HUFFMAN, Kenneth Glenn, 1940-
THE INTERACTION AND MERGING OF FLAMES FROM BURNING LIQUIDS.

The University of Oklahoma, Ph.D., 1968
Engineering, chemical

University Microfilms, Inc., Ann Arbor, Michigan

THE UNIVERSITY OF OKLAHOMA

GRADUATE COLLEGE

THE INTERACTION AND MERGING OF FLAMES FROM BURNING LIQUIDS

A DISSERTATION

SUBMITTED TO THE GRADUATE FACULTY

in partial fulfillment ot the requirements for the degree of

DOCTOR OF PHILOSOPHY

BY

KENNETH G. HUFFMAN

Norman, Oklahoma

1967

THE INTERACTION AND MERGING OF FLAMES

FROM BURNING LIQUIDS

APPROVED BY

C. M. Sliepcevich

C. V. Blair

F. M. Townsend

J. E. Fitzroy

Reed Wilson

DISSERTATION COMMITTEE

ACKNOWLEDGMENTS

I wish to express my gratitude and appreciation to the many people who gave assistance throughout the course of this study. I am especially indebted to my committee chairman, Dr. C. M. Sliepcevich, for his guidance and continuous support; to Dr. J. R. Welker, for his many helpful discussions during the study; and to the other members of the graduate committee, Dr. E. F. Blick, Dr. J. E. Francis, and Dr. F. M. Townsend.

Gratitude is due to Dr. O. A. Pipkin, for his helpful advice; to Mr. J. R. Hutchinson and Mr. B. L. Thomas for their valuable assistance in the experimental work; and to Mr. J. M. Bryan for his help in reducing the data. I also appreciate the efforts made by Mrs. Ruth Hogan and Mrs. Joyce Meyer in the preparation of this manuscript.

A special note of appreciation goes to those organizations who provided financial assistance during my graduate program: The National Bureau of Standards, the U.S. Army Physical Research Laboratory at Edgewood Arsenal, and the University of Oklahoma Research Institute.

Kenneth G. Huffman

TABLE OF CONTENTS

LIST OF TABLES

LIST OF ILLUSTRATIONS

THE INTERACTION AND MERGING OF FLAMES FROM BURNING LIQUIDS

CHAPTER I

INTRODUCTION

In the past, emphasis in fire research was directed mainly toward fire prevention and techniques for fire suppression. A large amount of information gained from this effort presently exists, but it has not answered many of the fundamental questions concerning fire behavior.

In recent years, fundamental fire research has received more attention. Importance has been placed on obtaining information on those variables which will lead to a basic understanding of the behavior and characteristics of fire. This information should give a better basis for determining standards and codes, as well as leading to new fire prevention and suppression methods.

A great deal of fundamental work has been directed toward the study of small laminar flames. Gaseous fuels have been used in most of this work. Lately there has been a growing interest in the study of larger, turbulent

fires, especially those supported by solid and liquid fuels. Information gained from these studies is more directly applicable to fires such as those involving buildings, forests, and fuel storage tanks. Since large-scale tests of such fires are expensive and difficult to conduct in a controlled manner, most of the experimentation has been done with small-scale models. In many cases, the data from these models have been correlated in such a manner as to predict the behavior of larger fires.

In the turbulent fire studies, particularly those involving solid or liquid fuels, conditions have usually been such that the flames could be described as uncontrolled, buoyant, diffusion flames. A flame is described as "buoyant" when the momentum forces that cause it to rise from its source are mainly due to the buoyancy of the hot flame gases. For gaseous-fueled fires, fuel is often fed to the fire at a rate such that the initial momentum of the fuel issuing from the source is large compared to the buoyancy forces of the hot flame gases. These are described as "jet" flames. The rate of burning of liquid and solid fuels is mainly determined by the characteristics of the fuel and the fire; therefore, these fuels produce "uncontrolled" flames. Gas flames are "controlled" since the burning rate is determined by the rate of fuel supply. "Diffusion" flames depend on molecular or eddy diffusion to mix the fuel and oxidizer at the combustion zone,

whereas "premixed" flames have fuel and oxidizer combined before the combustion zone is reached. The flames in the present study may also be described as uncontrolled, buoyant, diffusion flames.

Only a few investigators have considered flames from multiple sources. In most instances the work has been prompted by a desire to investigate the nature of either the "firestorm" or the "conflagration," both of which are multiple fire phenomena in that a large number of fuel elements are burning simultaneously.

Firestorms occur when there are many ignitions over a wide area such as might be caused by a nuclear blast. It is thought that under certain unstable meteorological conditions these fires will quickly coalesce into a single fire, burning intensely over a large area. A large convective column develops and rises almost vertically to considerable heights. The wind created by the air moving toward the center of the fire assumes gale-like proportions. This fire is characterized by its stationary behavior and complete destruction within the fire perimeter. The lack of spread is probably due to the strong indrafts; furthermore, firestorms appear to develop most readily under light wind conditions. Some examples of firestorms are the destructive fires which resulted after the attacks on the cities of Hamburg and Hiroshima in World War II.

The conflagration is a multiple fire which has a pillar of hot gases which slant considerably leeward as a result of prevailing winds. The chief characteristic of the conflagration is the presence of a fire front, which is an extended wall of fire moving leeward. Conflagrations sometimes occur in forest fires and have also occurred in city fires.

When the fuel sources of a multiple fire array are distant from each other, the fire from each source can be considered as a single flame and analyzed as such. As the distance between each source is reduced, the flames will start to influence one another. This condition will be termed "interacting" fires. As the spacing is reduced still further, each flame starts touching the adjacent ones. This condition is termed the onset of "merging." Further reductions in spacing increase the degree of merging, until the flames are combined into a single column of fire. They are then considered to be fully merged.

Most of the previous multiple fire studies have used small fires from gaseous fuels. Gas fires were used since their rate of fuel consumption is always fixed by the investigator. This control allows the use of widely varying fuel rates and fires ranging from small pilot flames to large jet flames; however, gas fuels also have a disadvantage in that there is no natural burning rate for gaseous fuels. In these previous studies, a great

deal of emphasis has been placed on the study of flame heights, particularly at the onset of merging.

Only very preliminary attempts have been made to study the merging of flames from liquid fuels. The degree of merging of liquid fuels, as well as solid fuels, influences the rate of heat feedback to the fuel source and therefore the rate of burning. The burning rate in turn affects the flame height and hence the degree of merging. The change in burning rate, and therefore the change in the size of the fire column of the array, also has a large affect on the rate of heat given off to the surroundings. The problem is complex, and little is known of the heat feedback mechanisms involved. By the use of gaseous fuels in the previous merging studies, flames could be analyzed in which heat flux back to the fuel would not be important in controlling the fuel flow rate. Such things as flame height could then be investigated without having to worry about the heat feedback problem. Since so little is known about the interaction and merging of separate fires, the present investigation was conducted under calm atmospheric conditions, without the additional complicating factor of an external wind source.

The present studies were made to obtain experimental data on the interaction and merging of flames from various liquid fuels in several spatial configurations. Since the burning rate of the liquid fuels is closely associated with

heat feedback, emphasis was placed on studying the burning rate and radiation flux to the fuel and surroundings. The objective was to correlate the burning rate data in such a manner that it could be used to predict the behavior of multiple fires in situations involving other liquid fuels and other numbers and arrangements of fuel sources. As will be seen, the rate of heat given off to the surroundings is greatly enhanced by the merging of separate fires, increasing the capacity of destruction to the immediate surroundings by a given quantity of fuel.

CHAPTER II

REVIEW OF PREVIOUS WORK

Although much fire research has been reported in the literature, the vast majority of this work has been concerned with single fires. The whole question of the interaction between two or more fires is nearly untouched.

In the following pages, some of the previous studies made on the more basic aspects of the single fire and of the interaction and merging effects of multiple fires are discussed. Only the single fire studies which are most directly related to the present investigation of flame merging are included, whereas essentially all of the previous fire merging studies reported in the literature are reviewed.

Studies of Single Fires

Small laminar flames, both of premixed and diffusion types, have been the subject of a large number of studies. Single turbulent fires from solid, liquid, and gaseous fuels have also been frequently investigated. Because of the complexity of the flow processes within the flame and surroundings, the freely burning turbulent flames have been analyzed in almost every case in terms of the gross properties of the flame.

In 1957 Blinov and Khudiakov (4) published the results of their work on burning pools of liquid fuels. Containers ranging from 3.7 mm to 22.9 meters in diameter were used. The fuels used were gasoline, tractor kerosene, diesel oil, and solar oil, all of which are mixtures of hydrocarbons.

In a review of Blinov and Khudiakov's paper (4), Hottel (12) showed that the behavior of the liquid-fuel fires could be explained qualitatively by considering the various heat transfer mechanisms which predominate in the laminar, transition, and turbulent burning regimes. Blinov and Khudiakov's data were plotted as burning rate per unit fuel surface area against burner diameter. For burners less than 3 cm in diameter the burning rate was seen to decrease as the diameter was increased. At these small diameters, the flames could be considered to be laminar. With further increases in burner diameter the burning rate changed slope and increased rapidly as flame turbulence began. At a pan diameter of about 1 meter, the burning rate leveled off with a fully turbulent flame being obtained. Further diameter increases showed essentially no effect on the burning rate. The ratio of flame height to burner diameter was seen to decrease as the diameter was increased. When the turbulent burning regime was reached, the flame height to burner diameter ratio leveled off.

The burning rate depends on the vaporization rate, which in turn is dependent on the rate of heat feedback from flame to fuel. Hottel showed that the vaporization rate per unit of fuel surface area would be proportional to the heat transfer rate to the fuel. He assumed that this heat transfer would be the sum of components due to conduction through the pan rim, and convection and radiation heat transfer to the fuel surface. The relation was expressed as

$$\frac{q}{\pi D^2/4} = \frac{4K(T_f - T_b)}{D} + U\,(T_f - T_b) + \sigma F(T_f^4 - T_b^4)(1 - e^{-\varkappa D}) \qquad (1)$$

where q = heat transfer rate to the fuel

K = conduction coefficient

U = convection coefficient

D = burner diameter

T_f = absolute flame temperature

T_b = absolute fuel temperature

σ = Stefan-Boltzman constant

F = view factor

$\varkappa$ = Beer's law extinction coefficient to allow for increasing opacity with thickness.

It is seen from the equation that at small diameters the conduction term will be dominant. At large diameters, the conduction term will become insignificant, and the convective term will be constant. The radiative term will be

dominant at large diameters due to the flame thickness. This behavior is reflected in the equation by the χD term becoming large. The burning rate will therefore be constant at large burner diameters. At intermediate diameters, the radiative term will be low due to the thinness of the flame, but the pan will be too large for conduction to be significant. The burning rate would therefore be at a minimum in this intermediate region.

The burning velocity of n-hexane and cyclohexane was studied by Fons (11) using pans ranging from 0.22 to 11.94 inches in diameter. The pan was provided with a water jacket to prevent heat conduction down the burner wall to the fuel. The pan was kept nearly full with a constant fuel level. The fuel temperatures were measured at two depths below the surface for the larger pans. The burning velocity of cyclohexane was plotted as a function of burner diameter and the slope was seen to be generally similar to the curves plotted by Hottel (12) from the data of Blinov and Khudiakov (4).

In furthering the study of the effect of pan diameter on burning rate, Emmons (10) burned methanol and acetone in shallow burners which were embedded in insulation up to their rims so that they were flush with the top of the table. The pans ranged from $\frac{1}{4}$ to 10 inches in diameter. He found that the burning rate continued to drop as the size of the pans decreased. His data did not agree with

that of Blinov and Khudiakov for the smaller pan sizes, although the two sets of data did agree for pans having diameters from 4 to 10 inches. By placing his pans on top of the table and exposing the rims, Emmons more nearly matched the data of Blinov and Khudiakov. A four-step heat transfer mechanism, taking the place of the simple conduction term assumed by Hottel (12), was postulated. In this mechanism, heat was first transferred from the flame to the table top by radiation, followed by convective heat transfer from the table top to the inducted air, convection transfer from inducted air to the pan rim, and finally conduction through the pan rim to the fuel. Heat was also transferred directly from flame to fuel by convection and radiation. The pans were blackened to note the effect of radiation to the pan bottom. It was found that the burning rate increased slightly for acetone when the shallow (¼ inch deep) pans were blackened. No effect was noted in the burning rate when methanol was burned in a blackened pan. The pan temperature during the acetone tests was measured by means of a thermocouple placed on the underside, center, bottom of the pan. The pan temperature was found to be well above the fuel boiling point during much of the burning time. Since the walls of the burner were surrounded by insulation, the high pan temperature indicated (in agreement with the blackened pan studies) that radiation direct to the pan bottom with

subsequent heat transfer to the liquid has the effect of increasing the burning rate somewhat (at least for shallow pans), when fuels which burn with luminous flames, such as acetone, are used. It might be noted that the burning tests of Emmons were at unsteady-state conditions since the burning rate was measured by igniting the fuel and noting the time elapsed until the fire burned out.

Rasbash, Rogowski, and Stark (17) burned several liquid fuels in a 30-cm diameter burner having an exposed rim. Alcohol, petrol, benzol, and kerosene were used as the fuels. Measurements were made, under steady state conditions, of the burning rate and temperature at several points below the fuel surface. They also measured flame shape and size, flame emissivity, and the upward velocity of the flame tip. Temperatures of the flames were taken using an optical pyrometer. From photographs the main part of the flames was seen to have the shape of a cylindrical column whose diameter was slightly less than that of the burner. They found that for petrol, benzol, and kerosene, the radiation was the dominant heat feedback mechanism, whereas convection was dominant for the alcohol fires.

In several articles, Burgess, et al. (5, 6, 8, 30) have reported their studies of the burning rates of liquid fuels. They extended the work of Blinov and Khudiakov by burning such fuels as butane, normal hexane, benzene,

methanol, and liquid hydrogen. These fires were burned outdoors under calm atmospheric conditions in pans ranging from 7 to 240 cm in diameter and 8 cm in depth. As in Hottel's (12) semiquantitative analysis of Blinov and Khudiakov's work, the radiative heat feedback to the fuel was considered to be dominant. Based on Hottel's expression for the radiative portion of heat feedback to the fuel, $\sigma F(T_f^4 - T_b^4)(1-e^{-\varkappa D})$, curves of liquid regression rate versus pan diameter were calculated and compared with experimental regression rate data for the larger burner sizes. The curves, which represented evaporation rates due exclusively to radiative heat transfer, were generally in good agreement with the data. These curves represent the empirical expression

$$v = v_\infty (1-e^{-kD}) \qquad (2)$$

where v = liquid level regression rate

v_∞ = liquid level regression rate for large pan diameters

k = a constant

D = pan diameter

The data were extrapolated to large pan diameters, and it was noted that the burning rates at large diameters were inversely proportional to $\Delta H_v/\Delta H_c$ where ΔH_v is the effective heat of vaporization (that is, the heat of vaporization

at the boiling point plus the integrated heat capacity of the fuel from ambient temperature to the boiling point) and ΔH_c is the heat of combustion. This ratio of $\Delta H_v/\Delta H_c$ is the fraction of the flame's heat that must be fed back to the fuel to maintain a steady rate of vaporization. The empirical correlation of burning velocity data had the form

$$v_\infty = 0.0076\,(\Delta H_c/\Delta H_v) \text{ cm/min} \qquad (3)$$

The radiant heat flux to the surroundings was measured, and found to be about 20 to 40 per cent of the heat of combustion. It was noted that the base of the flames of butane and benzene were particularly inclined to spread over a larger area than the fuel tray. This spreading was attributed to the density of the fuel vapors at the fuel boiling point being greater than the density of the surrounding air.

Spalding (20) attempted to show by means of convection theory that the dominant mechanism of heat feedback for large fires might well be convection rather than radiation. Using his earlier developed convection theory (19), he showed that burning rates of the same order of magnitude as those predicted by Equation 3 could be obtained. He stated that his earlier convection theory, when modified to take account of turbulence, predicted that the burning rate of liquid-fueled fires will be independent of tray diameter for large diameter fires.

In answer to Spalding, Burgess and Grumer (7) pointed out that flames above large liquid pools conform to the flame shapes reported by Rasbash, et al. (17), that is, there is a thick vapor zone between the luminous zone and the liquid surface. They also stated that the vapors immediately above the liquid are not necessarily very hot, and that in some cases there is no sharp discontinuity of temperature at the liquid surface. Under windless conditions, they had observed the sides of the flames in proximity to the fuel surface to be smooth and steady, thus making convection transfer less important.

In a study of fire involving liquid storage tanks, Magnus (14) investigated the behavior of gasoline and ethanol fires. He burned these fuels in tanks ranging from 12 cm to 120 cm in diameter and from 16 cm to 160 cm in height. The burning rate of the fuel and the temperature profile in the flame and convection column were measured under essentially calm conditions. He found that the burning rate per unit area increased with increasing diameter. He also investigated the effect of freeboard height (height of burner rim above the fuel surface) on the burning rate. The effect of the freeboard height on burning rate was found to be a complex function, depending on the test tank height to diameter ratio and fuel composition, as well as freeboard height. It was found that an increase in freeboard height caused the

burning rate and maximum flame temperature to decrease. The effect for the two fuels was such that at low freeboard heights, the ethanol burned more slowly than gasoline, but at freeboard heights greater than one-half the tank diameter, the burning rate for gasoline had decreased to a greater extent than the burning rate for ethanol so that ethanol burned more rapidly than gasoline. The temperature maximum in the flame was found to remain at almost a constant distance above the liquid surface, this distance being influenced by the tank shape.

Akita and Yumoto (1) measured burning rates of methanol in single burners and in concentric burners having three compartments. The single burners ranged from 1 to 60 cm diameter, and the concentric burners from 10 to 30 cm diameter. By use of empirical, local heat transfer coefficients, burning rates predicted by Hottel's (12) theory were compared with their data, showing that Hottel's theory apparently could be applied not only to the turbulent luminous combustion of liquid fuel, but also to nonluminous combustion under conditions of laminar flow. It was assumed that for methanol the radiation terms in Hottel's theory would be small compared with conduction and convection. It was found that the burning rate for methanol was much greater at the burner rim than at the center, particularly for small burners with laminar burning. This result would be expected, since radiation heat feedback

to the fuel would not be dominant, and conduction is limited to the burner rim. As shown by their treatment of Hottel's theory, the convection heat feedback in the small pools would decrease with distance from the burner edge.

Thomas, Webster, and Raftery (24) derived a relation between the height, L, of a turbulent, buoyancy-controlled diffusion flame, the linear dimension of the orifice, D, and the volumetric flow rate of fuel through the orifice, Q, using dimensional analysis. The relation for a particular fuel system was found to be

$$L/D = f\ (Q^2/gD^5) \qquad (4)$$

where g is the acceleration due to gravity. In this study the supply rate of fuel is considered to be independent of the heat feedback to the fuel. It was also noted that when buoyancy was important, the mean velocity of the flame gases increased rapidly with height, and turbulence could be induced at a small fraction of the total flame height even if the Reynolds number based on conditions of the emerging fuel showed this flow to be laminar. Single wood cribs with square horizontal bases were burned in still air. The burning rate was determined, and the flame heights from the turbulent fires were measured photographically. Since the whole crib was ignited at once,

these tests were unsteady state fires, the data being taken during a period when the burning rate was at a maximum value. The data were plotted as L/D vs $\rho Q^2/D^5$, where ρ was an assumed value of the density of the wood volatiles. The results were seen to conform to the derived correlation over the experimental range.

Thomas (25) extended the work of Reference (24). The quantity Q^2/gD^5 was presented experimentally as $m''/\rho_a\sqrt{gD}$, where m" is the mass flow rate of fuel per unit area and ρ_a is the density of the surrounding air. The relation obtained by plotting his data for wood cribs was

$$L/D = 42 \left(\frac{m''}{\rho_a \sqrt{gD}} \right)^{0.61} \qquad (5)$$

for fires burning under calm conditions from nearly radially symmetrical fuel beds. He also used the same dimensionless relationship between flame height, burning rate, and burner dimension to correlate data obtained by other investigators for liquid and gaseous fuel fires, and for large scale wood fires. The data covered a range of L/D from about 0.01 to 100 and a range of $\frac{m''}{\rho_a\sqrt{gD}}$ from 10^{-5} to 100.

Thomas, Baldwin, and Heselden (26) measured the flow to air into flames with thistledown used as a tracer. Circular fires, 91 cm in diameter, were studied using

both wood and ethyl alcohol as fuels. A smaller 30 cm square town-gas fire was also used in the studies. From the data it was seen that the air flow toward the flame was considerably in excess of both the stoichiometric requirement and the flow predicted from entrainment theory. A considerable part of the air flow did not enter the flame zone, but was dragged upwards outside the flame. The mean concentration of oxygen on the flame axis was measured. An appreciable amount of oxygen was present quite low in the flames, suggesting that even low in the flame, air penetrates to the flame center in some of the large turbulent fluctuations. The heat transfer back towards the fuel surface was also measured. Convection was found to be small in comparison with radiation as a heat-feedback mechanism at the center of the liquid fuel burner, with the convective contribution increasing somewhat nearer to the burner rim. This result is in accordance with Hottel (12), and Burgess, et al. (5), that radiation transfer is the predominant mechanism controlling the burning rate of large liquid fires.

In his studies of the effect of wind on uncontrolled buoyant diffusion flames from burning liquids, Welker (28) noted a trailing effect of the flame downwind from the fuel burner. This trailing effect apparently had not been noted in previous literature although Zabetakis and Burgess (30) had noticed that flames from some fuels

burning in still air would slip off the burner edges due to slight wind movements. The reason for the trailing effect seems to be that the density of the fuel vapor at the fuel boiling point is higher than that of the surrounding air, and therefore tends to descend until it has been heated. This flame trailing has not been reported for fires from solids or for gas fires. For fires from solids, pyrolysis must occur in order for vapors to be present and support a flame. This pyrolysis occurs at temperatures which are sufficiently high that the densities of the vapors are less than that of the surrounding air. For gas fires, the fuel usually consists largely of methane, the density of which is less than that of the surrounding air.

Studies of Multiple Fires

The multiple fire problem is very complex; theoretical analyses in the few studies made of multiple fires have been based on simple models. Much of the previous work has been concerned with the multiple fire only at the point where the individual fires just begin to coalesce to form a larger single fire. In these previous studies, gaseous fuels have been used most frequently, since the burning rate can be controlled for a gaseous fuel. The burning rate can then be considered independent of the heat feedback from flame to fuel, thereby considerably simplifying the problem.

Putnam and Speich (16) reported the preliminary findings of a study to establish modeling laws for partially

and fully-merged flames using gaseous fuels. Gaseous fuel was used since the flow rate could be controlled by the investigator and would be an independent variable in the establishment of modeling laws. Efforts were made to determine flow conditions and nozzle diameters which produce single turbulent, buoyancy-controlled flames. A range of flow rates and nozzle diameters was found so that the Reynolds number would be large enough for turbulent flow yet the Froude number would be small enough that the flame would be buoyancy controlled. Data for flames from different arrays of multiple jets were presented and analyzed by considering the total flame source either as a series of point sources of fuel or on an area basis. For a single flame, Putnam and Speich arrived at the equation

$$L/d_o = K\left(\frac{Q_o^2}{gd_o^5}\right)^{1/5} \qquad (6)$$

or

$$L = K' Q_o^{2/5} \qquad (7)$$

where L = flame height

K, K' = constants

Q_o = volumetric flow rate of the injected fuel

g = gravitational acceleration

d_o = nozzle diameter.

For both the single and multiple flames considered, the ratio of flame height to nozzle diameter was first assumed to be large (point source), so the nozzle diameter could be eliminated from the correlations. For multiple fires considered as point sources (small d_o), Putnam and Speich correlated flame lengths as

$$L'/L^* = \text{function}\left[\text{source shape factor, } n, \frac{S}{(Q_o^2/g)^{1/5}}\right]$$

where L' = multiple fire height

L^* = single fire height

n = number of jets

S = spacing between jets.

When the data for several source arrays and numbers of jets were plotted as a flame height function versus a spacing function, or

$$\frac{L'/L^*-1}{n^{2/5}-1} \text{ versus } \frac{S}{(Q_o^2/g)^{1/5}}$$

the flame height function was found to increase as the spacing function was decreased. This effect was considered to be caused by mutual entrainment. No consistent effect of jet number or source shape was noticed for the experimental data. At a value of spacing function of about 2, there was a rapid increase in the flame height function.

This increase was said to indicate that the jet flames changed abruptly from acting as single jet flames to acting as a mass fire. Treating the total flame source on an area basis, a correlation was obtained by plotting L/D vs q^2/gD^5 where q is the total flow rate. The principal dimension D was the side of an approximately square array.

Later, Putman and Speich (15) pursued further their study of multiple flames of various array patterns. It was assumed that the individual jets could be considered point sources. They attempted to show that flame arrays characterized by small ratios of flame height to overall diameter act as a line fire in which only one side is exposed to induced air. Putman (16) previously had developed the relation for a point source flame showing that the flame height is proportional to the flow rate to the 2/5 power. The data for arrays of various shapes and numbers of jets were plotted as L/D^* vs $q^{2/5}/g^{1/5}D^*$ where L is the array flame height, D^* is an equivalent diameter of the array, g is gravitational acceleration, and q is the total flow rate. The theoretical curves for a single point source and that of a line fire exposed to induced air on only one side were also plotted. An attempt was made to show by correspondence between data and theory that there was a close relation between line fires and area fires treated as if their perimeters were one-sided line fires.

Thomas, et al. (26) also studied the flame heights of merging fires. They were interested in the flame heights at the onset of merging, which they defined as being the point at which the flame tips are just touching. Only gaseous fuel was used so that the burning rate could be considered as being independent of the heat feedback to the fuel. A highly simplified theory was developed which considered entrainment and the motion of the flames. An expression for the flame height at the onset of merging of two rectilinear fuel burners was derived. It was noted that a column of hot rising gases entrains air from its surroundings, so that when one flame is placed in the neighborhood of another, the resulting restriction of the air flow causes a pressure drop in the space between the two. This pressure drop causes air flow toward the low pressure space, which in turn causes the flames to be deflected from the vertical. For buoyancy-controlled flames, the only forces acting on the flames would be a buoyancy force upward, and a resultant pressure thrust acting normal to the flame axis. The components of these forces normal to the flame axis were then equated. Thomas (25) assumed that the inward momentum of the entrained air is proportional to the local upward momentum. An expression for the upward velocity in the flame was given in terms of the height of the flame tip and its temperature as

$$w = K \left(\frac{2g\ \Theta_{fl}\ Z}{T_o} \right)^{1/2} \qquad (9)$$

The entrainment velocity could then be expressed as

$$V = K' \left(\frac{2g\ \Theta_{fl}\ L}{T_{fl}} \right)^{1/2} \qquad (10)$$

where g = acceleration due to gravity

K, K' = constants

L = flame height

T_{fl} = flame temperature

T_o = ambient temperature

V = mean entrainment velocity

w = mean upward flame tip velocity

Z = height

Θ_{fl} = flame temperature rise

Using this expression for the entrainment velocity and Bernoulli's equation, an expression was derived for the merging flame height in terms of the burner dimensions and the separation distance between the burners. This expression is

$$\frac{L}{D} = 9 \left(\frac{S^3}{DW^2} \right)^{1/2} \qquad (11)$$

where L = flame height

S = separation between fuel beds

D = tray diameter

W = length of long side of fuel bed

The authors noted that only approximate results could be expected from the above-mentioned expression for entrainment velocity used in the derivation. The data of Thomas, et al. (26) had shown the air flow toward the flame to be considerably in excess of that predicted by the entrainment theory. The flame merging data were taken using town gas in burners 60 x 30 cm and 30 x 30 cm arranged horizontally in pairs. There was only fair agreement between the data and theory.

These simplified flame merging calculations were later extended by Baldwin (3) in an attempt to predict the critical condition at which merging occurs in more complex situations. An expression for flame height of the array at the onset of merging was derived by considering a square array of n^2 fires arrayed in concentric rings. It was assumed that each of the fires in the array entrained air at the same rate; hence no account was taken of the variations of flame height from ring to ring nor of the variation of burning rate. Proceeding in the same manner as in Reference 26, the equation for the flame height was obtained in terms of separation distance and array dimensions. The authors presented no new data other than a few of the fires reported by Waterman (27). They observed that since there was very little experimental data on flame merging, the presented calculations could only be regarded as tentative.

Measurements by Strasser and Grumer (23) of static pressures between proximate wood fires showed pressure depressions on the order of 0.001 to 0.002 cm water below atmospheric pressure. A curve of pressure between the proximate fires versus time was seen to lag behind the curve of burning rate versus time because of time-dependent heating effects.

Waterman, et al. (27) analyzed the merging of free-burning fires. Preliminary tests were conducted with liquid fuel fires. Both laboratory and large-scale field tests were used. Wood cribs were used for the main experiments since the liquid fires were found to be very sensitive to any air motion. This difficulty was not encountered with the cribs. For the preliminary liquid fuel tests a single burner, 30 inches square, was used. A stable flame column could not be obtained due to sideward movement of the flame. In many cases fuel vapors moved horizontally across the floor for some distance before igniting, resulting in a disturbance to the main flame. Since part of the difficulty was thought to be due to uneven heating of the fuel, special fuel beds were designed containing ceramic beads which protruded above the liquid surface to help even out the heating. Although the flame was made a little more stable, the arrangement was still considered to be unsatisfactory. Tests with groups of burners of large dimensions were then conducted outdoors with No. 2 fuel oil being used as fuel.

These merging tests were not satisfactory due to wind effects. The experiments using wood cribs involved single crib fires, and multiple crib fires from as many as sixteen, 3 x 3 ft cribs. The dimensions per crib ranged from 2 x 2 to 6 x 6 feet. The multiple crib fires were conducted indoors with the cribs being set on fire so that all of them reached a fully involved state simultaneously. The tests indicated that the spacing at which merging occurs and the magnitude of the burning rate at this spacing are governed by the burning rate of a single crib and the total number of such fires. As the distance between individual cribs was increased, the total burning rate increased until a transition from a merged to non-merged fire occurred. This transition was accompanied by a sudden drop in burning rate. From the data obtained, a scaling law for merging was formulated as:

$$\left(\frac{\text{distance between cribs}}{\text{crib dimensions}}\right)_{peak} = 0.069\ (n\ R_s)^{0.4} \qquad (12)$$

where n = number of cribs

R_s = burning rate of a single crib, lb/min

The burning rate at the transition, R_{peak}, was given as

$$R_{peak} = 1.56\ (n\ R_s) \qquad (13)$$

Rios (18) studied the effects of wind on the flames from two proximate wood cribs. When burning in still air,

the two fires were observed to lean toward each other when the cribs were placed close together. As an external wind was applied to the closely spaced fires, the upwind fire was tilted from the vertical to a greater extent than was the downwind fire, showing that the upwind fire tends to exert a blocking effect on the air reaching the downwind fire. Rios found that the burning rates, length of flames, and propagation rates for the proximate fires could be correlated in terms of the depth of the flaming zone, irrespective of wind velocity and crib spacing.

The production of multiple fires on a large scale for purposes of investigation is extremely expensive. Only a very few large-scale field tests have been conducted. A large amount of data have been gathered from these tests, but little attempt has been made to correlate these data.

Countryman (9) described large-scale experiments in which multiple-pile plots of forestry fuels were burned. Plots of up to 2,200,000 square feet were used. Some measurements were made of the air flow into the fires, and the pressure within the burning plots was recorded. Temperatures in the fires and concentration of oxygen and noxious gases were also measured.

A preliminary analysis of data from other large-scale experiments was given by Western (29). In these experiments multiple piles of forestry fuels up to 1,620,000

square feet were burned. Temperatures, thermal radiation, toxic gas concentrations, and weight loss rates were briefly examined.

As can be seen from the previous pages, the amount of analysis and experimental work available on multiple fires is very limited. Most of these previous results have been based on data taken from multiple fires of gaseous or solid fuels, with liquid fuels being largely neglected.

Modeling and Dimensional Analysis

Since is is generally impractical to make full-scale fire studies, it has been the usual practice to use models to correlate the data from model tests. Hottel (13) discussed the general principles of similarity and modeling, and reviewed three methods for establishing dimensionless groups. The widely-used pi theorem defines a procedure which is largely mechanical in nature. It often yields dimensionless groups which are valid but are in an unfamiliar form. It therefore tends to mask the physical significance. Another approach is to formulate the equations applicable to the problem and to manipulate them until dimensionless groups appear. This procedure will work, but it requires enough knowledge of the systems to write the equations, which is not necessary in using other methods. The method favored by Hottel is to take ratios of forces, mass rates, and energy rates expected to enter the problem at hand.

Hottel gave examples to show the method of applying these ratios.

Spalding (21) discussed the art of partial modeling. He noted that the strict requirements of similarity theory are so numerous and restrictive that complete modeling of combustion processes is practically impossible. For this reason many model experiments have deliberately ignored some of the similarity rules which should ordinarily be followed. The author stated that experience has shown that in many cases flouting certain of these rules does not cause too large an inaccuracy in the result. Some of the more notable examples of this partial modeling and the procedure to be followed to obtain partial modeling are reviewed.

CHAPTER III

FACILITIES AND EQUIPMENT

The flame interaction and merging studies were carried out at the Flame Dynamics Laboratory Low Speed Wind Tunnel of the University of Oklahoma Research Institute. This wind tunnel was originally designed and constructed for the purpose of investigation of the effects of wind on buoyant diffusion flames from burning liquids. The wind tunnel facility consists mainly of a wind tunnel test section, an observation and instrumentation room, and a static test room. The present tests were conducted in the static test room. A photograph of the facility is given in Figure 1 and a layout diagram is given in Figure 2.

Static Test Room

The static tests room measure 20 x 20 x 16 feet high. It is located at the end of the wind tunnel test section. The static test room is designed to serve the dual purpose of providing a large space for tests under calm conditions, and serving as a surge chamber for tests in the wind tunnel section. The building is constructed

Figure 1. Flame Wind Tunnel.

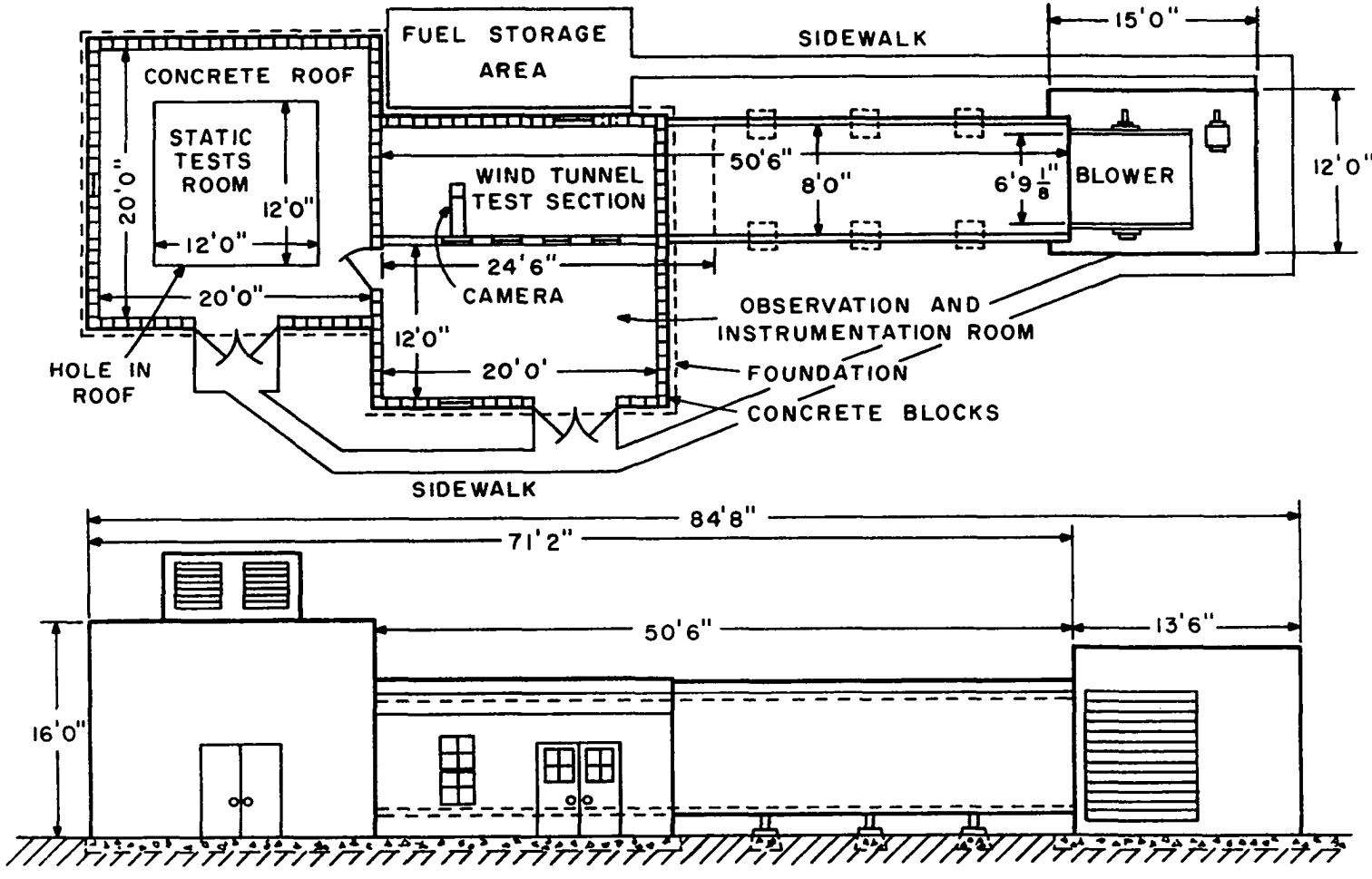

Figure 2. Layout of the Flame Wind Tunnel.

of concrete blocks with a concrete floor. No combustible materials of construction are used in areas near the test sections. For the testing of fires under calm conditions, a large hood, which extends down to a level about 8 feet from the floor, is suspended from the ceiling of the static test room. The purpose of this hood is to aid in collecting and venting smoke and soot. The combustion products are exhausted through a vent mounted on the roof. Spring-loaded shutters are provided in the walls of the vent, and a metal roof covers the top of the vent. The shutters allow combustion products to pass out, but they are closed by prevailing outside wind, thus preventing smoke from being blown back into the test room. A ½-HP constant speed fan is installed in one side of the vent in order to help exhaust smoke and fumes from the room.

The observation and instrumentation room measures 12 x 20 feet, is about 10 feet high, and connects directly to the static test room. For the purpose of observing the fires in the static test room, a glass panel was installed in the upper portion of the door leading from the observation room to the static test room.

An opening through the common wall between the observation room and the wind tunnel section is provided

with a small sliding glass door. This opening has dimensions of 16 by 32 inches and is about 5 feet above the observation room floor. A camera was positioned in the wind tunnel test section just below the sliding door, and just inside the wind tunnel test section as shown in Figure 2. The opening permitted access to the camera during a test. The camera arrangement is described in more detail later.

The fuel storage area is located outside the building on the opposite side of the wind tunnel section from the observation room. It is isolated from fire test areas and is surrounded by a high fence. Fuel is stored in 54-gallon drums on a concrete pad. The gates through the fence are kept locked while they are not in use.

Experimental Apparatus for Preliminary Studies

A number of preliminary tests were made before the final burning table was designed. The burners for these preliminary studies were placed on top of a flat surface during the tests; these burners were therefore "exposed rim" burners, in contrast to the "rimless" burners used for the main body of tests. The preliminary tests were unsteady state since the fuel burners were filled with a fixed amount of fuel, ignited, and allowed to burn until all the fuel was consumed.

The first series of preliminary tests was conducted using very small circular burners. The sizes used ranged from 1¼ to 2 9/16 inches in diameter. These burners were actually film cans and soup cans, the tops of which had been cut off to obtain containers one inch deep. The burning platform on which these burners were placed was light weight and was covered with asbestos paper. The platform surface was provided with markings for burner locations. This platform was attached to the end of a lever arm of adjustable length. The lever arm was connected to a Baldwin SR-4 Torque Pickup. Weights were hung at both ends of the lever arm so that the burning platform was balanced at the desired height. As the fuel in the cans was burned the burning platform was lightened and rose. This movement was transmitted through the counterbalanced lever arm to the shaft of the Torque Pickup. The signal from this Pickup was then recorded on a Bristol Dynamaster recorder. The lever arm was adjusted to give a full scale recorder deflection with only 10 ounces of fuel on the burning platform. This setup was reasonably satisfactory for measuring the burning rate of these very small unsteady state fires. The apparatus, however, was found to be unsuitable for measurement of flame lengths and radiation flux from the flame array to the surroundings due to the large amount of vertical movement which accompanied the burning process.

For the next series of preliminary tests, a weight-measuring apparatus was constructed which eliminated the problems caused by large vertical movement of the burning platform. In this second series of preliminary tests, circular burners of 4 3/16-inch diameter and square burners 3 inches in width were used. All of these burners had a depth of one inch. The tests were again for unsteady state burning, with only enough fuel being used to fill the burners initially flush full. The burning table, shown in Figure 3, had a circular, asbestos-insulated top, 64 inches in diameter. This platform was supported on three flexible beams equipped with strain gages. As burning proceeded during a test, the load on the strain gages decreased and the resulting change in resistance was reflected in the circuitry as a change in potential. This potential change was recorded on one channel of a 2-pen Honeywell recording potentiometer. The resulting strip chart record was used to calculate the burning rate. This weight measuring system was calibrated by placing standard weights on the burning platform and noting the recorder pen deflection. The radiation from the flame array to the surroundings was measured with a radiometer whose output was recorded on the second channel of the 2-pen recorder. This radiometer is described in more detail later. The height of

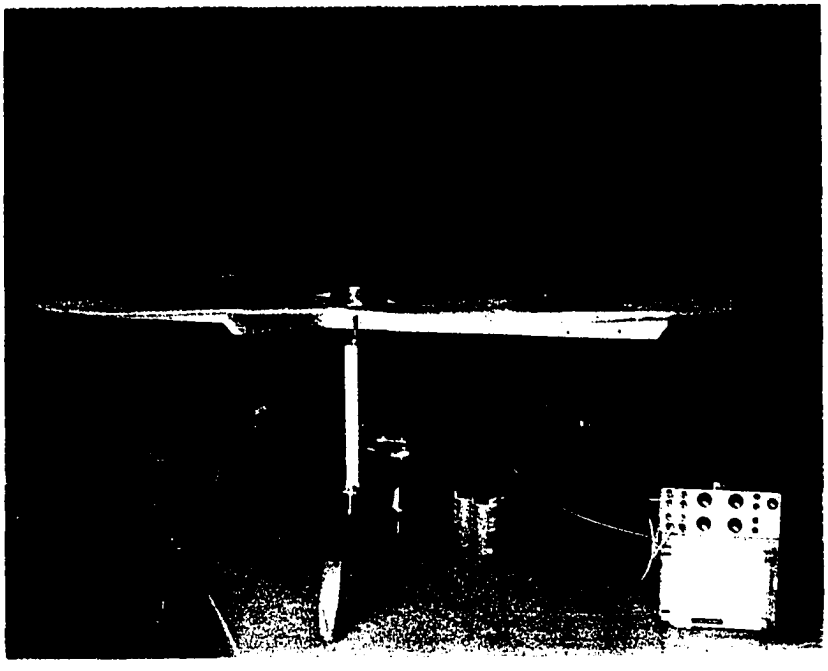

Figure 3. Flame Merging Test Apparatus for Exposed-Rim Burners.

the flames was measured using a Speed Graphic press camera containing a Polaroid film holder which used 4 x 5 Polaroid film packs.

Burning Table and Fuel Burners

For the main group of tests in the flame interaction and merging studies, it was desired to have steady state burning in burners of rimless design. The burners could be considered essentially rimless since they were embedded in insulation up to their rims. A new burning table, as shown in Figure 4, was constructed, and was made large enough to permit interaction-free burning as a limiting case. A nine-burner pattern was used for most of the tests with one burner positioned in the center of the pattern and eight burners placed symmetrically around the perimeter. In addition, a pattern was employed in which four burners would be placed between the eight peripheral burners and the center burner. Figure 5 shows a plan view of each of these burner placement patterns. The top of the table was made octagonal in shape. It measured ten feet between opposite sides and was 24 inches above the floor of the static test room. The framework of the table was constructed of slotted angle steel. Rails of angle steel on which the burners were to rest extended from the eight vertices to the center of the table top. The burners could then be placed on

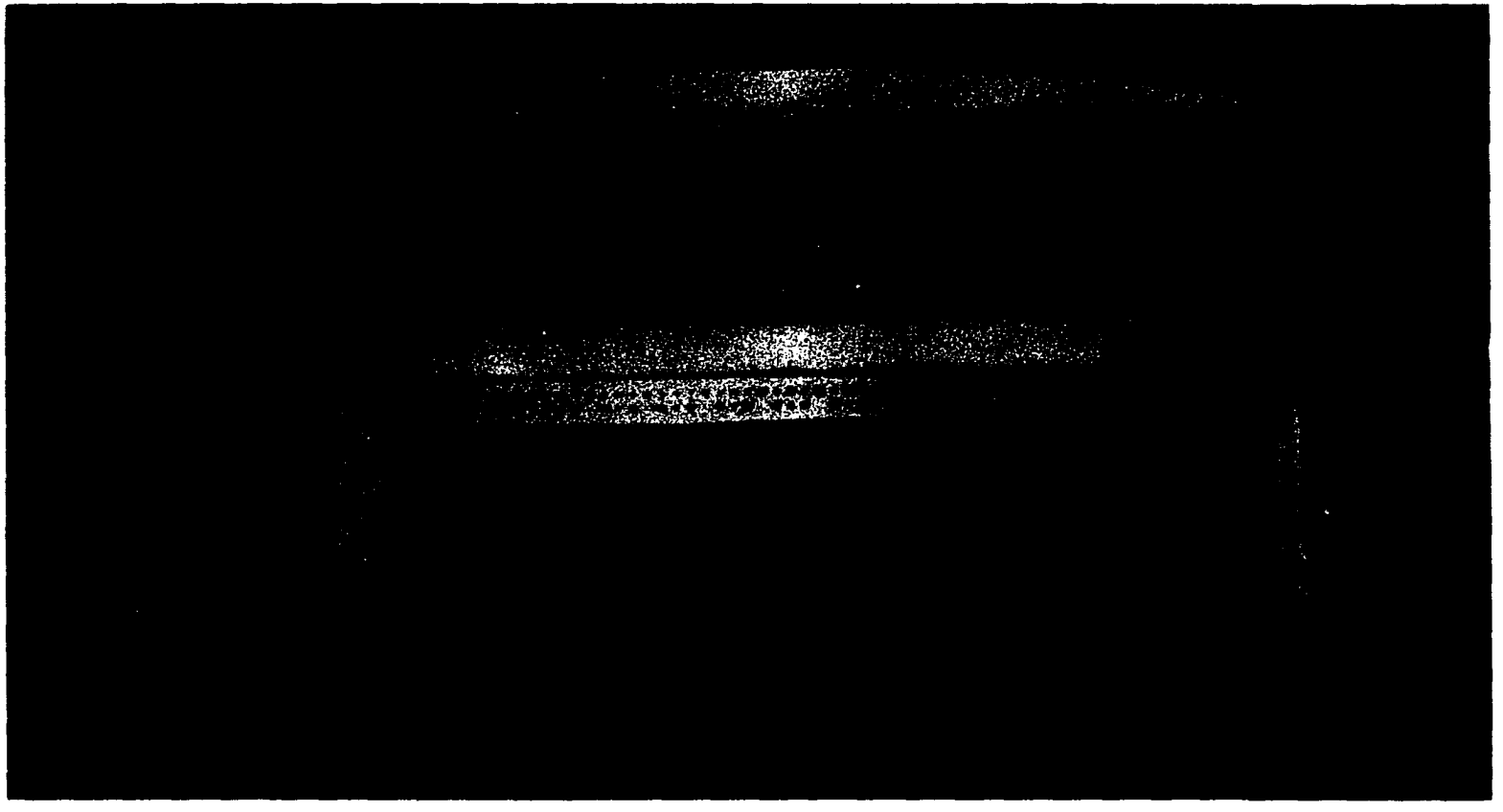

Figure 4. Flame Merging Burning Table for Rimless Burners.

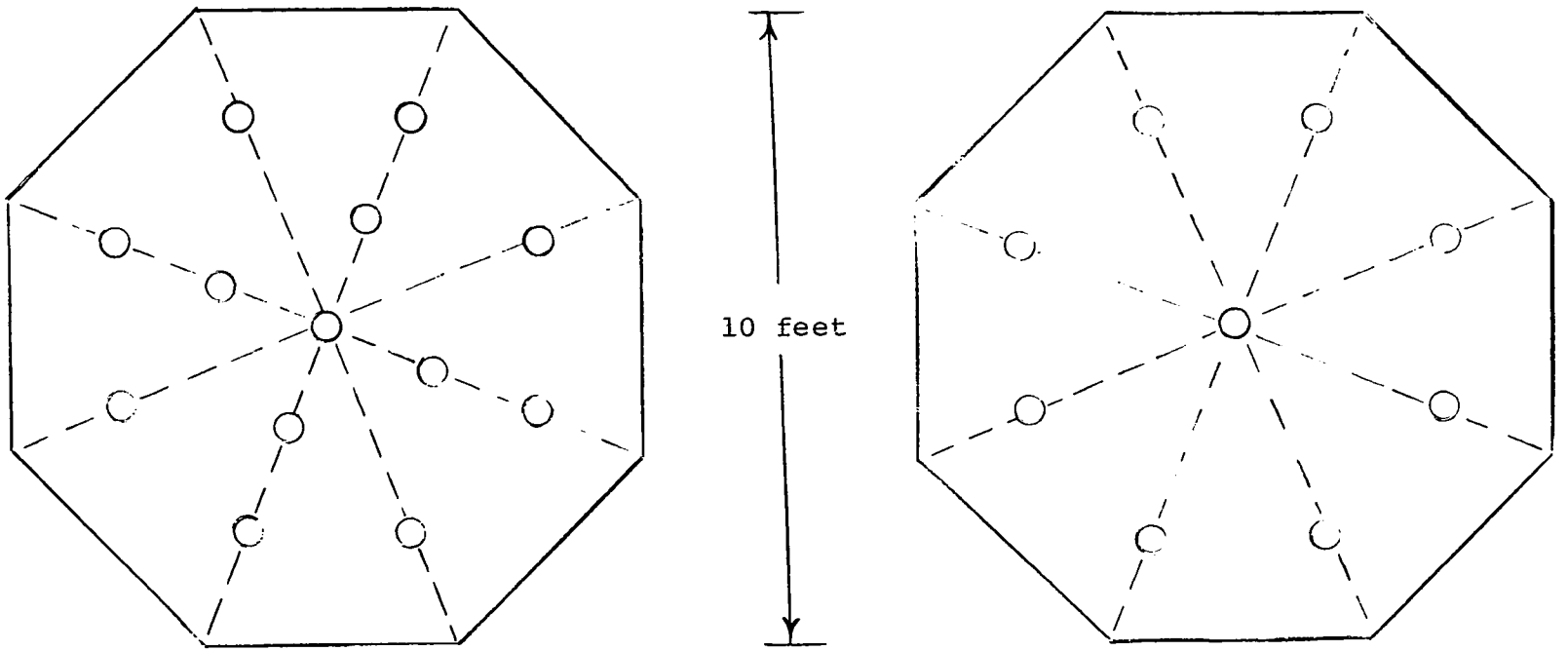

Figure 5. Schematic Diagram of Flame Merging Table-Plan View.

these rails at any desired distance from the center of the table. The burning table was positioned at the center of the static test room.

The entire top of the table framework was covered with 2-inch thick insulation. In order to change the position of the burners while keeping their rims flush with the table top, the insulation was made into fitted blocks of appropriate sizes and shapes. By inserting or removing the blocks around the fuel burners, the burner position could be easily changed. In the center portion of the table and along the burner rails, this insulation consisted of several layers of glass fiber mat covered with ½-inch thick asbestos millboard. These layers were held together with pins having small hooks in the top to facilitate the removal of blocks from the table top. To retard deterioration, the asbestos millboard in the immediate vicinity of the burners was painted with a high temperature coating cement. In the triangular-shaped areas between the burner rails where there would be no direct flame contact, the glass fiber mats were covered with a heavy grade of asbestos cloth instead of millboard to conserve millboard and to provide easier access to the center of the table. The large insulation sections which were covered with asbestos cloth were light enough to be removed easily, allowing accessibility to the table center. The height of the insulation blocks was such that when

the blocks were placed on the steel framework, a continuous, level surface was formed over the entire table for any desired burner position, with the burners being recessed into this surface. As a safety measure, sandbags were placed on the static test room floor completely around the perimeter of the burning table. In the event of a large spillage of burning fuel from the burners, the fire would be contained under the table and could not spread over the test room.

As the tests proceeded, it was found that a slight modification of the center portion of the burning table was necessary in some cases. For fuels such as n-hexane, cyclohexane, and benzene, the density of the fuel vapors is heavier than that of the surrounding air at the temperature of vaporization of the fuel. At small separation distances for which the flames were merging, a small blanket of unburned fuel vapor would cover the center portion of the burning array during a test. It was noted that in the area around the burners the heavy vapor from these fuels often seeped down into the cracks where the insulation blocks fitted together. The vapor was then absorbed into the glass fiber mats and would ignite. This vapor seepage problem was thought to be the cause of an accidental fire that occurred under the table during one of the tests. This fire will be elaborated upon later. To prevent the fuel vapor from getting into the insulation

and under the table, a large sheet of ¼-inch thick asbestos millboard was fitted into the center of the burning table. This sheet was necessary only for the smaller burner separation distances. Since close-fitting holes for the burners were cut out of the millboard sheet, it was necessary to use a different sheet for each burner size and separation distance. By using a large single sheet of millboard, there were no small breaks in the surface around the burners, and vapor could no longer collect in the lower layers of insulation and under the table.

Circular fuel burners having diameters of 2, 4 and 6 inches were used in the tests. Each burner was made by welding a circular piece of ¼-inch steel plate to a 2-inch long section of thin-walled steel pipe of the appropriate diameter. The pipe was tapered to a sharp edge at the top to minimize heat conduction to the fuel. The details of the construction of one of the burners are shown in Figure 6. In order to conduct tests with steady state burning, it was necessary to maintain a constant liquid level in the burners throughout an entire test. A 1/8-inch hole was drilled and tapped in the center of the bottom plate of each burner so that a fuel line could be connected to the burner. This hole was small enough that when the fuel level was dropped back into the fuel lines below the bottom of the

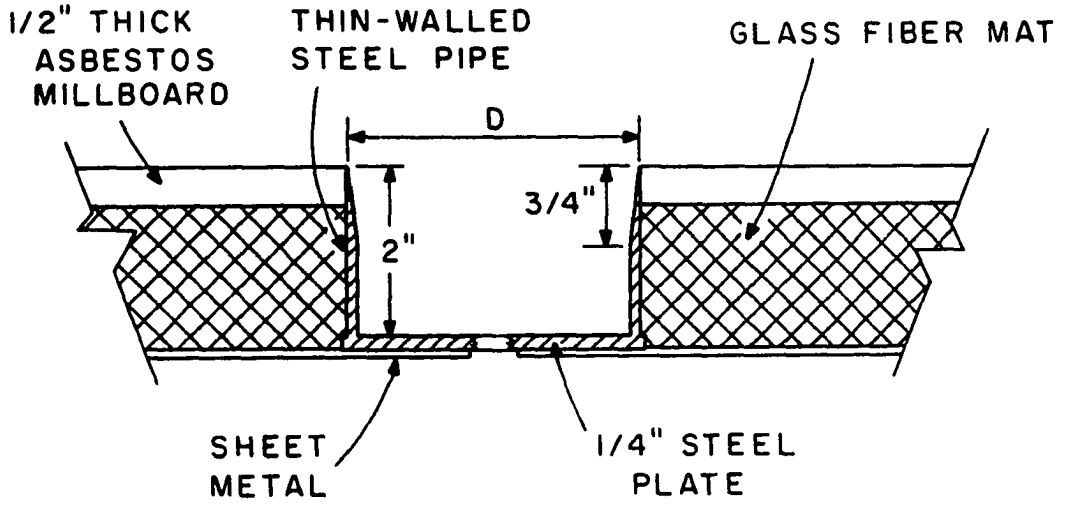

NOMINAL DIAMETER (INCHES)

2
4
6

Figure 6. Detail of Rimless Burner.

pan, the fire would be snuffed out. The burners were made two inches deep to allow for enough fuel thickness to absorb most of the radiative energy incident on the fuel surface. When the burners were filled as nearly flush full with fuel as possible, the radiant heating of the burner bottom with subsequent conduction to the fuel would be made negligible. Tests at the Bureau of Mines (6) indicate that the two-inch fuel depth would be more than sufficient to absorb all the back radiation.

As mentioned above, the burners were recessed into the insulation so that their rims were flush with the top of the table surface. Thus, heating of the burner walls with subsequent conduction to the fuel was small enough to be considered negligible.

To study the effects of burner size and burner array pattern on flame interaction and merging, nine-burner and thirteen-burner patterns, shown in Figure 5, were chosen for the main body of tests. These particular patterns were chosen since they would provide a simple, symmetrical array, and would give flames small enough to be studied in the static test room. The nine-burner pattern was also used in the preliminary tests. The preliminary tests had indicated that burners smaller than 2 inches in diameter would probably not show a significant amount of merging with the number of burners to be used. Six-inch diameter burners were chosen for

the largest size in the nine-burner pattern since fires from these burners, after merging, are as large as can be tolerated in the static test room. By using 4-inch diameter burners, the results of the rimless burners could be compared with the results of the exposed-rim burners used in the preliminary tests. Furthermore, in the thirteen-burner pattern only the 4-inch diameter burners were used due to the limited size of the static test room.

Fuel Delivery System

The fuel reservoirs used in the flame interaction and merging tests were those employed by Welker (28) in his flame bending studies. The fuel reservoir and delivery system are shown schematically in Figure 7. The system is basically a constant head siphon which uses the liquid fuel in the delivery lines to provide a liquid seal between the burner and the fuel reservoir. The bottom end of the breather tube is positioned at a level the same as the desired fuel level in the burners. During the filling of the burners, the fuel level rises until the liquid head at the burner and at the end of the breather tube balance; the fuel flow will then stop. The liquid level inside the reservoir is under a slight vacuum caused by the removal of fuel. As fuel is burned, the level in the burner starts to drop. Air is then sucked in through the

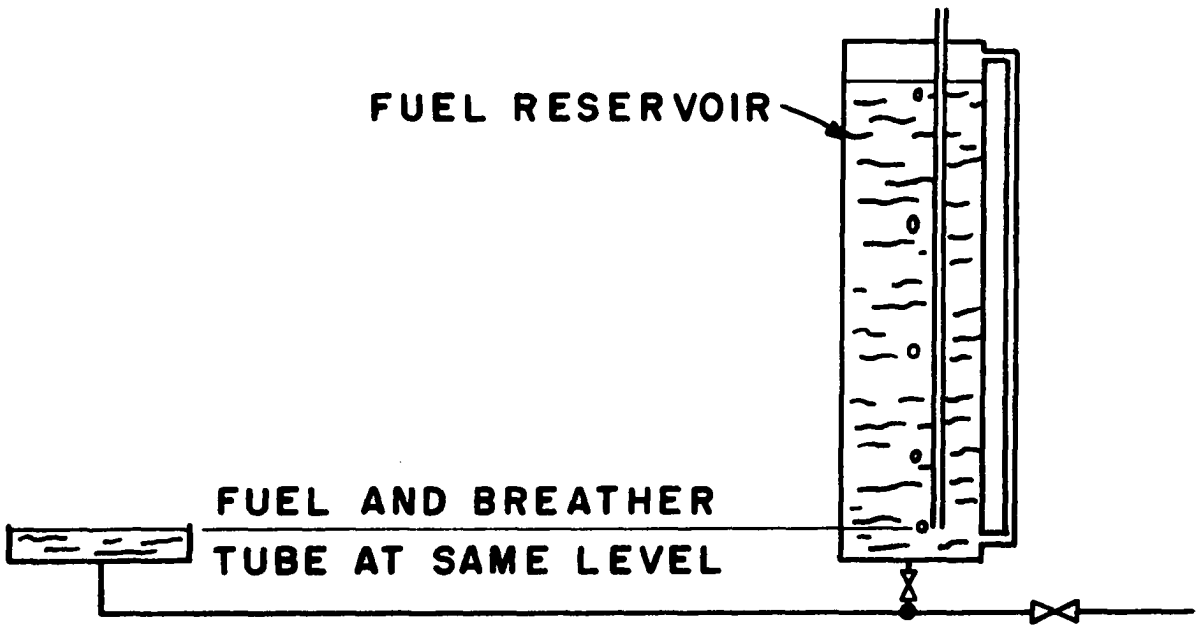

Figure 7 Schematic Diagram of Fuel Level Control System

breather tube allowing the pressure to rise slightly, and more fuel flows out until the liquid heads again balance. When the fuel consumption rate is constant, accurate control can be easily established, and the fuel level is accurately maintained without much attention. Since air is being continuously sucked into the reservoir, no fumes escape into the observation room where the reservoirs are kept, which is desirable from the safety viewpoint.

In order to ensure accurate measurement of fuel consumption over the wide range of fire sizes employed, it was necessary to use several sizes of fuel reservoirs. The four reservoirs which were used measured 2, 4, 6, and 10 inches in diameter. The details of construction of the fuel reservoirs are shown in Figure 8. The four reservoirs were made from thin-walled aluminum tubing, and the breather tubes were stainless steel. Fuel measurement was made by noting the drop in liquid level in a reservoir by means of a sight glass. The reservoir sight glasses were covered by clear acrylic shields to prevent accidental breakage. Each fuel reservoir was calibrated volumetrically using water, and a linear relationship between fuel level in the sight glass and volume of fuel was found for each reservoir. The four reservoirs were hung on the wall of the observation room. They were positioned so that the bottom of the reservoirs would be slightly below the bottom of the burners on the

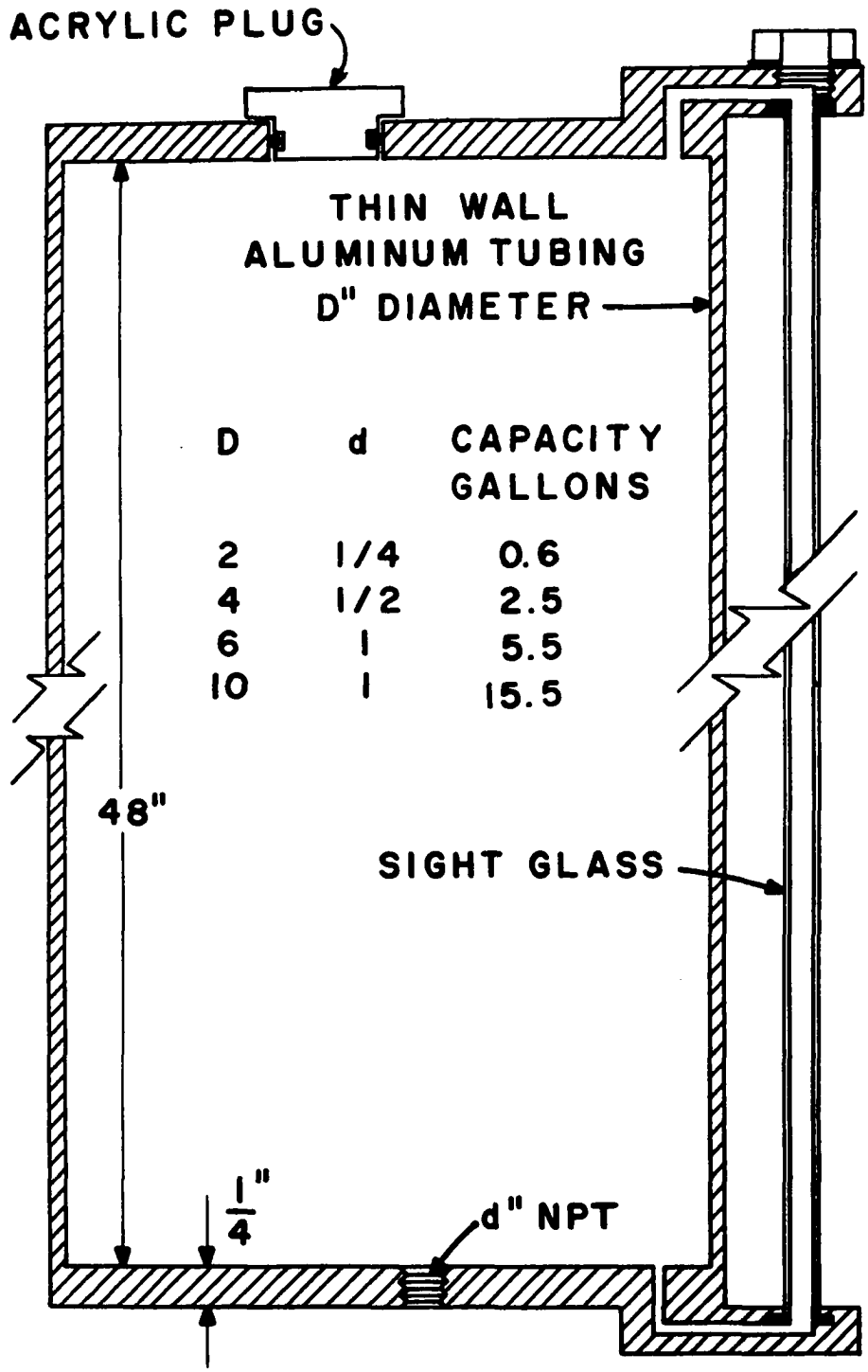

Figure 8. Detail of Fuel Reservoir.

burning table in the static test room. In this way the breather tube of the reservoir was placed so that the fuel level in the burners could be positioned at any level in the burners, or could be kept in the fuel lines slightly below the bottom of the burners.

The fuel reservoirs were connected to the burners on the burning table by a combination of copper lines and polyethylene tubing. These fuel lines were connected so that each of the reservoirs would be completely independent of all the other reservoirs and could be drained separately.

With this arrangement, the center burner was connected to one reservoir, and the peripheral burners were connected to another. The burning rate of the center burner could then be measured separately from the burning rate of the peripheral burners. In the thirteen-burner pattern, a third reservoir was used to measure the burning rate of the four intermediate burners. Copper tubing ran from the valve at the bottom of a reservoir through the wall between the observation room and the static test room, and underneath the burning table. This hard copper tubing was of one-inch diameter for the two larger reservoirs and of ½-inch diameter for the two smaller reservoirs. The end of the copper tubing under the table was connected to a manifold. The manifold consisted of a solid cylindrical block of aluminum in which eight holes had been drilled and tapped around the perimeter. These holes

were connected to a hole drilled and tapped up from the base of the block. Polyethylene lines ran from the manifold to the individual burners. The copper lines were positioned so that both the reservoir and the copper tubing leading to the manifold could be completely drained by gravity flow to a drain valve located on the outside of the building. The test fires could be quickly extinguished by shutting off the valve at the bottom of the reservoir and then draining enough fuel from the lines to empty the burners. All the valves used were brass ball valves with teflon seals and packing.

During a series of tests, the position of the peripheral burners would range from near the burning-table edge to the center of the table as separation distances were varied. Since all of these peripheral burners were to be connected to a single fuel reservoir, flexible fuel lines were necessary to connect the manifold to the individual burners. One-half inch polyethylene tubing was chosen since it was sufficiently flexible and would be little affected by the fuels which were to be burned. The use of polyethylene would appear to have a distinct disadvantage in view of its low melting temperature, yet the use of this tubing was found to be generally satisfactory. Since the polyethylene lines were only used underneath the burning table and the table surface had a two-inch thick layer of insulation,

the temperature under the table rose only slightly above ambient temperature during the larger tests. In addition, cool fuel was continuously flowing through these lines as burning proceeded. The polyethylene lines were connected to the bottoms of the individual burners by means of 6-inch long galvanized pipe nipples.

Soft copper tubing was used for the center burner connection in place of the polyethylene tubing since the center burner was always in the same position.

The fuel was stored in 54 gallon drums in a fenced-in area outside the building. For easy filling of the fuel reservoirs, a copper line was run from the storage area to a reversible, self-priming gear pump in the observation room. Polyethylene tubing was used to connect the storage area end of the copper line to any of the fuel barrels in this area. Another length of polyethylene tubing, which was connected to the pump, could be inserted into a fuel reservoir in the observation room. Fuel could therefore be pumped directly from a storage barrel to a reservoir. If only part of the fuel in a reservoir was consumed during a test, the remaining fuel could be pumped back to its particular storage barrel.

Instrumentation

The instrumentation of the flame interaction and merging tests was designed so that the data could be

taken and any movement of instruments in the test room could be accomplished without having to enter the static test room during a test. As far as possible, instruments were used which provided a continuous recording of the test variables, or at least a direct readout.

The burning rate was monitored by using an electric timer and noting the position of fuel in the reservoir sight glass at various times.

Two asymptotic radiometers were used to measure flame radiation. This type of radiometer was discussed briefly by Stempel and Rall (22). The instrument measures a temperature difference over a finite thickness of material which is so oriented that the heat will pass through the desired path to ensure that the temperature difference measured will be directly proportional to the incident flux. The asymptotic radiometer consists basically of a thin, blackened constantan foil suspended over a cavity in the copper radiometer body. This foil is bonded to the body at the periphery of the cavity. By attaching a fine copper wire to the center of the foil, a differential thermocouple is formed with the hot and cold junctions at the foil center and periphery, respectively. The temperature difference between the center and periphery of the foil is directly proportional to the incident flux over the surface of the foil.

One of the radiometers was used to measure the radiation given off by the flame array to the surroundings. This radiometer had a range up to 3 solar constants (about 0.36 Btu/ft^2-sec) with an output of 0 to 5 millivolts. For extended exposure to radiation, the radiometer had provisions for water-cooling of the radiometer body. The radiometer also had a window over the receiver to prevent convective cooling effects at the receiver foil. This window was made of optically ground and polished quartz. The use of quartz has a slight disadvantage because it absorbs flame radiation at longer wavelengths. The quartz window will not transmit wavelengths longer than about 4 microns; therefore some of the infrared flame radiation is cut off.

The second radiometer was placed next to the center burner, facing upward with the face flush with the burning table surface. This instrument had a range up to about 15 Btu/ft^2-sec with an output of 0 to 10 millivolts. This radiometer was directly exposed to the flame, and for long duration tests or high heat fluxes it could be water cooled and gas purged. A sapphire window was used in this higher-range radiometer. Sapphire is a somewhat better material for use as a radiometer window in flame radiation measurements than quartz, becuase it will transmit slightly longer wavelengths (up to about 5 microns). Each of the two

radiometers was connected to one channel of a two-pen Honeywell recording potentiometer. The output in millivolts was converted to the appropriate heat flux units by means of a calibration curve which was provided with each radiometer.

Measurements of the radiation flux from the entire flame array to the surroundings were taken at various distances from the center of the array. It was assumed that the flame array would radiate symmetrically. Since these readings were taken at steady state conditions, a single radiometer would suffice by changing its position several times during the test. To move the small-range (up to 3 solar constants) radiometer to the desired positions, a V-shaped track was built, and a sled for holding the radiometer was placed in this track. The track was ten feet long and positioned horizontally. The radiometer was placed so that the receiver face was in a vertical plane and facing the flame array. The sled could be moved forward or backward by means of a reversible motor and a system of pulleys and cables. To stop the radiometer sled at the desired positions along the track, several switches were installed on the track. When the sled hit the contact point of a switch, the circuit would be broken and the sled would stop. After a satisfactory reading at each position was obtained, the radiometer could be moved to a new position by closing

the circuit with a button on the control box. This box was located in the observation room.

In order to determine flame heights and the areas of the merging flame columns, photographs were taken of each of the flame arrays. The use of photography is more desirable than visual observation in determining flame height, because the height of the flame fluctuates irregularly for the turbulent fires encountered in the tests. Short-duration time exposures were used, since a photograph with instantaneous exposure might catch the flame in an unusual position. A Speed Graphic press camera was fastened to a tripod head which was attached to two telescoping rails. The rails could be extended to about a 3-foot length. These rails were positioned on the wall of the wind tunnel section just below an opening in the wall between the wind tunnel section and the observation room. This opening (16 x 32 inches) was about 5 feet above the floor and was provided with a sliding glass door. Having been previously positioned on the tripod head and focused, the camera could be loaded with film and cocked while it was against the wind tunnel wall. When the photograph was to be taken, the sliding door was opened, and the loaded camera was pushed out to the full length of the rails. The camera was then in the desired position for taking pictures and the shutter could be tripped by means of a long cable release. The entire

picture-taking process could be performed without leaving the observation room. When not in use, the camera was pushed back against the wall with a piece of asbestos millboard being placed between the camera and the burning table. The asbestos millboard protected the camera from the heat produced by the larger fires. By having the camera positioned in the wind tunnel section, the camera was far enough away from the table that it could see the entire burning table surface as well as the tallest fires encountered in the tests.

Two types of Polaroid film were used to photograph the flames. A very fast film (ASA 3000) was used for the less luminous flames such as methanol, and for some of the smaller acetone fires. A two-second time exposure was used for all of the photographs with the camera set at f/32. This long film exposure made the use of a slower speed film (ASA 400) necessary for the larger, more luminous fires. A Polaroid film was also used which permitted both a positive and a negative copy to be taken. Before the present merging tests were conducted, the positive-negative film was used to photograph a grid positioned over the burning table. After processing, the negative was used as a template for measuring the sizes of the photographed flames. The grid was 8 feet square and was painted black with white lines running horizontally and vertically every inch. The position of the flames to

be photographed would vary from the perimeter of the burning table to the center, but the camera position would be fixed. The grid was therefore positioned vertically at several places over the table in order to account for the distortion in the photographed flame sizes with depth. The camera position for photographing the grid was the same as that used in the actual tests. The grid was placed at the end of the table nearest the camera, half way between the near end and the table center, at the table center, half way between the center and the end farthest from the camera, and at the farthest end of the table. By use of these negatives, the sizes of the photographed flames at any position on the table could be measured.

Several photographs of the interacting flames were taken with a Polaroid Model 180 camera. These pictures were taken with the camera being hand held at a distance of about 4 feet from a particular flame. These photographs were used in studying the flame trailing effect. In addition to the still photographs, a small amount of moving pictures was taken of several of the merged fire columns.

The velocity of air entrained into the burning array was measured in a number of the tests by placing an Alnor Type 8500 Thermoanemometer just outside one of the peripheral burners of the array. This anemometer

differs from the usual hot-wire anemometer in that it uses a thermocouple-type readout instead of a constant current probe. The anemometer basically consists of a piece of fine wire connected to two supports. The supports supply electrical current to the fine wire, which is heated to about 350°F in calm surroundings. As the air flow across the wire increases, the wire's temperature decreases. A fine thermocouple junction at the center of the wire measures the wire's temperature, and the resultant reading is shown on a scale calibrated to read the air velocity in feet per minute. The fine cross wire and the thermocouple wires are 0.002 inches in diameter and provide rapid response. In addition, the thermocouple has a built-in reference junction which is also exposed to the air stream in order to compensate for differences in readings due to varying air temperatures. The accuracy of the instrument is stated to be ± 2 ft/min or ± 3 per cent of the indicated value, whichever is larger. The range is 10 to 2000 ft/min with two range scales. Since it is a hot-wire device, the anemometer is calibrated under conditions of known mass flow; therefore a correction must be applied for air densities other than 0.075 lb/ft^3. The instrument had a 2-foot long probe and a power cord 25 feet long. With this length of cord, the indicator box for the anemometer could be positioned in the observation room.

An optical pyrometer was used to measure the flame brightness temperature of the fire arrays from the various fuels. With an optical pyrometer, the unaided eye of the observer is used to match the brightness of one source of light against that of another. A red filter is interposed between the object and the eye to increase the accuracy of the brightness comparison, since red rays have a wavelength of maximum sensitivity to the eye. The instrument is sighted on the object under study, and the light from the hot body is matched optically in the pyrometer with that received from a constant comparison lamp in the instrument. When the two light sources are matched, the temperature of the object can be read directly from a scale located on the instrument. The accuracy of the pyrometer used was given to be ½% of the temperature being measured. The pyrometer was not entirely satisfactory for the present work due to the difficulty of sighting the instrument on a turbulent fire. In addition, radiation corrections must be made for the measurement on the flame, because the pyrometer is calibrated to give temperatures by assuming that the object under study radiates as a black body. To make the correction, it would be necessary to know the emissivity (ratio of the radiant energy emitted by a heated body to that emitted by a black body) of the flame being studied at the wavelength of the red radiation (0.65 micron) allowed to pass through the monochromatic pyrometer filter. The optical pyrometer could

not be used to study the nonluminous methanol flames.

A grid network of thermocouples was used to measure the temperature of the hot gases over the flame array. Fine nichrome wires were strung in a parallel manner along the bottom of the hood suspended from the ceiling of the static test room. These wires, which were about 10 feet above the test room floor, were spring loaded at each end to support the thermocouples. The thermocouples were attached to these wires at various points over the burning table. A diagram of the thermocouple placement is shown in Figure 9.

Two types of thermocouples were used. Iron-constantan thermocouples were used around the outer portion of the burning table for reading temperatures up to 400°F, and Chromel-Alumel thermocouples, which were available for temperatures up to 1500°F, were used over the center of the table. The hot junctions were made by twisting the wires together and welding them with an oxy-acetylene torch. The temperatures were recorded on two 12-point multipoint recorders, one of which was calibrated for use with iron-constantan thermocouples and the other for Chromel-Alumel thermocouples. In order to make reliable temperature measurements, it was necessary to shield the thermocouples from the flame radiation. The shield design used is shown in Figure 10. The shield was made from thin-walled brass tubing

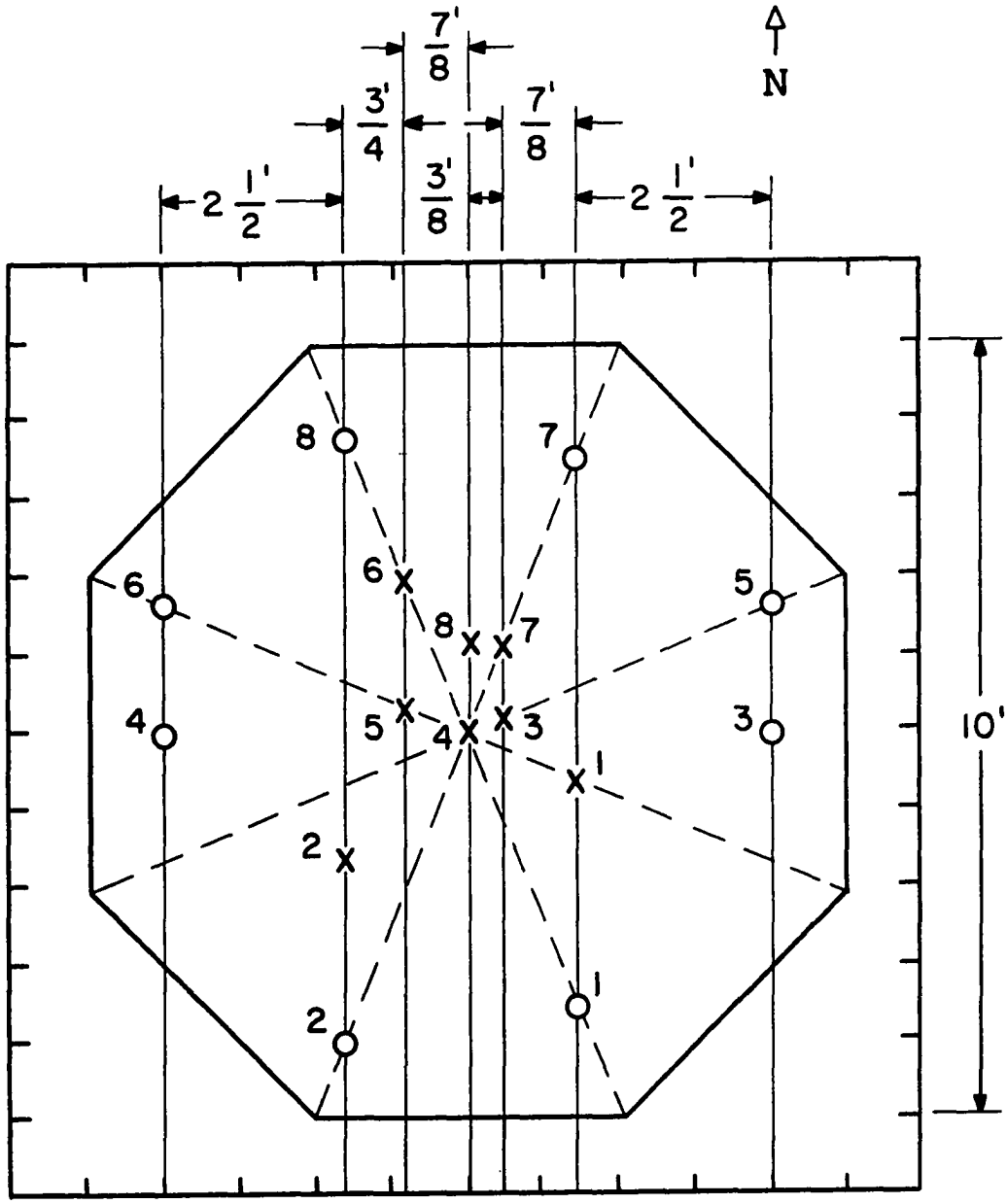

Figure 9. Location of Thermocouples Over Burning Table.

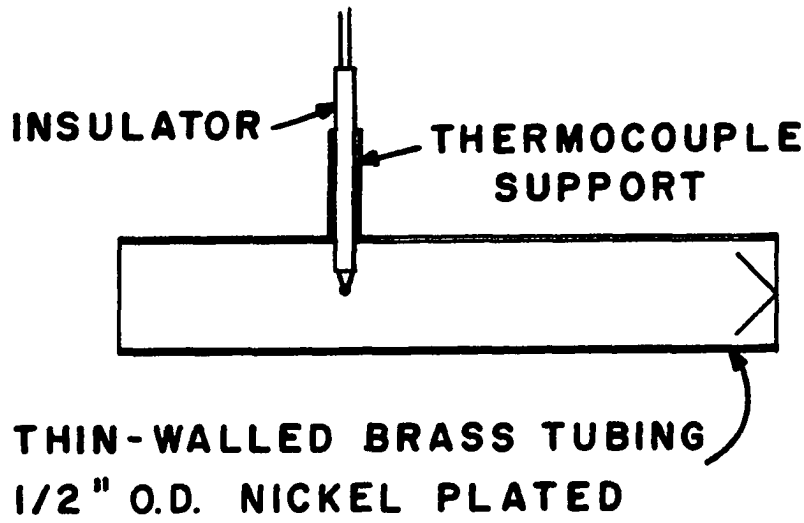

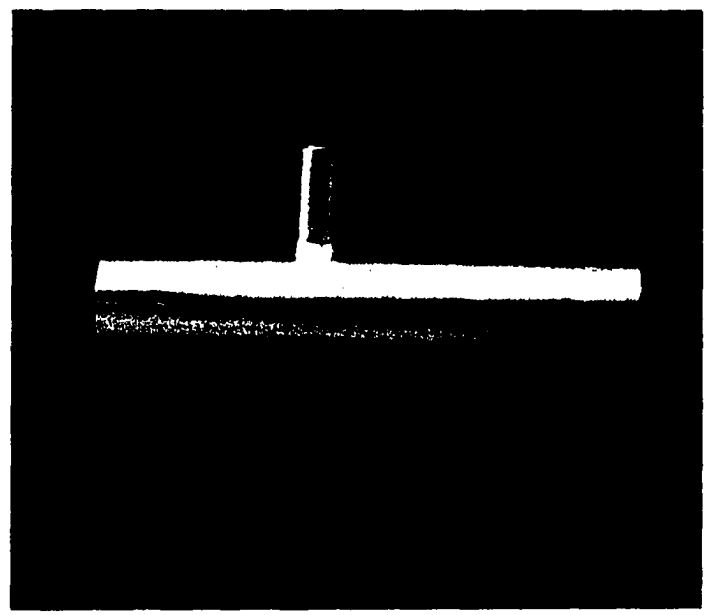

Figure 10. Thermocouple Shield.

and had a cone-shaped copper shield placed in the tubing near the entrance. The thermocouple was inserted through a smaller diameter tube on the side of the thermocouple shield. Contact between the tube and the thermocouple wires was avoided by means of a ceramic insulator. The thermocouple was located so that the hot junction would be perpendicular to the air flow through the shield tube and would be shielded from direct flame radiation by the cone in the nose of the tube. The shields were plated with a bright nickel coating so that they would reflect as much radiation as possible.

Fuel Selection

Five fuels were selected for use in the flame interaction and merging studies; these were methanol, acetone, normal hexane, cyclohexane, and benzene. These fuels can be obtained in a reasonably pure state and at a moderate cost. This selection of fuels gives a sufficiently wide variation in heat output, burning rate, chemical type, and amount of expected flame radiation. Methanol burns slowly with a low heat of combustion, and its flames are a pale blue, resulting in low radiative transfer. Acetone burns with a bright flame but with no smoke, a somewhat higher heat of combustion, and medium radiative output. Cyclohexane and normal hexane both burn with a smoky flame and

high heat of combustion. Both also have a high radiative output. The benzene flame is optically more dense than that of the other fuels selected and has a high radiative heat output.

CHAPTER IV

EXPERIMENTAL PROCEDURE

A brief explanation of the experimental procedure used in the flame interaction and merging studies is provided in the following pages. Some of the problems encountered during the tests are also discussed.

Exposed-Rim Burner Tests

Both circular and square burners were used in the exposed-rim burner tests. The circular burners were used in the nine-burner circular pattern described previously. The square burners were arranged in a nine-burner square pattern, as sketched in Figure 16, which consisted of eight burners arranged symmetrically around the perimeter of the square and one burner in the center of the square. Burning of the fuel in the exposed-rim burners was done under unsteady-state conditions. The fuel containers, having a depth of one inch, were filled flush full with fuel, ignited, and allowed to burn until all the fuel was consumed.

The tests using the circular, exposed-rim burners with diameters of 1¼, 2 1/16, and 2 9/16 inches were

conducted on the previously mentioned apparatus which employed a burning platform located at the end of a long lever arm. Due to the limitations of the apparatus, only burning rate data were taken for these tests.

The tests using the 4 3/16-inch diameter circular burners and the 3 x 3-inch square burners were conducted on the previously described burning table which made use of strain gages to measure the weight loss of fuel. Both the burning rates and radiation flux to the surroundings from these fires were measured. In addition, some photographs of the flames were taken.

Rimless Burner Tests

Most of the rimless burner tests were conducted by varying only the position of the peripheral burners. One particular fuel was used, and the size and number of burners was the same throughout a series of tests. A typical series of tests began by positioning the peripheral burners far enough apart for interaction-free burning to be obtained. In succeeding tests, the separation distance between the peripheral burners and the center burner was decreased until the burners were finally very close together. Two burner patterns were used for the rimless burner tests (the nine-burner and the thirteen-burner patterns described previously). All the burners used for a particular test were always of the same size.

For the rimless burner tests with n-hexane, cyclohexane, and benzene, a slightly different procedure was followed at the small burner separation distances. In these tests, a large sheet of insulation was used which had holes cut for a particular arrangement of the burners; therefore, a different sheet was used for each position of the burners. As mentioned previously, this insulation sheet was necessary to prevent fuel vapors from penetrating beneath the table. The various fuels were used at a particular burner separation distance before that position was changed, due to the inconvenience of changing the burner positions with the insulation sheet arrangement.

The sizes of fuel reservoirs selected for a particular test depended on the size and number of burners to be used, as well as the fuel to be burned. The separation distance between the burners was also a factor in the reservoir selection. The separation distance greatly affects the burning rate, as will be discussed later. One of the reservoirs was used to supply fuel to the center burner, and a larger reservoir was used with the eight peripheral burners. With the thirteen-burner pattern, the four intermediate burners were supplied by a third reservoir.

An experimental test started with the positioning of the fuel burners. If a new set of burners was being

used, these burners were screwed onto the pipe nipples which were attached to the ends of the polyethylene fuel lines. The burners were set on the rails of the burning table framework at the desired separation distance from the center burner. The insulation blocks were then placed in front of and behind the burners in order to provide a continuous surface around the burner array. When one of the large insulation sheets was used, the sheet was positioned so that the burner rims would fit snugly in the holes provided in the sheet. The radiometer at the center of the burning table was pushed up from underneath the table through a hole provided in the insulation. The radiometer face was positioned flush with the top of the insulation surface. The hole for the radiometer was in the insulation block which fitted around the center burner. The center of the hole was one inch from the edge of the center burner rim. It was necessary to remove the center radiometer when changing burner sizes, since different insulation blocks had to be used to fit around the various sizes of center burners. When burner sizes were not being changed, the position of this radiometer was left unchanged.

With the burners positioned, the fuel lines connected, and the insulation in place, the fuel reservoirs were ready to be filled with fuel. The end of the polyethylene fuel supply line in the outside storage area was connected to a fuel barrel. The other end of the

line in the observation room was placed in the proper fuel reservoir, and the pump was started. If a new fuel was being used, the reservoirs and fuel lines would be rinsed with the new fuel before the reservoirs were filled. After the reservoirs were filled, the reservoir breather tubes were positioned at the proper depth and the burners were slowly filled. The center burner fuel line was sloped so that air bubbles could not collect in the line when it was being filled with fuel. The range of peripheral burner positions made necessary the use of flexible polyethylene fuel lines from the manifold to the burners. At burner positions close to the table center, these flexible lines were coiled on the floor under the table. During the initial filling, air bubbles became trapped in these lines, stopping the flow of fuel into the burners. In this case it was necessary to go under the table to raise the lines until the bubbles rose and were dispelled into the burners. After these lines were initially filled with fuel, no further trouble with air bubbles was experienced. The flexible fuel lines under the table were always checked for entrapment of air after the burners were filled and prior to ignition of the fuel. In addition, all the fuel lines were closely monitored for leaks.

A thermometer was also positioned outside the building in order to obtain the ambient air temperature at the time of the test.

The burners were filled as nearly flush full with fuel as possible, with the fuel level usually being about 1/8 inch below the burner rim. Since all of the eight peripheral burners were connected to the same reservoir, it was necessary for all these burners to be at the same height in relation to the bottom of the reservoir breather tube. The rails on which the burners rested were connected to the framework so that the burners would be at the same height; therefore, all of the peripheral burners could be filled with fuel to the same depth.

After the fuel level in the burners rose to the desired height, the level in the fuel reservoir sight glass became stationary. The sight glass levels of the reservoirs used for the tests were watched closely for several minutes after they had become stationary to check for air leaks in the reservoirs. If a small air leak had developed in a reservoir, the level in the reservoir would continue to drop very slowly, eventually overflowing the burners. While the sight glass levels were being monitored, the radiometer which was located on the track was brought into position. The radiometer was first positioned at the end of the track nearest the burning table edge. The position was changed several times during the test, with the radiometer being moved farther away from the fire each time. The anemometer was placed on the burning table at a position 6 inches above the

table and 12 inches out from the edge of one of the peripheral burners. The anemometer readings were always obtained with the anemometer located on the same side of the burning table. A test tube stand and a clamp were used to hold the anemometer probe. The cooling water was then turned on for both the track radiometer and the center radiometer. In addition the nitrogen, which was used as a gas purge for the center radiometer, was turned on. The gas purge for this radiometer was supposed to keep condensed moisture and soot off the radiometer window, since the window was in direct contact with the flame. The nitrogen flow rate across the radiometer window was kept rather low to avoid disturbing the flame column.

After having observed that the sight glass levels were still stationary, the fires were ignited by means of a match at the end of a holder 3 feet in length. The fires were ignited one at a time, but as quickly as possible. Since the fires had to burn for several minutes to reach a steady state fuel consumption rate, it was not necessary that all the fires be ignited simultaneously. After the fires were ignited, the chart paper drive was started for the two-pen recorder (connected to the two radiometers) and the two multipoint recorders (connected to the thermocouples over the burning table). The amplifiers for these three recorders were always left on unless the tests were to be discontinued for a

day or more. The recorder for the radiometers was zeroed prior to the fuel ignition. The calibration of this radiometer recorder was checked periodically during the course of the series of tests to make sure that the calibration had not changed. The timer was started as soon as the fuel was ignited, and the exhaust fan in the ceiling of the static test room was turned on. The camera was then loaded with film and cocked.

Several minutes were required for the burning rates to become constant so that a steady reading could be obtained for the radiometers. The length of this initial burning period depended on the fuel, burner size, and burner location. Reservoir sight glass levels were usually recorded every three minutes throughout the test. This time interval was varied somewhat for the different tests, depending on the magnitude of the drop rate in the sight glass fuel level. It was observed that the center radiometer (which had a fast response time) reached its steady reading about the time that the burning rate became steady. The radiometer on the track was considerably slower in reaching its steady value since this radiometer had a rather slow response time (on the order of several minutes).

When the track radiometer had obtained a steady output on the recorder chart, the fire was considered to have reached steady state. An anemometer reading

was usually taken at this time. The camera holder was then pushed out to the full length of its rails, and a picture was taken. The camera was pulled back, and the film was removed from the camera and processed. The immediate processing of the film was done to ensure that a good photograph had been taken. After taking the picture, the track radiometer was moved to its second position, which was located at about the middle of the track length. The reading from the track radiometer gradually decreased after the radiometer was brought into its new, more distant position from the fire, and the value of the reading leveled off after a few minutes. For some of the tests, a picture was taken of the flame trailing effect from one of the peripheral burners. To take this close-up shot, a camera was taken into the static test room and hand held for the shot. This photograph was also immediately processed. Optical pyrometer readings of the fires were also taken for many of the tests. The pyrometer was taken into the static test room after the fire reached the steady state condition, and a pyrometer reading was obtained. After a steady reading was obtained at the second position, the track radiometer was moved back to the third track position. This third radiometer position, which was not used for the smallest fires, was located at the end of the track farthest from the burning table. After a steady reading had been obtained at the third

position, the fires were extinguished. For the largest fires, the burning rates and radiometer readings came to steady values very quickly so that these large fires were usually not burned longer than 15 minutes.

In order to extinguish the fires, the valves at the bottom of the reservoirs were shut off. Then the outside drain valves were opened and fuel was allowed to drain from the lines into a container. Enough fuel was allowed to drain to lower the fuel level down into the fuel lines below the burners, causing the fires to recede greatly, although they continued to burn for about a minute after the fuel level was lowered. The bottom of a fuel burner was not sloped toward the center hole; therefore a very slight amount of fuel would not drain and would be left in the bottom of the burner. The outside door to the static test room was opened after the fires were extinguished in order to help clear the room of any smoke.

Several problems were encountered in the course of the experimental tests. During several of the tests, part of the fuel vapor evolving from the burners would seep down into cracks in the insulation between the burners before it would ignite. These cracks were present where the insulation blocks fitted together. This trouble was encountered during the hexane tests at small separation distances where the fires were merging. As mentioned previously, this seepage of vapor was the cause

of an accidental fire encountered during one of the tests. Vapor accumulated in the insulation and apparently was burning on the underside of the insulation surrounding some of the burners. At least one of the polyethylene fuel lines was heated enough to melt, and fuel was spilled under the table. This fuel ignited, melting the rest of the polyethylene lines. When this spillage occurred, the fuel level in the reservoir sight glass started to drop rapidly. The valve at the bottom of the reservoir was immediately shut off, and the fire under the table was quickly extinguished by means of a dry-chemical fire extinguisher. Except for melting the polyethylene fuel lines, little damage was done to the apparatus by this fire. The previously-mentioned large insulation sheet was used in all subsequent tests to prevent an accumulation of burning vapor under the table, and no further trouble of this kind was encountered. Only a few tests using hexane had been made prior to the accidental fire. These hexane tests were subsequently run again with the new insulation setup. There was a possibility that vapor had been burning within the insulation layers during these tests, although this burning had been detected in only one test immediately preceding the accidental fire.

Several times during the course of the tests, difficulty was encountered with air leaks in the fuel

reservoirs. As noted previously, these leaks would prevent a slight vacuum from forming above the fuel in the reservoir, and fuel would continue to flow into the burners, causing these burners to overflow. These air leaks were always detected before the fuel in the burners had been ignited because the fuel level in the burners was allowed to stabilize before it was ignited. The trouble was traced to the gaskets above and below the sight glasses. These gaskets apparently became brittle due to contact with the fuel vapor. After these gaskets were replaced, the trouble was eliminated for several weeks.

Spring-loaded shutters were located near the floor of the static test room to provide incoming air for the fires. There was one set of shutters located at the bottom of each of the three walls of the test room, and one set in the adjoining wind tunnel test section. On days when the outside wind was gusty, some of these air-inlet shutters would often have to be sealed to prevent stray air currents from disturbing the flames. Nevertheless, on several of the windiest days, stray air currents disturbed the flames to such an extent that the tests had to be discontinued until calmer wind conditions prevailed. To seal off the part of the wind tunnel section behind the camera location, plastic sheeting was stretched across the tunnel section and taped to the sides. This sheeting worked fairly well,

but the tape had a tendency to pull loose, and it had to be checked each day.

A more serious problem was encountered with the larger, smokier fires due to the limited size of the static test room and the inadequate ventilation system. For several of the very largest merging fires encountered, the tips of the flames would almost touch the concrete beams located across the ceiling of the test room. The smoke and combustion gases were vented to a series of shutters located around a hood in the ceiling of the test room. The shutters in the ceiling were spring loaded and were supposed to allow smoke to escape from the room while being closed to outside winds. This shutter arrangement was designed primarily for the wind tunnel tests in which air was forced through the wind tunnel and the adjoining static test room by means of a large blower located upwind of the wind tunnel section. An exhaust fan was also located in the ceiling vent in the static test room to help exhaust the smoke during tests under calm conditions. The use of the exhaust fan did not tend to disturb the fires, but the fan did not pull enough air out of the static test room to dispel the accumulation of smoke in the room during the more smoky fires. The buildup of smoke proved to be so bad for the benzene fires using 4-inch diameter burners, that the tests for benzene with the 4- and 6-inch diameter burners had to

be discontinued. For some of the large hexane and cyclohexane fires, as well as some of the small benzene fires, the readings obtained with the track radiometer would start to decrease even though the radiometer position had not been changed. This decrease in detected radiation flux to the surroundings was caused by the accumulation of smoke and combustion gases in the room during the latter part of the test. This smoke buildup also caused difficulty in obtaining good pictures of some of the fires.

CHAPTER V

DISCUSSION OF THE RESULTS

In the present investigation, emphasis was placed on correlating the burning rate data of the interacting and merging fires in such a manner that this data could be used to predict the behavior of multiple fires in situations involving other liquid fuels, and other sizes of fuel sources. Since the burning rate of the liquid fuels is closely associated with the heat feedback from the flame, the radiative heat feedback from the flame to the fuel was studied. The radiative heat flux given off to the surroundings is greatly affected by the merging of the separate fuel sources; therefore, this effect was also investigated. Additional data such as the brightness temperature of the fires and the temperature of the convective columns over the fires were also taken during the tests. Although some of this additional data was insufficient to lend itself to adequate correlation, it assisted in evaluating the experimental techniques and equipment.

A number of burner sizes and burner arrangement patterns were studied in the tests. In addition, different numbers of burners and various fuels were used. The effect of exposing the burner walls to radiation from adjacent fires was also

investigated by studying fires burning in both exposed-rim and rimless burners. The interacting or merging fires from the burner arrays ranged from the small, laminar flames of methanol in nine, 1¼-inch diameter burners to large, highly turbulent fires from burning cyclohexane using nine, 6-inch diameter burners.

For both exposed-rim and rimless burners, the separation distance between the peripheral burners and the center burner was varied for the different tests while keeping the same shape of burner pattern. A test consisted of burning a particular fuel in an array of burners of a particular size, with the burners being placed a certain distance apart.

Some qualitative observations of the flame interaction and merging phenomena will be given in the following pages. The comments generally apply to both the exposed-rim and rimless burner tests unless otherwise noted. These observations are followed by a presentation of the results of the present studies and the correlations developed during the studies.

Qualitative Observations

The present interaction and merging studies showed rather dramatically the effects that the merging of a number of small fires into one fire column can have on the burning rate, flame height, and heat given off to the surroundings. Since the largest single burner size employed in the tests was 6 inches in diameter, the flames from the individual burners were never over about 30 inches in height when the burners

were spaced far enough apart that the individual fires had little or no effect upon one another. Yet, when nine of the same 6-inch burners were spaced close enough together that the individual fires merged, fire columns as large as 2 feet in diameter and about 9 feet high were obtained from certain fuels. Figure 11 shows three photographs of interacting n-hexane fires from nine rimless 4-inch diameter burners. In the first photograph tilting of the flames is observed; in the second the fires are interacting but have not yet merged; and in the third the flames have merged and the heat feedback to the fuel has been reinforced to the extent that the flame column is approximately 81 inches high.

For the rimless burner tests conducted on the large burning table, all the individual fires were observed to behave in approximately the same manner when the peripheral burners were positioned close to the edge of the table. At this large burner spacing, the fires would exhibit little or no interaction effects upon one another, although flames from some of the largest size burners could not be spaced far enough apart on the table to prevent the peripheral flames from leaning slightly in toward the middle of the burner array. This leaning was due to air entrainment into the fire array.

As the burner separation distance was decreased, the peripheral flames would begin to lean more toward the center of the array. As noted by Thomas, Baldwin, and Heselden (26)

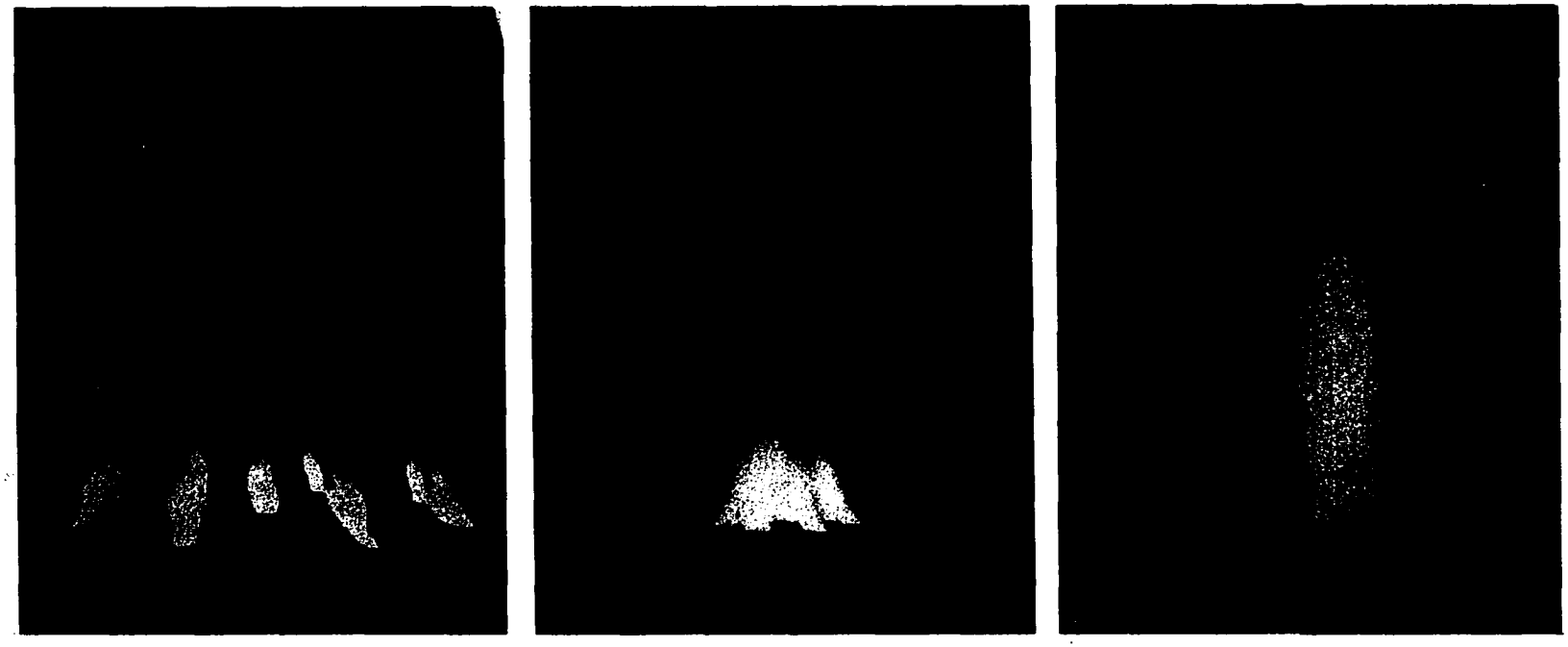

Individual Fires Interacting Fires Merged Fires

Figure 11. Test Fires Burning on Flame Merging Table (For n-Hexane in nine, 4-inch diameter burners).

in their flame merging studies, a column of hot rising gases entrains air from its surroundings, so that when several flames are placed in the neighborhood of one another, the resulting restriction of air flow causes a slight pressure drop in the space between the flames. This pressure drop causes air flow toward the low pressure space, deflecting the flames from the vertical. Measurements by Strasser and Grumer (23) of static pressures between proximate wood fires showed pressure depressions that reached a few hundredths of a millimeter of water. In most instances the air entrainment for the present merging studies was approximately symmetrical with respect to the fire array, causing the flames to lean toward the center to about the same degree.

Particularly with fuels such as cyclohexane, the center flame was often observed to move slightly off its burner, first to one side and then another for burner spacings at which little interaction between the fires occurred. For the rimless burner tests, this movement was generally caused by fuel vapors moving horizontally across the table surface for an inch or more before finally being consumed with a resulting disturbance in the main flame. As the cool air being entrained into the outer edge of the fire array moved through the spaces between the peripheral burners, it was heated by the fires from the peripheral burners and consequently began to rise. The air turbulence resulting from this heating also contributed to the slightly unstable nature of the center flame

at the intermediate burner spacings.

At these intermediate burner spacings, where the fires were beginning to interact but had not yet begun to merge, the peripheral flames were observed to exhibit a trailing effect as they leaned in toward the center of the table. This effect was noted particularly for n-hexane, cyclohexane, and benzene, although acetone showed trailing to a certain extent. As mentioned previously, this trailing effect was noted by Welker (28) in his studies of the effect of wind on liquid-fueled fires. The trailing effect seems to be caused by the density of the fuel vapor at the fuel boiling point being higher than that of the surrounding air; therefore, the vapor tends to layer until it has been heated. Due to the air entrainment toward the fire array, this vapor from the peripheral burners started moving toward the center of the array, in some cases for 6 inches or more, as it began to ignite. The trailing effect was noted both for the exposed-rim and rimless burners. The flame trailing was less noticeable for the exposed-rim burners, however, since the entire burner was above the table surface. For the exposed-rim burners the fuel vapor layering over the edge of the burner was apparently heated sufficiently in its travel down the outside of the hot burner wall to become buoyant before it could travel very far over the burning table surface. A photograph of the flame trailing effect is given in Figure 83 and this effect is discussed further in the following pages.

As the burners were moved still closer together, a spacing was reached at which the individual flames approached the onset of merging. As this critical spacing was approached closely, the individual flames could still be discerned, although they were just about to touch. The entrainment of air to the peripheral flames at this burner spacing was restricted mainly to the side of these flames facing the outside of the array, and the air flow into the center burner was restricted to an even greater extent. Less air could be entrained into the lower portion of one of these interacting flames than when no other flames were present. The height of these multiple flames therefore had to increase to entrain as much air as when the entrainment restriction was not present. The flame height then increased still further due to the increased heat feedback to the fuel at these close burner spacings. This increased heat feedback resulted in a greater fuel vaporization rate and therefore a larger flame.

When the spacing was reached that the onset of merging occurred, the individual flames began to merge into one large flame column. At this spacing, the air flow to both the peripheral burners and the center burner was restricted to a greater extent than at the slightly larger burner spacings. This greater restriction of air entrainment, as well as the more greatly reinforced heat feedback to the fuel, caused the height of the fire column to be greatly increased. These merged fire columns, particularly at spacings for which the

individual fires were just starting to become fully merged, were much more stable than a fire produced from a single large burner of fuel surface area comparable to that of the combined small multiple burners.

When the burner separation distance was decreased further, the flames became fully merged into a single fire column. At these very close burner spacings, the center burner was entirely surrounded by the merged flames from the peripheral burners so that sufficient air could not be entrained to maintain the fuel consumption rate of the center burner at its former peak level, although some air could probably be swept to the center of the lower portion of the merged fire column due to the highly turbulent nature of the fire. For some of the merged rimless-burner fires, a blanket of unburned fuel vapor formed over the center portion of the burner array surface. Apparently, the heat feedback from the surrounding fire caused the fuel in the center burner to vaporize at a faster rate than it could be burned.

Waterman, et al. (27) burned several individual fires indoors using a single 30-inch width square burner and JP-4 as fuel. He observed that the fire column was unstable, with fuel vapors moving horizontally across the floor for some distance before finally being consumed with a resulting disturbance in the main flame column. In a few of the present tests, the fires, when fully merged, tended to act in a manner similar to the single-container fire burned by Waterman.

Particularly for some of the largest, fully merged cyclohexane fires, part of the base of the fire column spread out several inches on the outside of the burner array, first to one side and then another.

Exposed-Rim Burner Tests

Hottel (12), in his review of work done by Blinov and Khudiakov, postulated that the conduction of heat through the burner walls was a significant mode of heat feedback for small-sized single burners containing burning liquid. To show that the effect of heat conduction through the burner walls was also significant for small-sized multiple burners with exposed rims, tests with both exposed-rim and rimless burners were conducted in the present studies of flame interaction and merging.

Circular burners of four sizes and square burners of 3-inch width were used in the exposed-rim burner tests. The circular burners, 1¼, 2 1/16, 2 9/16, and 4 3/16 inches in diameter, were used in the nine-burner circular pattern described previously. The square burners were arranged in a nine burner square pattern shown in Figure 16. A total of 162 tests were conducted with the exposed-rim burners.

The tests conducted with the exposed-rim burners were of a preliminary nature in that the variables involved were in some cases less well controlled than in the later tests with rimless burners. Burning of the fuel in these exposed-rim burners was done under unsteady-state conditions. The

fuel containers were filled flush full with fuel, ignited, and allowed to burn until all the fuel was consumed. Since pans approximately 4 inches or less in diameter were used in these preliminary tests, the total burning time of fuels such as benzene was only about 3 minutes in some cases. Although the total burning times for some of the fuels were rather short, a period of steady fuel consumption rate was always observed after the fuel had burned long enough to be heated to boiling. This steady fuel consumption rate was the value taken to represent the steady state burning rate of the fuel.

Methanol and acetone were the only fuels burned in the three smaller sizes of circular, exposed-rim burners. These particular tests were conducted on the previously mentioned apparatus which employed a burning platform located at the end of a long lever arm. A typical weight loss (or burning rate) curve as a function of time as obtained from the recorder is shown in Figure 12. The top of the S-shaped curve in Figure 12 represents the warmup period of the fuel prior to the period of steady fuel consumption rate. The value of the slope of the constant-slope portion of the weight loss curve was taken to be the burning rate of the fuel for the test. At the bottom of the curve, the weight loss rate declines as the fuel is eventually consumed. The experimental results recorded in Table 1 are plotted in Figure 13 as the average burning rate of all nine burners

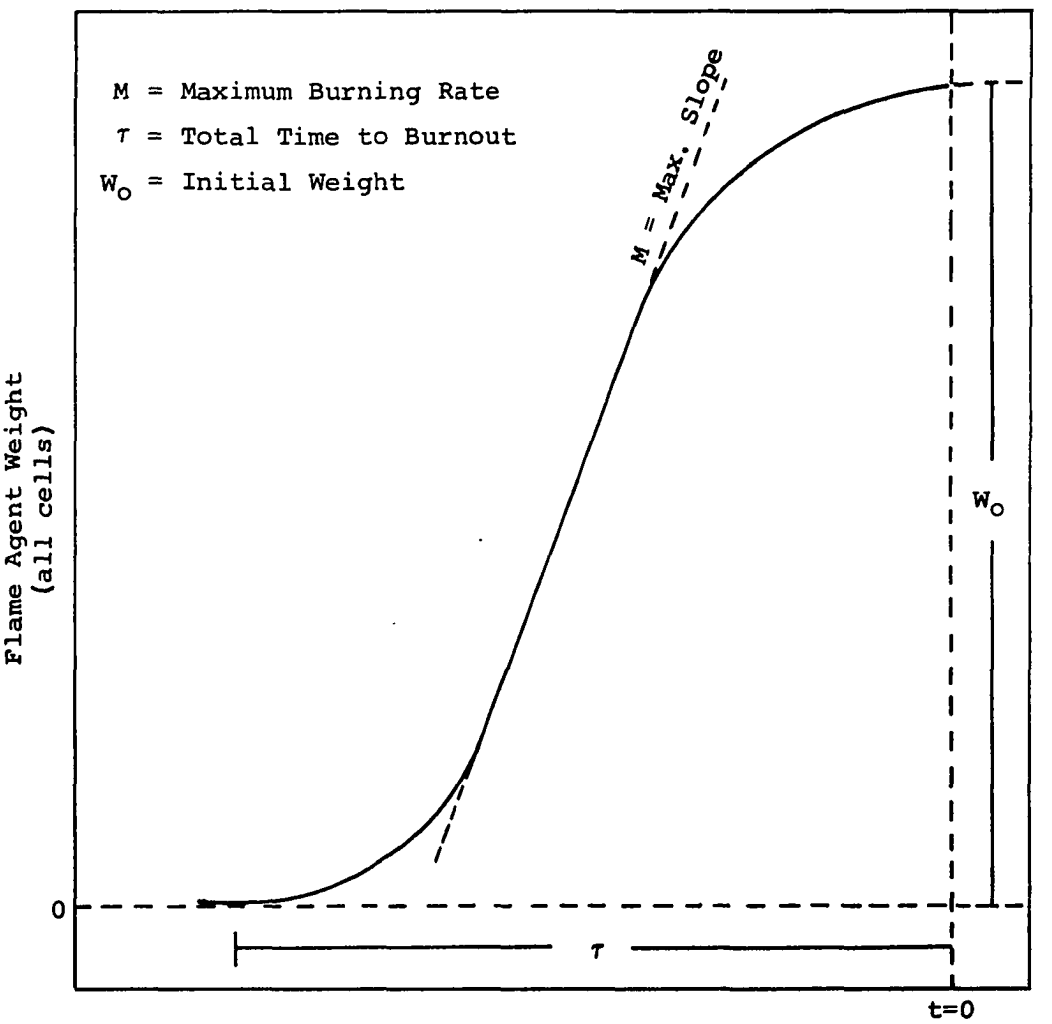

Figure 12. Typical Burning Rate Curve for Merging Flames Using Exposed-Rim Burners.

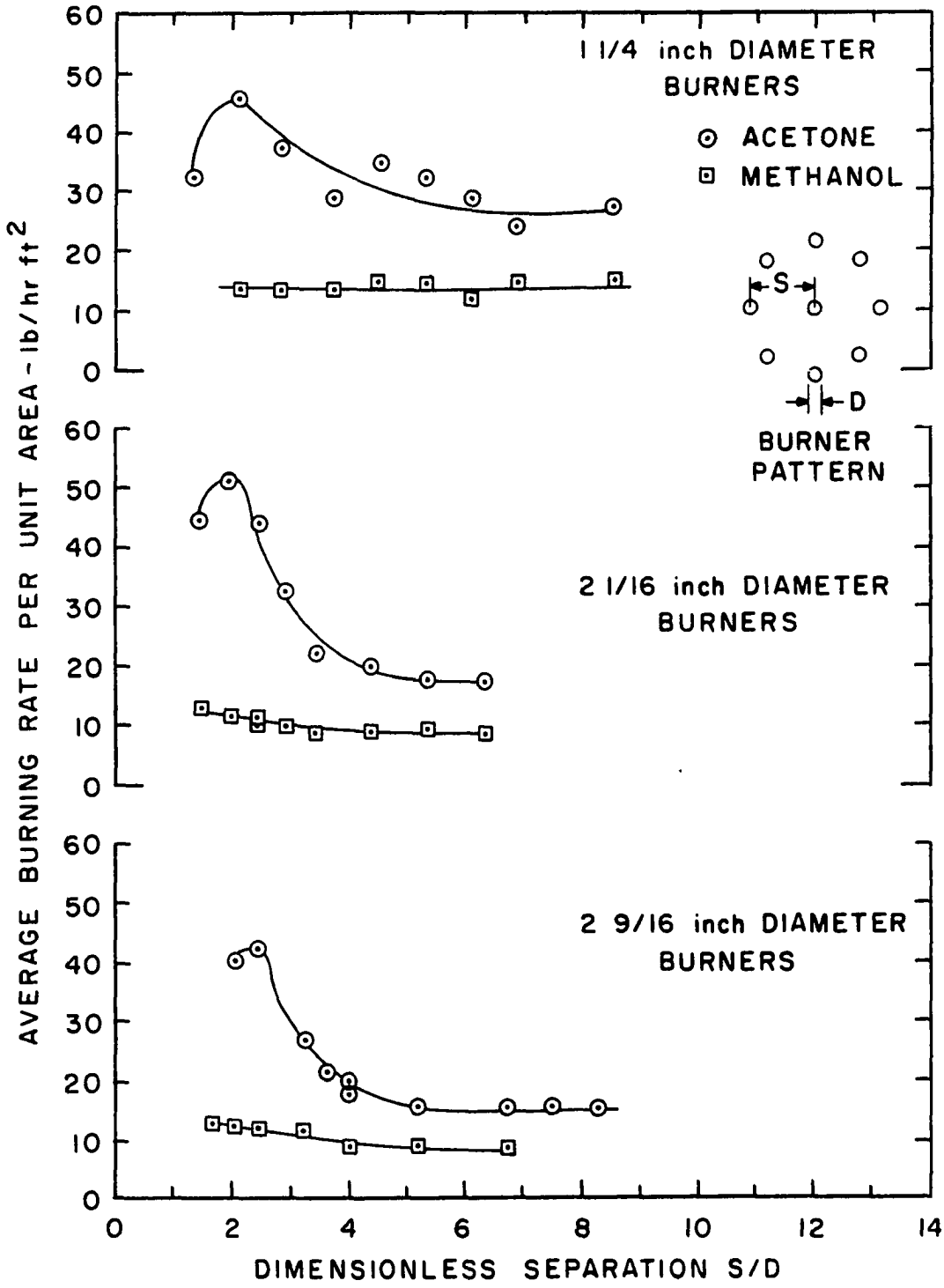

Figure 13. Flame Merging Burning Rate Data (Circular Exposed-Rim Burners).

in lb/hr-ft^2 versus the dimensionless separation distance. The dimensionless separation distance (S/D) is the ratio of the distance between the centers of the center burner and one of the peripheral burners to the diameter of a burner. From the burning rate curve of Figure 13 it is seen that the burning rates for methanol are hardly changed as the burners are brought very close together. For the small, laminar methanol flames, no merging was ever observed. The burning rate curves for acetone fires in the 1¼-, 2 1/16-, and 2 9/16-inch diameter burners are seen to have a peak at the smaller separation distances. Similar peaks were observed for the burning rate curves of the 4 3/16-inch burners, as will be discussed below. For the acetone tests, the flames were observed to begin to merge at very small separation distances. This merging caused an increase in the height of the fire column above the burners.

The tests using the 4 3/16-inch diameter circular burners and the 3 by 3-inch square burners were conducted on the previously described burning table which made use of strain gages to measure the weight loss of fuel. Methanol, acetone, n-hexane, cyclohexane, napalm test solvent*, and

---

*Napalm test solvent has the following approximate composition:

	Weight Per Cent
n-heptane	57
benzene	18
cyclohexane	20
iso-octane	5

benzene were used as fuels with these two sizes of burners. The fires from the fuels other than methanol showed rather vividly the effects of flame merging upon the flame height, burning rate, and radiation flux to the surroundings. Typical weight loss and radiometer output traces are given in Figure 14. For these tests, the radiometer was placed just above the level of the burning table surface at a distance of 64 inches from the center of the table, with the radiometer sensing element positioned vertically and facing the fire array.

The values of burning rate per unit area and radiation flux to the surroundings are plotted versus dimensionless separation distance in Figures 15, 16, and 17 for the arrays of 4 3/16-inch diameter and 3-inch square burners. The data are recorded in Table 2. As with the very smallest burners used, the fires from methanol did not merge. This absence of merging is reflected in the lack of increase of the methanol burning rate curves of Figures 15 and 16 as the burner separation distance was decreased.

For the fuels other than methanol, sharp peaks occurred in the burning rate curves at the smaller burner separation distances. The maximum in a burning rate curve for a test was observed to occur at about the same separation distance that the individual fires of the array began to merge into one large fire column. At this critical burner separation distance, the flame height of the array was also seen to increase greatly

Notes:

(a) Chart Speed: 1-inch/min.
(b) Radiometer Scale: 0-100 = 5 millivolts
(c) Fuel Weight Scale: 0-100 = 2 millivolts

Figure 14. Typical Strip-Chart Readout of Merging-Flame Radiation and Burning Rate for Exposed-Rim Burners.

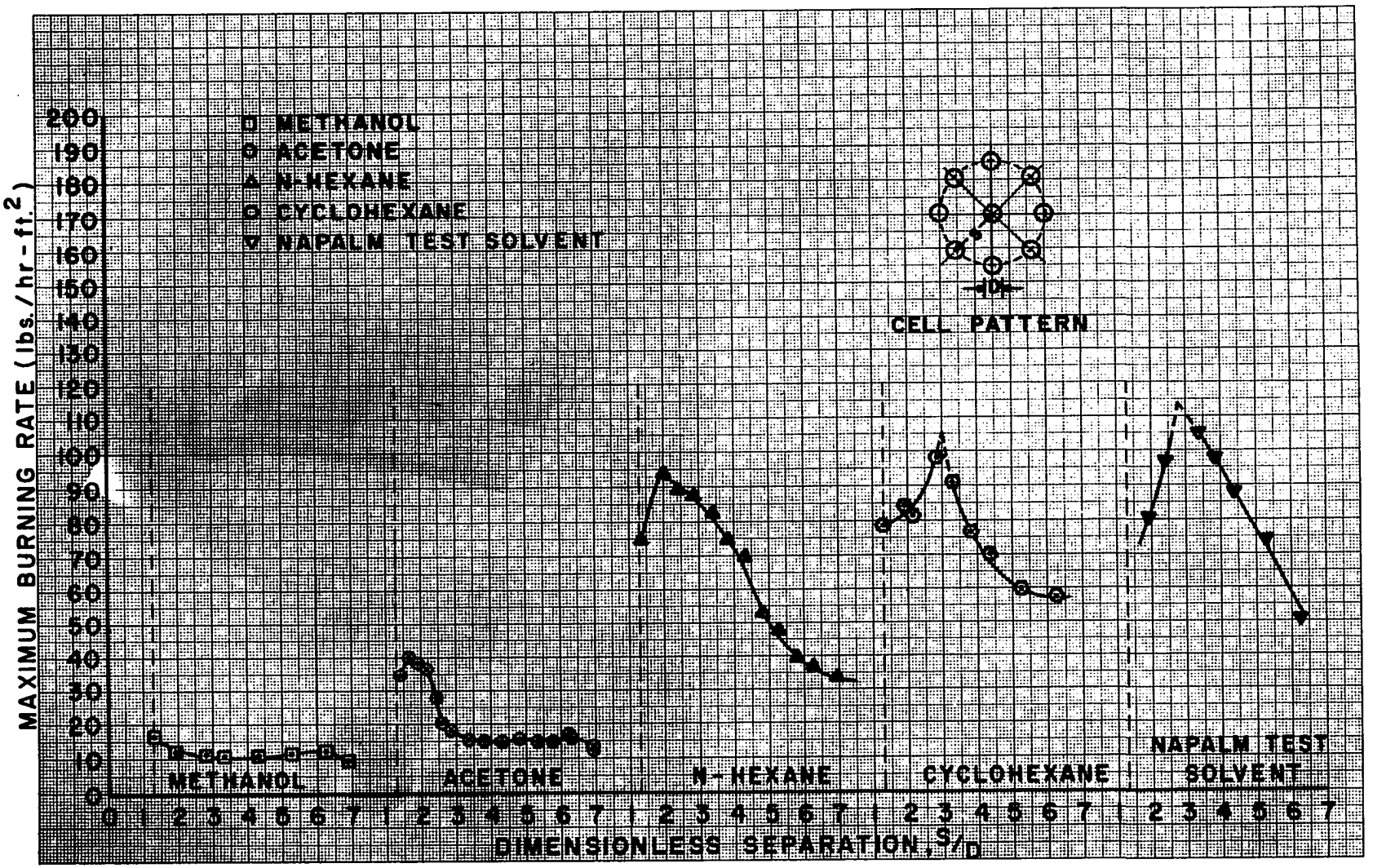

Figure 15. Merging-Flame Burning Rate Data (4 3/16-Inch Circular Burners, Exposed Rims).

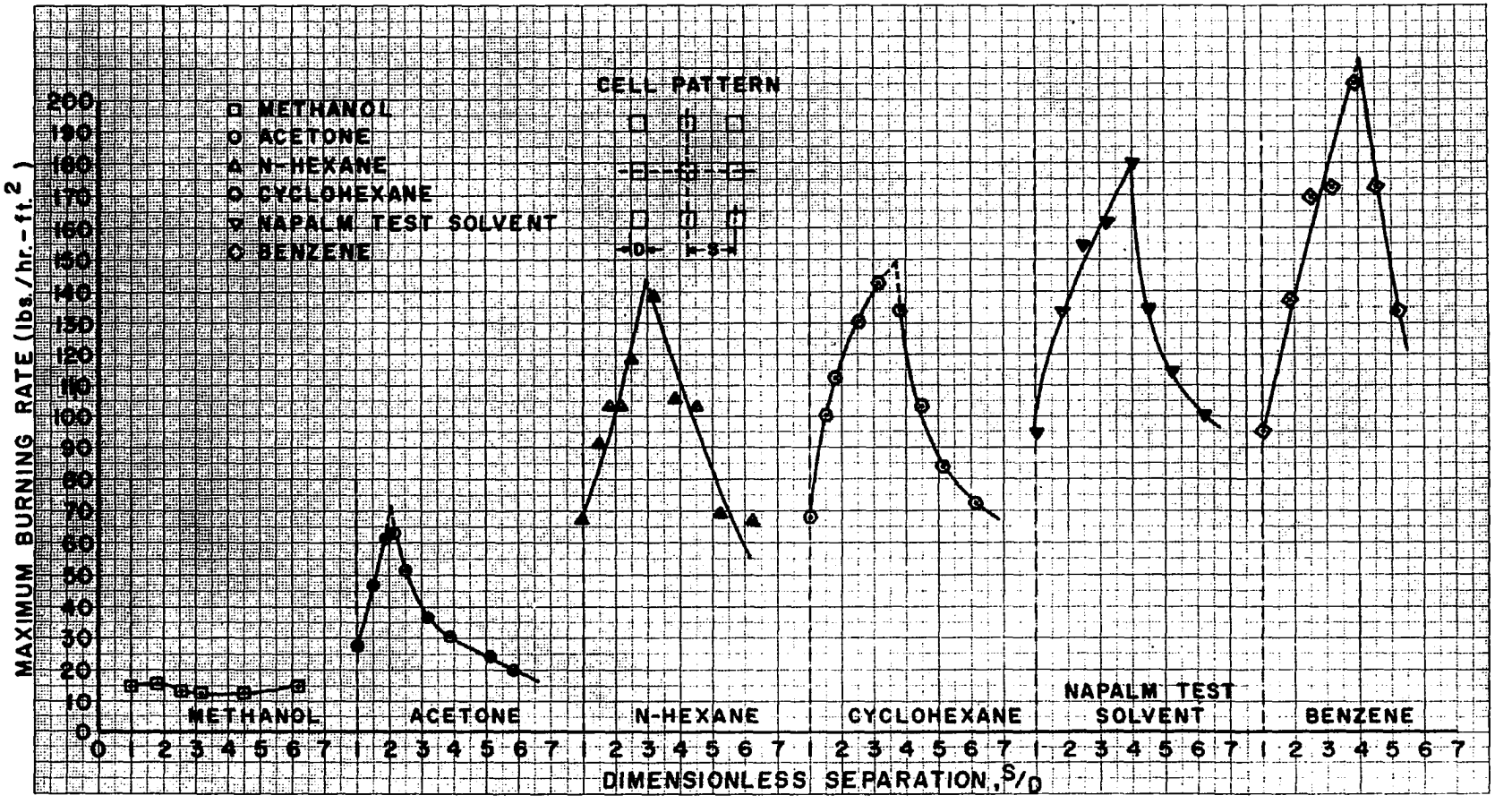

Figure 16. Merging-Flame Burning Rate Data (3 x 3-Inch Square Burners, Exposed Rims).

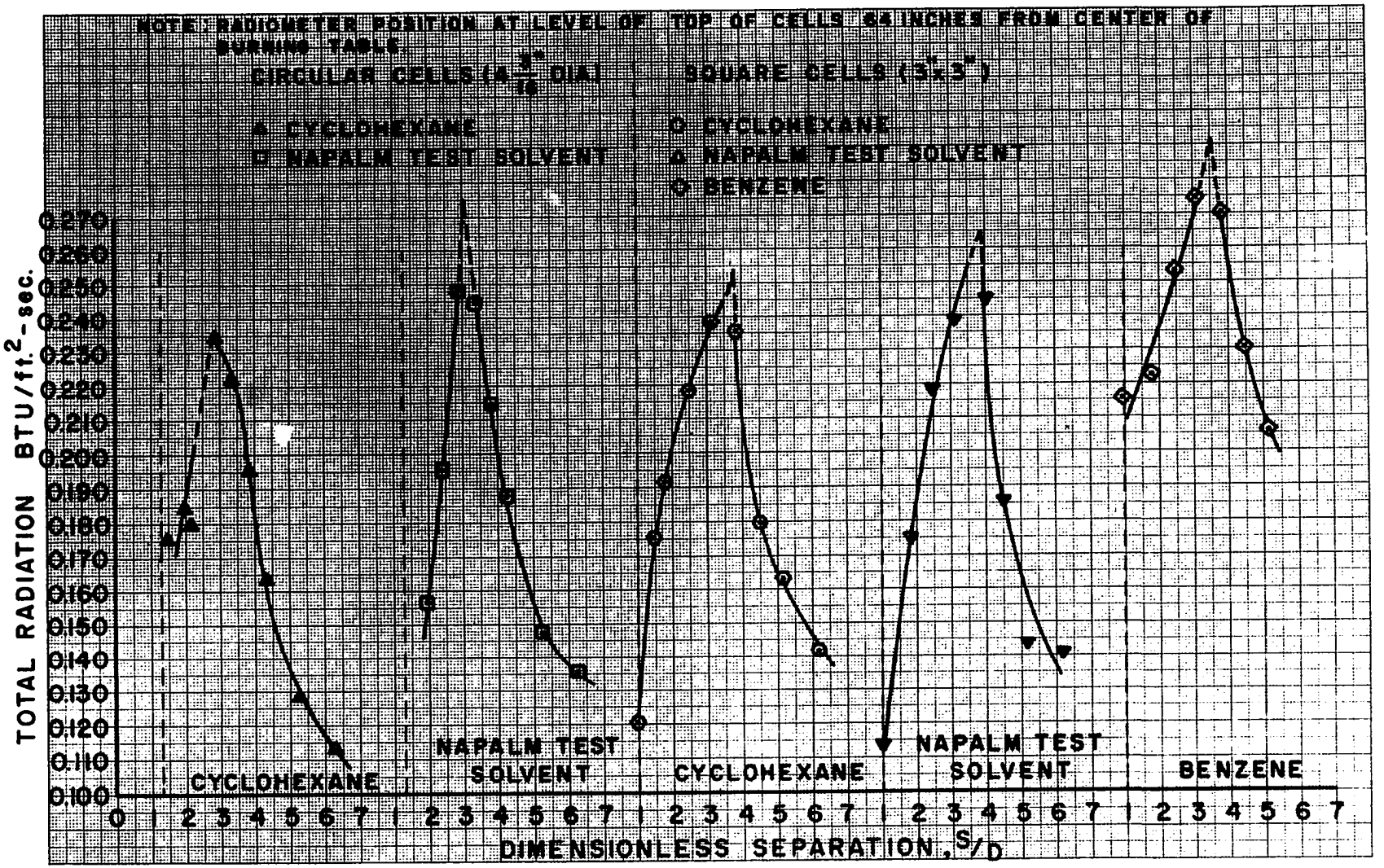

Figure 17. Merging-Flame Radiation Data for Exposed-Rim Burners. (Circular Burners Used in Circular Patterns, Square Burners Used in Square Patterns.)

as the individual flames began to merge. The onset of merging was therefore defined to be the condition at which the individual flames from the various fuel sources begin to combine into one fire column. This onset of merging was accompanied by a large increase in burning rate, flame height, and radiation flux to the surroundings. When the spacing between burners was decreased still further, the flames became fully merged and the burning rates dropped sharply.

From the burning rate curves, it is seen that the burning rate peaks occurred at the greatest separation distances for the fuels which showed the greatest values of burning rates at these peaks; that is, the onset of merging occurred with the burners farthest apart for fuels which had the greatest peak burning rates. The burning table was not large enough to permit interaction-free burning, except for the tests using methanol and acetone. To approximate interaction-free burning, burning rates were taken for the fuels using a single 3-inch square burner. It is also seen from these burning rate curves that the greatest peak burning rates occurred for the fuels which had the greatest burning rate per unit area for single, non-interacting fires.

The comparison of the burning rate per unit area curves given in Figures 15 and 16 for the 4 3/16-inch diameter circular and the 3-inch square burner configurations shows important differences. For a particular fuel the burning rate curves for the square burners and square burner

pattern have a consistently higher burning rate per unit area than the corresponding burning rate curves using the circular burners and circular pattern. From Figures 15 and 16 the ratio of the value of peak burning rate per unit area of the square burners to the peak burning rate per unit area value for the circular burners has a value of approximately 1.5 for each fuel considered, except for methanol. The methanol fires did not merge, and showed little difference in burning rate values for the two burner patterns.

Furthermore, the amount of heat conducted through the burner wall to the fuel is proportional to the circumference of the burner; therefore, per unit area, the wall's contribution to the evaporation rate of the fuel is proportional to $(\text{diameter})^{-1}$ for the 4 3/16-inch diameter of the circular burners and to $(\text{width of side})^{-1}$ for the 3-inch width of the square burners. The difference in the surfaces of the circular and square burner walls also contributes to the difference in burning rate. The outside surface of the circular burner wall was polished and tended to reflect part of the radiation received from the adjacent flames. The square burner wall was made of dark, non-reflective steel plate and absorbed more radiation than the polished circular burner wall. The square burner therefore became hotter than the circular burner and the fuel evaporation rate was greater.

Both the outside and inside surfaces of the burner wall were being heated during a test. The outside wall was heated both by heat received from adjacent fires and the burner fire itself, which was noted to spill over the burner rim in some cases. In addition, the inside wall of the burner was heated because the fuel level was not maintained flush with the burner rim, but continued to drop during a test. This drop in fuel level allowed the flame from the burner to come more thoroughly into contact with the wall.

The radiation flux curves in Figure 17 are similar in shape to the burning rate curves. In addition, the peaks of these radiation flux curves occur at the same separation distances as the peaks of the corresponding burning rate curves. The increased burning rates produced at the onset of merging produce large fire columns, which give off more radiation to the surroundings.

The radiometer (with a range of 0 to 3 solar constants) from which the radiation measurements were obtained was the same instrument used later in the rimless burner tests and, as mentioned previously, it had a slow response time. For some of the tests, particularly those with benzene used as fuel, the burning time was so short that there might be some question as to the reliability of the flux values obtained with this radiometer. The values of radiation flux used were the peak values on the radiation curves as shown in Figure 14.

For a few of the more violently burning, merging fires, the rapid entrainment rate of air into the fires caused the light-weight burning table surface to oscillate up and down very slightly. This oscillation would sometimes cause difficulty in reading the slope of the constant-slope portion of the weight loss curve; however, for most of the tests, the burning rate, and therefore the air entrainment rate, was not great enough to cause noticeable oscillation and the slopes of the weight loss curves could be read with more confidence. As mentioned previously, only the square burners were used to obtain the single burner measurements. The single burner data from the square burners were used for the burning rate correlations for both the circular and square burner patterns.

As seen from the curves of burning rate per unit area versus dimensionless distance given in Figures 15 and 16 for the various fuels and burner patterns, very little scatter from the general trends of the data was found. Apparently the reproducibility of the burning rate measurements was quite good although the only exposed-rim burner tests which were repeated were several using acetone at the larger separation distances.

The burning rates recorded in Table 5 give an illustration of the magnitude of the merging phenomenon. From Table 5 it is seen that the ratio of the peak burning rate per unit area (burning rate at the onset of

merging) to the burning rate per unit area from a single burner was greatest for acetone, that is, 4.36 compared with 2.10 for benzene when the square burner array was used. Even though benzene had the greatest burning rate at the onset of merging, it had the least burning rate enhancement due to merging. On the other hand, acetone had the least burning rate at the onset of merging but the greatest percentage increase due to merging. As will be discussed more thoroughly later, much of the radiation from opaque flames such as those produced by benzene is absorbed by the flame itself before it can get back to the fuel surface. The radiation from adjacent fires would thus have less effect on the fuel evaporation rate than if the flames were more transparent and most of the radiation from the surrounding flames could reach the fuel surface, as is the case with the acetone flames.

From the burning rate curves the burner separation distances at the onset of merging for the various fuels were observed to be greater for the fuels with the greater single-burner burning rates. The burner separation distances at the peak burning rates might therefore be considered to be a function of the single-burner burning rates of the particular fuels. An empirical relationship was developed for predicting the burner separation distance at the onset of merging for the liquid fuels. This relation is similar to that given by Waterman, et al. (27) for predicting the separation distance at the onset of merging for multiple wood cribs in square

arrays as given in Equation 12.

The relationship for the burner separation distance at the onset of emerging developed for the present exposed-rim burner studies is given as

$$\left(\frac{S}{D}\right)_p = 0.55\ (m_s)^{0.40} \qquad (14)$$

for the circular burner pattern, and

$$\left(\frac{S}{D}\right)_p = 0.59\ (m_s)^{0.46} \qquad (15)$$

for the square burner pattern where m_s has the units of lb/hr-ft^2. In Figure 18 the burning rates per unit area for the square array are plotted versus the burning rate function, $\frac{S}{D}\ (m_s)^{-0.46}$. From Figure 18 it is seen that the peaks of the burning rate curves for the various fuels all have a value of approximately 0.6 for this burning rate function.

It was noted by Burgess, et al. (5), who measured the burning rates of liquid fuels in single burners, that the burning rate appeared to be a function of $\frac{\Delta H_v}{\Delta H_c}$. ΔH_v is the heat of vaporization at the fuel boiling point plus the integrated heat capacity of the fuel from ambient temperature to the fuel boiling point, and ΔH_c is the standard, lower heat of combustion. This ratio is essentially the fraction of the flame's heat that must be fed back to the fuel to maintain a steady rate of vaporization.

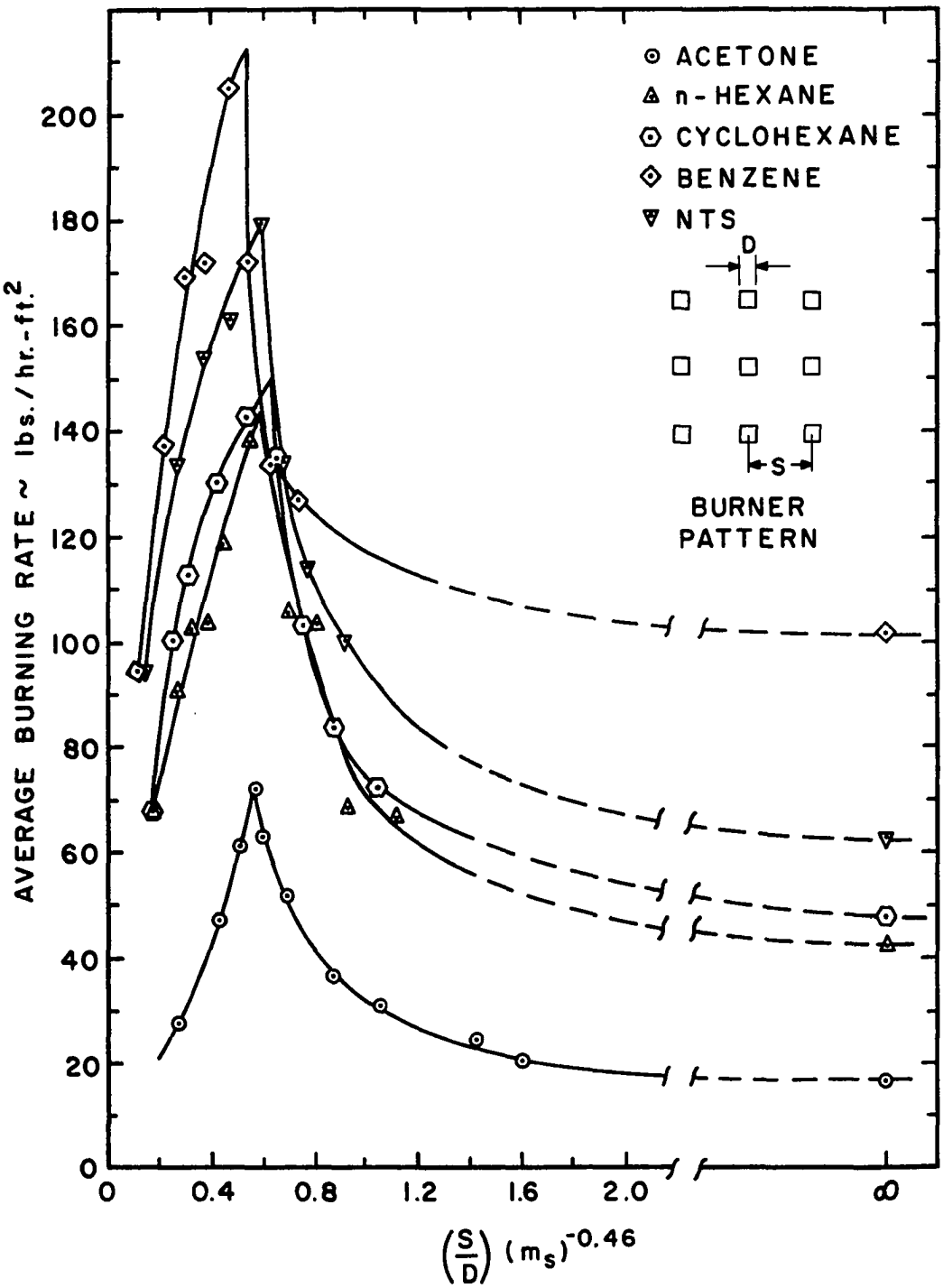

Figure 18. Effect of Flame Interaction on Exposed-Rim Burner Burning Rate (Nine-Burner Square Pattern).

From the data of Table 5 and Figures 15 and 16, it was seen that the fuels with the greatest values of burning rate per unit area at the onset of merging (m_p) had the smallest values of the ratio of (m_p/m_s). It therefore appeared that the burning rates at the onset of merging (m_p) might be a function of both (m_p/m_s) and ($\Delta H_v/\Delta H_c$). Using the data from the present exposed-rim burner studies, an empirical relationship for the burning rates at the onset of merging was found for the circular burner pattern. This relation is given as

$$m_p = 0.53 \left[\left(m_s\right)\left(\frac{\Delta H_c}{\Delta H_v}\right)^{1.35}\right]^{0.5} \text{ lb/hr-ft}^2 \qquad (16)$$

for the square burner pattern, the relation

$$m_p = 13.2 \left[\left(m_s\right)\left(\frac{\Delta H_c}{\Delta H_v}\right)^{0.80}\right]^{0.5} \text{ lb/hr-ft}^2 \qquad (17)$$

was obtained. The large differences in the coefficients of Equation 16 and 17 are due mainly to the different exponents of the $\Delta H_c/\Delta H_v$ terms. The burning rate data for both circular and square burner patterns were plotted in Figures 19 and 20, respectively, as $m\left(\frac{m_p}{m_s}\right)\left(\frac{\Delta H_c}{\Delta H_v}\right)^b$ versus $(S/D)(m_s)^a$. Both a and b are empirical constants; for the circular burners a = -0.4 and b = -1.35, and for the square burners a = -0.46 and b = -0.80.

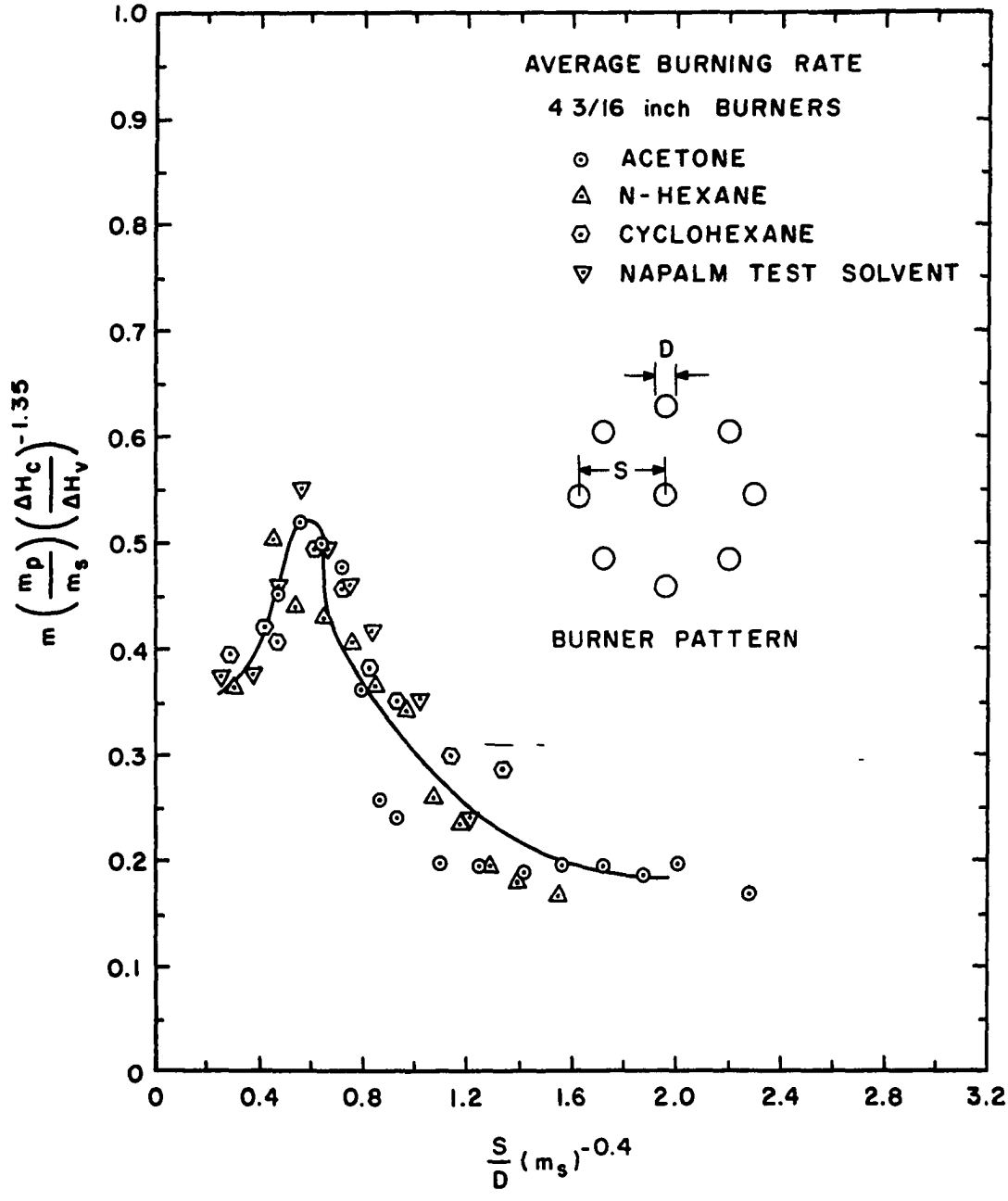

Figure 19. Burning Rate Correlation for Multiple Fires from 4 3/16-Inch Circular Exposed-Rim Burners

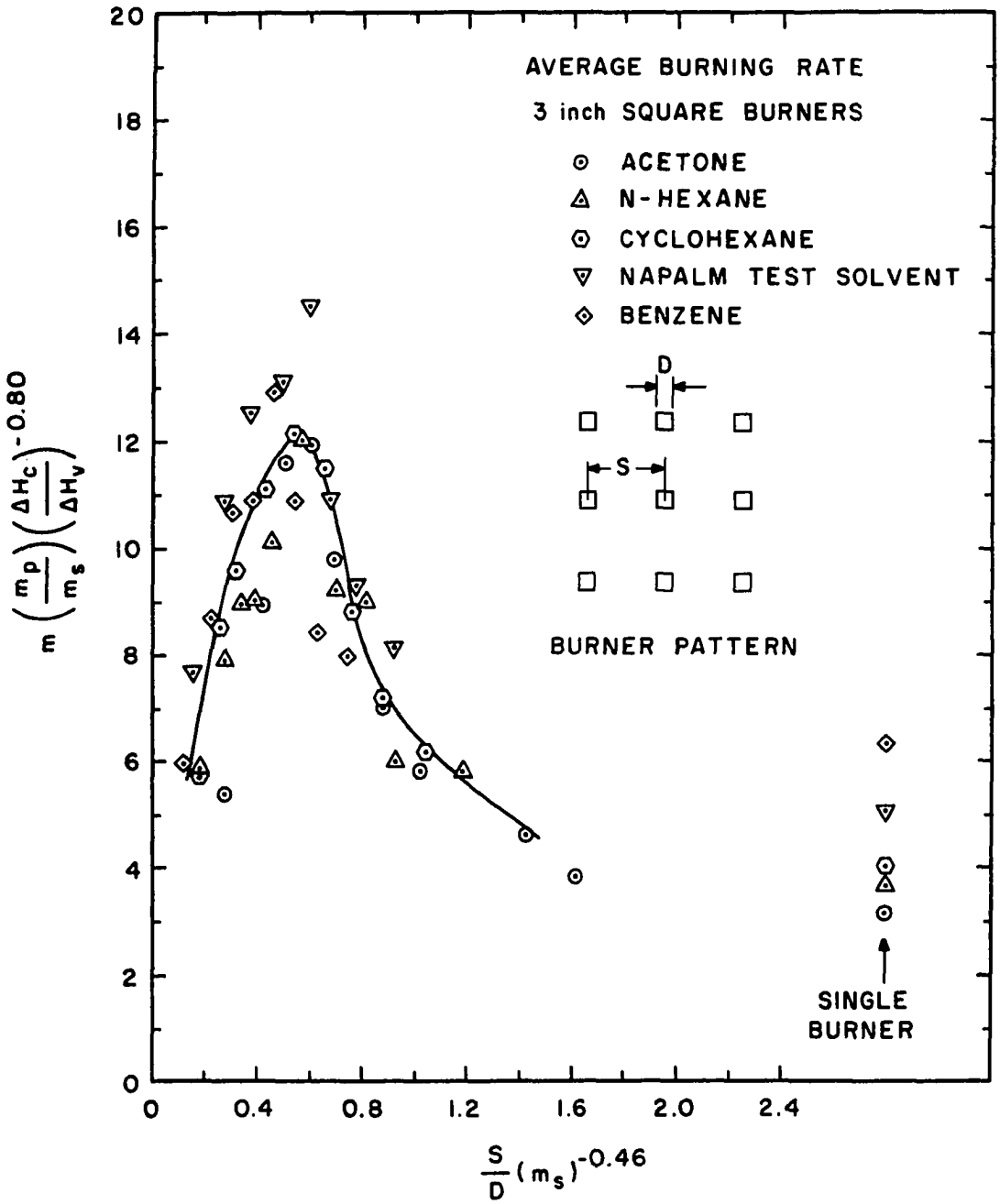

Figure 20. Burning Rate Correlation for Multiple Fires from 3-inch Square Exposed-Rim Burners.

As stated previously, ΔH_v in Equations 16 and 17 is defined as the sensible heat of raising the fuel from ambient temperature to its boiling point plus the heat of vaporization. In reality, for the exposed-rim burner tests only a fixed quantity of fuel was used, and the burning rates used in the correlations were those corresponding to the short period during which the burning rate was approximately constant. Therefore, the temperature of the fuel during this period was something greater than ambient so that the values of ΔH_v calculated on the basis of an ambient temperature of 70°F are slightly, but insignificantly, larger than the true values of ΔH_v in the tests.

In summary, sharp peaks in the burning rate curves for all fuels except methanol were observed at the small burner separation distances as shown in Figure 15, when the exposed-rim burners were used. The individual fires of the array began to merge into a single column, with an accompanying large increase in flame height, at about the same separation distance that these peak burning rates were measured. The ratios of these peak burning rates to that of a single burner ranged from 4.36 for acetone to 2.10 for benzene when the 3-inch square burners were employed. The curves of radiation flux to the surroundings followed closely the trends in the corresponding burning rate versus burner separation curves, with a sharp peak in measured radiation

flux occurring at the same burner separation as the burning rate peak. The peak burning rates per unit area for the 3-inch square burners were approximately 1.5 times as great as those of the 4 3/16-inch circular burners due to the greater effect of heat conduction through the burner wall. The greater conduction effect for the smaller, square burners can be mainly attributed to their larger wetted surface to fuel volume ratio.

Correlations for the 4 3/16-inch circular and 3-inch square exposed-rim burners were developed which have the general form

$$\dot{m}\left(\frac{m_p}{m_s}\right)\left(\frac{\Delta H_c}{\Delta H_v}\right)^b \text{ versus } \left(\frac{S}{D}\right)\left(m_s\right)^a$$

where "a" and "b" are empirical constants having different values for the circular and square burners. As seen from Figures 19 and 20, these burning rate correlations were quite successful in bringing together the burning rate per unit area curves for the various fuels, especially when considering the wide range of burning rates found in these particular exposed-rim burner tests. The correlations can be used for predicting the flame merging behavior of other fuels with similar burners and burner patterns. Only the single-burner burning rate needs to be measured, or estimated from other sources of information such as the Bureau of Mines data of References 5 and 29. With the single-burner burning

rate known, the peak burning rate for the particular burner pattern under consideration, as well as the dimensionless burner separation distance at which this peak occurs, can be predicted from Equation 16 or 17. The success obtained with the exposed-rim burner correlations led to the more comprehensive modeling involved in connection with the rimless burners.

Rimless Burner Tests

The rimless burner tests comprised the majority of the tests conducted during the present studies on flame interaction and merging. Three burner sizes, two burner patterns, and five fuels: methanol, acetone, n-hexane, cyclohexane, and benzene, were studied. Circular burners of 2-, 4-, and 6-inch diameter were employed in the same nine-burner circular patterns used in the exposed-rim tests. The 4-inch burners were also used in a thirteen-burner pattern described previously. The results from 207 of these tests are reported in the following pages. The tests were conducted on the previously mentioned burning table which was large enough to allow interaction-free burning as a limiting case. The burners and burning table were designed to minimize heat conduction from the burner walls to the fuel. In addition, the burners were constructed so that steady state burning could be obtained in the tests. The data taken for fires from these rimless burners included burning rates, radiation flux to the

surroundings, radiation flux back to the base of the merging flame column, flame heights, flame brightness temperatures, and temperatures of the convective columns above the fire arrays.

Burning Rates

The burning apparatus was designed so that the burning rates of several individual burners of the array or several groups of these burners could be measured separately. For all of the tests using the nine-burner circular pattern, the burning rate of the center burner and the total burning rate of all eight peripheral burners were obtained separately. For the thirteen-burner circular pattern, an additional burning rate comprising the burning rates of all four of the intermediate burners was obtained.

The burning rates for the center and for the peripheral burners using the nine-burner pattern are plotted as burning rate per unit area versus dimensionless separation distance in Figures 21 through 32. The dimensionless separation distance (S/D) is the ratio of the distance between the centers of the center burner and one of the peripheral burners and the diameter of a single burner. The average burning rate per unit area for all nine burners of the array is plotted for the various burner sizes and fuels in Figures 33 through 44. These average burning rates per unit area were obtained by combining the center and peripheral fuel consumption rates and dividing by the total fuel

surface area of all nine burners. In Figures 45 through 47 the burning rate per unit area curves for the center burner, the four intermediate burners, and the eight peripheral burners in the thirteen-burner pattern are given. The averaged burning rates per unit area for all thirteen burners are plotted in Figures 48 through 50.

The burner spacing exhibited only a slight influence on the burning rate of methanol in the 4- and 6-inch diameter burners. From Figure 21 and 22 only the center burning rates for the 4- and 6-inch burners showed a slight increase at the closest separation distances. A small increase in flame height was also observed for the flame array at this closest burner position, indicating a small interaction effect between the separate fires, although no merging of the flames was ever detected. Due to the very slight interaction effects observed with these two sizes of methanol burners, tests with the 2-inch and thirteen 4-inch diameter burners were not conducted for methanol.

All three sizes of burners were used for the acetone tests. For a particular burner size, the acetone burning rates per unit area for the center and for the peripheral burners were approximately the same for the larger burner separation distances. There were few if any interaction effects at these large separation distances. As the separation distance was decreased, the center-burner burning rate per unit area always increased more rapidly and had a much

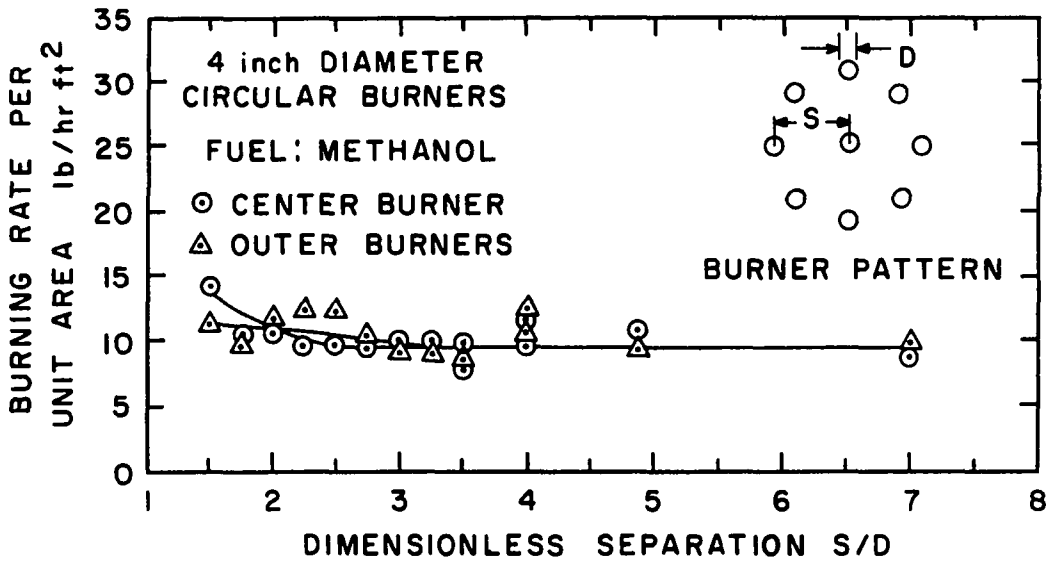

Figure 21. Burning Rates of Interacting 4-Inch Methanol Fires.

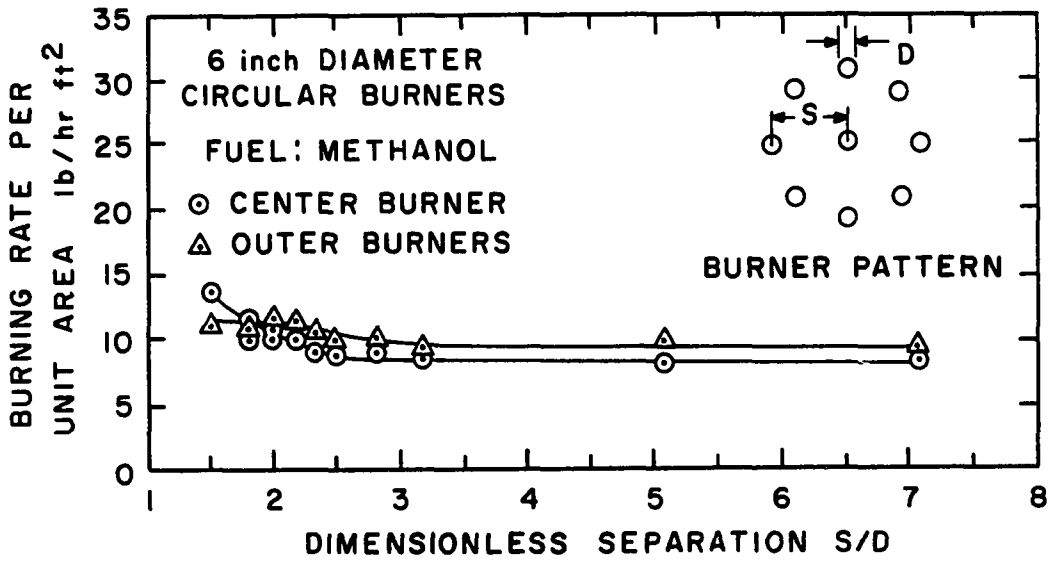

Figure 22. Burning Rates of Interacting 6-Inch Methanol Fires.

larger maximum burning rate at the onset of merging than did the burning rate per unit area of the peripheral burners. The interaction and merging effects for acetone became more pronounced, particularly for the center burner, as larger burner sizes were used, as shown by the peaks in the burning rate curves in Figures 23 through 25. For the 4- and 6-inch burners a very sharp drop in burning rate was observed at the smallest separation distances where the flames were fully merged. It was also noted that the peak in the acetone burning rate curves (at the onset of merging) occurred at the same dimensionless separation distance for both center and peripheral burners. In addition, the peaks for all three burner sizes occurred at approximately the same dimensionless separation distance.

The burning rates per unit area versus dimensionless separation distance are given for the center burner and the peripheral burners in Figures 26 through 28 and Figures 29 through 31 for n-hexane and cyclohexane, respectively. The burning rate curves for these two fuels, when the same burner size was used, are quite similar; although the burning rates for cyclohexane were usually slightly greater than those for n-hexane at the corresponding burner positions. As with acetone, the burning rates of center and peripheral burners for each fuel are approximately the same at the larger separation distances, and the center-burner burning rate becomes much larger than that for the peripheral burners

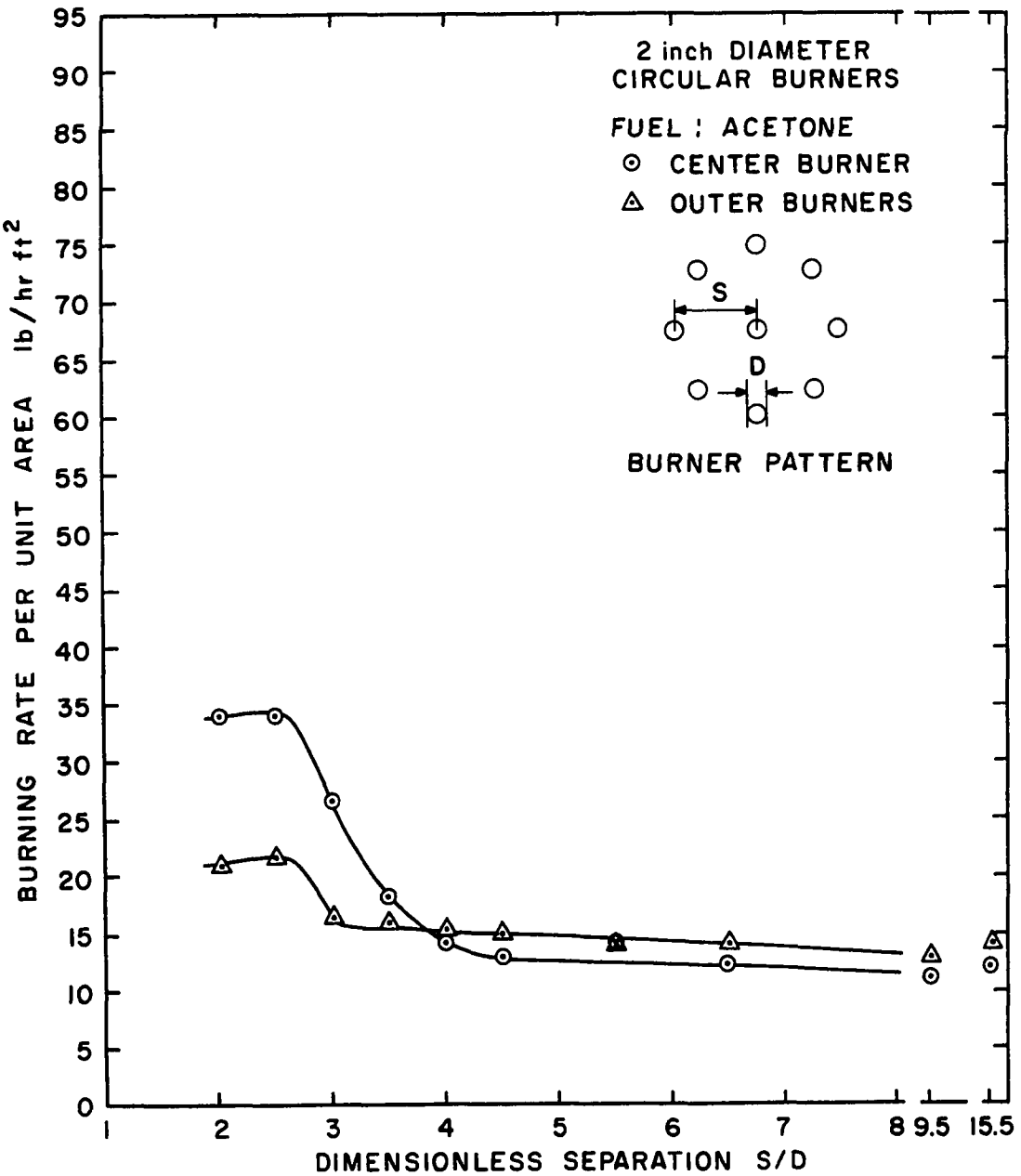

Figure 23. Burning Rates of Interacting 2-Inch Acetone Fires.

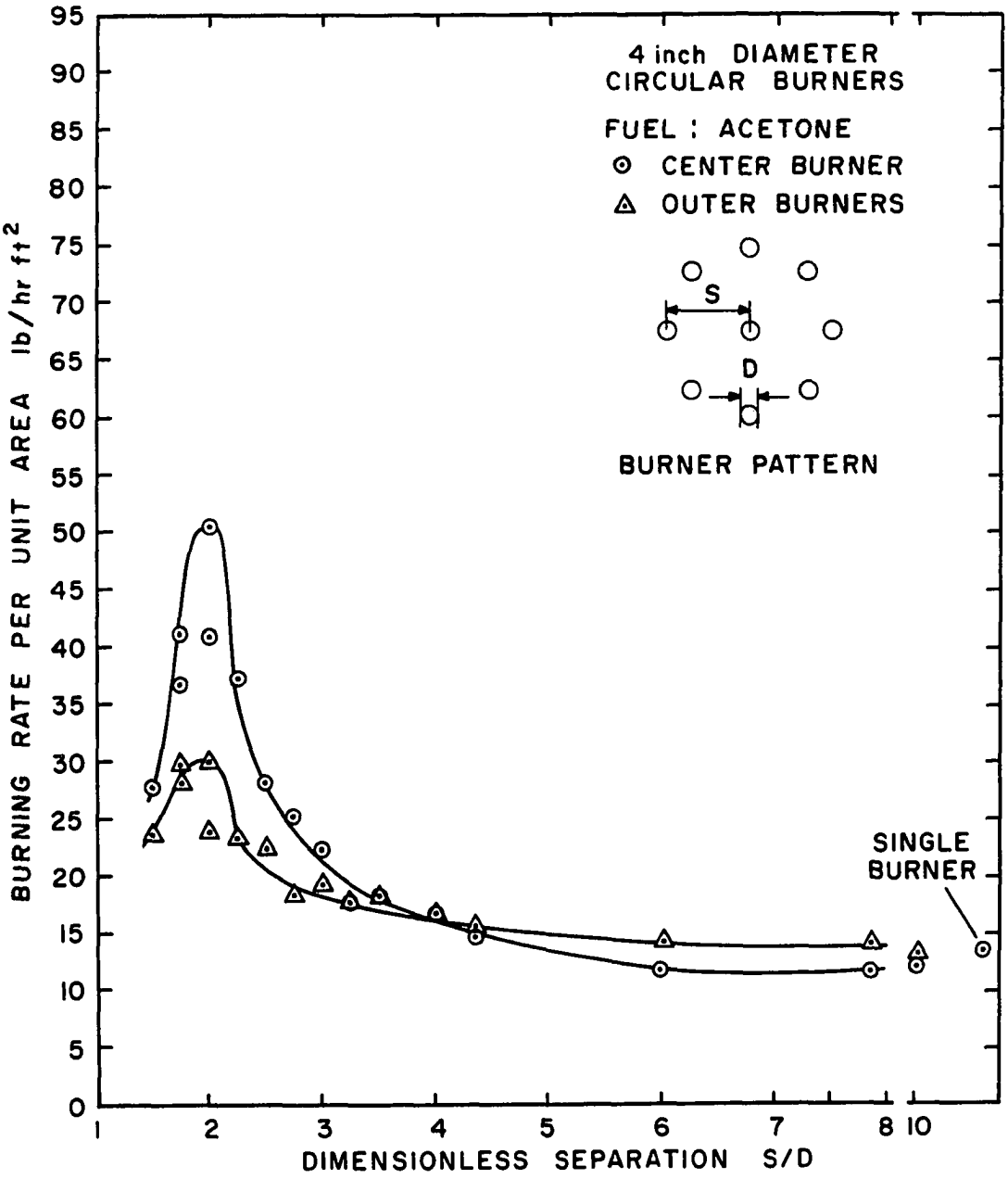

Figure 24. Burning Rates of Interacting 4-Inch Acetone Fires.

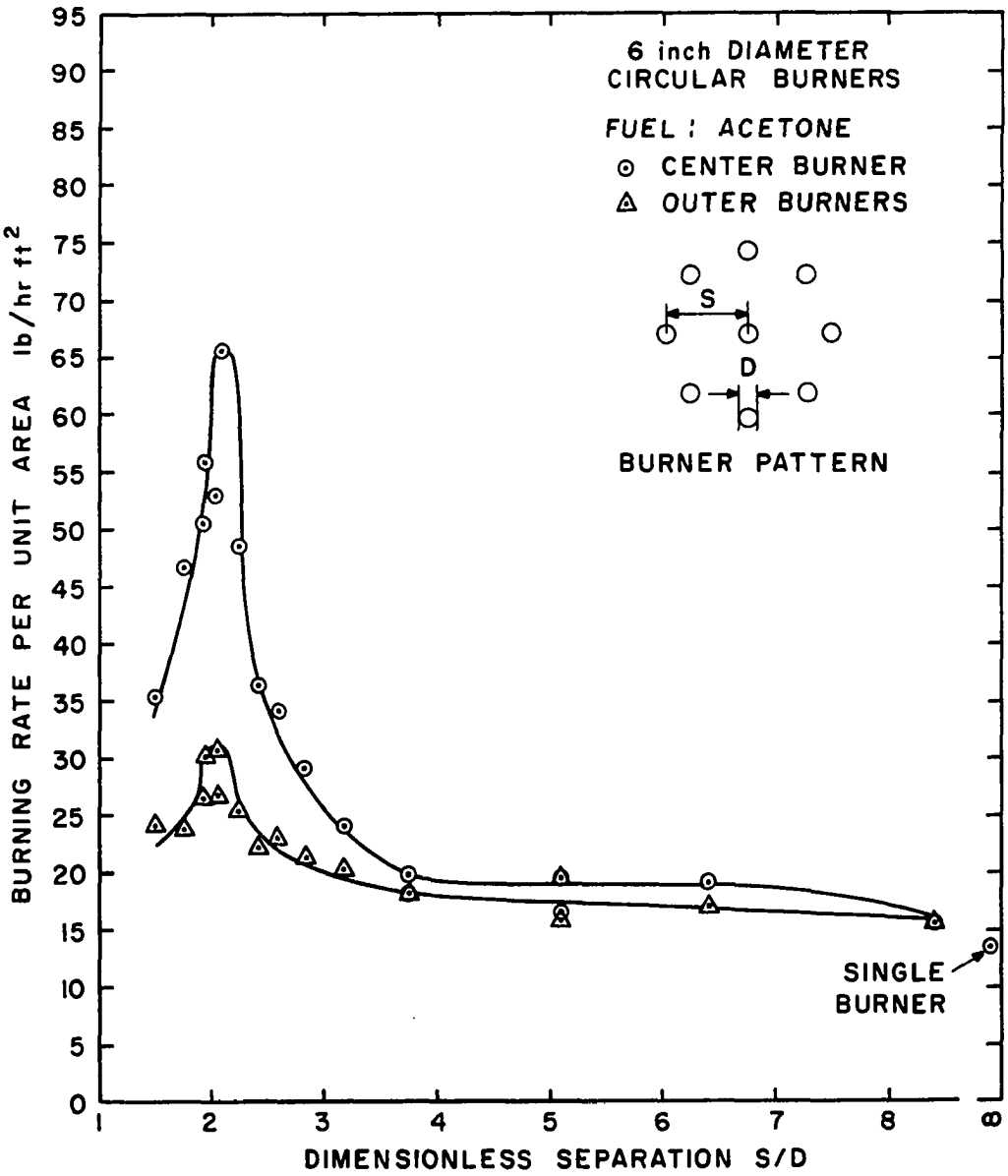

Figure 25. Burning Rates of Interacting 6-Inch Acetone Fires.

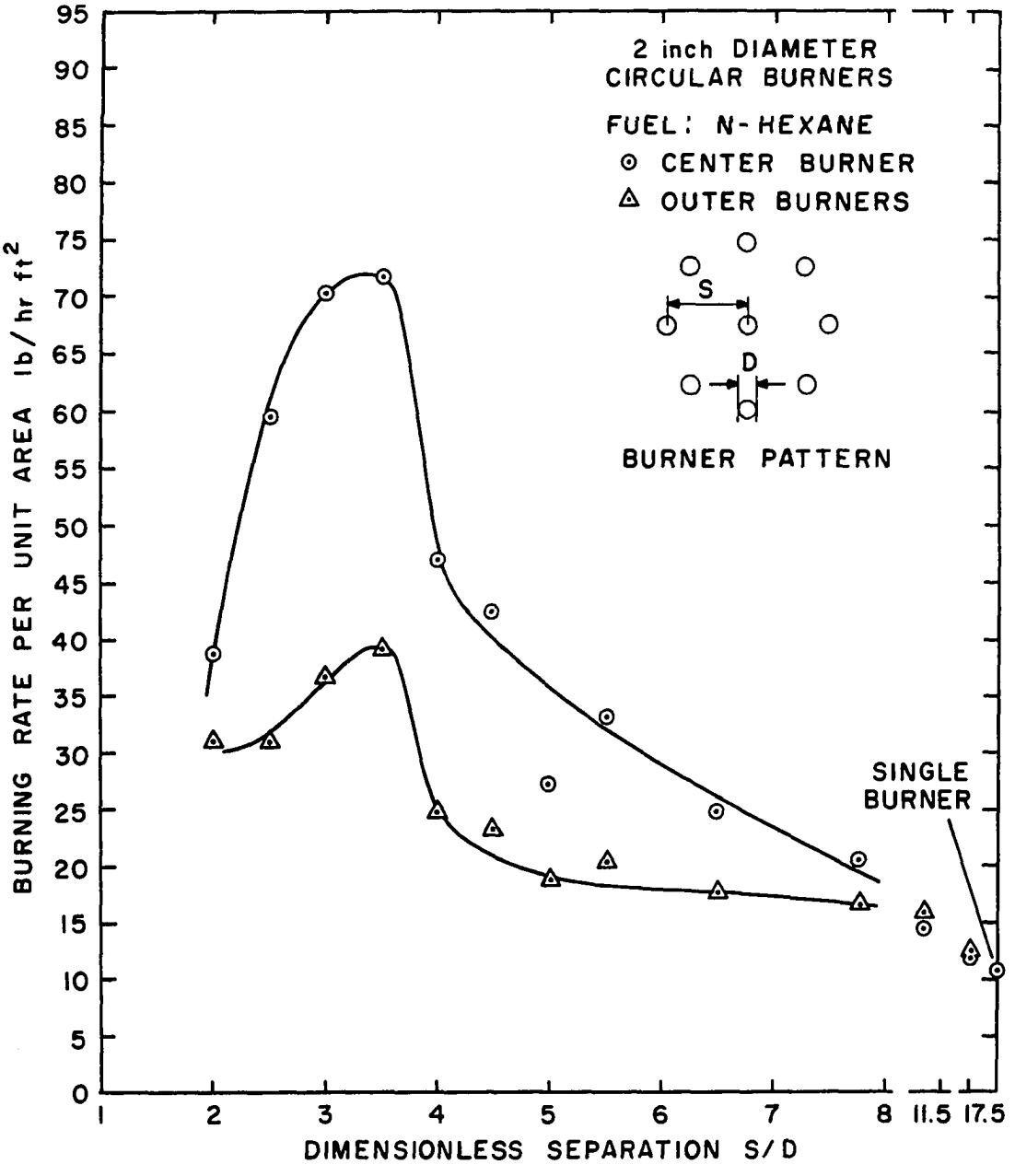

Figure 26. Burning Rates of Interacting 2-Inch n-Hexane Fires.

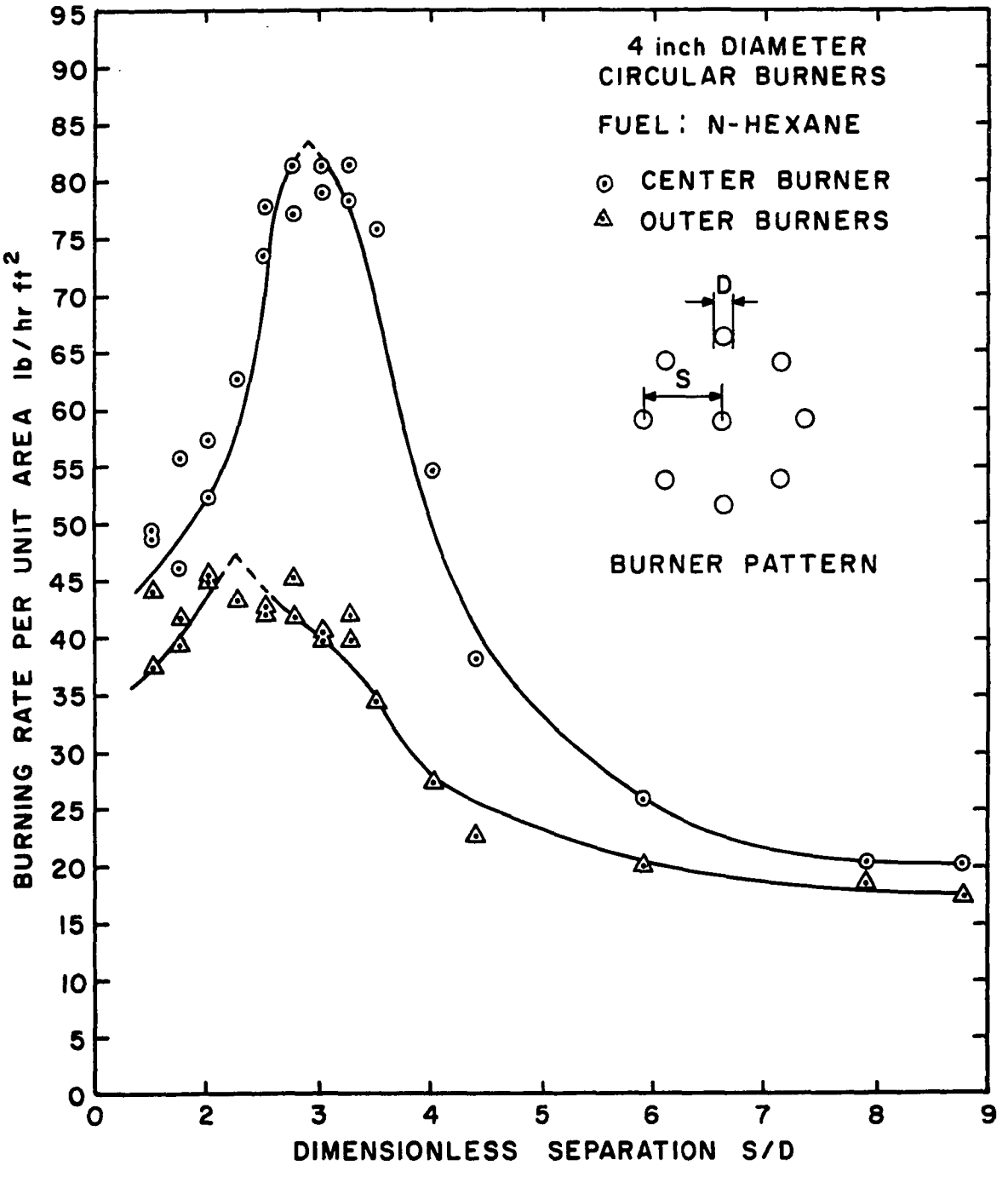

Figure 27. Burning Rates of Interacting 4-Inch n-Hexane Fires.

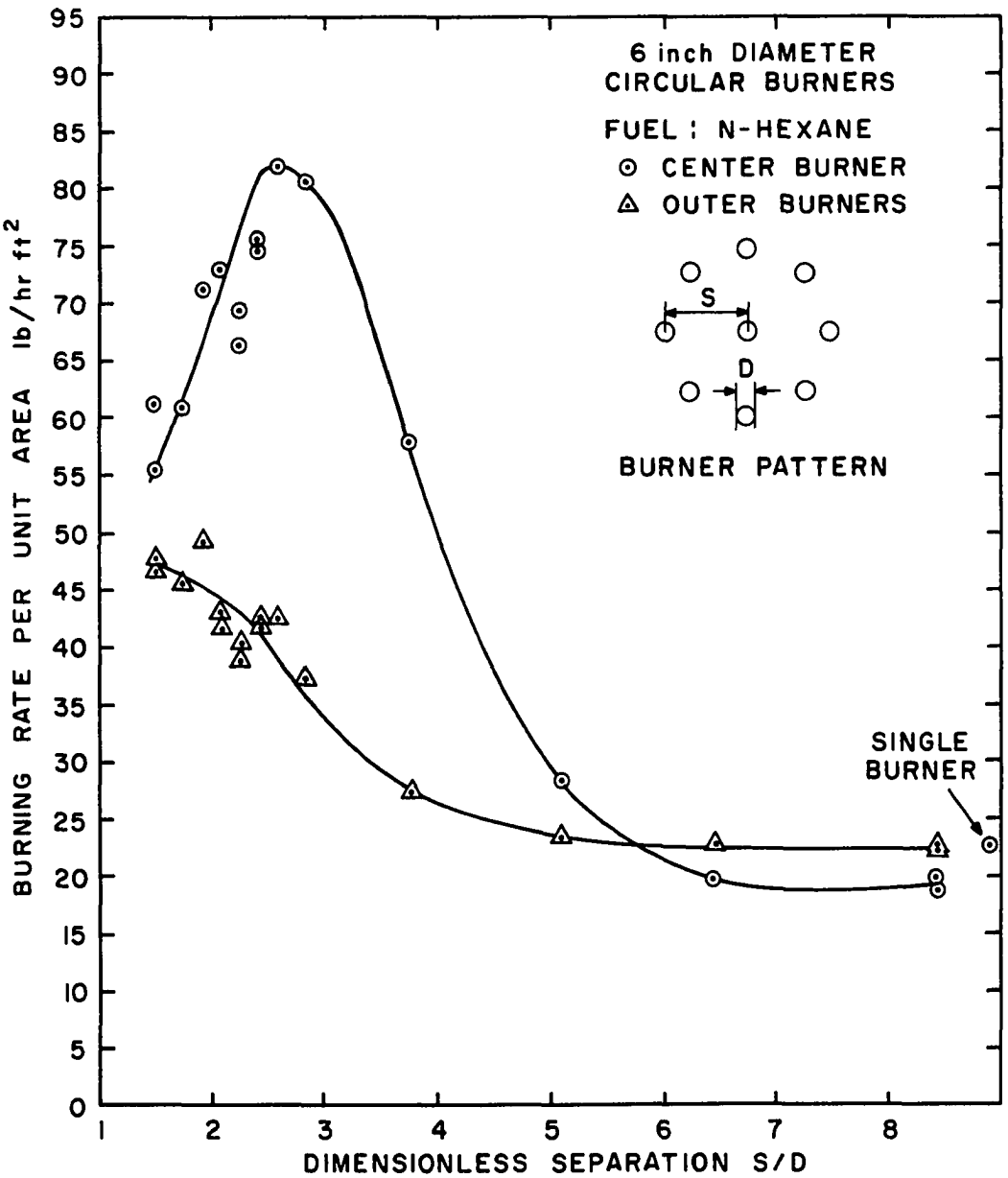

Figure 28. Burning Rates of Interacting 6-Inch n-Hexane Fires.

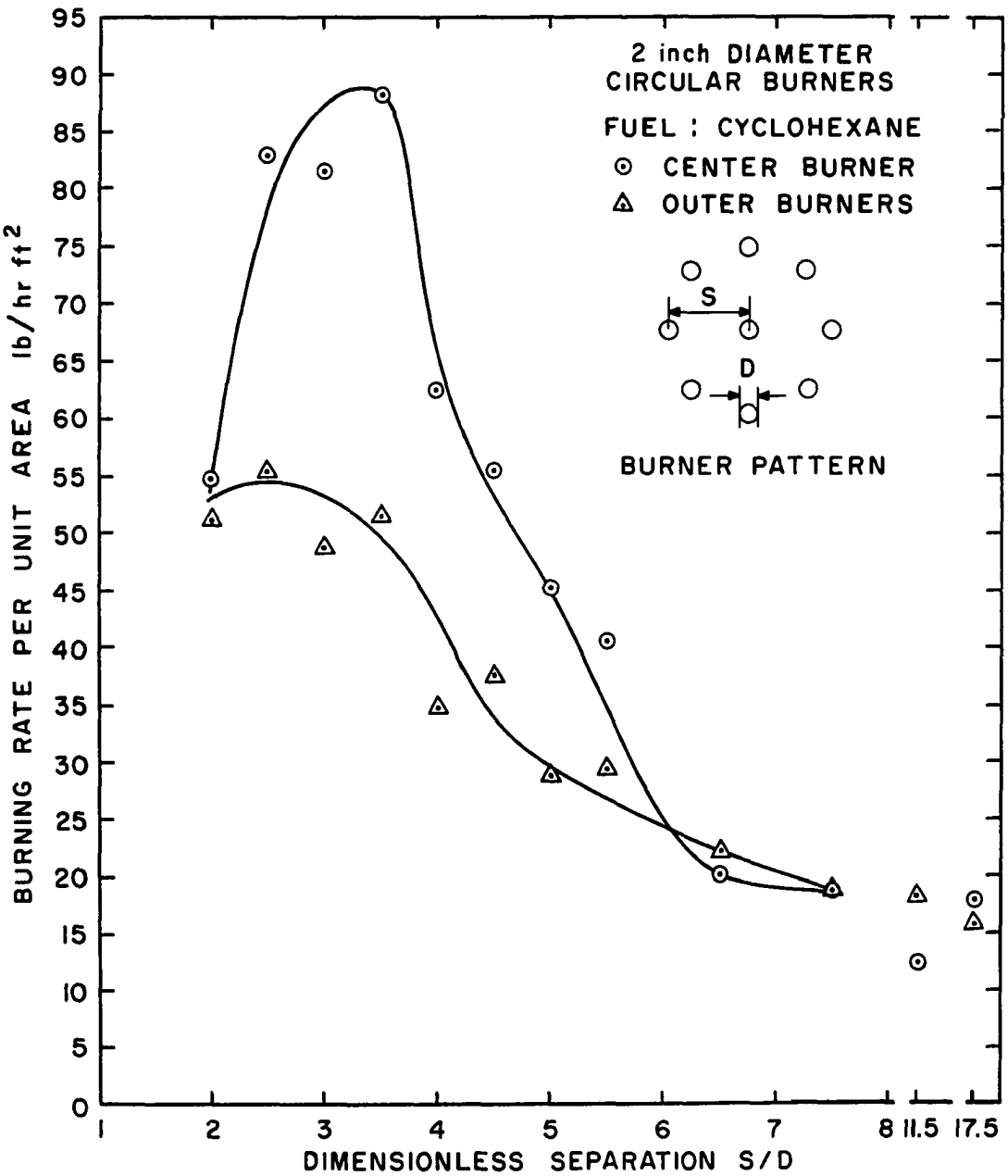

Figure 29. Burning Rates of Interacting 2-Inch Cyclohexane Fires.

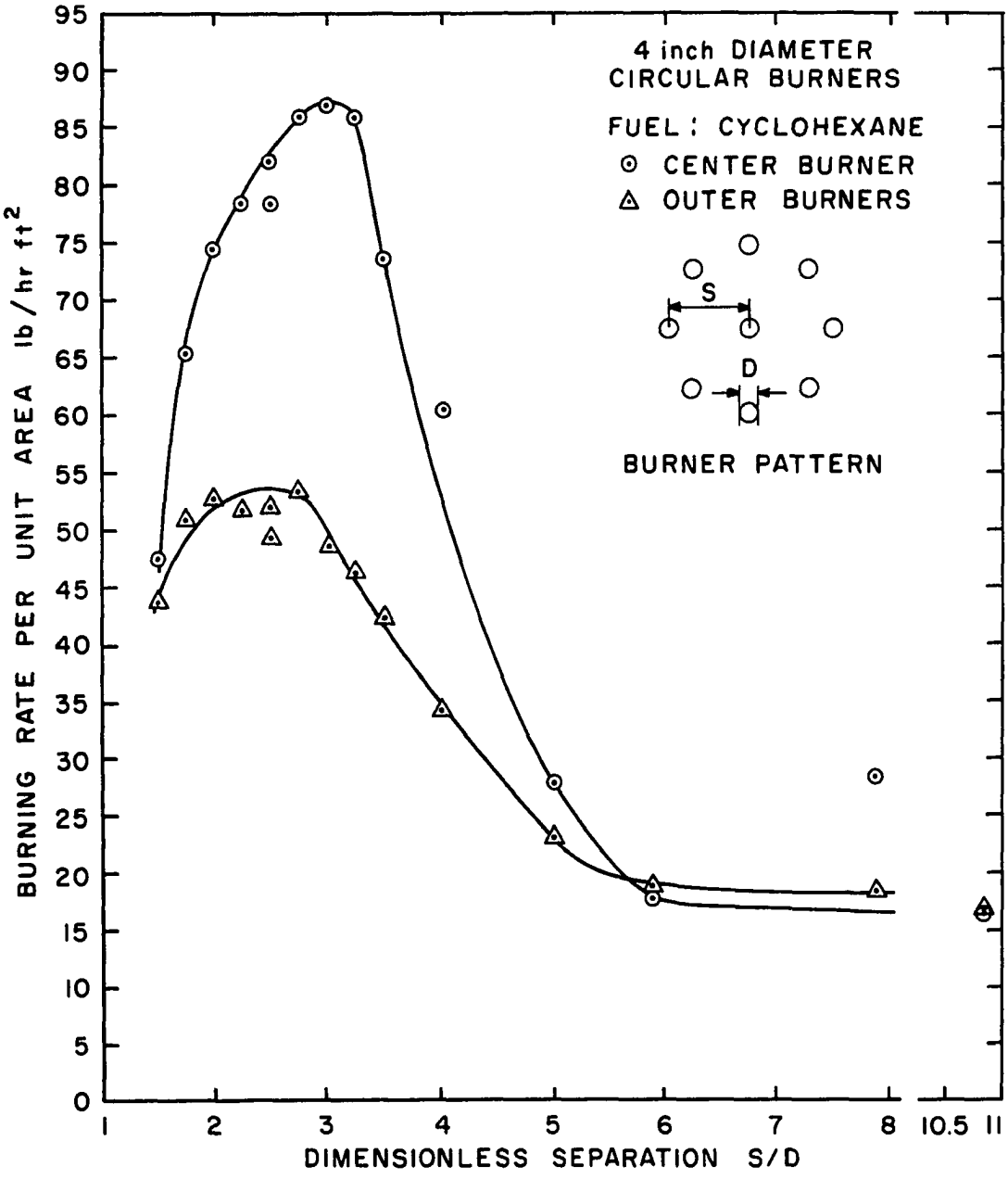

Figure 30. Burning Rates of Interacting 4-Inch Cyclohexane Fires.

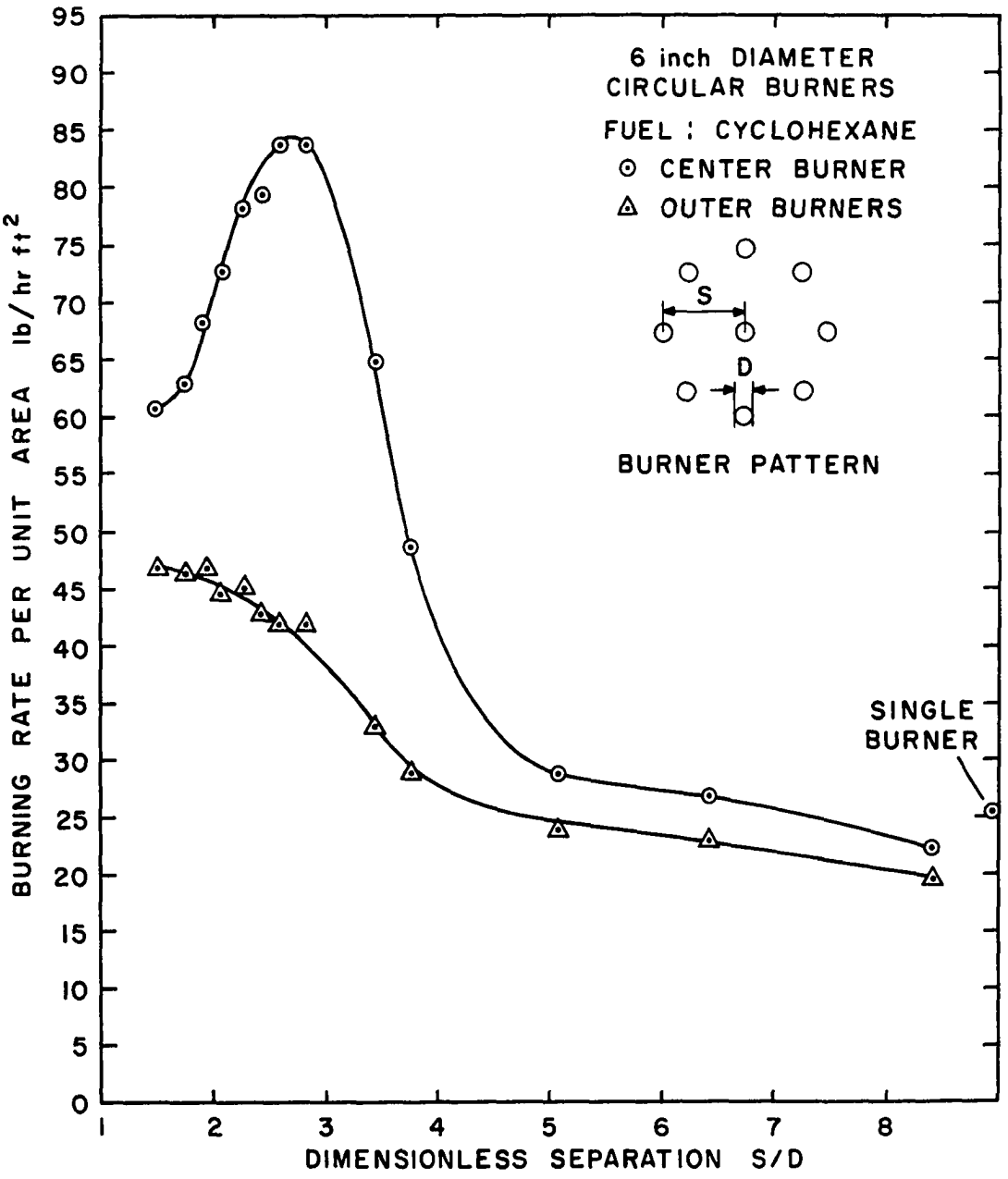

Figure 31. Burning Rates of Interacting 6-Inch Cyclohexane Fires.

as the fires begin to interact and merge. With both the larger n-hexane and cyclohexane fires, the burning rate curves of center and peripheral burners peak at different values of dimensionless separation distance for a particular fuel and burner size. This spread in the peaks of the burning rate curves is seen to become greater as larger burner sizes are employed; in fact, the peripheral-burner burning rate curves for both hexane and cyclohexane in the 6-inch burners do not peak at all, but continue to increase with apparently a slight leveling off occurring at the smallest separation distances used. As would be expected, the beginning of the merging effect, as shown by the sharp increase in burning rate, was observed to occur at greater burner separation distances for the fires from the larger burners, although as seen from the burning rate curves for n-hexane and cyclohexane, the ratio of burner separation distance to burner diameter at the onset of merging decreases slightly for the larger burner sizes.

As mentioned previously, only the 2-inch diameter burners were used for the benzene tests. The ventilation facilities in the static test room proved to be inadequate for the tremendous amount of smoke produced from benzene fires in the rimless burners larger than 2 inches in diameter. Nevertheless, the largest values of burning rate per unit area at the onset of merging for any of the rimless-burner, nine-burner pattern tests were obtained

with these small benzene fires. A very sharp peak was obtained for the center-burner burning rate curve for benzene, as shown in Figure 32. The burning rate for the peripheral burners continued to climb, even for the closest separation distances used, similar to the observations for large n-hexane and cyclohexane fires in 6-inch diameter burners.

The average burning rates for nine-burner arrays, obtained by combining the center and peripheral fuel consumption rates and dividing by the total fuel surface area of all nine burners, are strongly influenced by the burning rates of the eight peripheral burners. These average burning rate curves are therefore similar to the peripheral-burner burning rate curves discussed in the previous pages. The average burning rate per unit area curves shown in Figures 33 through 44 for all fuels therefore do not show sharp peaks at the onset of merging, as did the center-burner burning rate curves. The average burning rates for the hexane and cyclohexane fires in 6-inch burners, shown in Figures 40 and 43, respectively, continue to increase as burner distance is decreased and do not show a distinct maximum value at all.

The curves of burning rate per unit area as a function of dimensionless burner separation are given for the center burner, four intermediate burners, and eight peripheral burners using the 4-inch diameter, thirteen-burner pattern in Figures 45, 46, and 47 for acetone, n-hexane and cyclohexane,

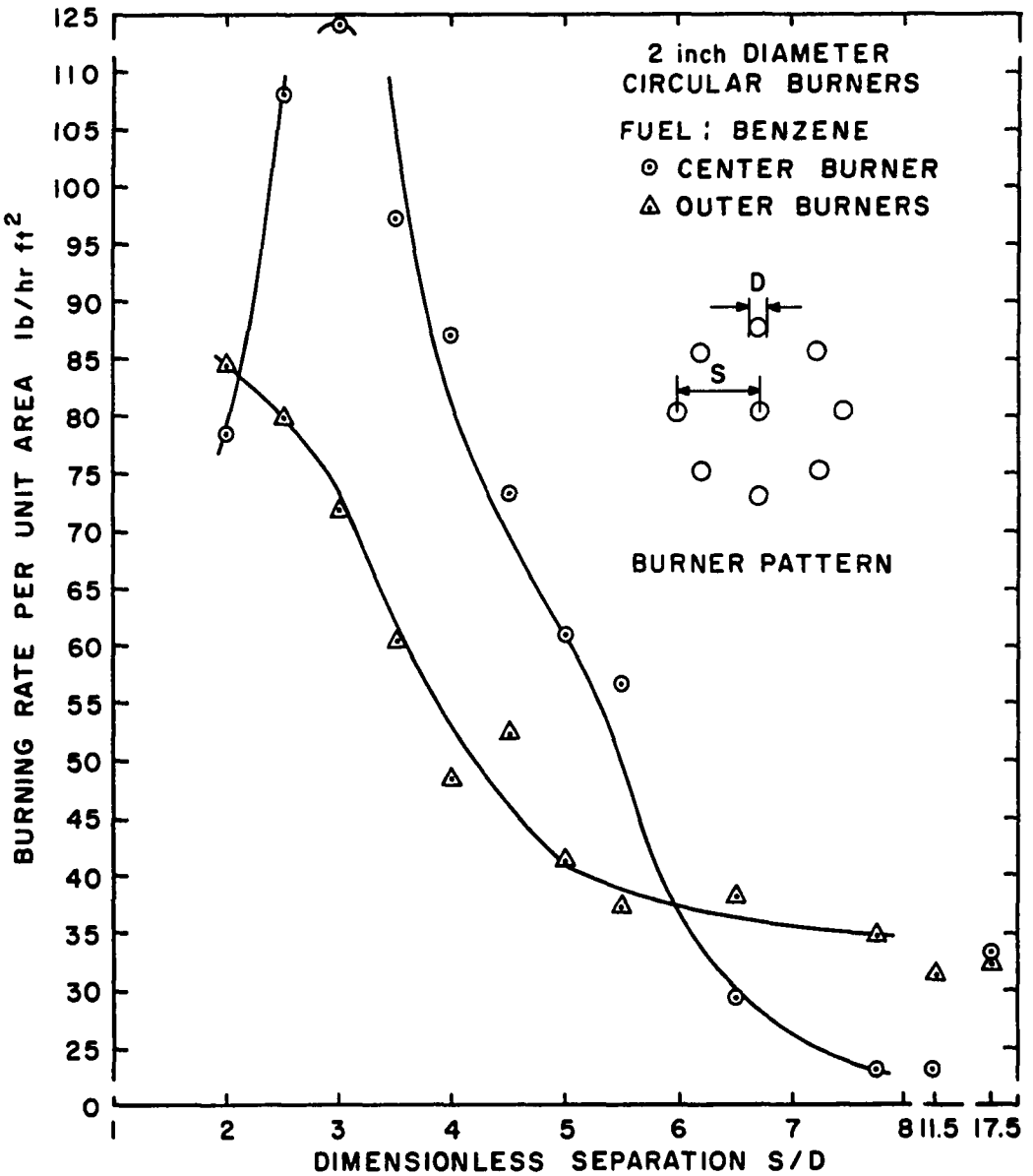

Figure 32. Burning Rates of Interacting 2-Inch Benzene Fires.

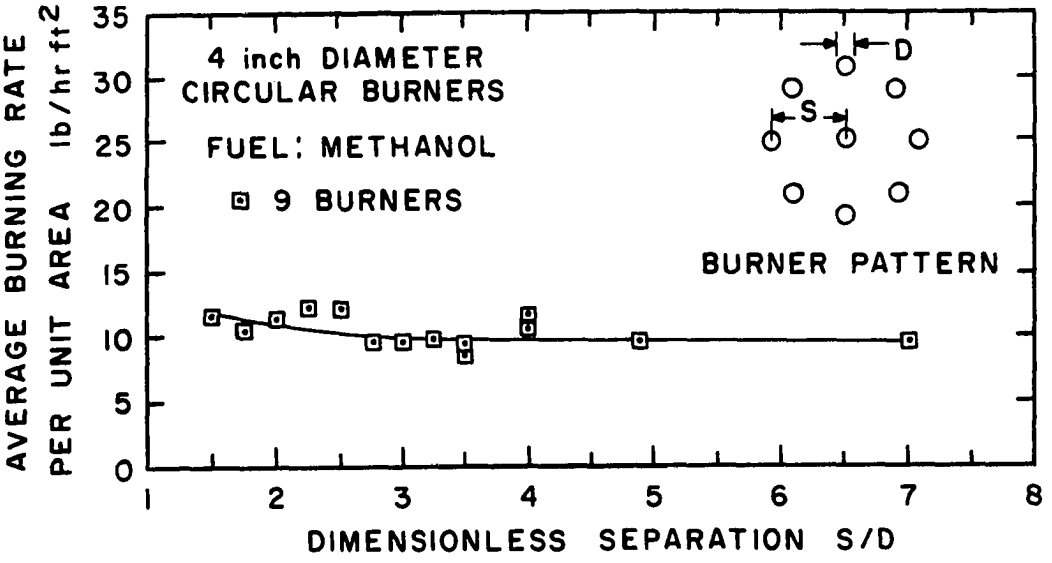

Figure 33. Average Burning Rates of Interacting 4-Inch Methanol Fires.

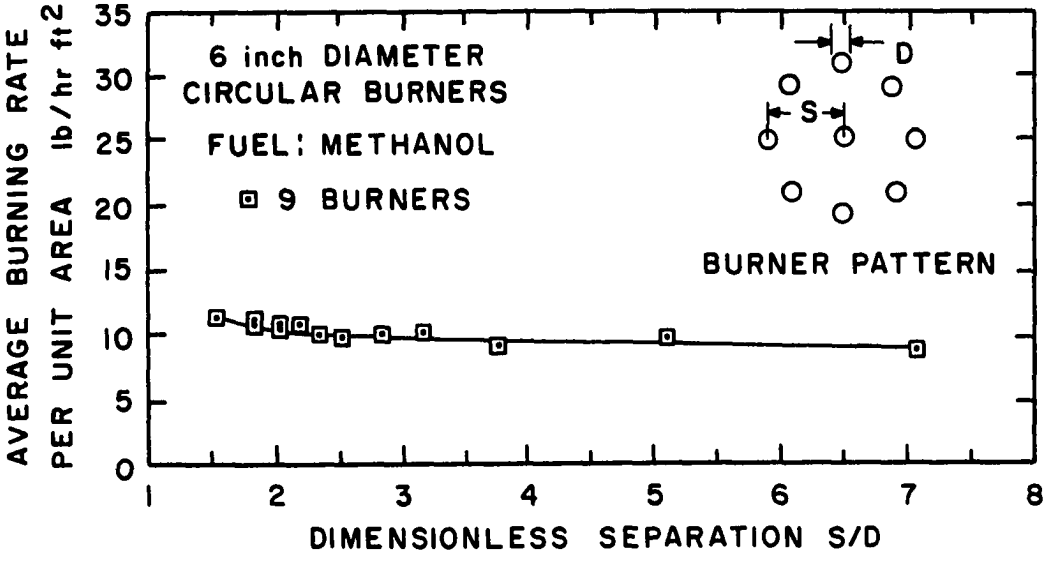

Figure 34. Average Burning Rates of Interacting 6-Inch Methanol Fires.

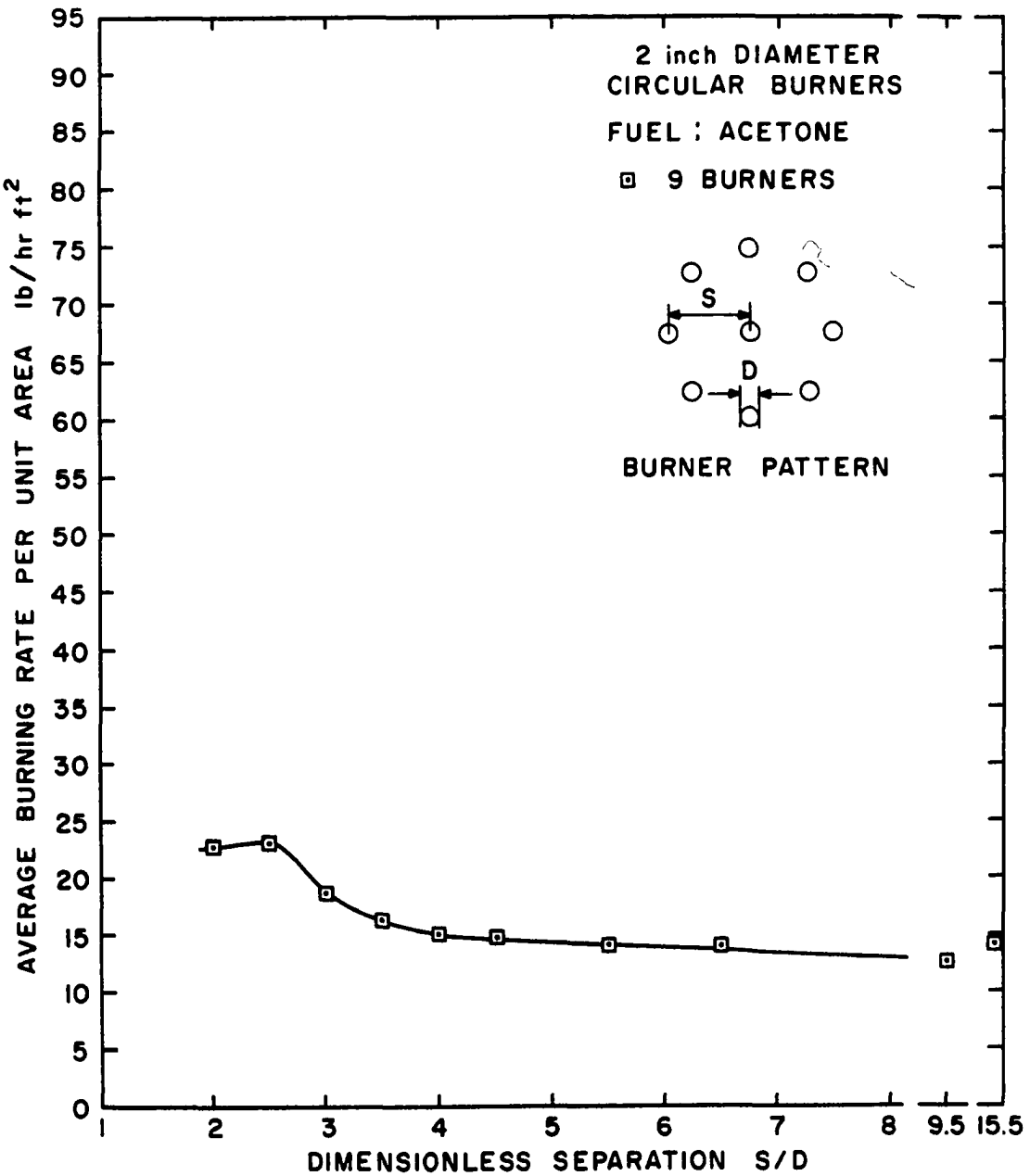

Figure 35. Average Burning Rates of Interacting 2-Inch Acetone Fires.

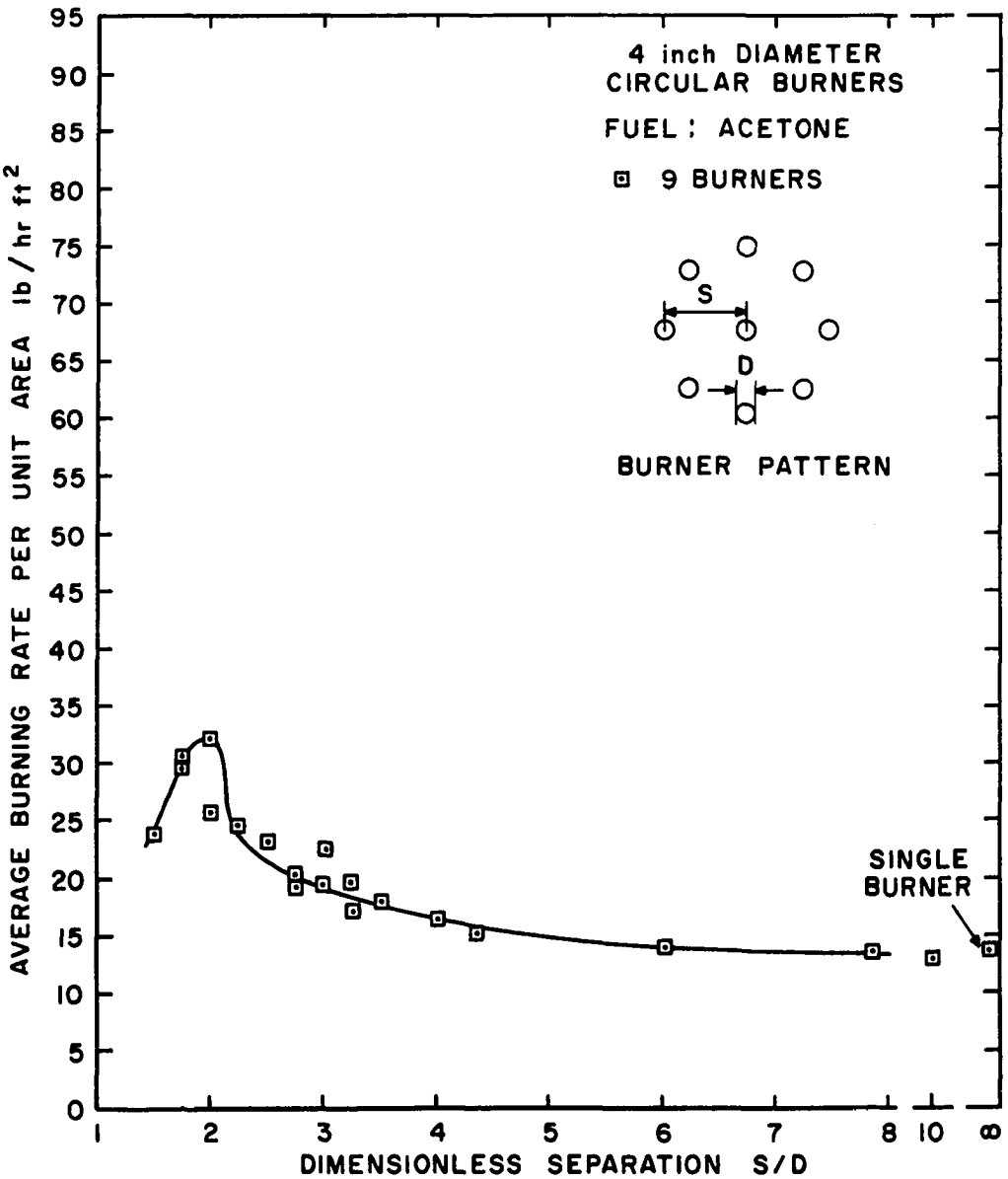

Figure 36. Average Burning Rates of Interacting 4-Inch Acetone Fires.

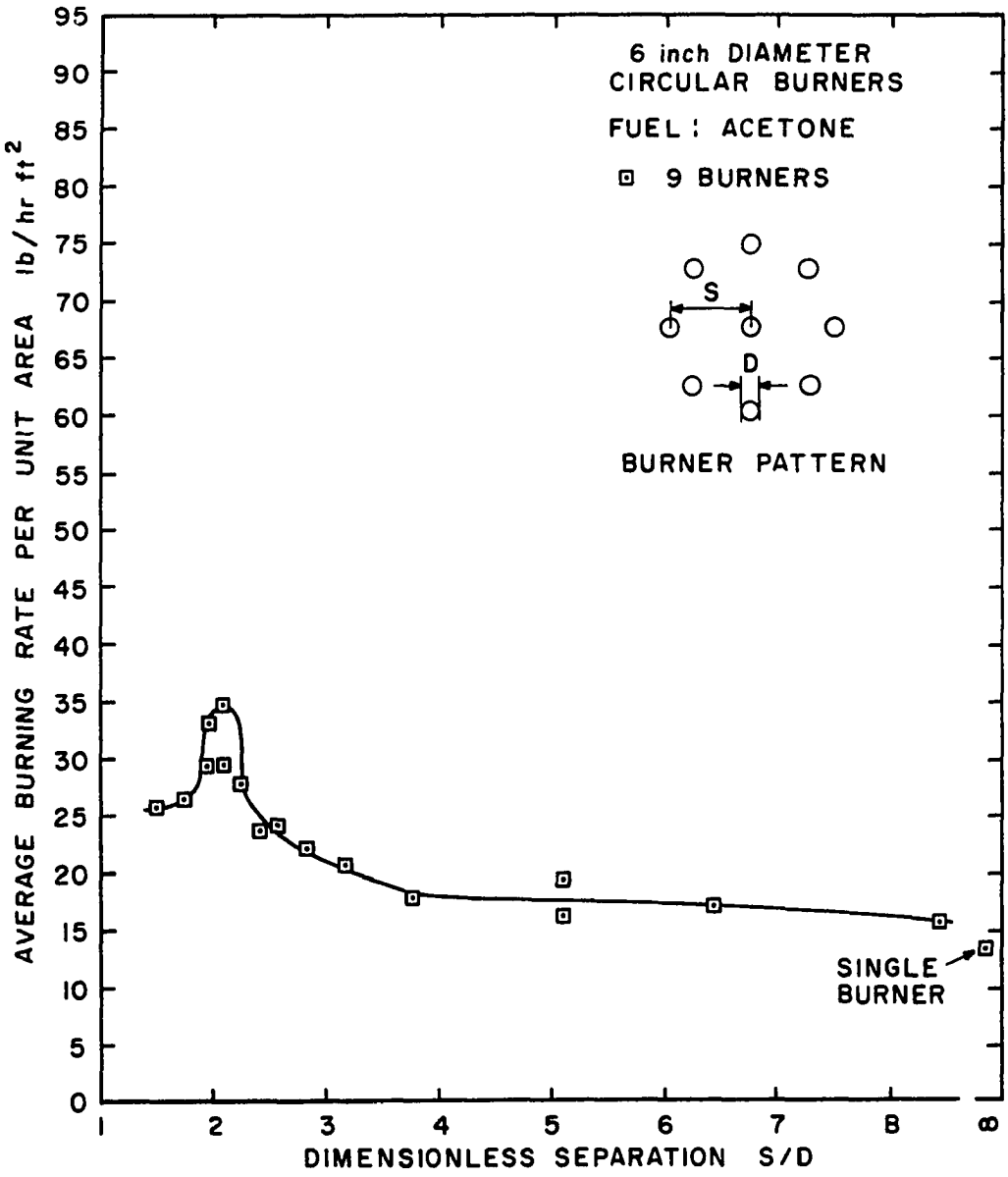

Figure 37. Average Burning Rates of Interacting 6-Inch Acetone Fires.

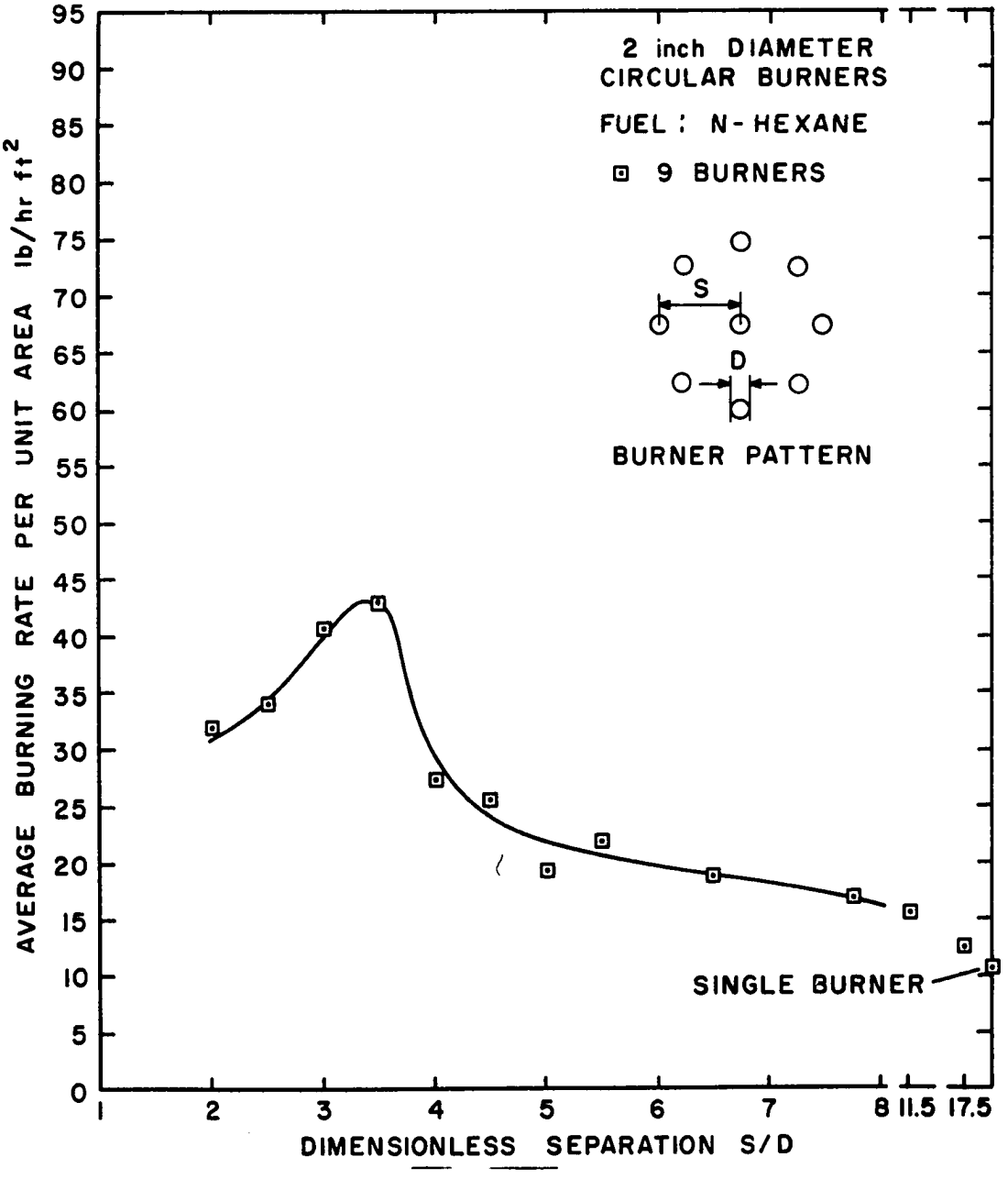

Figure 38. Average Burning Rates of Interacting 2-Inch n-Hexane Fires.

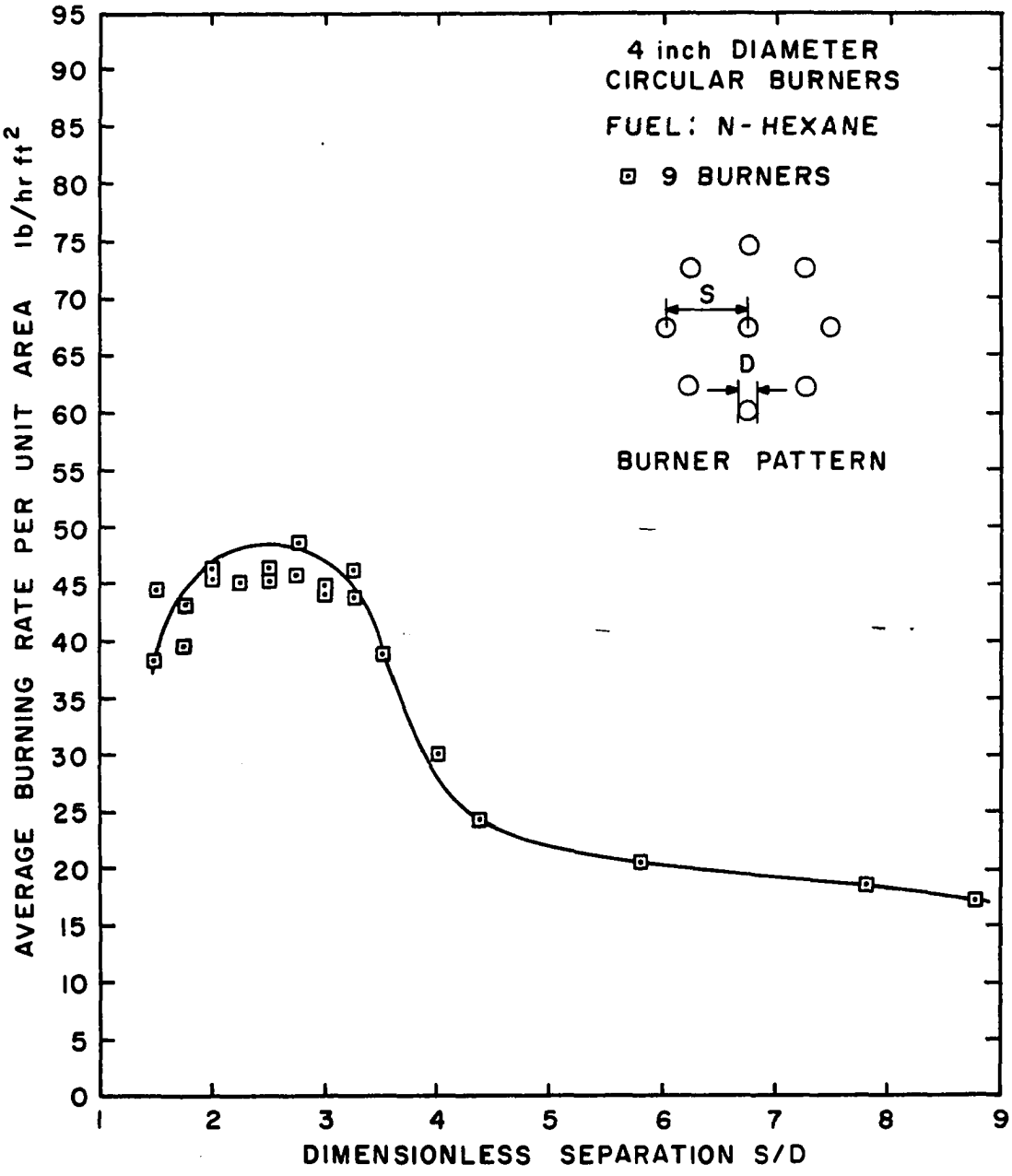

Figure 39. Average Burning Rates of Interacting 4-Inch n-Hexane Fires.

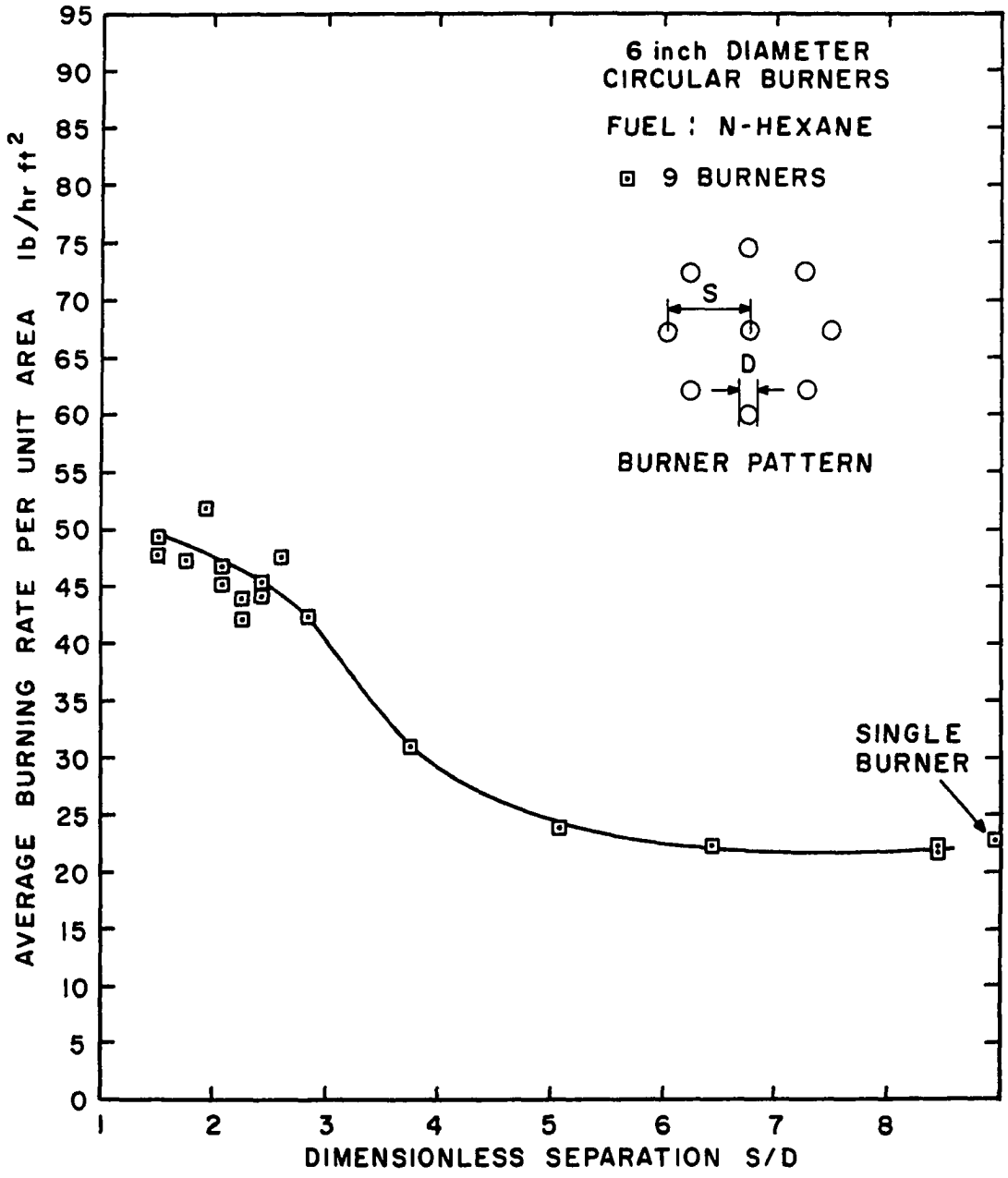

Figure 40. Average Burning Rates of Interacting 6-Inch n-Hexane Fires.

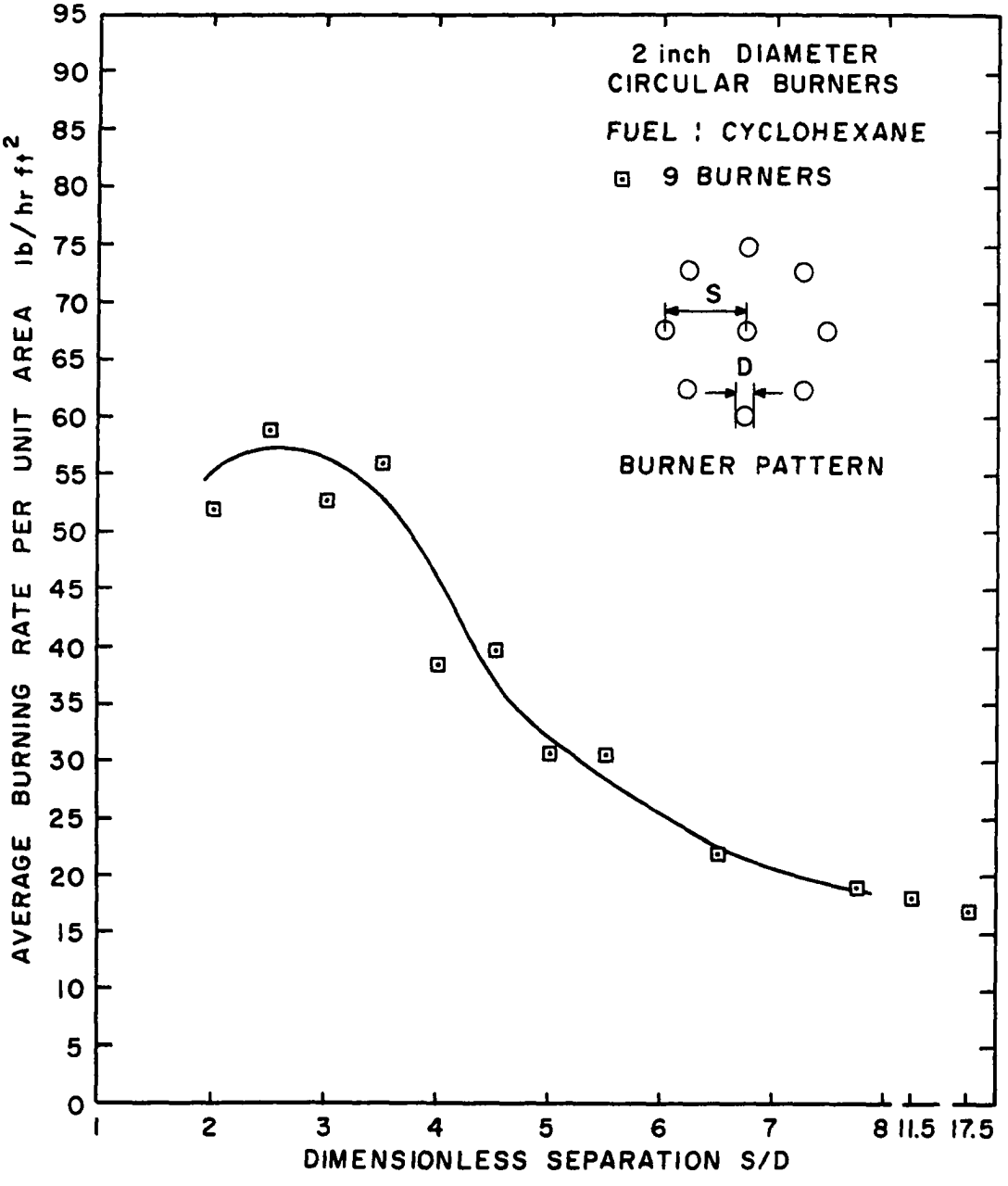

Figure 41. Average Burning Rates of Interacting 2-Inch Cyclohexane Fires.

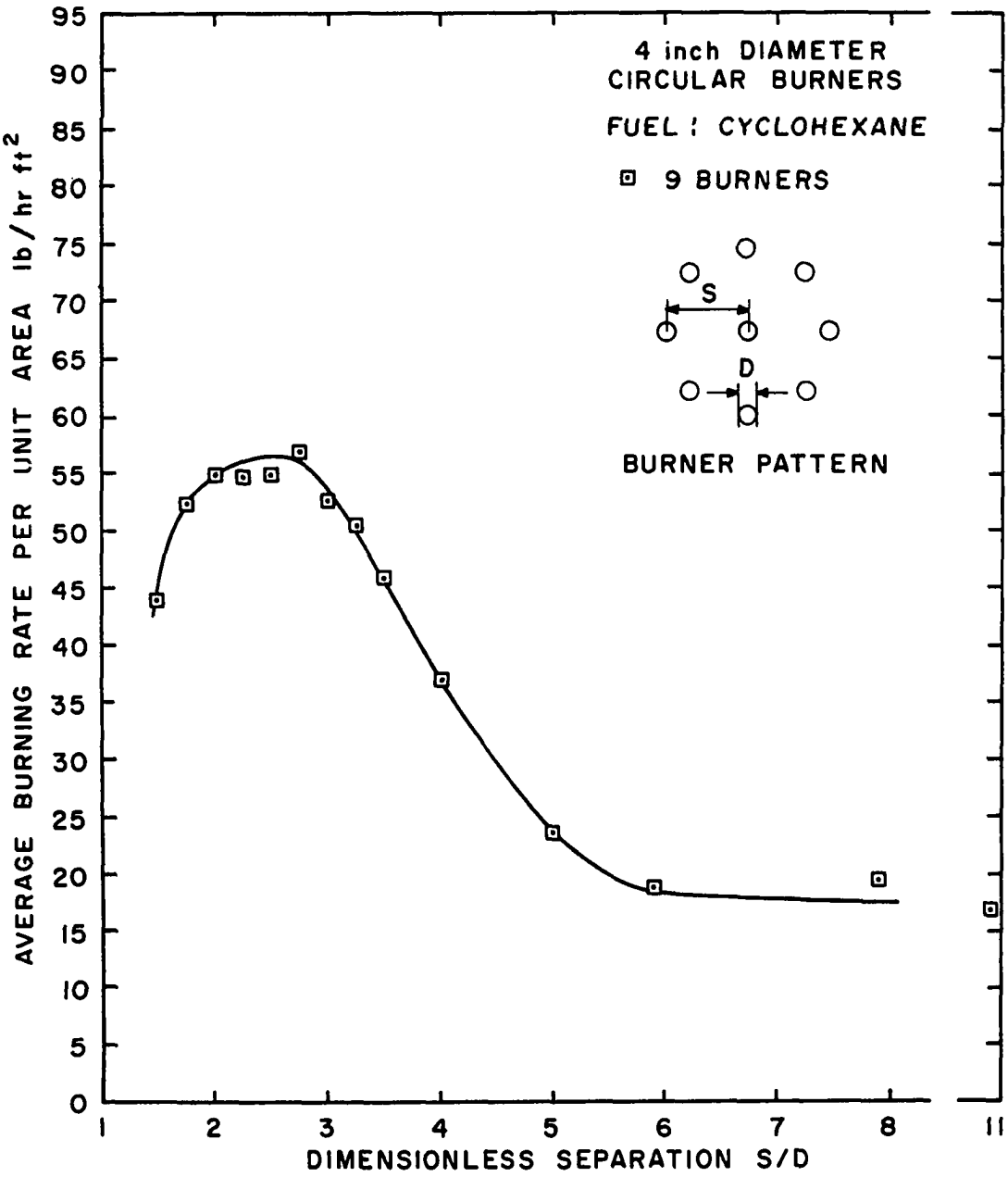

Figure 42. Average Burning Rates of Interacting 4-Inch Cyclohexane Fires.

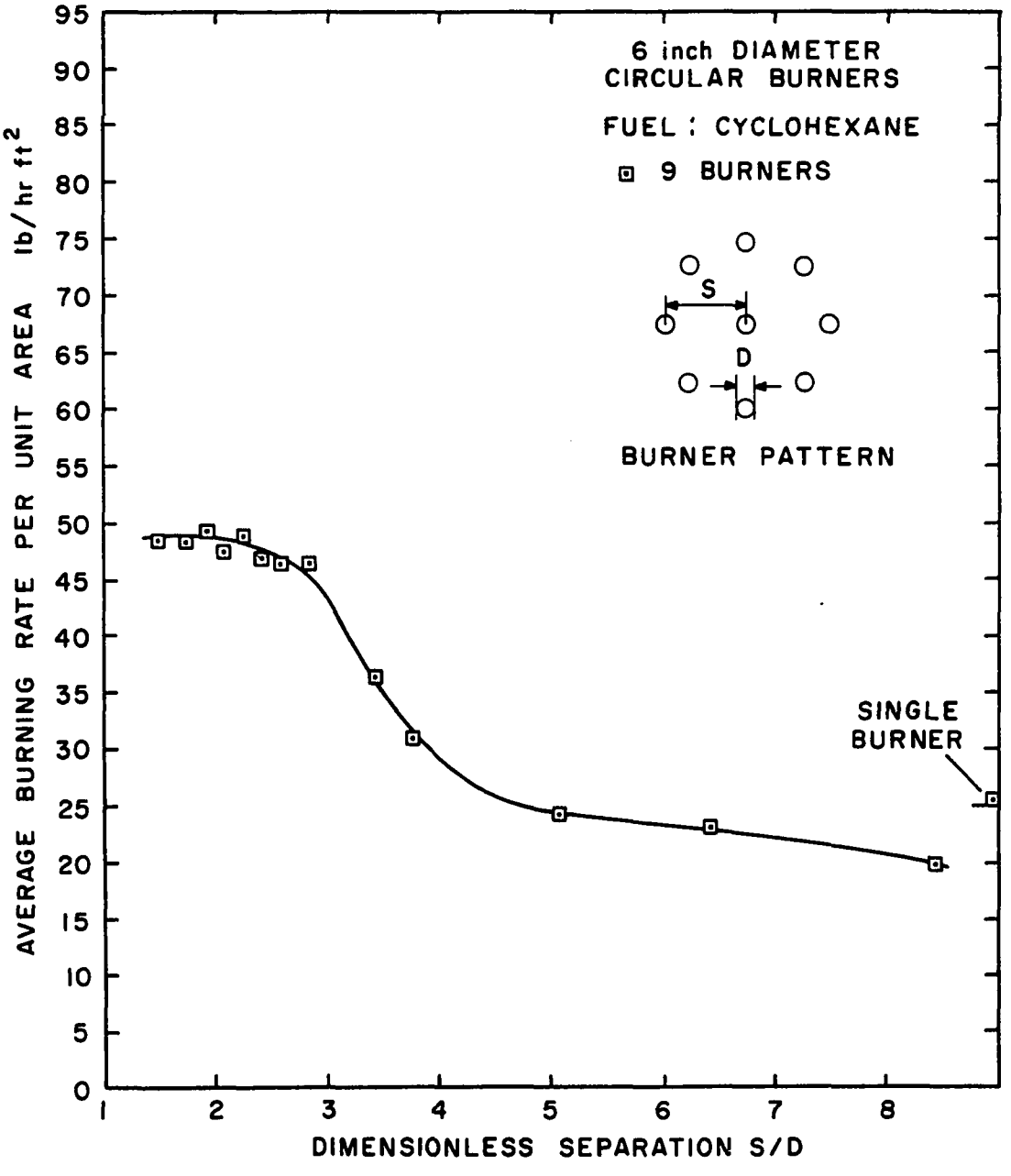

Figure 43. Average Burning Rates of Interacting 6-Inch Cyclohexane Fires.

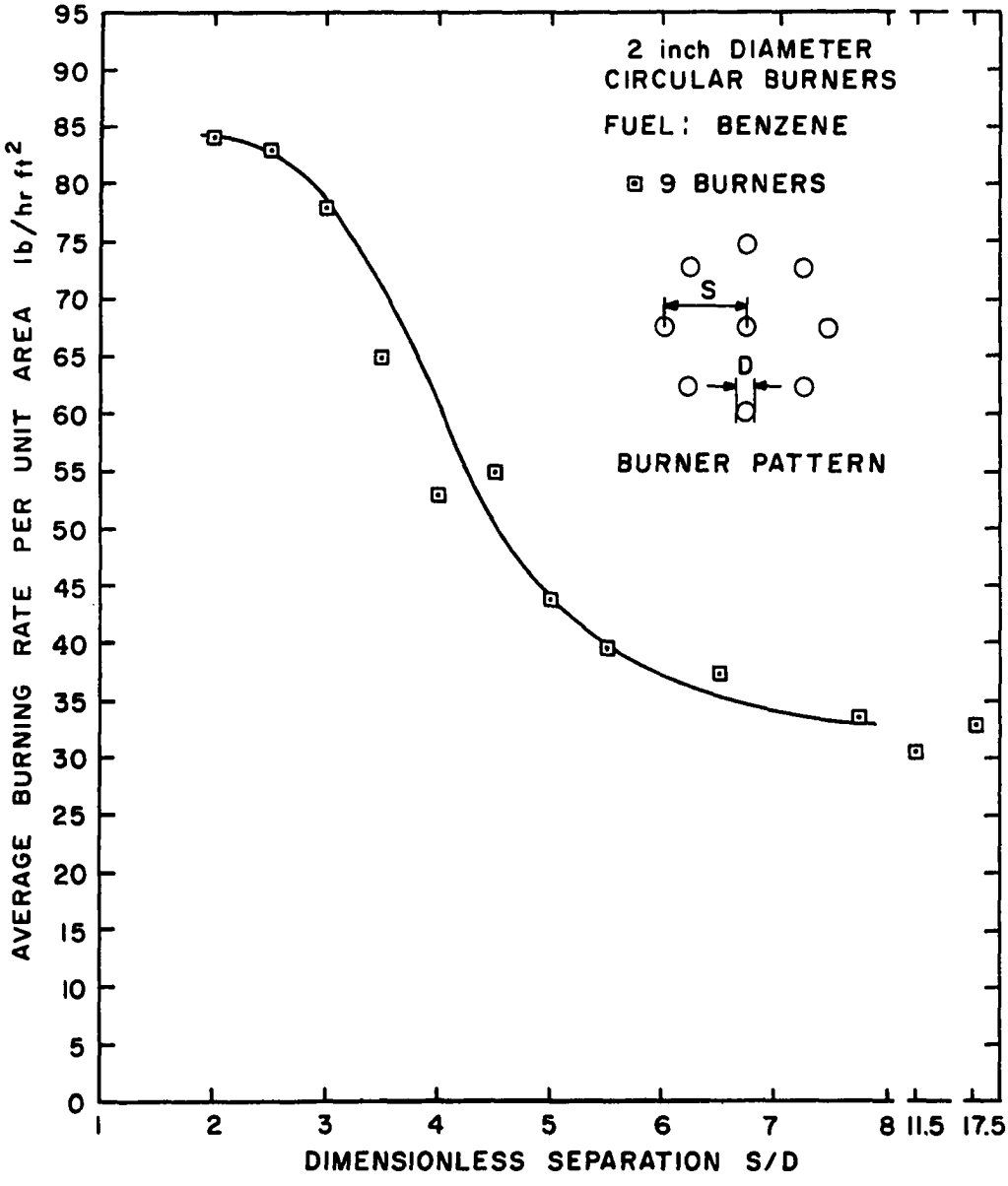

Figure 44. Average Burning Rates of Interacting 2-Inch Benzene Fires.

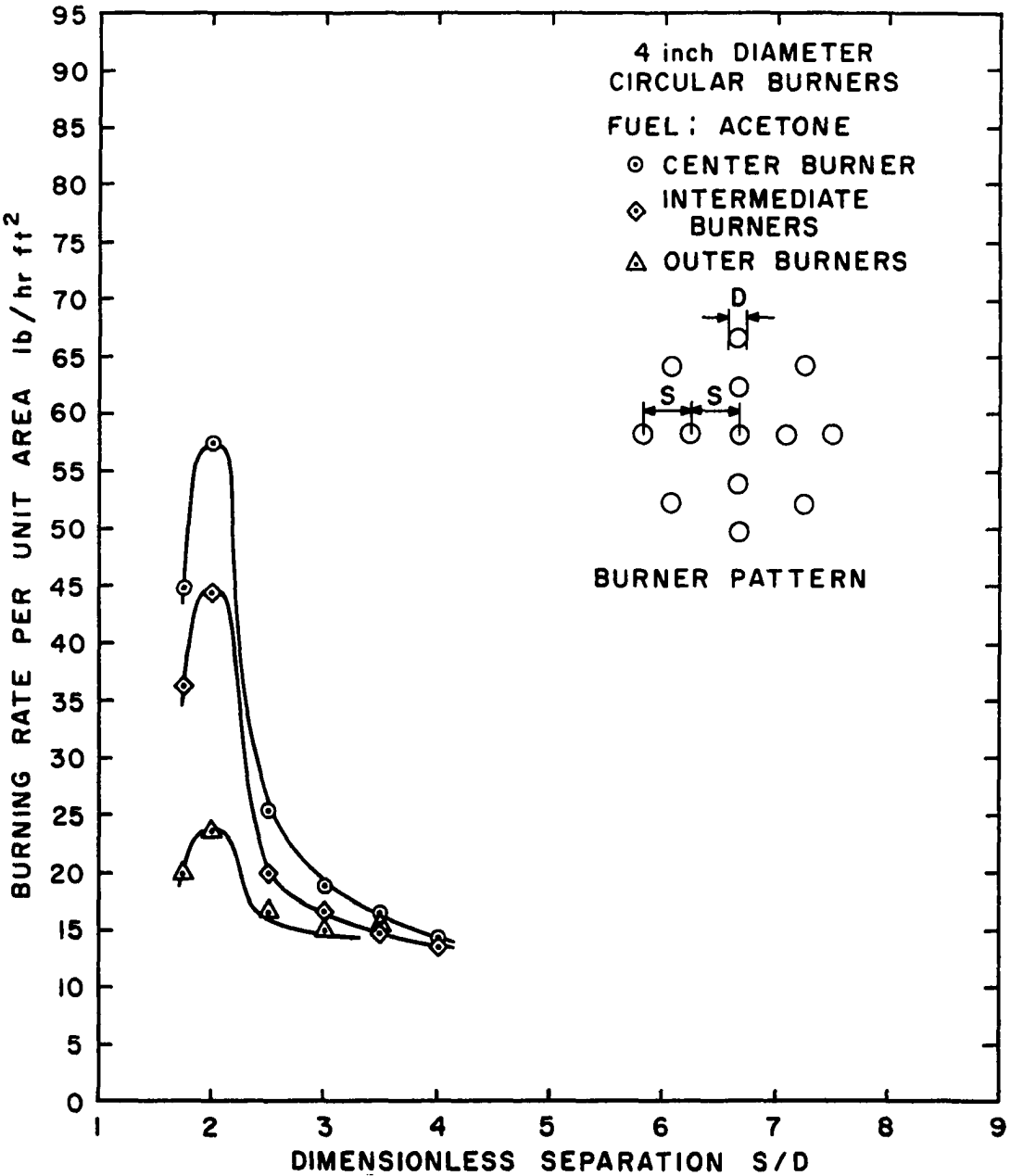

Figure 45. Burning Rates of Interacting 4-Inch Acetone Fires (Thirteen-Burner Pattern)

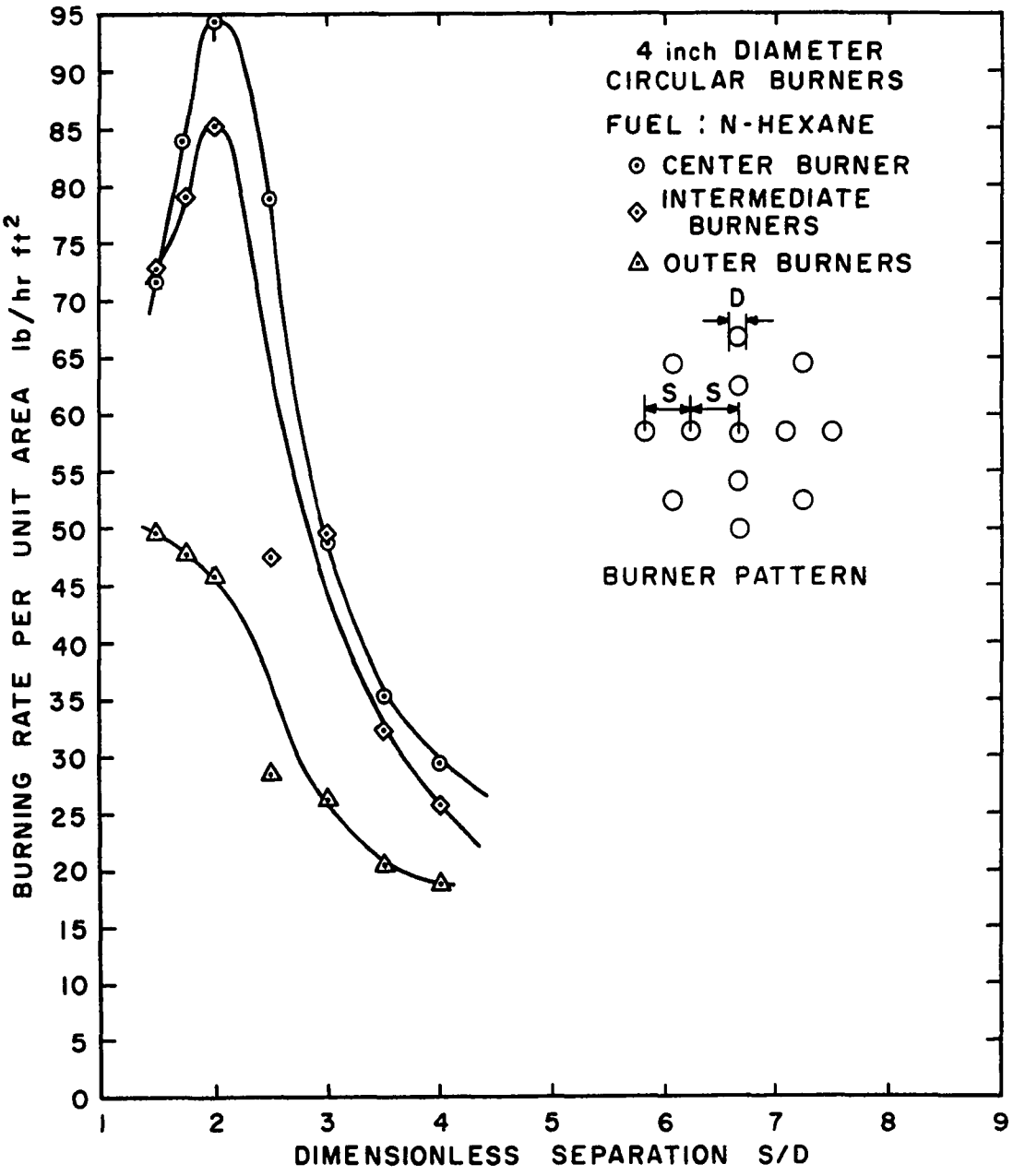

Figure 46. Burning Rates of Interacting 4-Inch n-Hexane Fires (Thirteen-Burner Pattern).

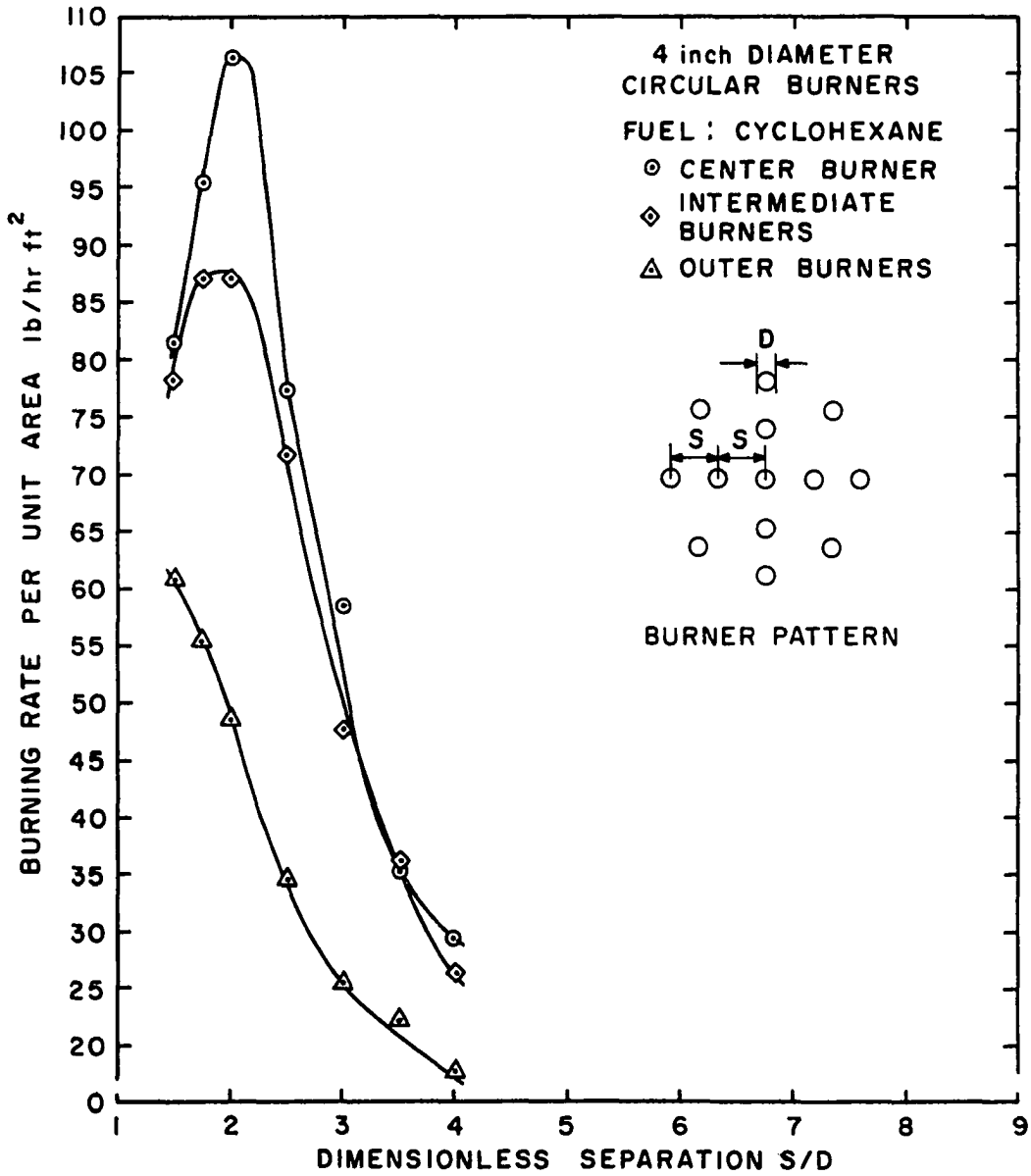

Figure 47. Burning Rates of Interacting 4-Inch Cyclohexane Fires (Thirteen-Burner Pattern).

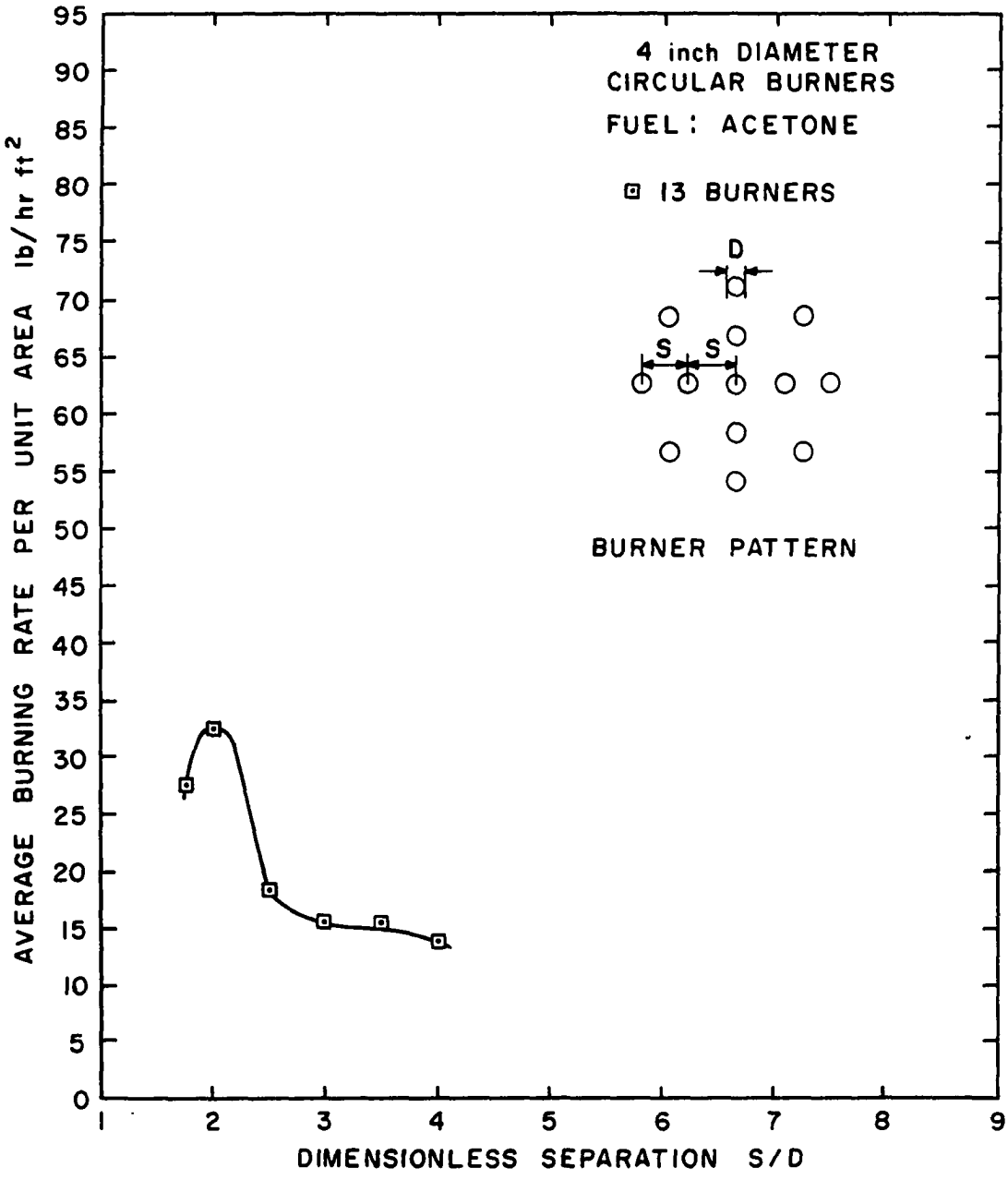

Figure 48. Average Burning Rates of Interacting 4-Inch Acetone Fires (Thirteen-Burner Pattern).

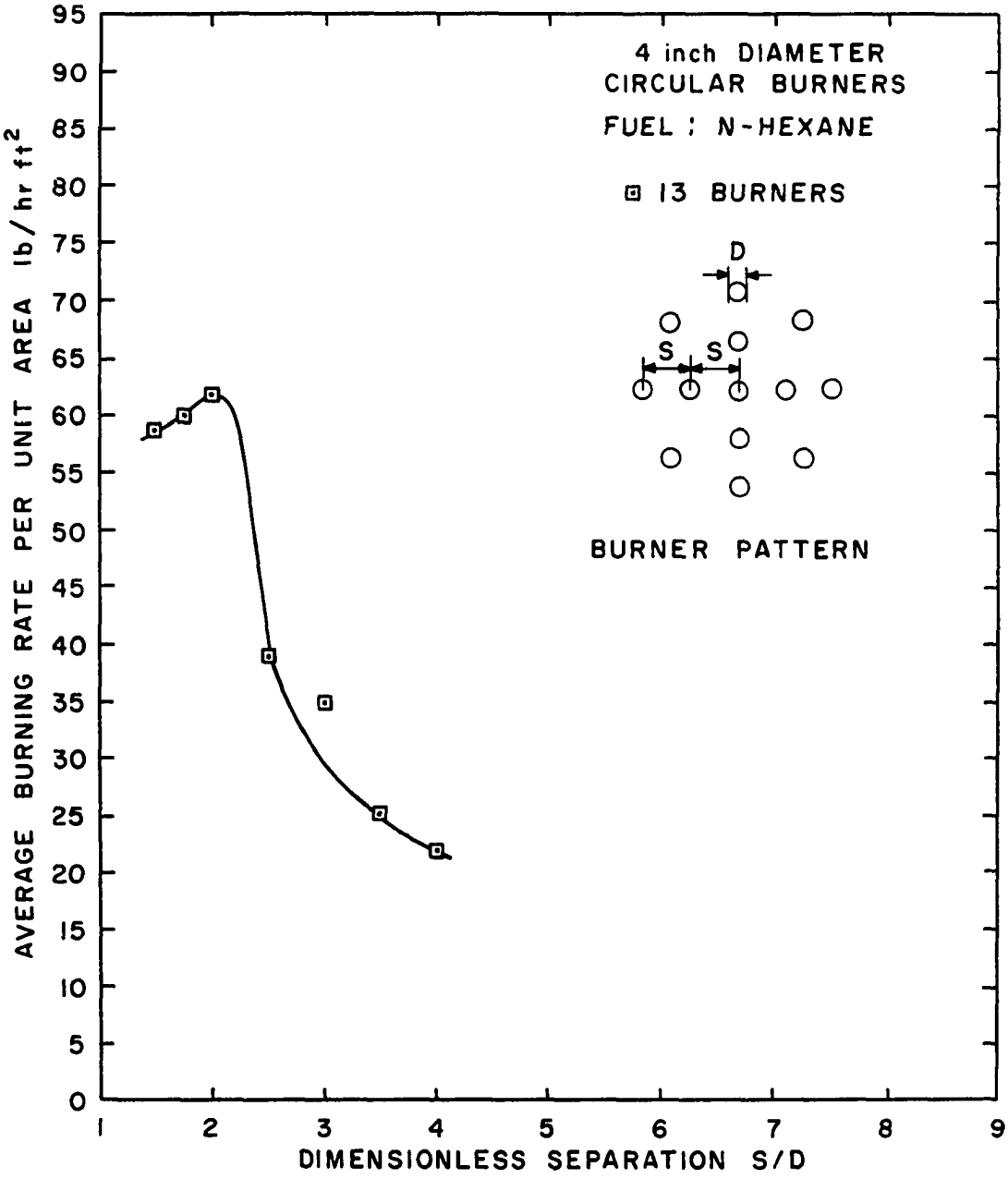

Figure 49. Average Burning Rates of Interacting 4-Inch n-Hexane Fires (Thirteen-Burner Pattern).

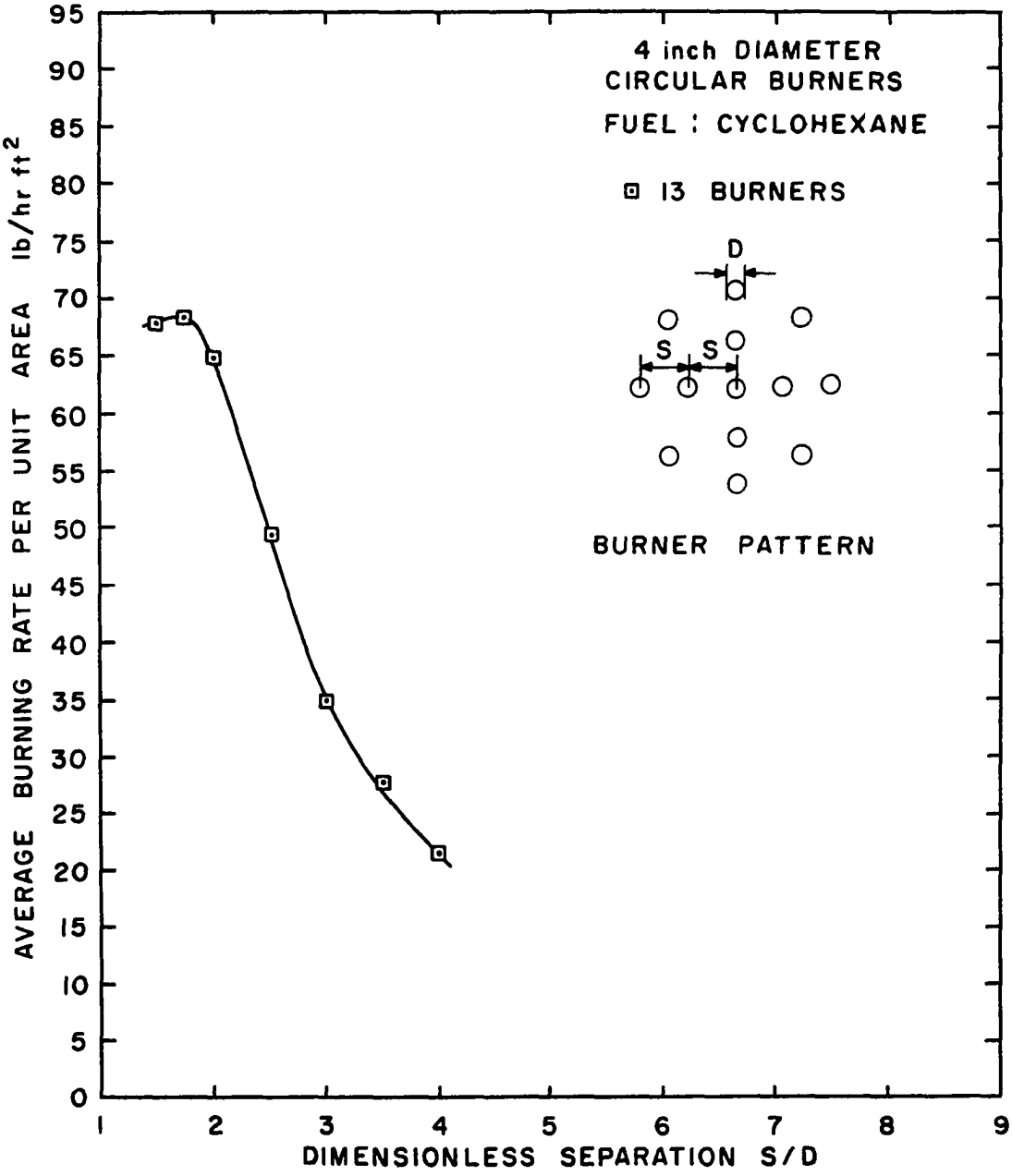

Figure 50. Average Burning Rates of Interacting 4-Inch Cyclohexane Fires (Thirteen-Burner Pattern)

respectively. The dimensionless burner separation for this burner pattern is the distance between the centers of the center burner and the four intermediate burners divided by the burner diameter. The distance between the center burner and each of the eight peripheral burners was always equal to twice the distance between the center burner and the four intermediate burners. These fires were never spaced far enough apart for interaction-free burning to occur, but they could be expected to behave in a manner similar to the fires of the nine-burner pattern at the very large burner spacings. For all three fuels, the burning rate per unit area of the center burner always had the greatest value with the peripheral burners having the lowest burning rate value at a particular burner position. The burning rate curves reached a maximum and then decreased for the center and intermediate burners, but the peripheral-burner burning rates for n-hexane and cyclohexane continued to climb as the burners were moved to their closest spacings. A comparison of the curves of average burning rate for all burners using the 4-inch burners in the nine-burner and thirteen-burner patterns shows that the number of burners employed has an effect on the total burning rate per unit area of the array. The effect is caused mainly by the different burner pattern employed as shown in Figure 5. For the thirteen-burner pattern, five of the burners were surrounded on all sides by adjacent fires,

compared with only one burner of the nine-burner pattern.

A number of the flame interaction and merging tests were repeated under as nearly the same conditions as possible in order to test the reproducibility of the experiments. Inspection of the data for the center and outer burning rates in Figures 21 through 32 shows that the difference between the burning rates for the repeated tests was nearly always much less than 10 per cent of either of the burning rate values. From Figures 24 and 25 for the 4- and 6-inch acetone fires, respectively, several of the repeated burning rates for the merged fires were somewhat higher than the values from the original tests, although these fires were not repeated under exactly the same conditions. These original merging acetone tests were made on the burning table before the previously mentioned modifications had been made at the center surface of the table. The trends in the burning rate data also showed little scatter. The data for slightly different burner separation distances showed the most scatter for the small fires under conditions of interaction-free burning and for the largest fully merged fires. The small fires, when widely separated, were very sensitive to any stray air flow in the room. As mentioned previously, the large fully merged fires tended to act like a fire from a large single burner and the fire column was also sensitive to stray air flow in the room.

In summary, the trends in the burning rates as burner separation distance was varied depended both on the fuel and burner size used. The burning rate of multiple methanol fires increased very little as the burners were brought very close together; no merging of the methanol flames was even observed. For large burner separation distances, the acetone burning rate values did not change, although the burning rate of the center burner was increased to approximately 350 per cent of its interaction-free value when the burner spacing was such that the flames began to merge, the burning rate peaked and then dropped with further decreases in the burner separation distance, as shown in Figure 25. Both the n-hexane and cyclohexane burning rates for the 2- and 4-inch burners peaked at the onset of merging as did the acetone burning rates, although for the 6-inch burners, as shown in Figure 31, the peripheral-burner burning rates for these two fuels did not drop as the flames became fully merged but continued to increase as the burner separation was decreased. The maximum burning rates per unit area were obtained at the onset of merging of the benzene flames, even though only 2-inch burners were used. The burning rates for benzene behaved similarly to those for the largest cyclohexane fires in that the peripheral-burner burning rates continued to increase as the flames became fully merged.

Effect of Heat Feedback to the Fuel on the Burning Rate

The burning rate of liquid-fueled fires is heavily dependent on the heat feedback from the flame to the fuel. Radiation and convection were the main heat feedback mechanisms from the fire to the fuel for the rimless burner tests since the burners were embedded in insulation up to their rims, which were tapered to minimize conduction effects. In addition, the burners were always kept essentially flush full with fuel. The conduction of heat from the burner walls to the fuel was therefore considered negligible. The flames studied in the tests ranged from the essentially transparent flames of methanol, where radiative heat feedback to the fuel is probably minor compared to convection, to the opaque flames of benzene where radiative heat feedback predominates. Many of the trends of the burning rate curves mentioned previously can be explained by considering the increases or decreases in radiation and convection heat feedback to the fuel and the relative importance of one of these modes of heat feedback in contrast to the other for the various fuels and spatial arrangements.

Burgess, Strasser, and Grumer (6) studied some of the radiative properties of several liquid fuels. Among those fuels studied were methanol, n-hexane, and benzene. They found that radiation from methanol flames was very strongly absorbed by liquid methanol. Liquid benzene absorbed its flame radiation less readily than methanol,

and liquid hexane absorbed its radiation to a slightly greater extent than benzene. They also found that methanol vapor absorbed more of its flame radiation than did either hexane or benzene.

A study of the burning rates of the various fuels indicates that the main cause of the very great increase in burning rate as the fires begin to merge is the increase in radiation to the fuel surface from the adjacent flames. The radiative output from the methanol flames was very low compared to that of the other fuels burned in the present studies. As noted above, the methanol vapor over the liquid surface tends to absorb the flame radiation, reducing the amount of radiation reaching the fuel surface. Only a slight turbulence if any was observed in these methanol flames. The amount of convection from the flame to the fuel was therefore held to a lower value than if these flames had been highly turbulent. In highly turbulent flames, the hot gases in the lower portion of the flame tend to sweep across the fuel surface due to the turbulence in the flame columns. The ratio of the heat of vaporization to the heat of combustion (the fraction of the heat liberated by combustion that must be fed back to the fuel to maintain a steady vaporization rate, as described previously), is also much greater for methanol than for any of the other fuels studied due to the higher heat of vaporization of methanol. The rather small amount of heat transfer back to the fuel

therefore keeps the methanol burning rate low. The small burning rate enhancement observed for the center burner as the methanol flames were brought close together was probably due to slightly increased convection transfer to the fuel in this burner rather than any influence of radiation from the adjacent flames.

The flames from acetone fires had a much greater radiative output than the methanol flames, and the acetone burning rates were seen to increase sharply as the acetone fires were brought close together. A comparison of the peak burning rates of acetone flames from the three sizes of burners shows that the peak burning rate per unit area increases considerably as larger burner sizes are used, but the burning rates at large separation distances for these three burner sizes increase very little. The flames of acetone, while being luminous, were less opaque to their own radiation than the other fuels such as cyclohexane and benzene; therefore less of the flame radiation was absorbed by the acetone flame itself before it could penetrate to the fuel surface. The burning rate per unit area for the merging fires was increased as larger burner sizes were used, due to the much larger column of flame which was present over the fuel surface. When the acetone fires were brought very close together, so that the flames were fully merged, the burning rate was observed to drop sharply. This burning rate drop was caused by the blockage of air to

the burners due to the adjacent flames. The extreme closeness of the flames restricted the convective heat transfer from flame to fuel at the center burner. The resulting decrease in burning rate also decreased the size of the fire column over the fuel. The acetone flame is probably transparent enough to its radiation that radiation from most parts of the fire column can get to the fuel before being absorbed by the flame itself. The smaller fire column therefore reduced the amount of radiation back to the fuel and further reduced the burning rate.

The flames from both n-hexane and cyclohexane had a large radiative flux output and the burning rates of these fuels were also greatly increased by the presence of adjacent flames. The burning rate curves for these two fuels were quite similar, particularly for the larger burner sizes. In addition the values of measured radiative flux output and the ratio $\Delta H_v/\Delta H_c$ were nearly the same.

Both hexane and cyclohexane flames are much more opaque to their own radiation than is acetone. The effects of this opaqueness can be seen by comparing the burning rate curves for the various fuel burner sizes used. The burning rates per unit area at the onset of merging increased as the burner size was increased from 2 to 4 inches in diameter, but as the burners were increased from 4 to 6 inches in diameter the peak burning rates per unit area remained nearly the same.

The ratio of burning rate at the onset of merging to the single-burner burning rate was used in the merging studies as a measure of the burning rate enhancement due to flame merging. The values of this ratio for the various fuels and rimless-burner sizes are given in Table 6. It is seen from this table that the (m_p/m_s) ratio decreases as larger burner sizes are used for the rather opaque hexane and cyclohexane flames. However, for the more transparent acetone flames, this ratio continues to increase with burner diameter but at a progressively reduced rate. The values of the (m_p/m_s) ratios as well as the burning rate per unit area values at the onset of merging mentioned in the preceding paragraph indicate that the effect of merging on the burning rate will become less as the flame size becomes larger.

As the merged flame column becomes large, the radiation from part of the opaque fire column is absorbed by the flame itself before it can reach the fuel surface. An increase in the size of the merged flame column therefore contributes less additional radiation flux to the fuel surface than when the flames were smaller.

As the flames were moved close enough together to be fully merged, the center burning rate of hexane or cyclohexane always dropped sharply due to insufficient air and a possible decrease in convective effects, as was noted in connection with acetone. As mentioned previously, a layer of unburned fuel vapor was observed to form over the center

burner at these fully merged burner positions. This blanket of vapor probably absorbed some of the flame radiation.

It was noted in the burning rate curves for hexane and cyclohexane in the 6-inch burners that the burning rate of the eight peripheral burners continued to climb as the burner separation distance was decreased, while the center-burner burning rate dropped sharply as the fires became fully merged. The radiation from the hexane and cyclohexane flames plays a very important part in determining the burning rate of these fuels; therefore the shape of the flame over the fuel is important. As the flames were brought close enough together to interact, the peripheral flames were rather small and leaned toward the center of the burner array producing a conical flame shape, in which case less radiation was directed back to the fuel surface of the peripheral burners. As the flames were brought close enough together to begin to merge, the flame shape once again became cylindrical, so that the flames were more directly above the peripheral burners. More radiation was thus directed back to the fuel to increase the burning rate even though the convective effect decreased as the flames merged.

The flames from benzene were very opaque. This opaqueness apparently caused the burning rate per unit area curves for benzene in the 2-inch burners to behave in a manner similar to the burning rate curves for the above-mentioned large hexane and cyclohexane flames.

In summary, the trends in the burning rate versus burner separation curves can be explained by considering the increases or decreases in radiative and convective heat feedback to the fuel and the relative importance of one of these modes of heat feedback in contrast to the other. The increase in radiation to the fuel surface from the adjacent flames is the main cause of the large increase in burning rate as the fires begin to merge although increased convective heat feedback due to the proximity of other fires contributes to the burning rate increase. For the smaller as well as the more transparent fully-merged fires, the blockage of air to the fire array center by the outer portion of the fire array caused a decrease in heat feedback to the fuel with a resulting drop in burning rate. For the larger as well as the more opaque merged fires, the increased radiative heat feedback to the peripheral-burner fuel due to the change in fire column shape was enough to offset any decrease in convective heat feedback; therefore, the peripheral-burner burning rates did not drop as these fires became fully merged. As shown in Figures 38 through 40, the peak values of n-hexane burning rate per unit area at the onset of merging showed little or no increase as the burner size was increased. For opaque flames from fuels such as n-hexane, much of the radiation from the merged fire column is absorbed by the fire itself before it can reach the fuel; therefore, the larger flame columns

over the fires from the larger burners contribute little extra radiation back to the fuel surface.

Comparison of the Burning Rates for Exposed-Rim and Rimless Burners

Emmons (10) examined the effect of exposed burner rims on the burning rate of a liquid fuel. He burned acetone in single shallow pans (¼-inch deep) of several sizes. His burning tests were conducted both for the pan on top of a table surface and the pan embedded in the surface in a manner similar to that used in the present merging studies. For pan diameters less than 4 inches, he found that the burning rate was greater with the pan placed on the table (exposed-rim pan) than for the pan embedded in the surface (rimless pan). The effect of the exposed pan rim appeared to make little difference in the burning rate for pans about 4 inches or larger in diameter. (The larger effect for the small pans can be attributed to their larger wetted surface to fuel volume ratio.) Emmons postulated a four-step mechanism for heat transfer from flame to the fuel by way of the exposed pan rims. This mechanism consisted of radiation from the flames to the table top, convection heat transfer from the table top to the induced air, convection transfer from the induced air to the pan rim, and conduction through the rim to the fuel.

For multiple burner tests, the effect of the conduction of heat from an exposed burner wall to the fuel

can be shown by comparing the burning rate curves obtained in the present studies for the 4 3/16-inch diameter exposed-rim burners and the 4-inch diameter rimless burners. The difference in the burning rates obtained from the two types of burners also includes the effect of heating the burner bottom since the tests for the exposed-rim burners were not conducted under steady state conditions but contained a limited amount of fuel which was burned until the fuel was consumed. This heat of the pan bottom is probably not significant compared with the exposed-rim effects since the exposed-rim burning rate was obtained while the burners still contained enough fuel to absorb the majority of the radiation from the flame before it could reach the burner bottom. As noted previously, Zabetakis and Burgess (30) found that most of a flame's radiation was absorbed by a very small depth of the liquid fuel for fuels such as those used in the present tests.

The burning rate curves in Figures 15 and 33 for the methanol flames are essentially the same for both exposed-rim and rimless burners. If Emmons' four-step heat transfer mechanism (mentioned above) is considered, the amount of radiation from the flames to the table top would be small for the non-luminous methanol flames. The lack of significant radiation heating of the table top would subsequently result in reduced heating of the induced air and therefore a smaller amount of heat conduction through the

burner rim to the fuel. Radiation from adjacent flames directly to the exposed burner wall would also be too small to affect the methanol burning rate significantly.

The curves of burning rate per unit area for acetone with the exposed-rim and rimless burners are shown in Figures 15 and 36, respectively. Both of these burning rate curves are based on the average burning rates of all nine burners of the array. The acetone curves for both cases are seen to have similar shapes, and the burning rates per unit area at the largest burner separation distances are nearly identical for the two types of burners. At these large burner separation distances the acetone flames have little effect on one another; therefore they can be considered as being single burner fires. The results given by Emmons, as mentioned above, also showed that exposing the burner rim had little effect on the acetone burning rate for single pans 4 inches or larger in diameter.

As the acetone flames began to interact and merge, the burning rates with the exposed-rim burners increased to greater values than for the rimless burners. The greater exposed-rim burning rates were caused by the increased heating of the burner walls due to radiation from the adjacent flames directly to the burner walls. The adjacent flames also heated the burner wall by the additional heating of air induced to the flame with subsequent convective heating of the wall. The burning rate of the center burner

of the array was particularly affected by radiative and convective heating of the exposed center burner wall when the fires were interacting or merging. The increase in the center burning rate was reflected in the average burning rate of the array.

A comparison of the burning rate curves for hexane, given in Figures 15 and 39 for the exposed-rim and rimless burners, respectively, shows the effect of burner-wall heating by the adjacent flames even more clearly. At corresponding burner positions, the burning rates were always much higher for the exposed-rim burners at the burner spacings used. Hexane burning rates for the exposed-rim burners were not obtained at large enough burner spacings to have interaction-free burning, but such interaction-free burning would be expected to be only slightly higher, if at all, than the corresponding interaction-free burning in the rimless burners. The exposed-rim burning rate values for hexane ranged from 1.5 times as great at the larger burner spacings used to over 2 times as great as the rimless burner values at the onset of merging. Hexane flames give off much more radiation than acetone flames; therefore, the heating of the exposed burner walls by radiation transfer directly from the adjacent flames is greater. According to Emmons' heat transfer mechanism, the large radiation flux from these hexane flames would also increase the convective wall heating due to the adjacent

flames. However, the contribution of these convective effects due to the exposed rim is relatively less significant in the case of multiple fires than for single fires.

An additional factor in increasing the hexane burning rates of the exposed-rim burners over those of the rimless burners is flame trailing. As noted previously, flame trailing was observed for the hexane fires from both types of burners. The presence of other fires, even at large burner spacings, caused the outer fires to lean toward the center of the array. For the exposed-rim burners, the leaning flame was in direct contact with part of the burner wall as it trailed over the rim and down on to the table. The subsequent radiative heating of this portion of the burner wall further increased the burning rate of the exposed-rim burners over that of the rimless burners.

With cyclohexane used as fuel, effects of the exposed burner walls were similar to those described above for n-hexane.

It is therefore seen that, except for methanol, the burning rates of the interacting or merging flames were always higher for the exposed-rim burners than for rimless burners of the same size; in fact, the peak hexane burning rate for the exposed-rim burners was over two times as great as the peak burning rate for the rimless burners. The greater burning rates of the exposed-rim burners were caused by the conduction of heat through the exposed burner wall to the fuel. The burner wall was heated by the hot air entrained into the

burner array and the radiation from adjacent fires directly to the exposed burner wall. Additional wall heating was caused by direct contact of the flame and the burner wall due to the flame trailing effect.

Burning Rate Correlations

Burning rate correlations similar to those previously described for the exposed rim burners were obtained for the various fuels and burner sizes in the rimless burner tests. Again the objective was to predict the behavior of multiple fires for other sizes of fuel sources and other liquid fuels. Correlations were developed both for the center-burner burning rates and for the average burning rates based on all nine burners of the array.

The burning rates of most interest in the present studies were those obtained as the individual flames actually began to merge since these burning rates were the largest obtained for a particular fuel and burner size. It was therefore desired to obtain a burning rate function which would have the same value for the various fuels and burner sizes at the onset of merging. A burner spacing function was also needed which would have a common value at the onset of merging for all the fuels and burner sizes. In most cases, it was found that when such functions were obtained, their values for the different fuels and burner sizes were approximately the same for conditions under which interaction-free burning was obtained, or even when the flames were fully merged.

The amount of enhancement of the burning rate due to the merging of the fires played an important part in determining the separation distance at which the flames merged. The ratio of the burning rate at the onset of merging to the burning rate for interaction-free burning (m_p/m_s) is taken as a measure of this burning rate enhancement. The ratio (m_p/m_s) reflects the variations in heat feedback to the fuel, such as changes in radiation due to changes in flame volume, flame shape, or amount of unburned fuel vapor above the liquid surface. The ratio also reflects changes in opaqueness and luminosity of the flames from the various fuels.

The flame trailing effect also influences the separation distance at which the flames merge. This influence is stronger for the center burning rate than for the burning rate from the peripheral burners. The flame trailing causes the actual separation distance between the individual flames to be less than the burner separation distance. As mentioned previously this flame trailing is influenced by the density of the fuel vapor at the fuel boiling point as compared to the density of the surrounding air. The ratio (ρ_g/ρ_a) is therefore taken as a measure of the flame trailing effect. In addition, the sizes of burners used is expected to affect the burner separation distance at the onset of merging. Therefore,

$$S_p = f(D, m_p, m_s, \rho_g, \rho_a) \qquad (18)$$

The empirical burner spacing function, which was best able to provide the same value for all fuels and burner sizes at the onset of merging, was found from the data to be

$$(S/D)_p \left[\left(\frac{m_p \text{ center}}{m_s}\right)\left(\frac{\rho_g}{\rho_a}\right)\right]^a$$

for the center-burner burning rate and

$$(S/D)_p \left(\frac{m_{p \text{ ave.}}}{m_s}\right)^a$$

for the average burning rate based on all nine burners, where "a" is an empirical constant and has different values for the various correlations. The value of "a" was found by using a least-squares fit on the peak values of (S/D).

The burning rate at the onset of merging is strongly influenced by the degree of burning rate enhancement due to the flame merging. As noted above, the ratio (m_p/m_s) can be taken as a measure of this enhancement and reflects, among other things, changes in the heat feedback to the fuel due to the different flame properties for the various fuels and changes in flame size. The peak burning rate is also affected by the burning rate for interaction-free burning (m_s). When different fuels are used, the fraction of heat generated by combustion that needs to be fed back to the fuel to maintain fuel vaporization will affect the burning rate. As noted previously this heat feedback requirement is denoted by ($\Delta H_v/\Delta H_c$). In addition, the amount of flame

trailing, as represented by (ρ_g/ρ_a), influences the burning rate since the shapes of the flame columns as they begin to merge affect the amount of radiation back to the fuel and the degree of blockage of air to the burning fuel, which in turn influences the burning rate. An increase in the amount of radiation given off by the flames tends to increase the burning rate, while the blockage of air due to the surrounding flames will cause the burning rate to decrease. The burning rate at the onset of merging can therefore be expressed as

$$m_p = \text{function } (m_s, \Delta H_v, \Delta H_c, \rho_g, \rho_a) \qquad (19)$$

The burning rates were correlated using the data for a particular fuel and all burner sizes, and using the data for a particular burner size and all fuels. The burning rate data for all fuels and all burner sizes using the nine-burner pattern were then combined into a single correlation. These correlations were obtained for the center-burner burning rate and for the average burning rate and are shown in Figures 51 through 64.

The form of the best empirical burning rate function was found to be $m\left(\frac{m_p}{m_s}\right)^b$ for the correlations involving one particular fuel and all the burner sizes. For the correlations involving a particular size of burner and all fuels, the function which best correlated the data was

$$\left(\frac{m}{m_s}\right)\left(\frac{\Delta H_c}{\Delta H_v}\right)\left(\frac{\rho_g}{\rho_a}\right)^b .$$

The values of the empirical constant "b" were different for the various correlations.

The burning rate correlations for the center-burner burning rates, shown in Figures 51 through 57 were quite effective in bringing together the burning rate per unit area data. It is of interest to note the values of the exponent "b" in the burning rate function

$$\left(\frac{m}{m_s}\right)\left(\frac{\Delta H_c}{\Delta H_v}\right)\left(\frac{\rho_g}{\rho_a}\right)^b$$

when the three correlations were obtained using all fuels and a particular burner size. The exponent of the density term has a value of -3.6, -2.9, and -1.8 for the 2-, 4- and 6-inch diameter burners, respectively, and -2.9 for the 4-inch diameter, thirteen-burner pattern. As mentioned earlier, the radiative heat feedback to the fuel for the more opaque flames became less dependent on the total size and shape of the entire flame columns as the flame size (or burner size) was increased; therefore, the burning rates for the larger burner sizes were less affected by changes in flame column shape due to the flame trailing effect. This lessening dependence on flame trailing is reflected in the smaller absolute value of the exponent for the density ratio term as the burner size increases.

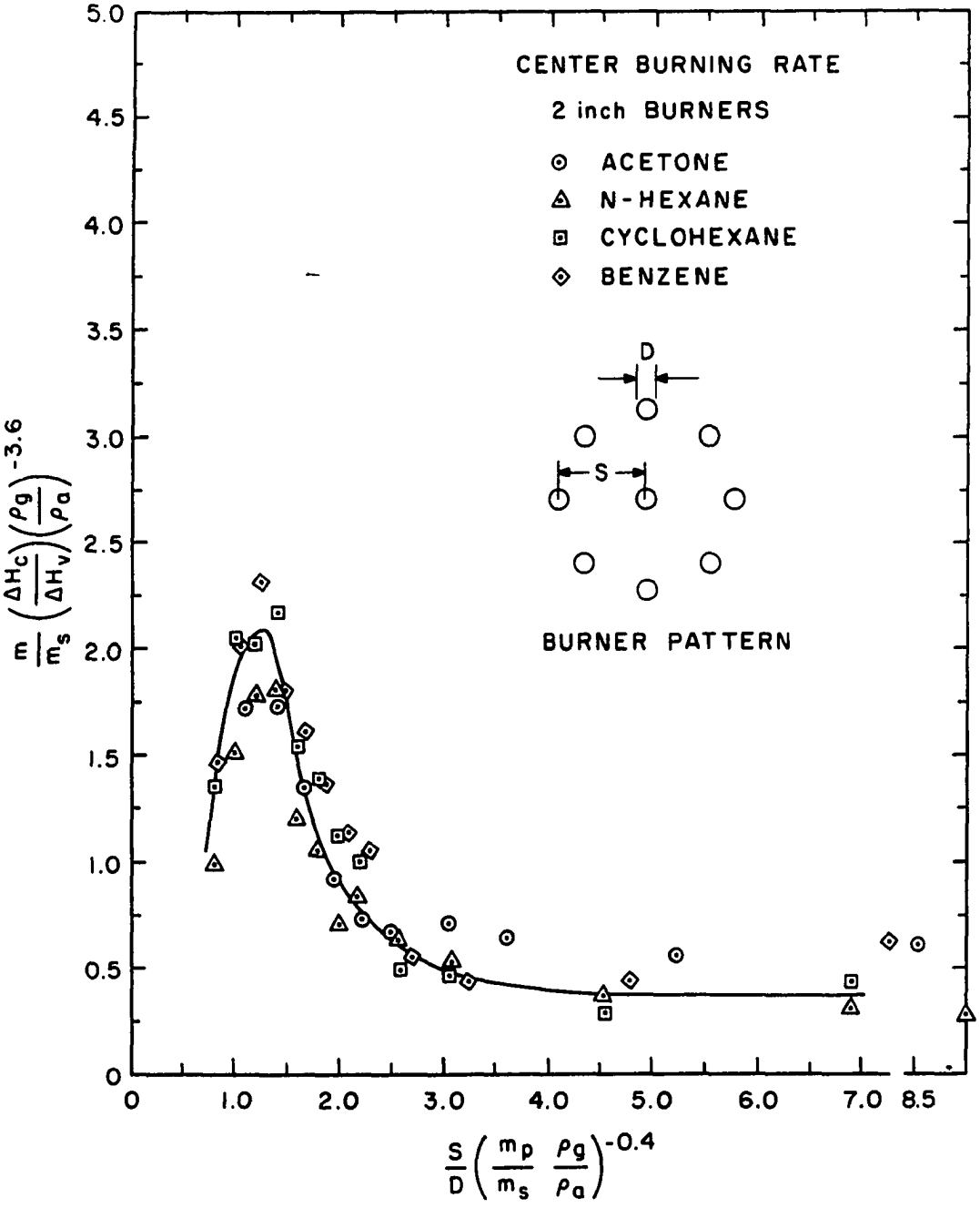

Figure 51. Correlation of Center Burning Rates for 2-Inch Rimless Burners.

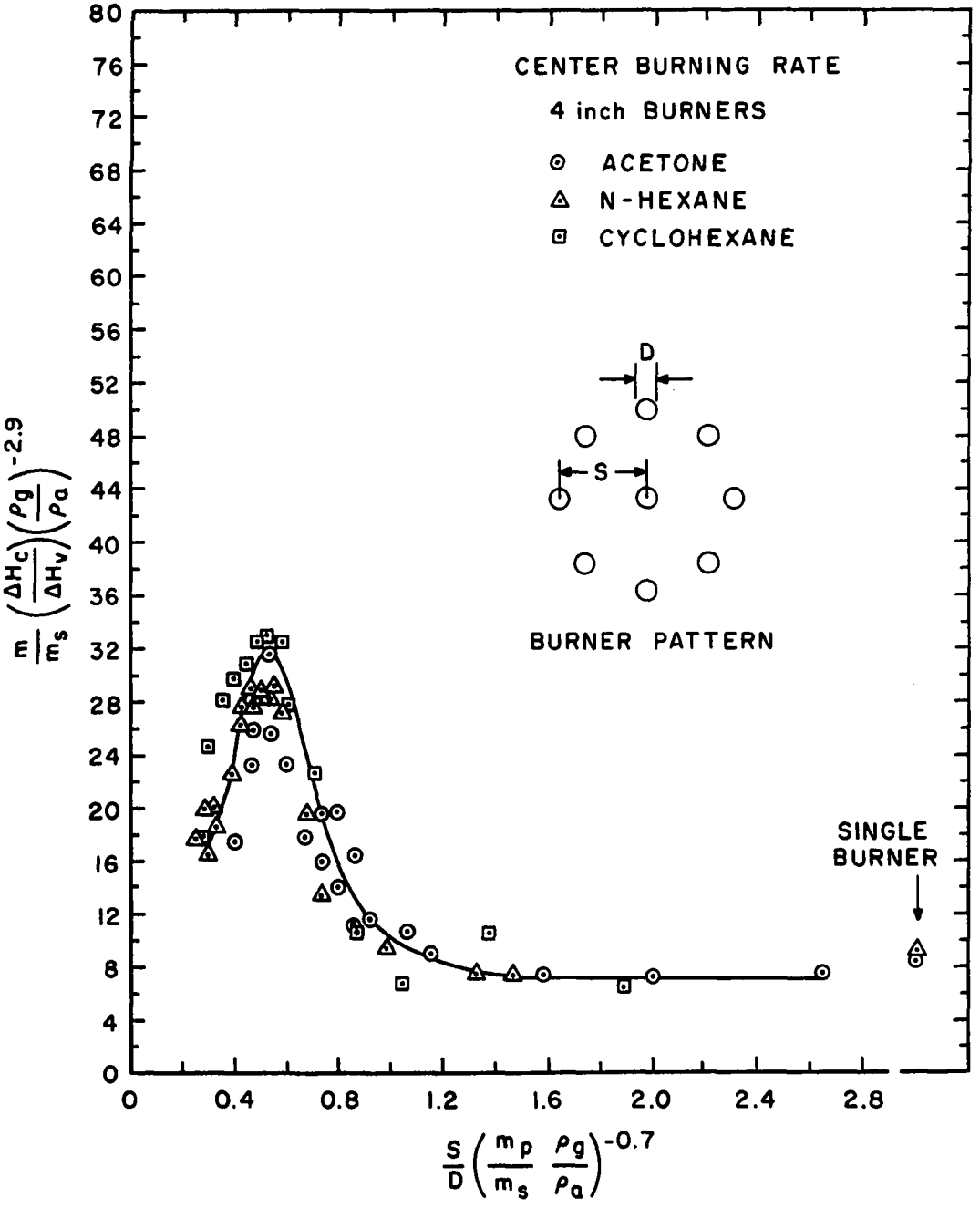

Figure 52. Correlation of Center Burning Rates for 4-Inch Rimless Burners.

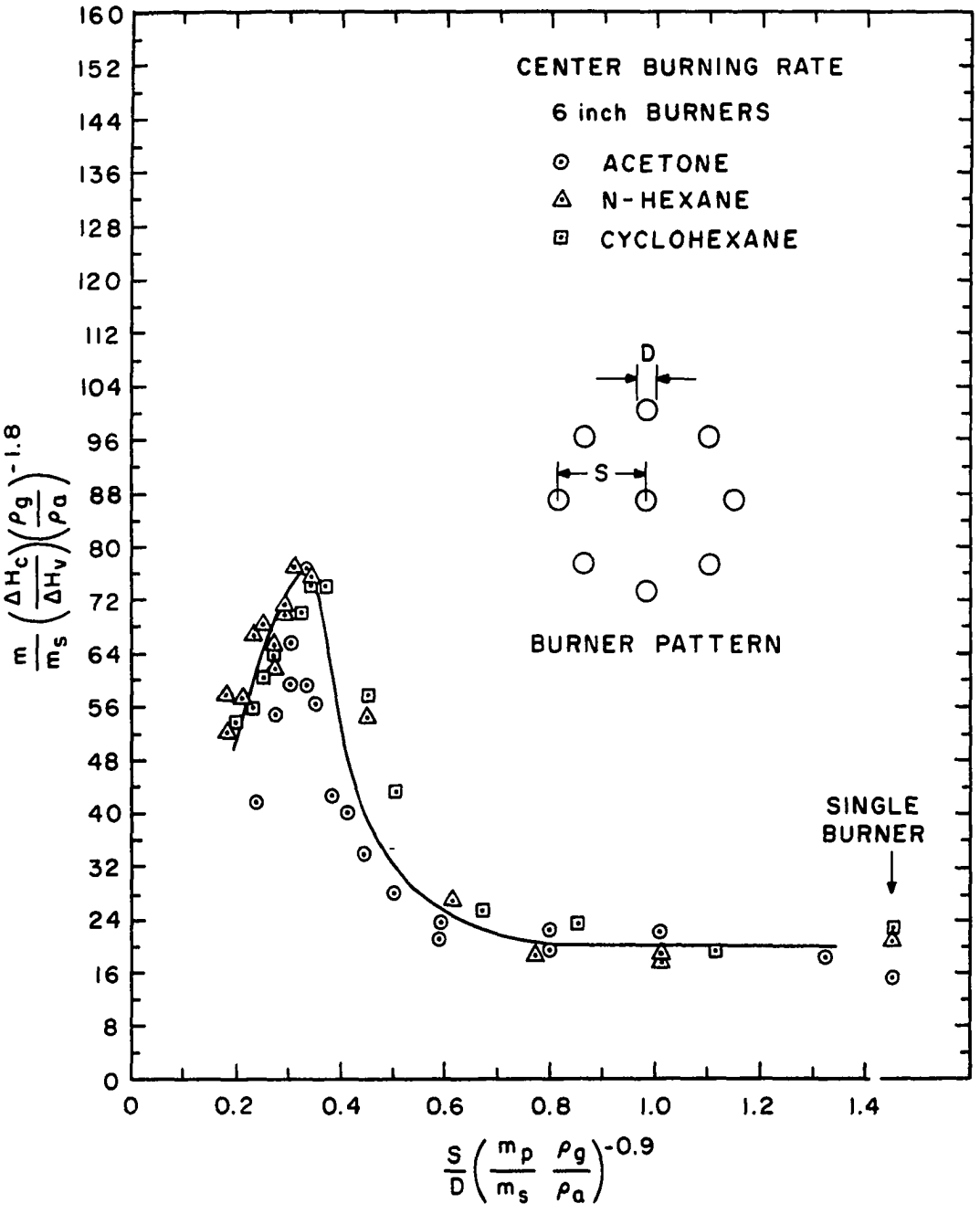

Figure 53. Correlation of Center Burning Rates for 6-Inch Rimless Burners.

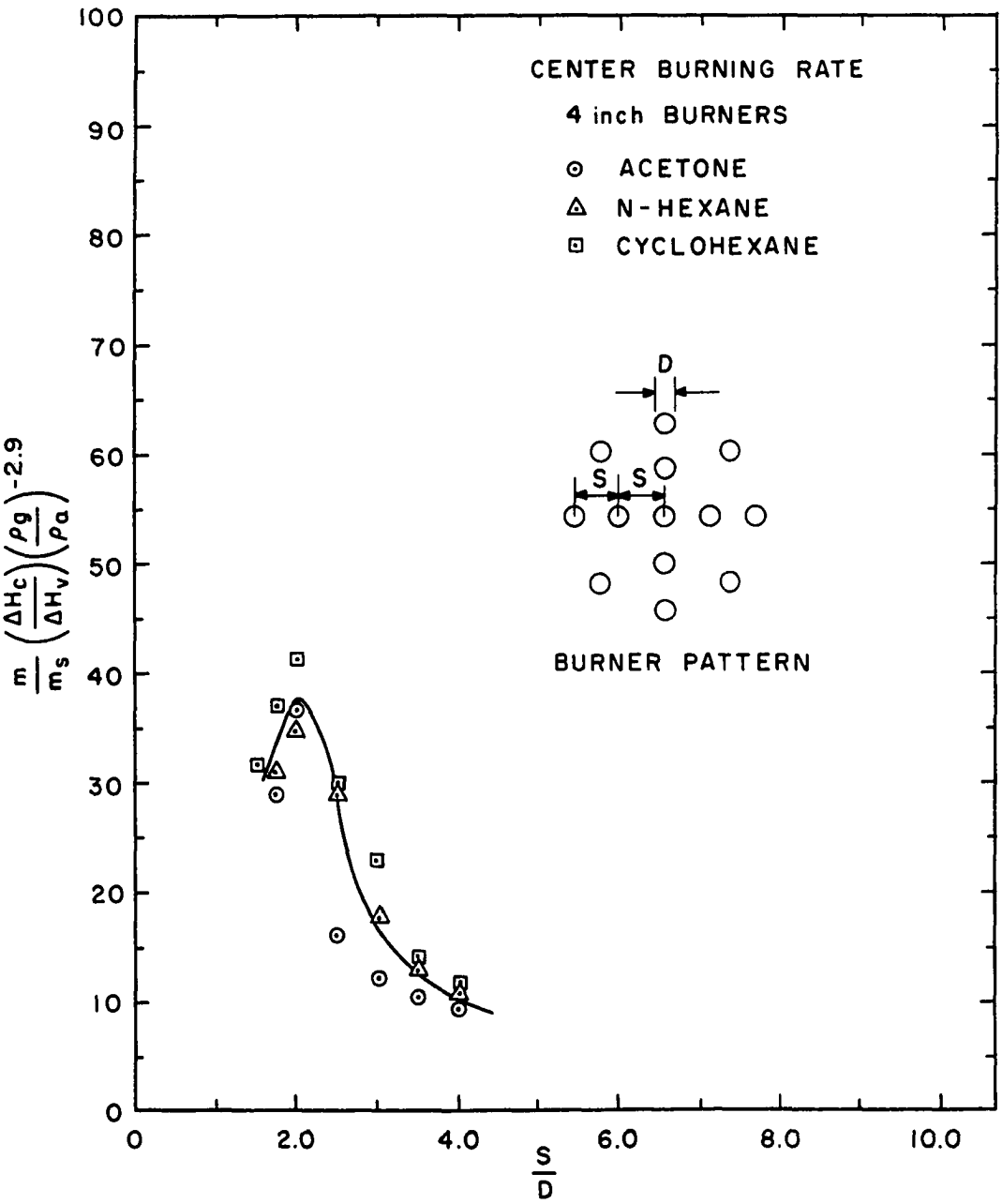

Figure 54. Correlation of Center Burning Rates for 4-Inch Rimless Burners (Thirteen-Burner Pattern)

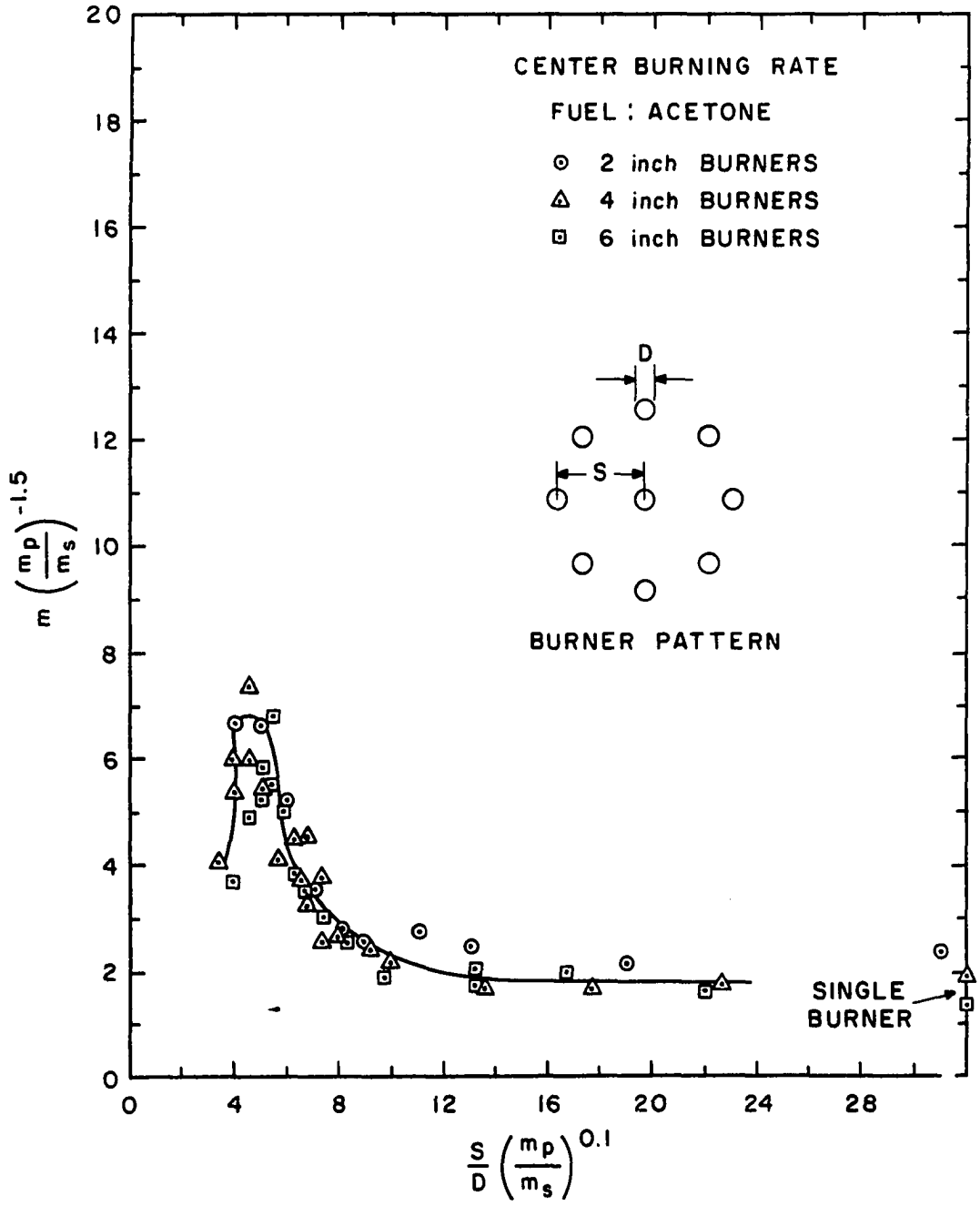

Figure 55. Correlation of Center Burning Rates for Acetone in Rimless Burners.

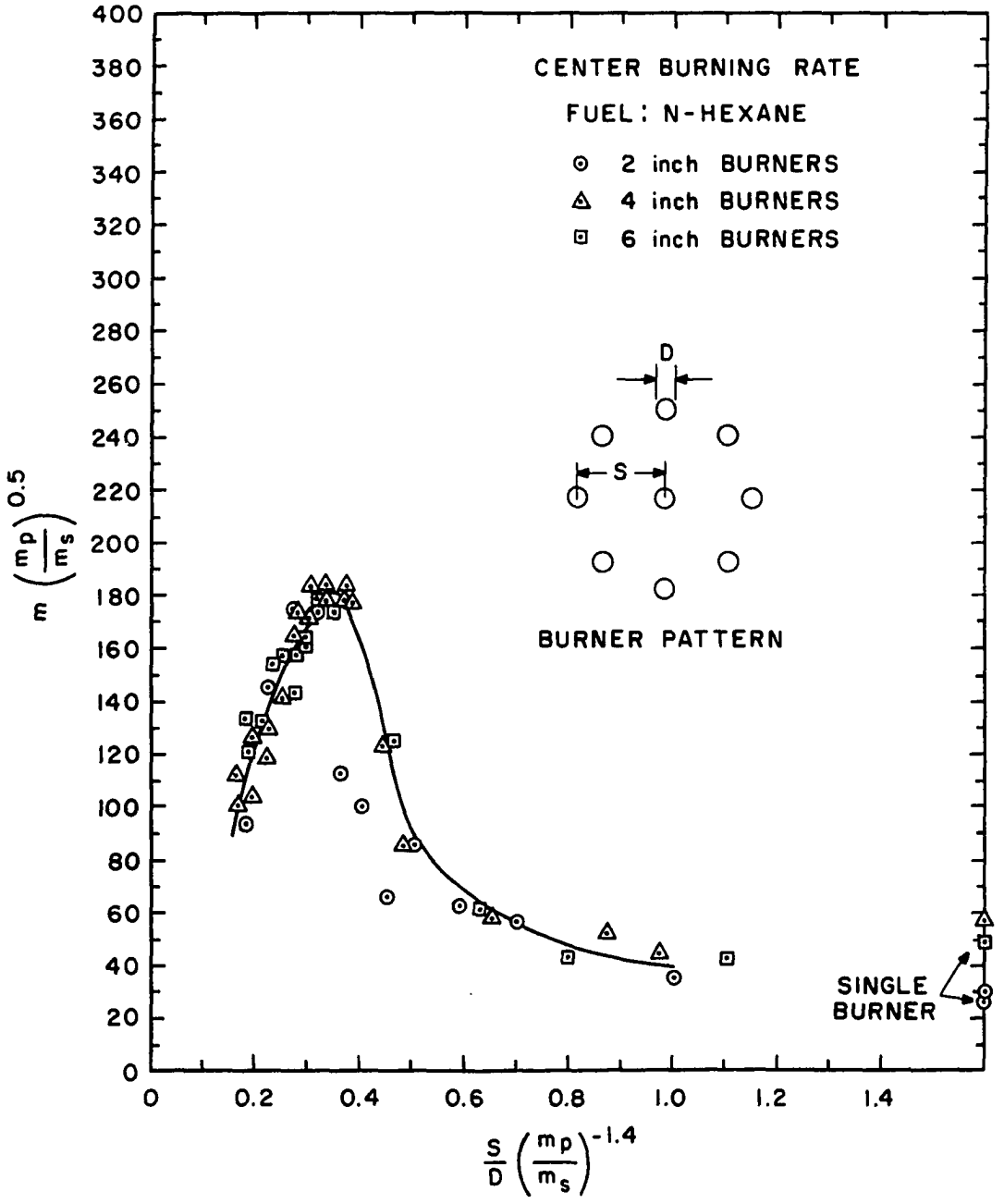

Figure 56. Correlation of Center Burning Rates for n-Hexane in Rimless Burners.

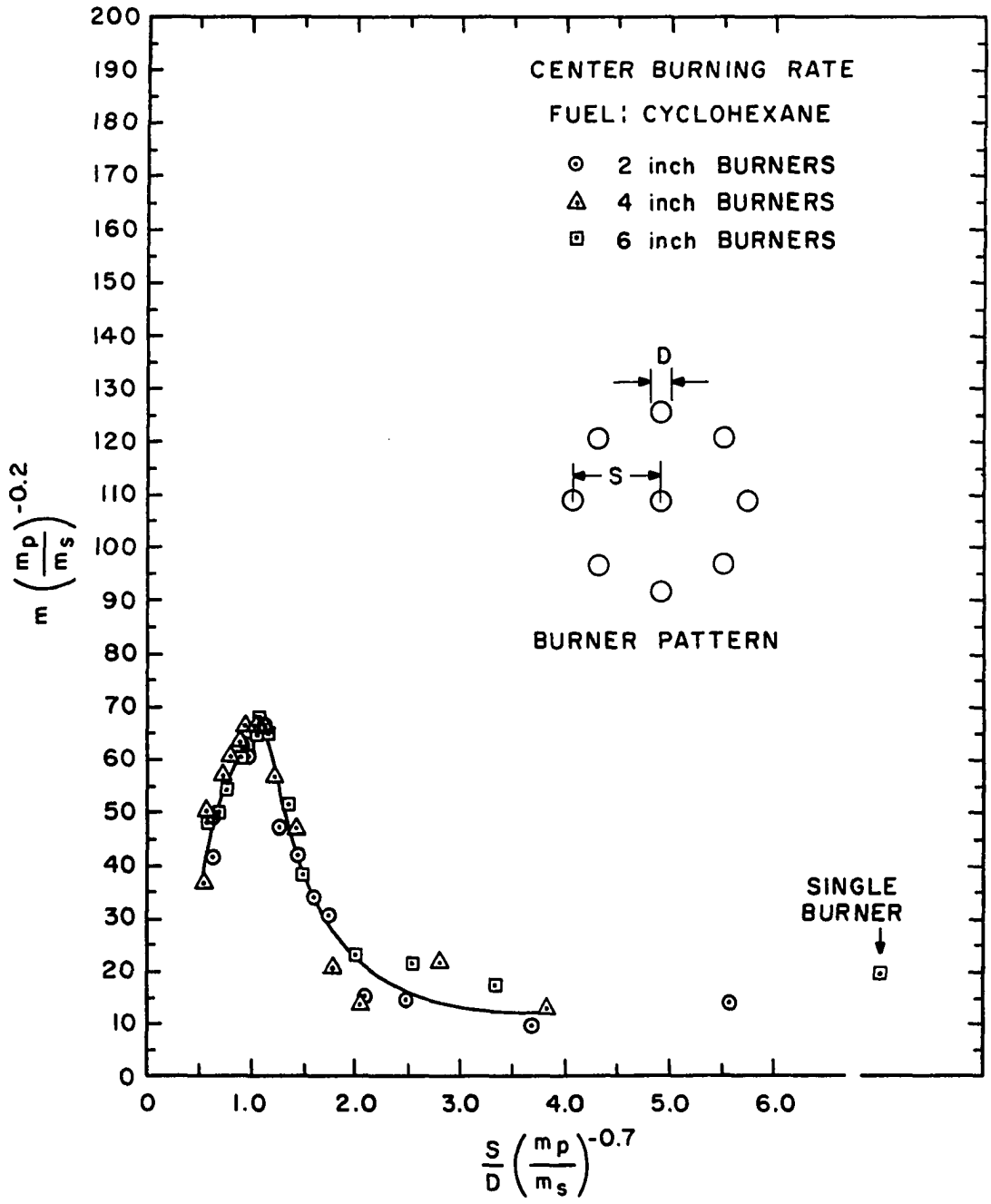

Figure 57. Correlation of Center Burning Rates for Cyclohexane in Rimless Burners.

For the center burning rate correlations involving one fuel and several burner sizes, shown in Figures 55 through 57, the burning rate function $m\left(\frac{m_p}{m_s}\right)^b$ was used. The meaning of the value of the exponent "b" is somewhat obscured. In this case, the ratio $\frac{m_p}{m_s}$ reflects a combination of changes in such things as fuel properties and modes of heat feedback to the fuel, as mentioned previously.

The burning rate correlations for the average burning rates, as shown in Figures 58 through 64, were in some cases slightly less successful in bringing the burning rate data for the various situations under a single curve. Due to the rather large amount of scatter in the values of burning rate function at small burner separations, curves were not drawn through the data of some of these figures. As noted previously, the peripheral-burner burning rates for several combinations of fuel and burner size did not drop as the flames became fully merged but continued to climb. Since they greatly reflect the behavior of the peripheral-burner burning rates, the average burning rate curves in these few cases showed a rather flat peak or did not decrease at all as the separation distance was decreased to its smallest values. The values of $(S/D)_p$ and m_p as obtained from these burning rate curves were rather difficult to determine. The uncertainty in the selection of these peak values for use in the correlations tended to be a cause of scatter in some of the average burning rate

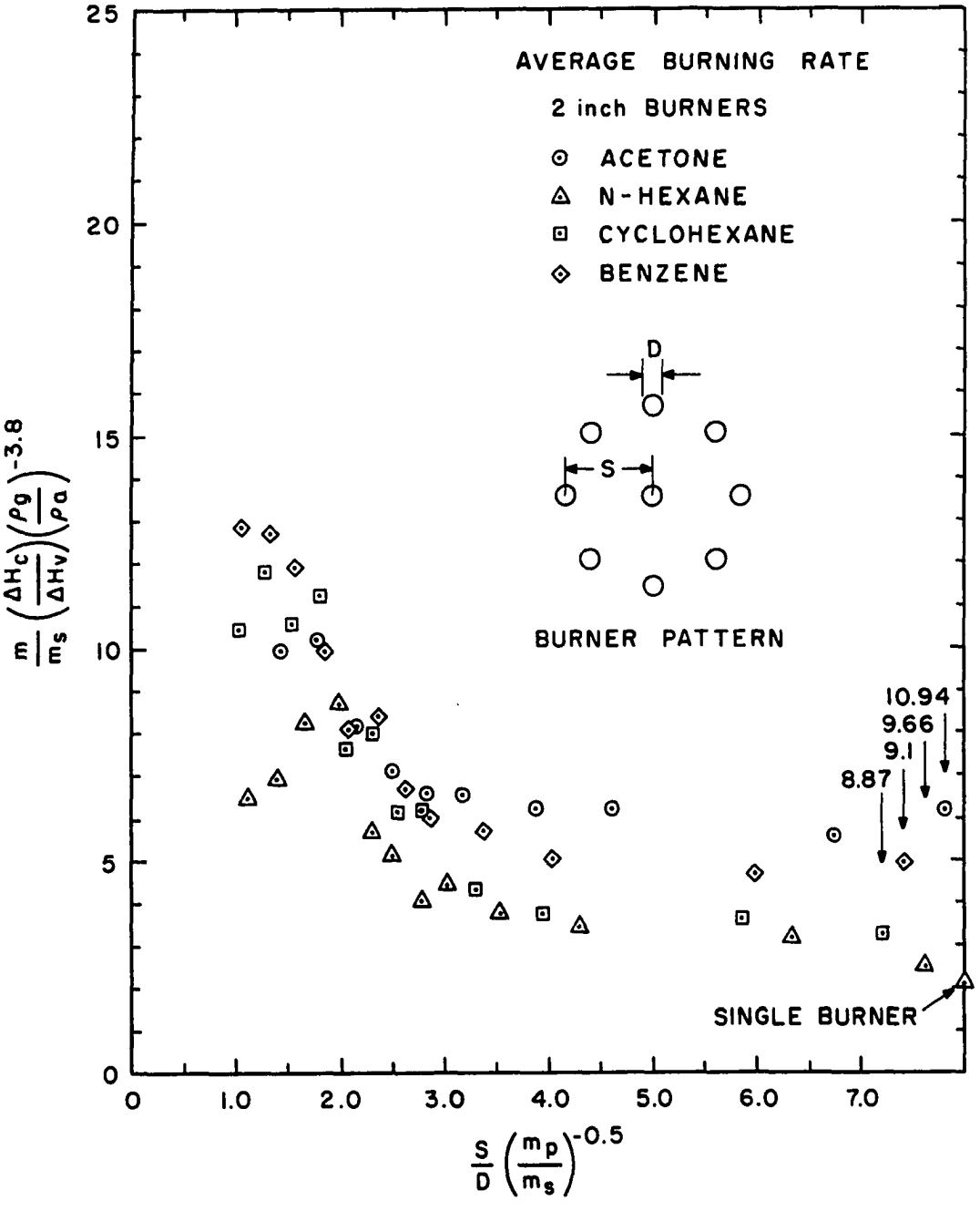

Figure 58. Correlation of Average Burning Rates for 2-Inch Rimless Burners.

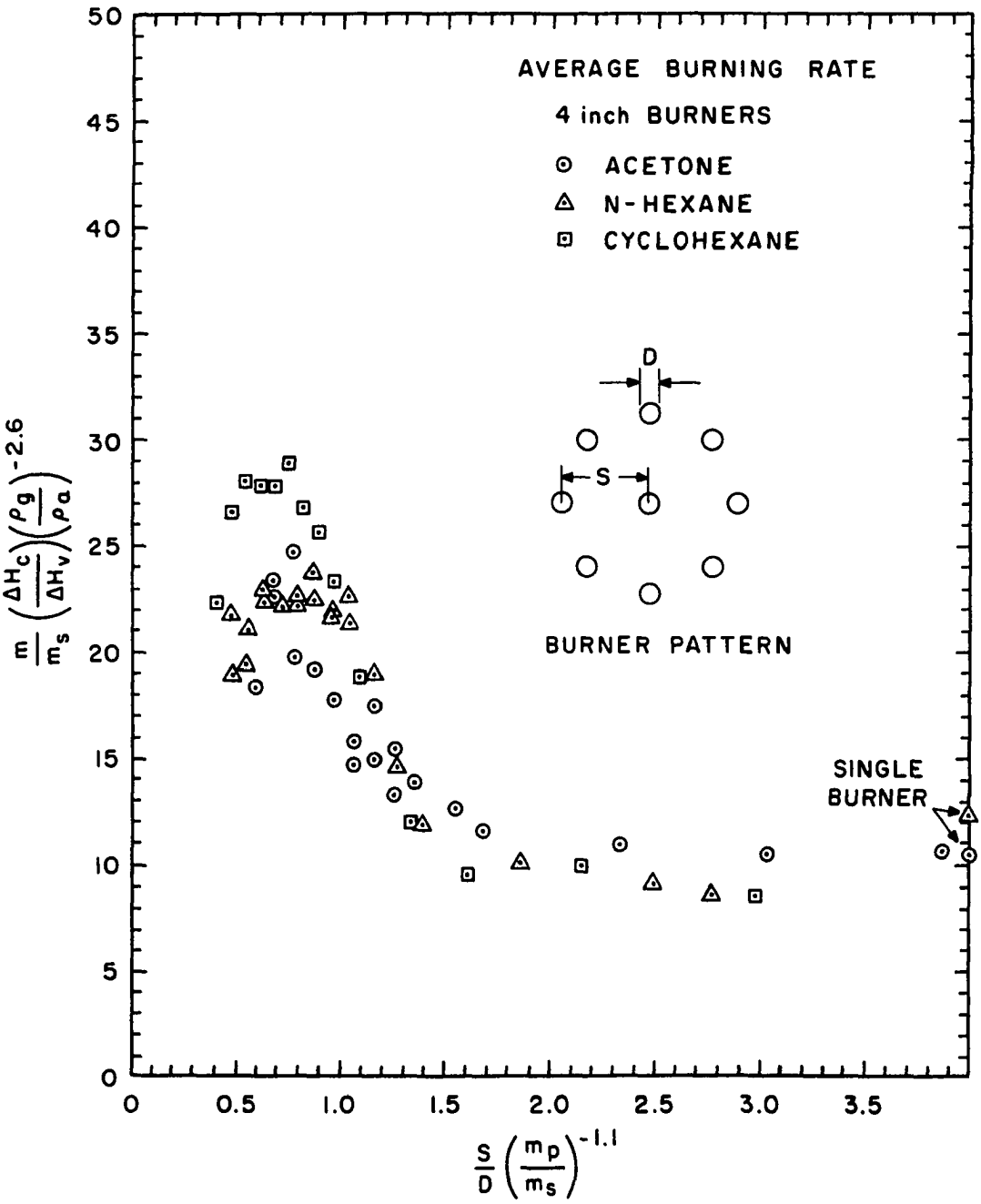

Figure 59. Correlation of Average Burning Rates for 4-Inch Rimless Burners.

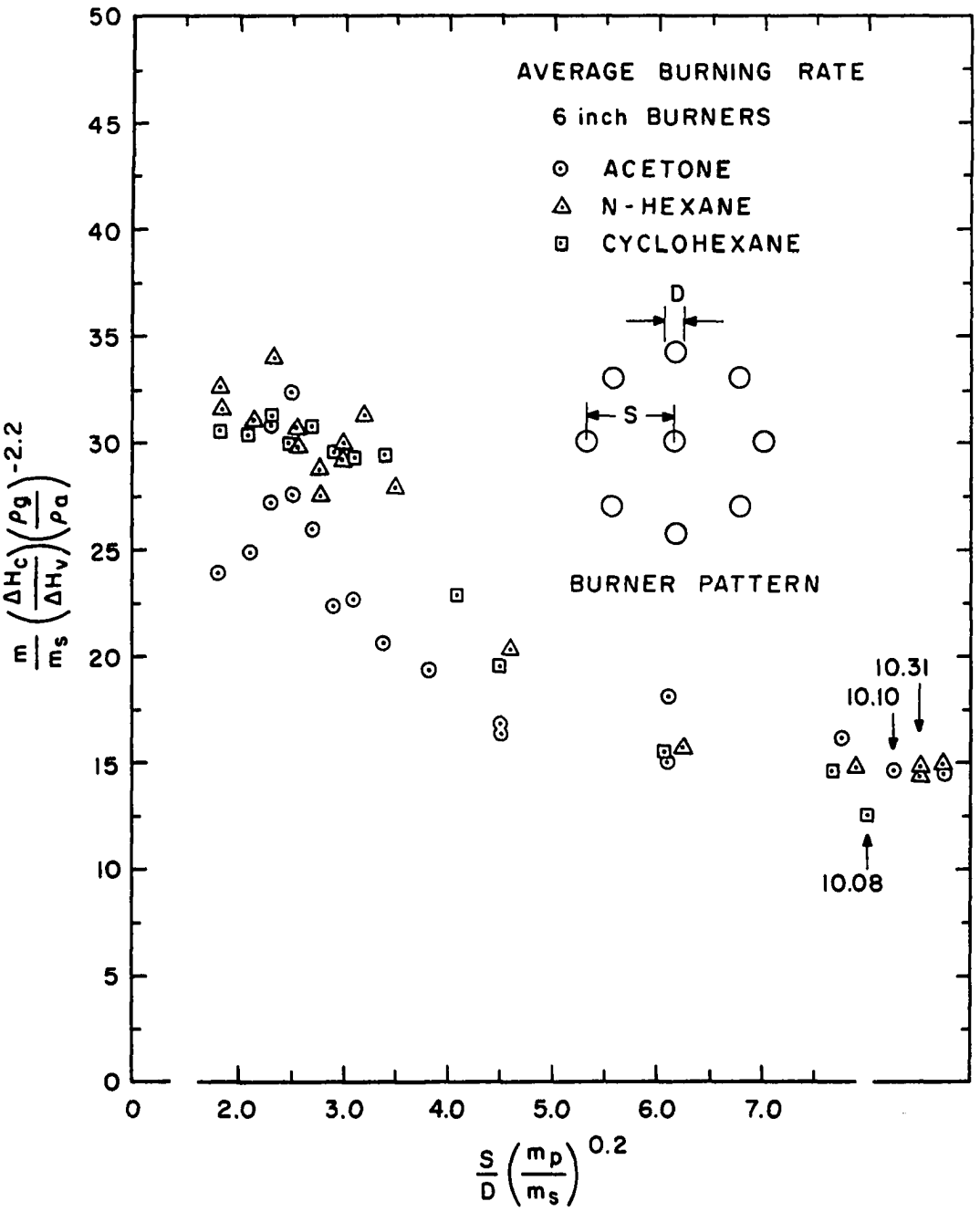

Figure 60. Correlation of Average Burning Rates for 6-Inch Rimless Burners.

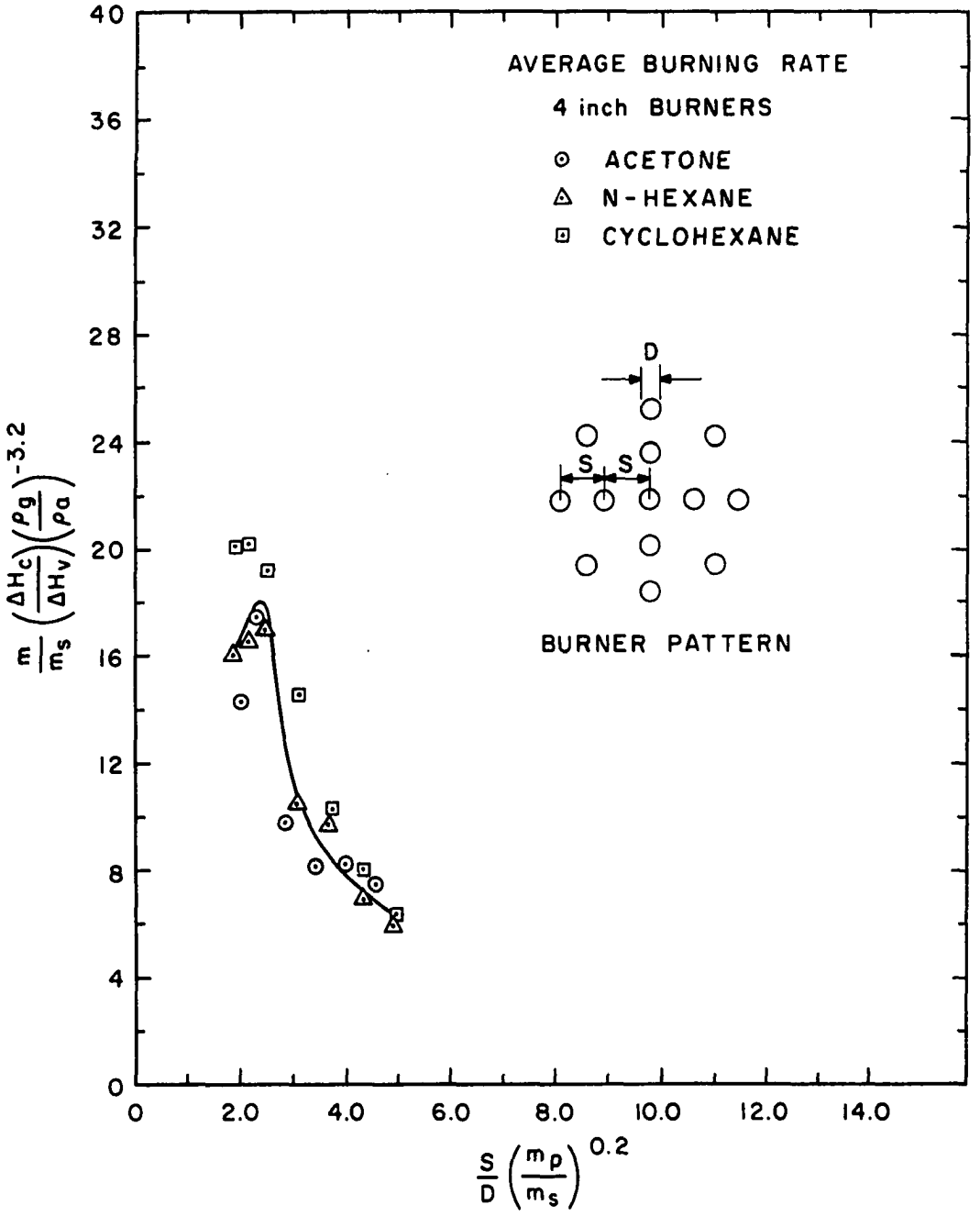

Figure 61. Correlation of Average Burning Rates for 4-Inch Rimless Burners (Thirteen-Burner Pattern).

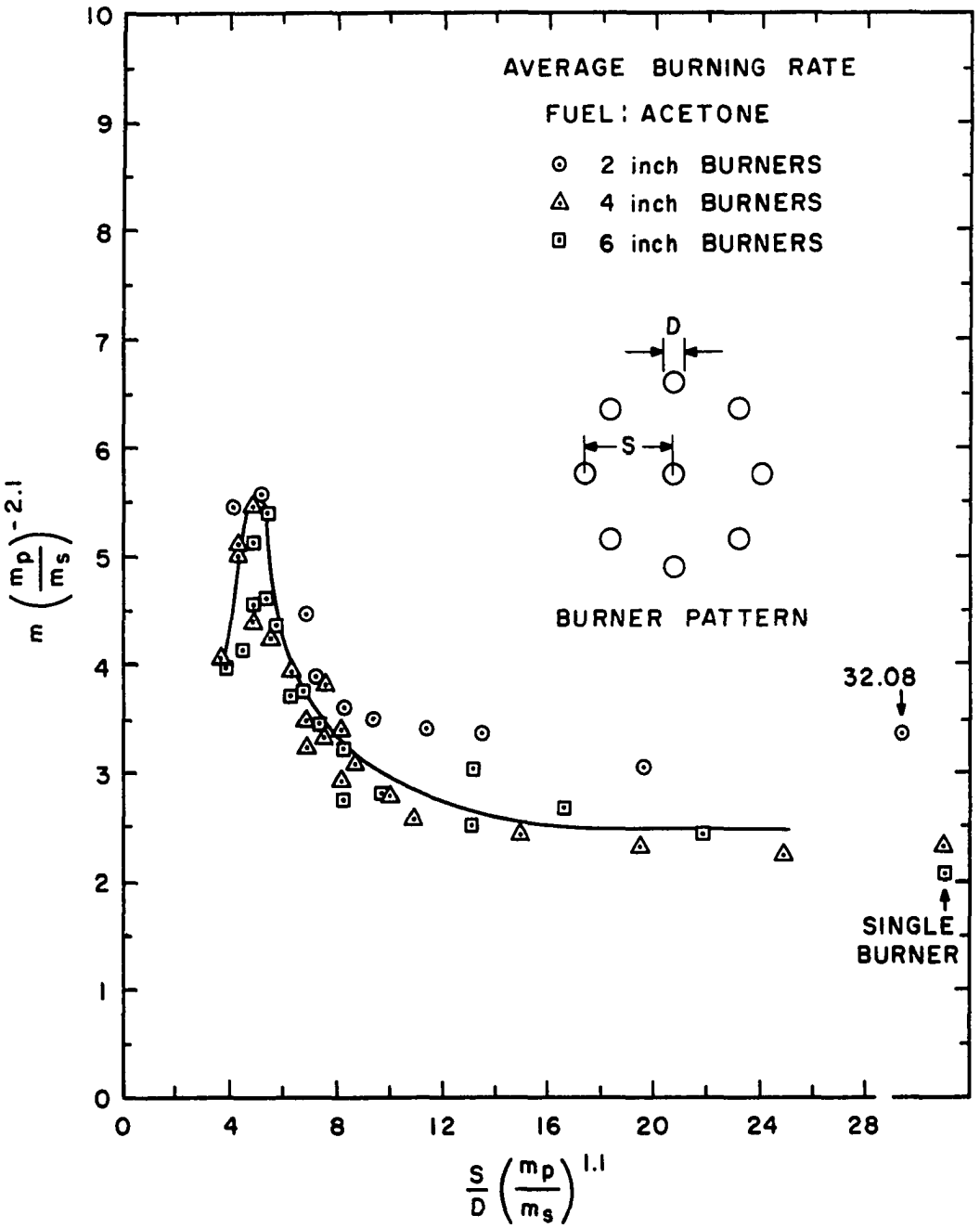

Figure 62. Correlation of Average Burning Rates for Acetone in Rimless Burners.

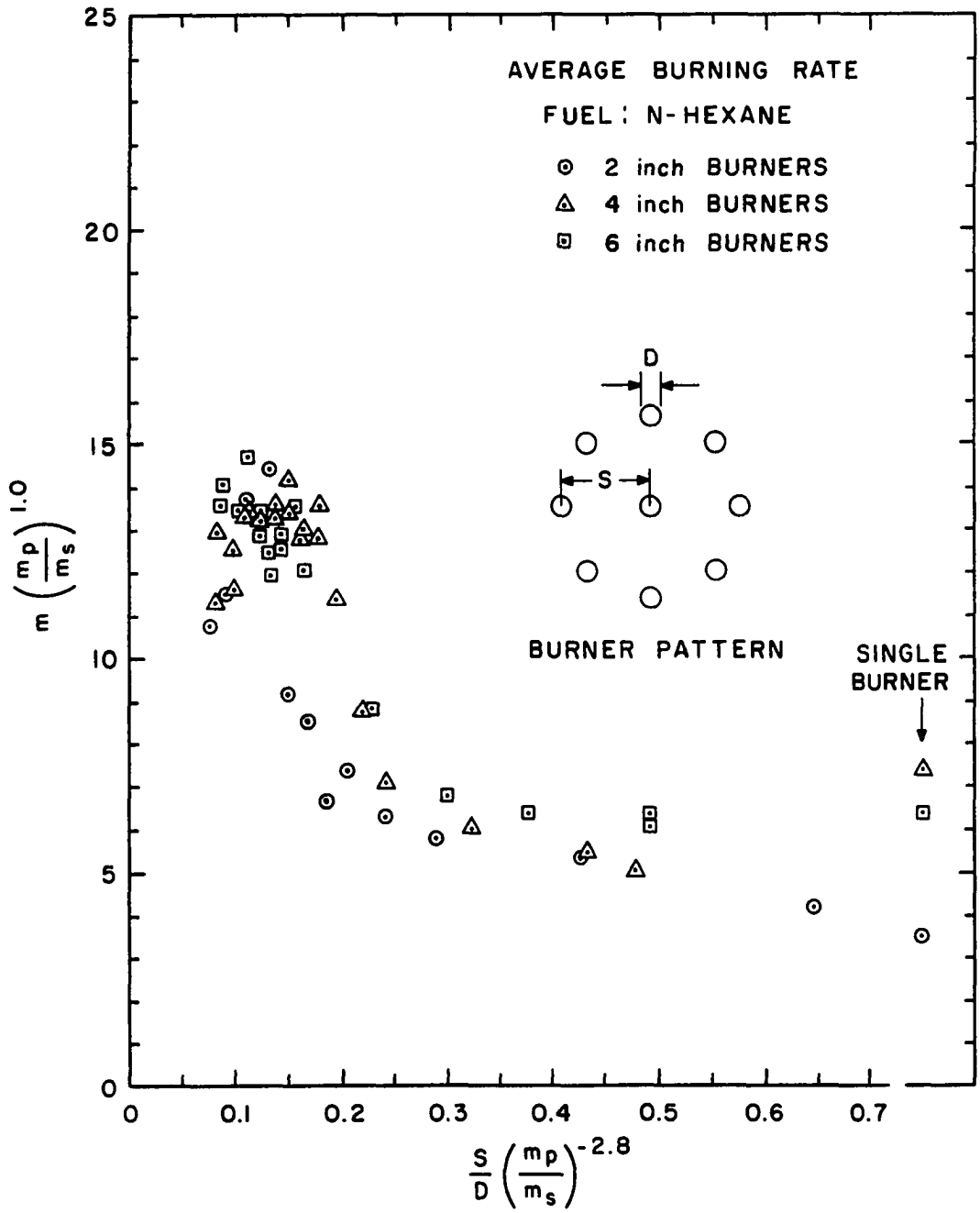

Figure 63. Correlation of Average Burning Rates for n-Hexane in Rimless Burners.

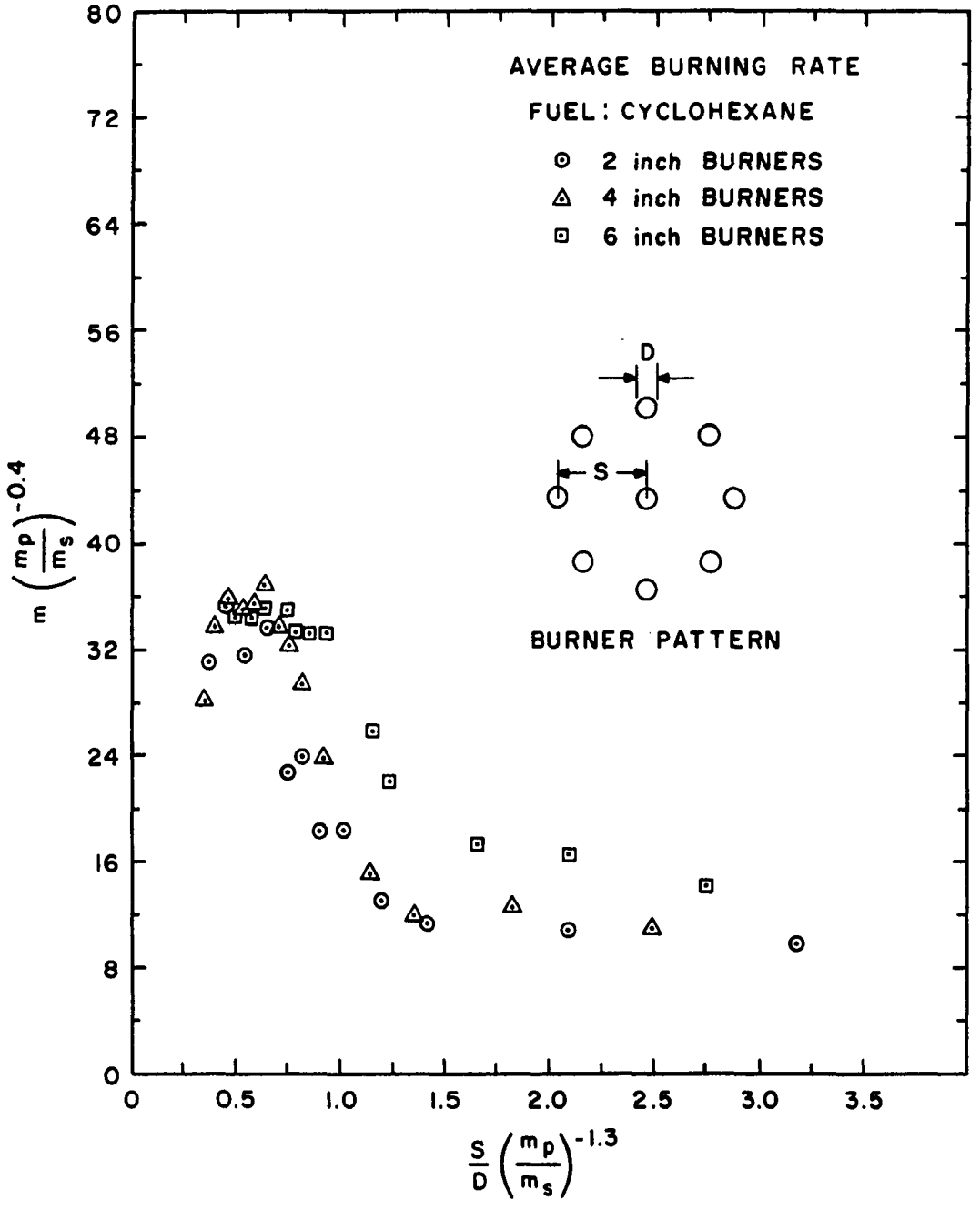

Figure 64. Correlation of Average Burning Rates for Cyclohexane in Rimless Burners.

correlations. The values of the exponent (ρ_g/ρ_a) term in the burning rate function for the correlations involving various fuels for a particular burner size might be noted. The absolute value of this exponent decreased as larger burner sizes were used, as was the case for the center-burner burning rates.

The correlations combining the burning rates for all the fuels and burner sizes used with the nine-burner pattern are shown in Figures 65 and 66 for the center burning rate and average burning rate, respectively. The correlation for the center burning rates was successful in combining the burning rates of the various fuels and burner sizes, for conditions varying from interaction-free burning to fully merged burning. The fires burned ranged from the small 2-inch burner acetone fires to large 6-inch burner cyclohexane fires. The correlation involving the average burning rates was less successful at combining the burning rates in the region where the fires were merging. Due to the large amount of scatter in the values of the burning rate functions at small burner separations, a curve was not drawn through the data of Figure 66. It is noted from the average burning rate correlation that the data for the various fuels in the 2-inch burners were consistently higher than the data for the 4- and 6-inch diameter burners when the fires begin to interact and merge.

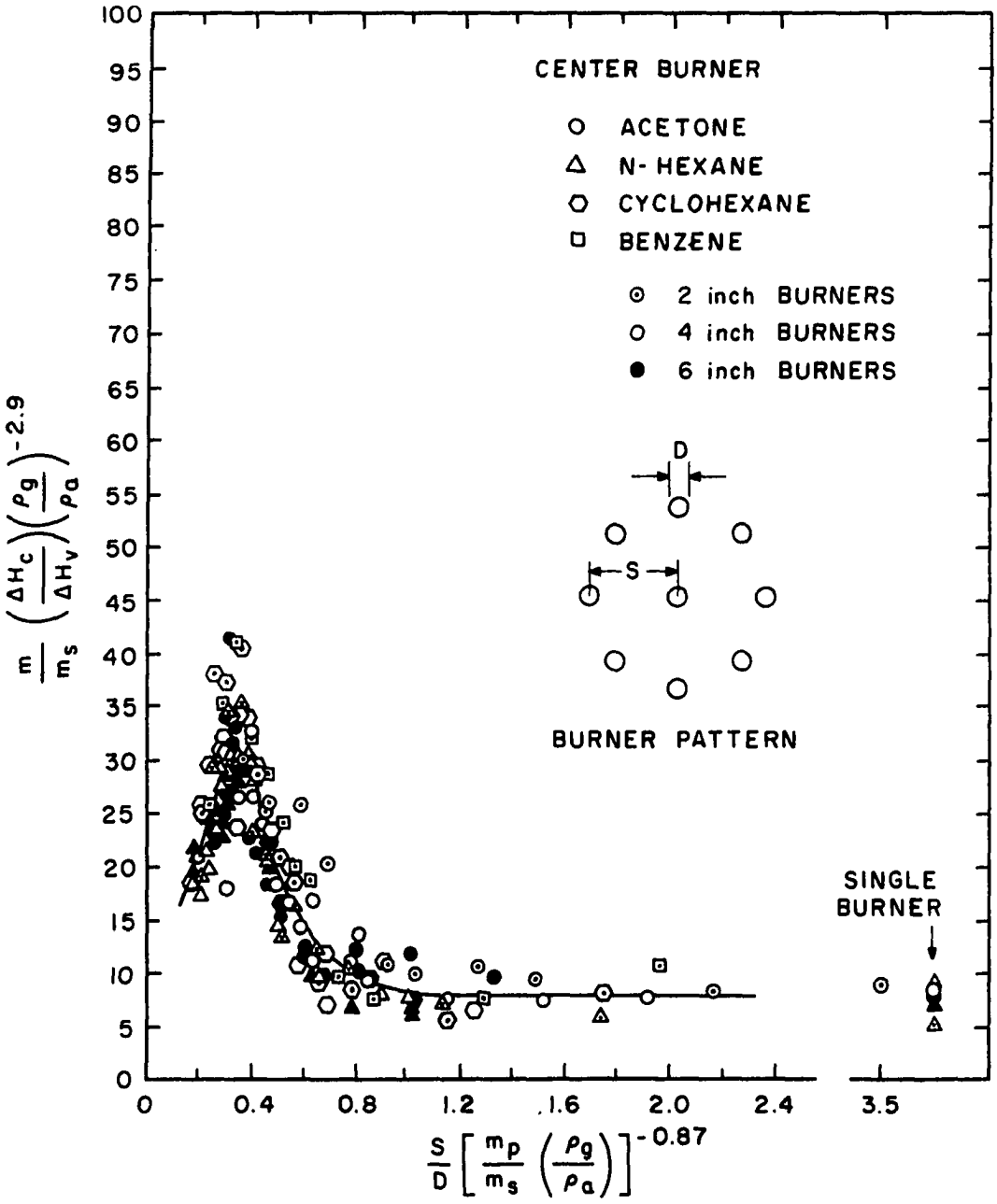

Figure 65. Correlation of Center Burning Rates for All Fuels and Rimless Burner Sizes (Nine-Burner Pattern).

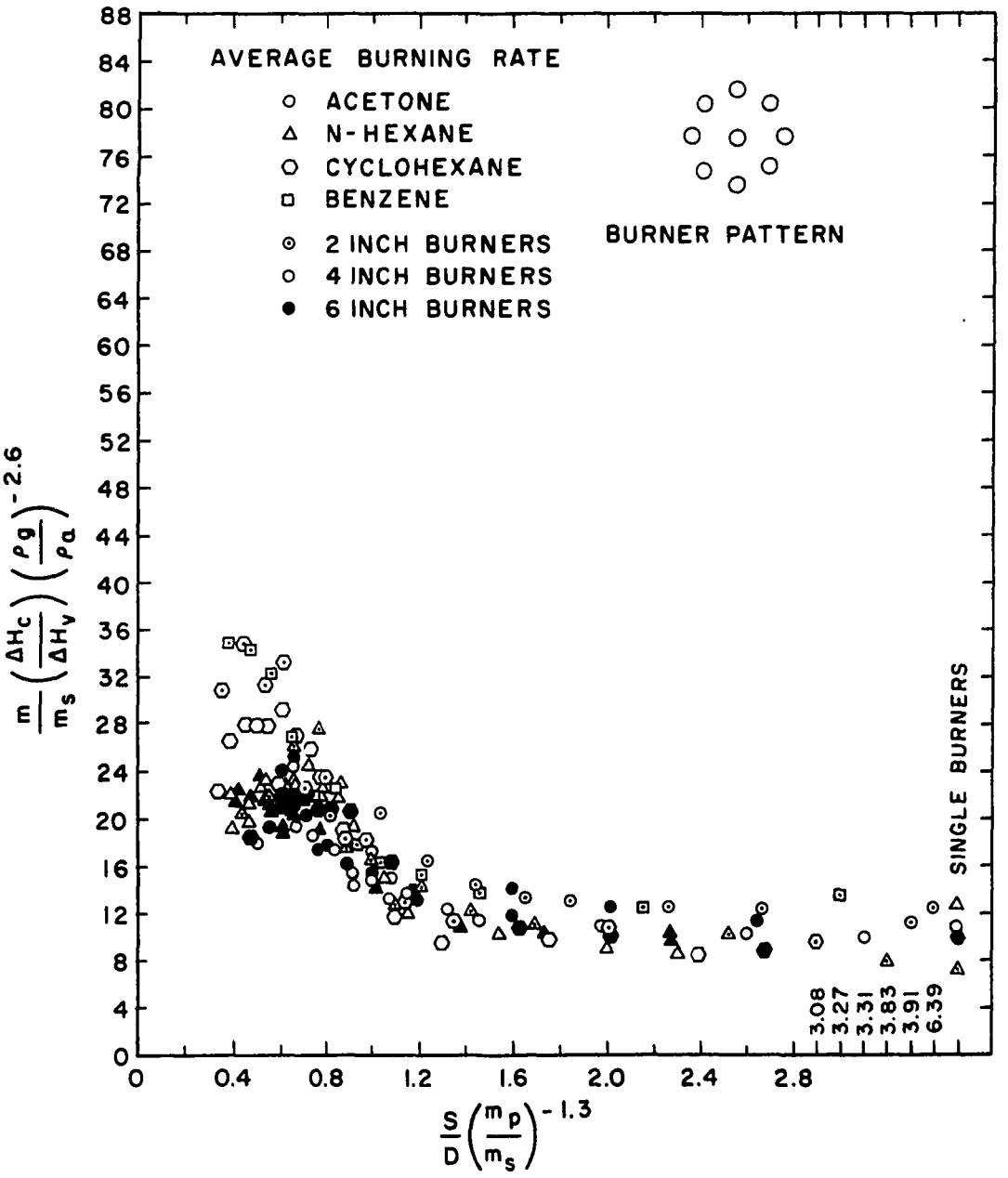

Figure 66. Correlation of Average Burning Rates for All Fuels and Rimless Burner Sizes (Nine-Burner Pattern).

The difference between the average burning rate functions for the 2-inch burners and the larger burners is probably caused by the effect of changes in the proportion of total emitted radiation which reaches the fuel surface. These differences in the proportion of the radiation which returns to the fuel are caused by the large differences in the sizes of the opaque flame columns from these fires. From Figure 65 it is seen that the center burning rate functions for the 2-inch burners are only slightly higher than the functions for the larger burners.

In summary, correlations have been developed which allow the burning rate of interacting or merging, multiple, liquid-fueled fires to be predicted. These correlations have the general form of

$$\frac{m}{m_s}\left(\frac{\Delta H_c}{\Delta H_v}\right)\left(\frac{\rho_g}{\rho_a}\right)^b \text{ versus } \frac{S}{D}\left[\frac{m_p}{m_s}\left(\frac{\rho_g}{\rho_a}\right)\right]^a$$

for the center-burner burning rate and

$$\frac{m}{m_s}\left(\frac{\Delta H_c}{\Delta H_v}\right)\left(\frac{\rho_g}{\rho_a}\right)^b \text{ versus } \frac{S}{D}\left(\frac{m_p}{m_s}\right)^a$$

for the nine-burner average burning rate. "a" and "b" are empirical constants having different values for the center and average burning rates. Only the burning rate of a single source of the fuel, along with several properties of the fuel such as heat of combustion, the heat of

vaporization plus the heat necessary to bring the fuel from ambient temperature up to the boiling point, and the ratio of fuel vapor density to ambient air density, needs to be known. The burning rate at the onset of merging, as well as the separation distance between the multiple fuel sources at which this merging occurs, can be predicted from Figures 65 and 66, or for more restricted situations from Figures 51 through 64. These correlations can be used for a burner pattern similar to that employed in the tests and for situations where conduction of heat through the fuel source rim is not an important mode of heat feedback to the fuel.

Radiation from Interacting Fires

Measurements of flame radiation were made exterior to the flame array for all of the interacting and merging tests conducted with the rimless burners. As mentioned previously, radiometer readings for most of the tests were taken at positions 77.5, 106.5, and 153.75 inches from the center of the burning table in order to determine the decay in radiation intensity with increasing distance from the flame column.

The curves of radiation flux data to the surroundings as a function of burner separation are seen in Figures 67 through 80. They correspond very closely to the average burning rate curves for the corresponding tests. As the burning rate increased, a larger flame column formed over

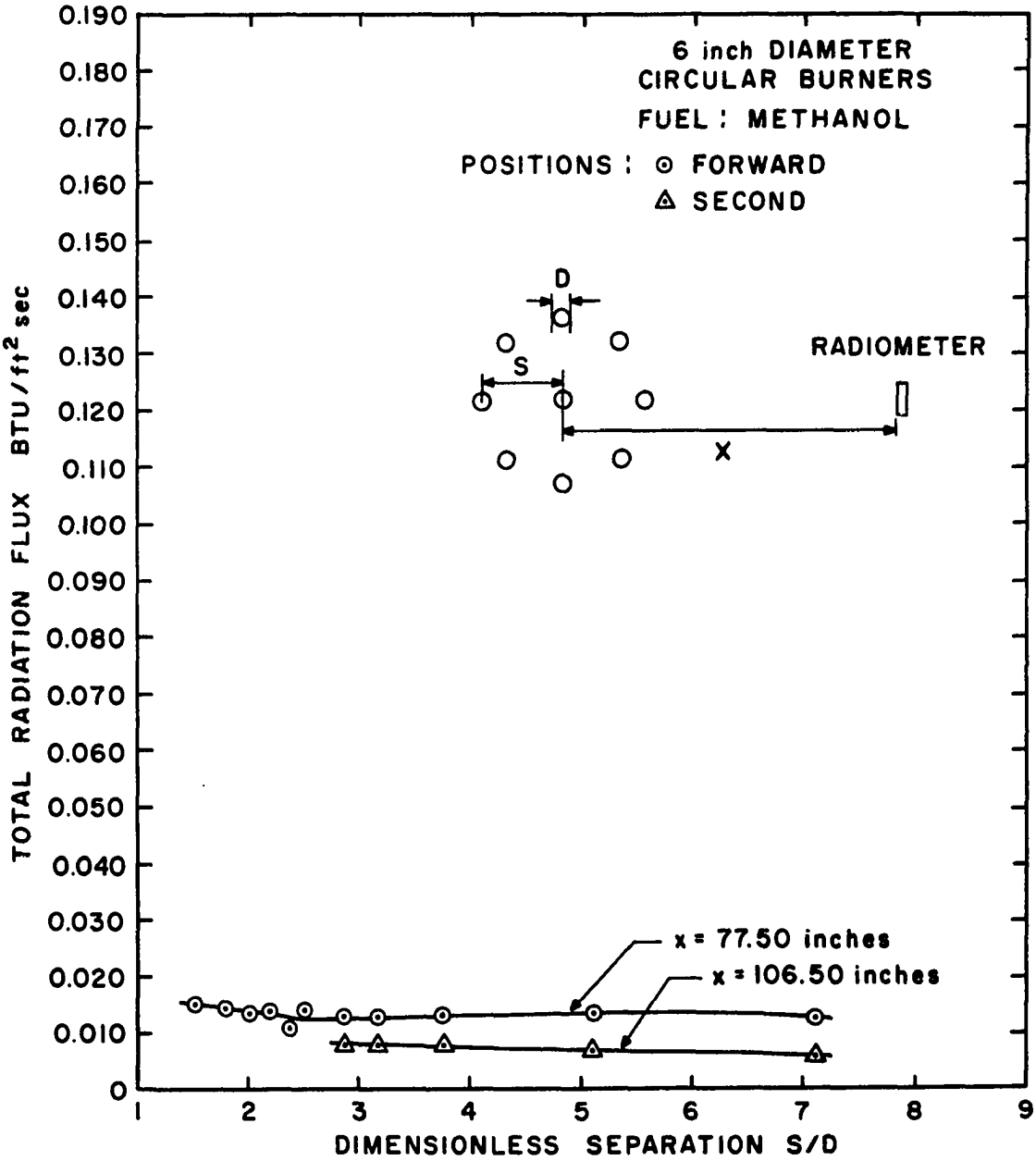

Figure 67. Radiation Flux of Interacting 6-Inch Methanol Fires.

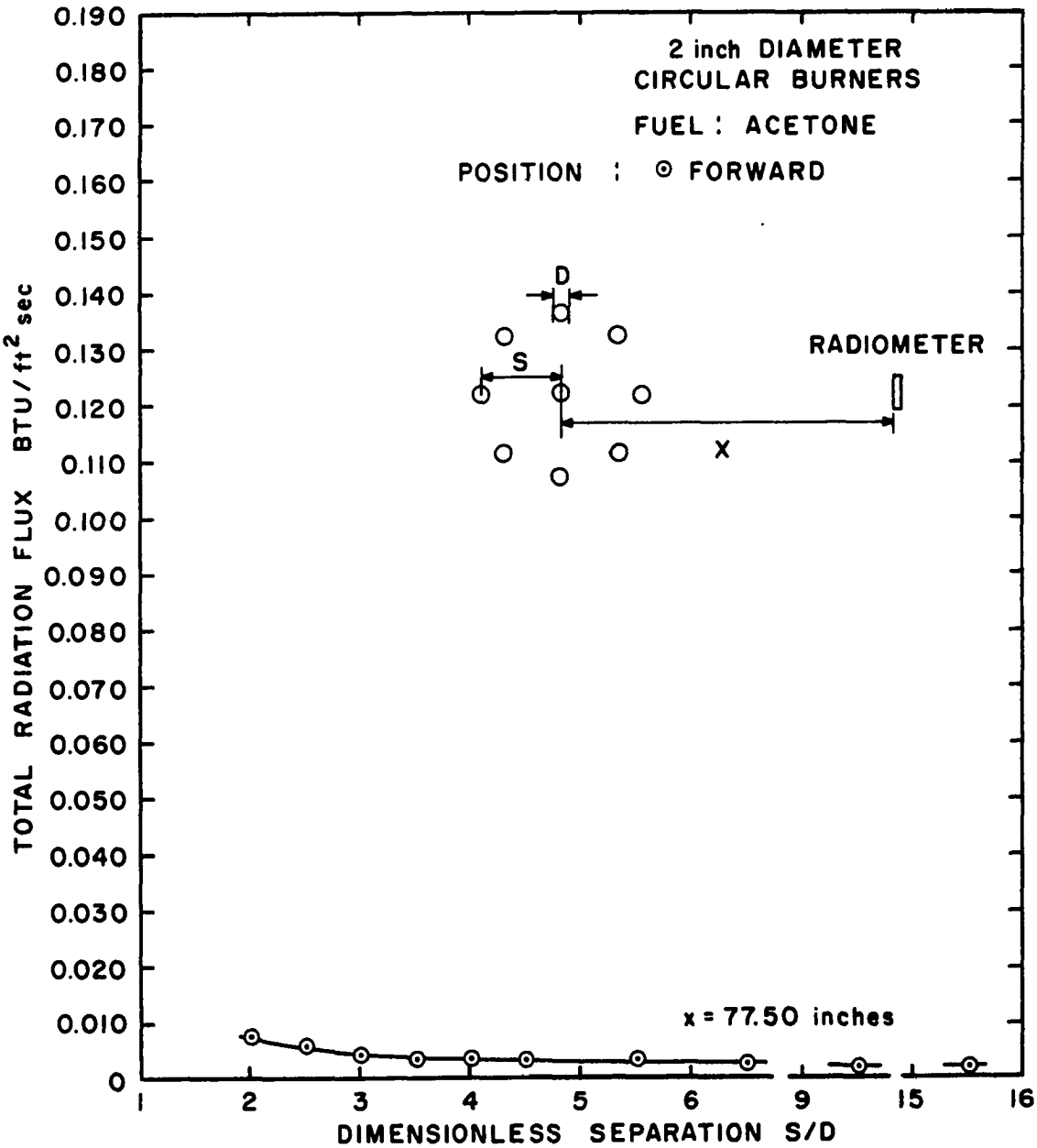

Figure 68. Radiation Flux of Interacting 2-Inch Acetone Fires.

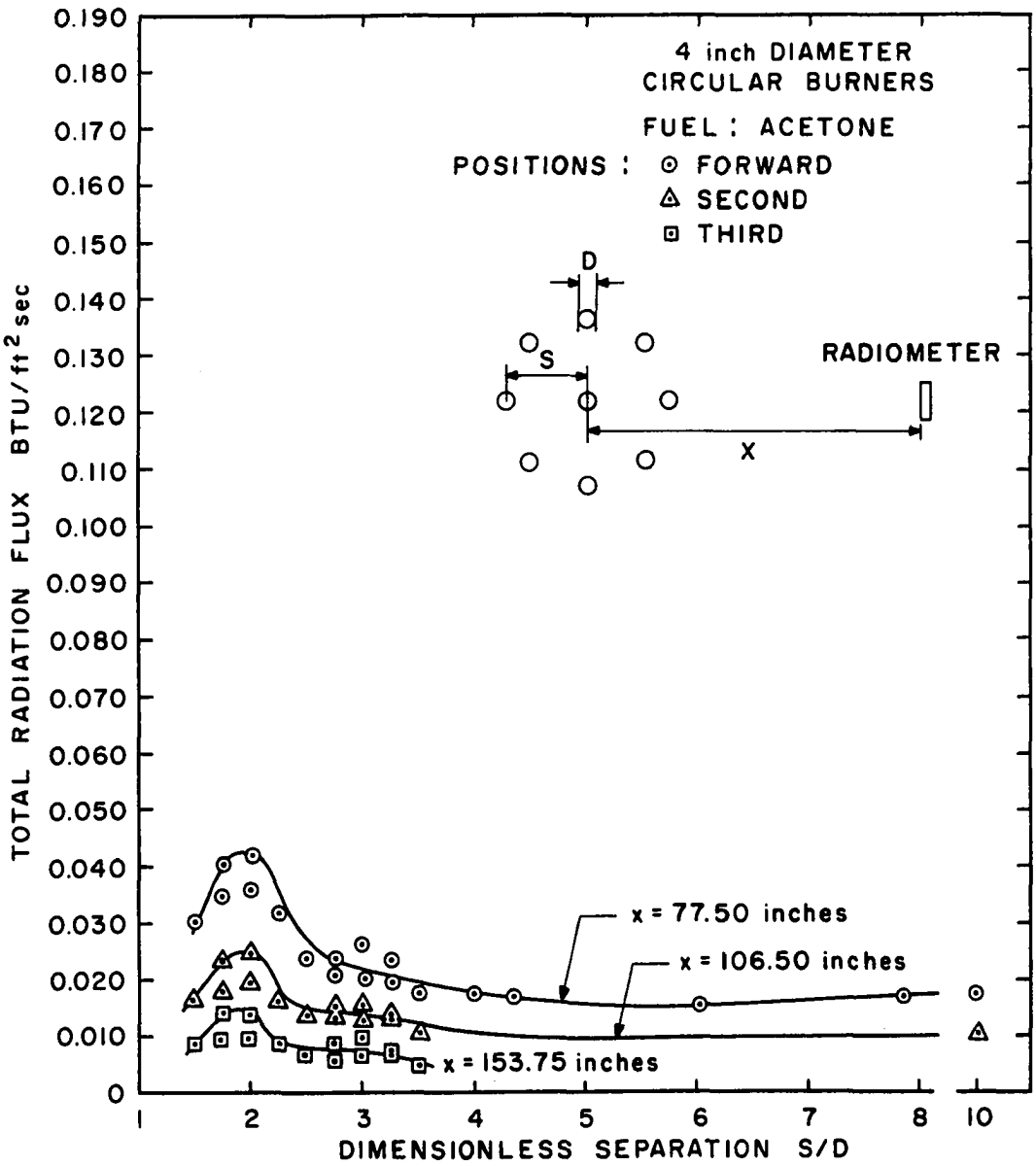

Figure 69. Radiation Flux of Interacting 4-Inch Acetone Fires.

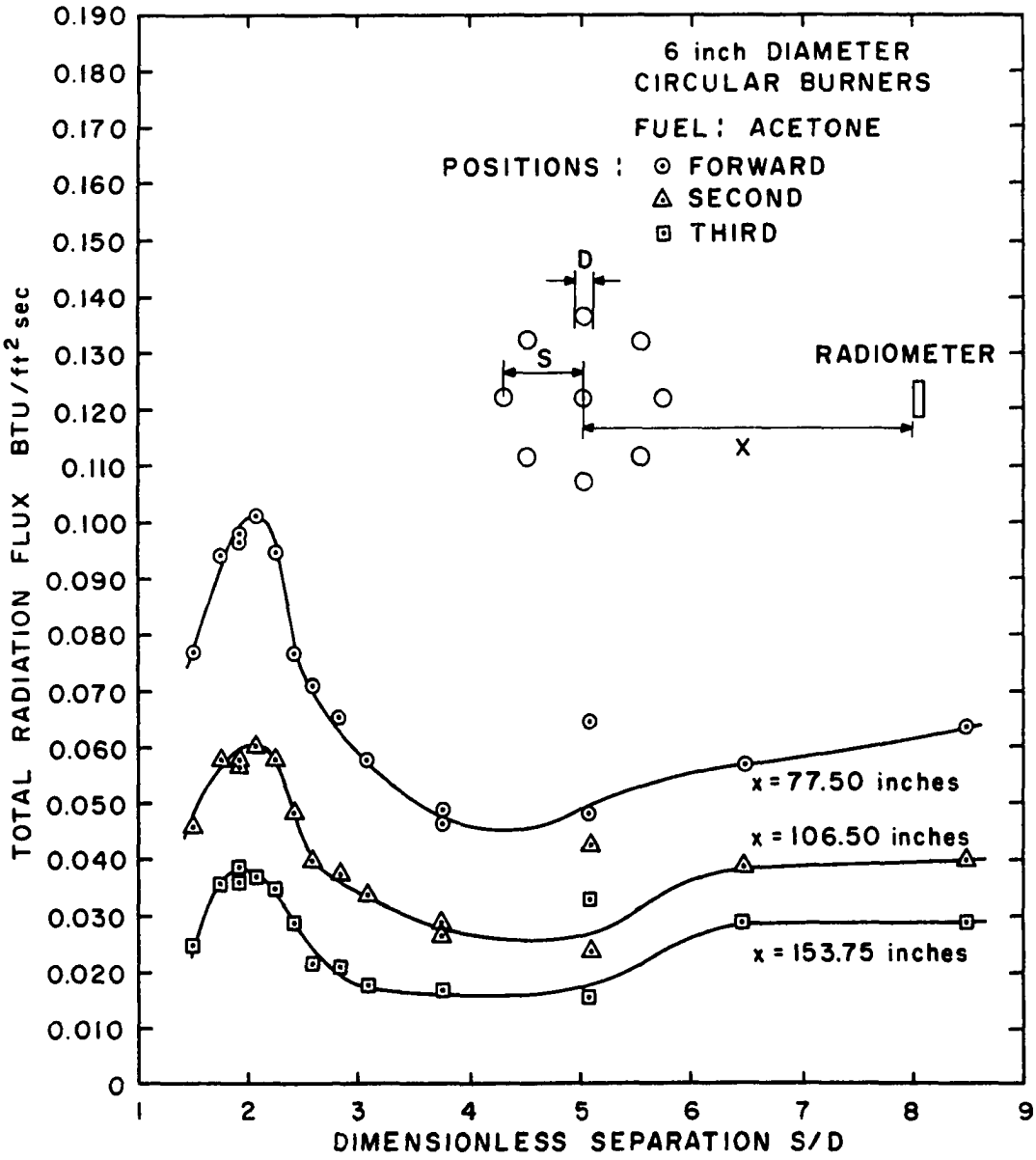

Figure 70. Radiation Flux of Interacting 6-Inch Acetone Fires.

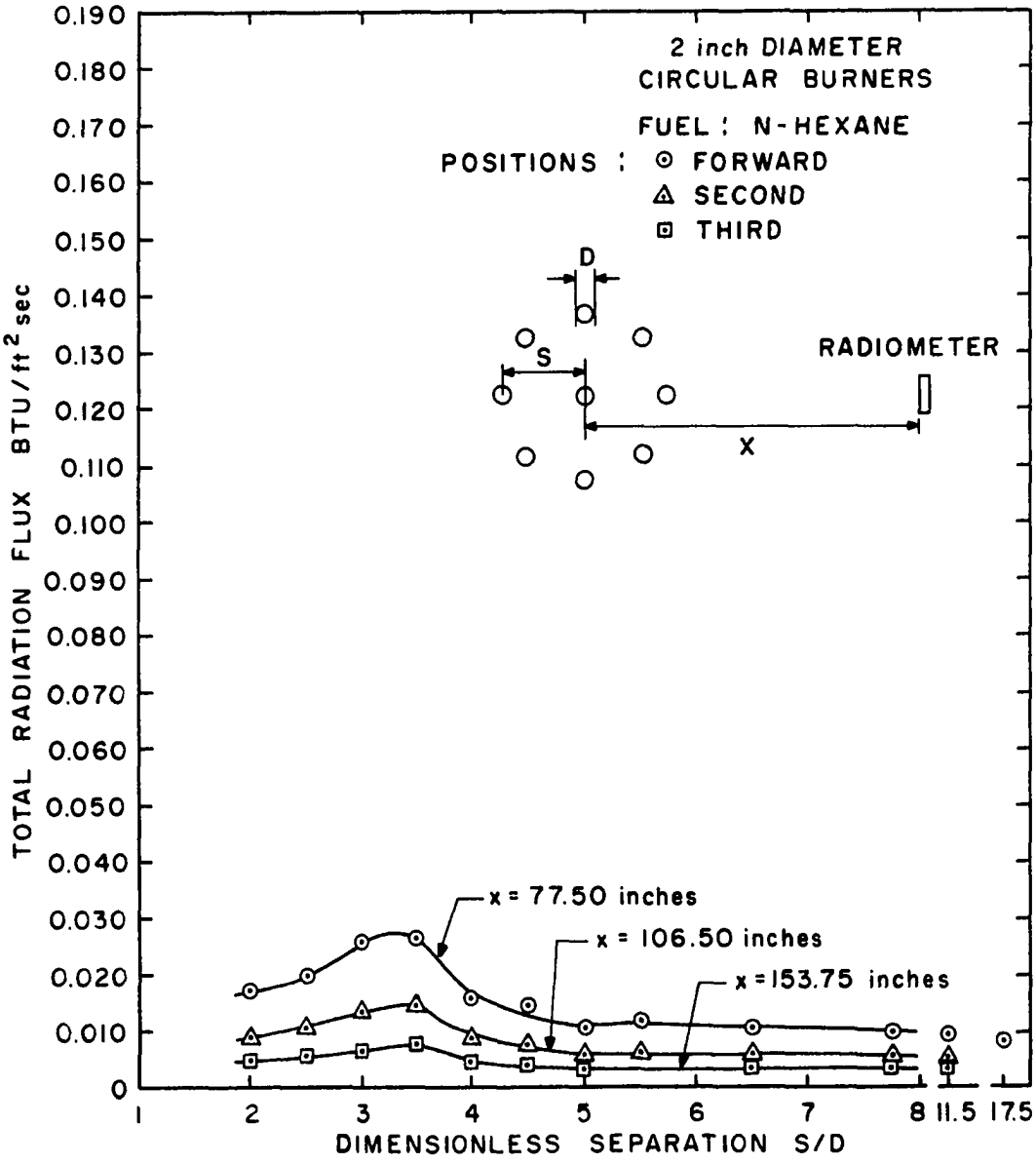

Figure 71. Radiation Flux of Interacting 2-Inch n-Hexane Fires.

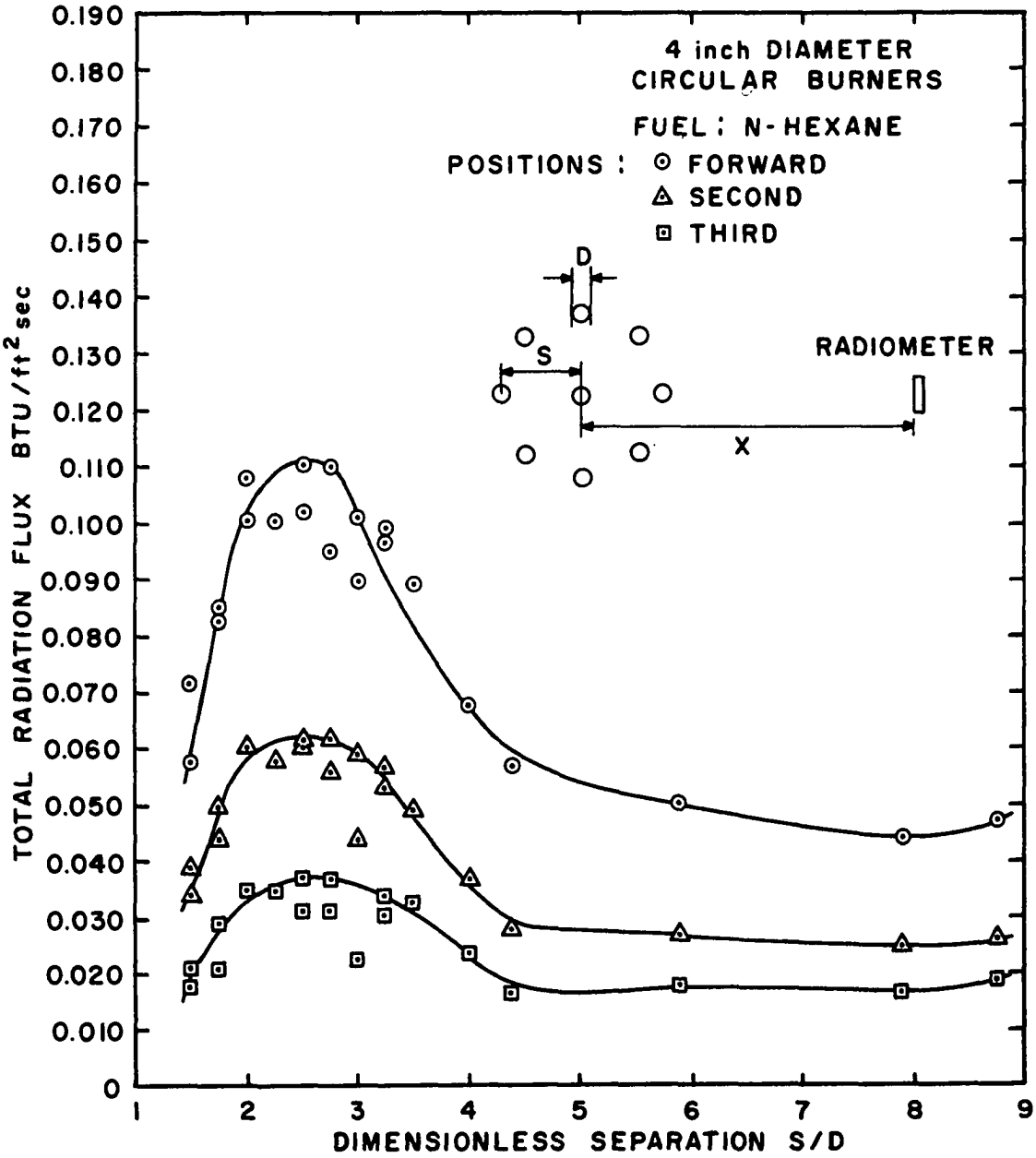

Figure 72. Radiation Flux of Interacting 4-Inch n-Hexane Fires.

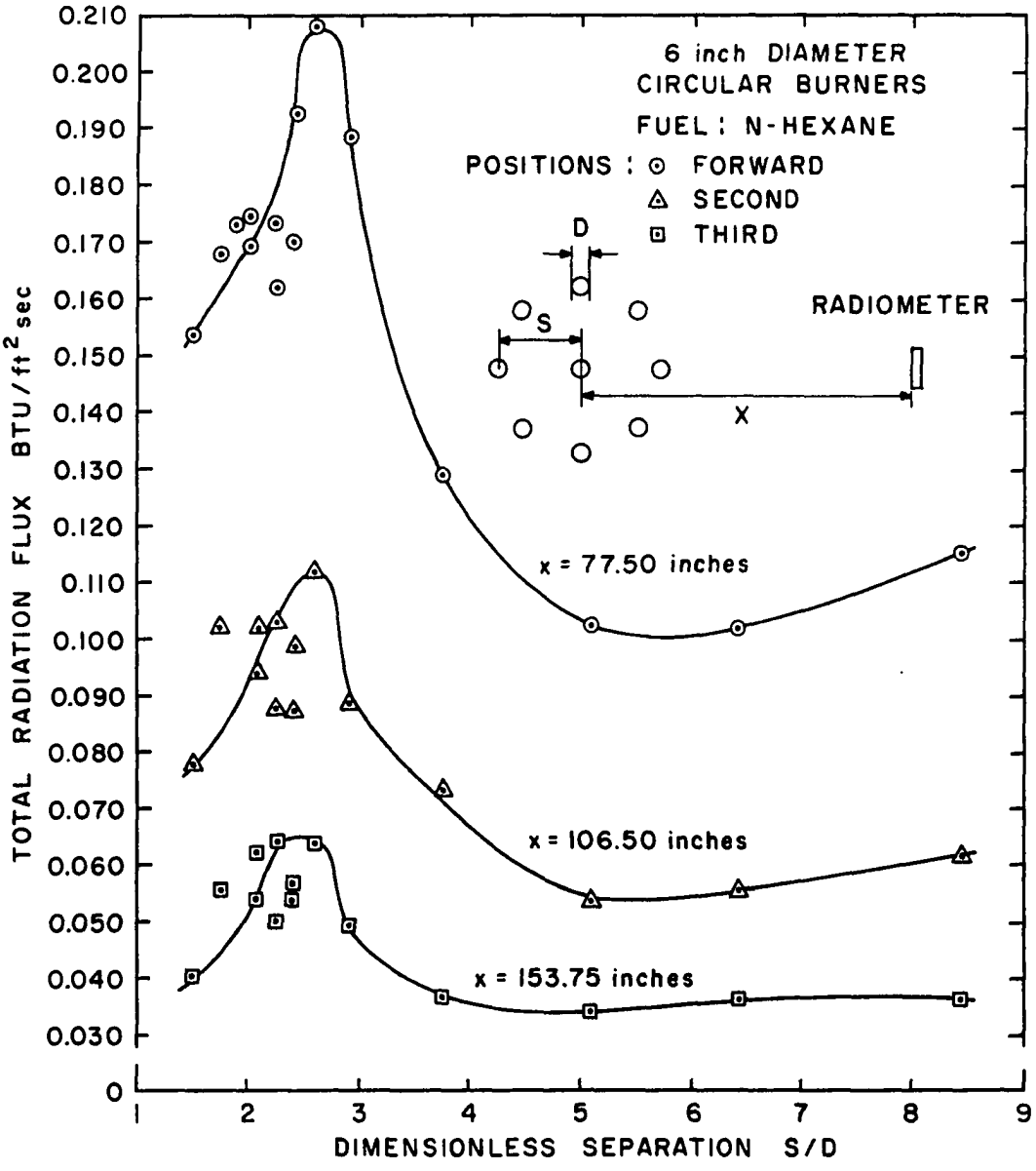

Figure 73. Radiation Flux of Interacting 6-Inch n-Hexane Fires.

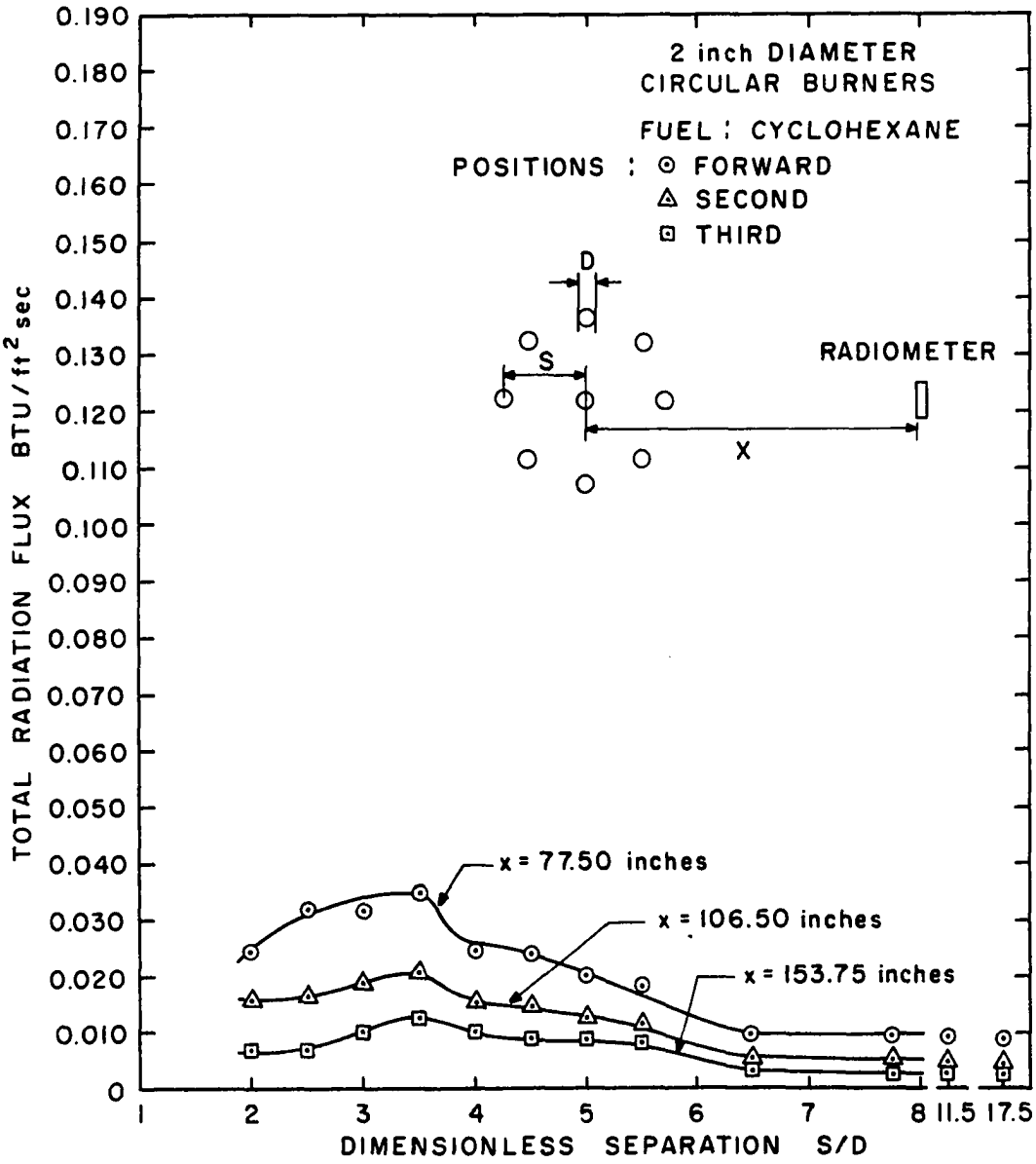

Figure 74. Radiation Flux of Interacting 2-Inch Cyclohexane Fires.

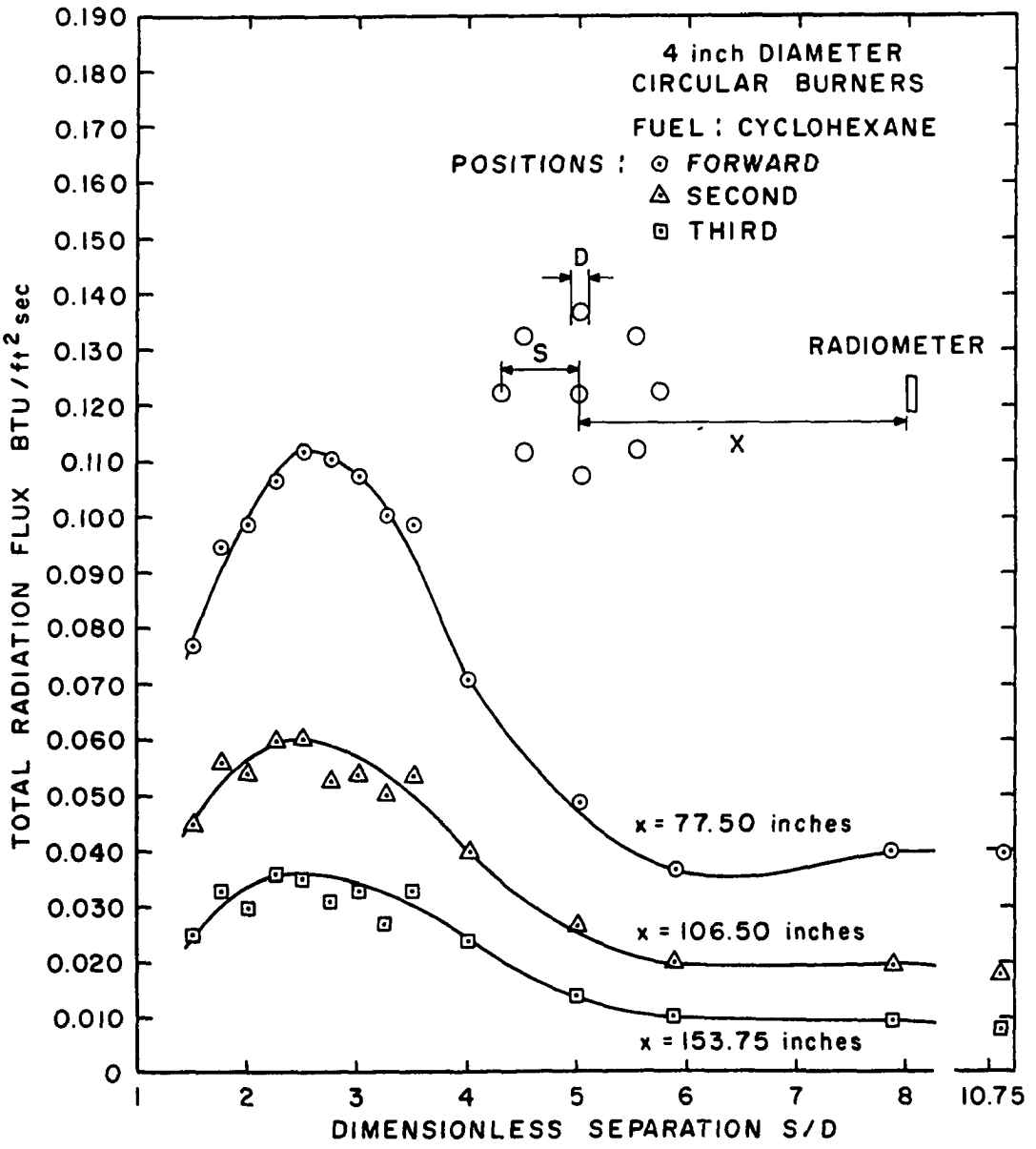

Figure 75. Radiation Flux of Interacting 4-Inch Cyclohexane Fires.

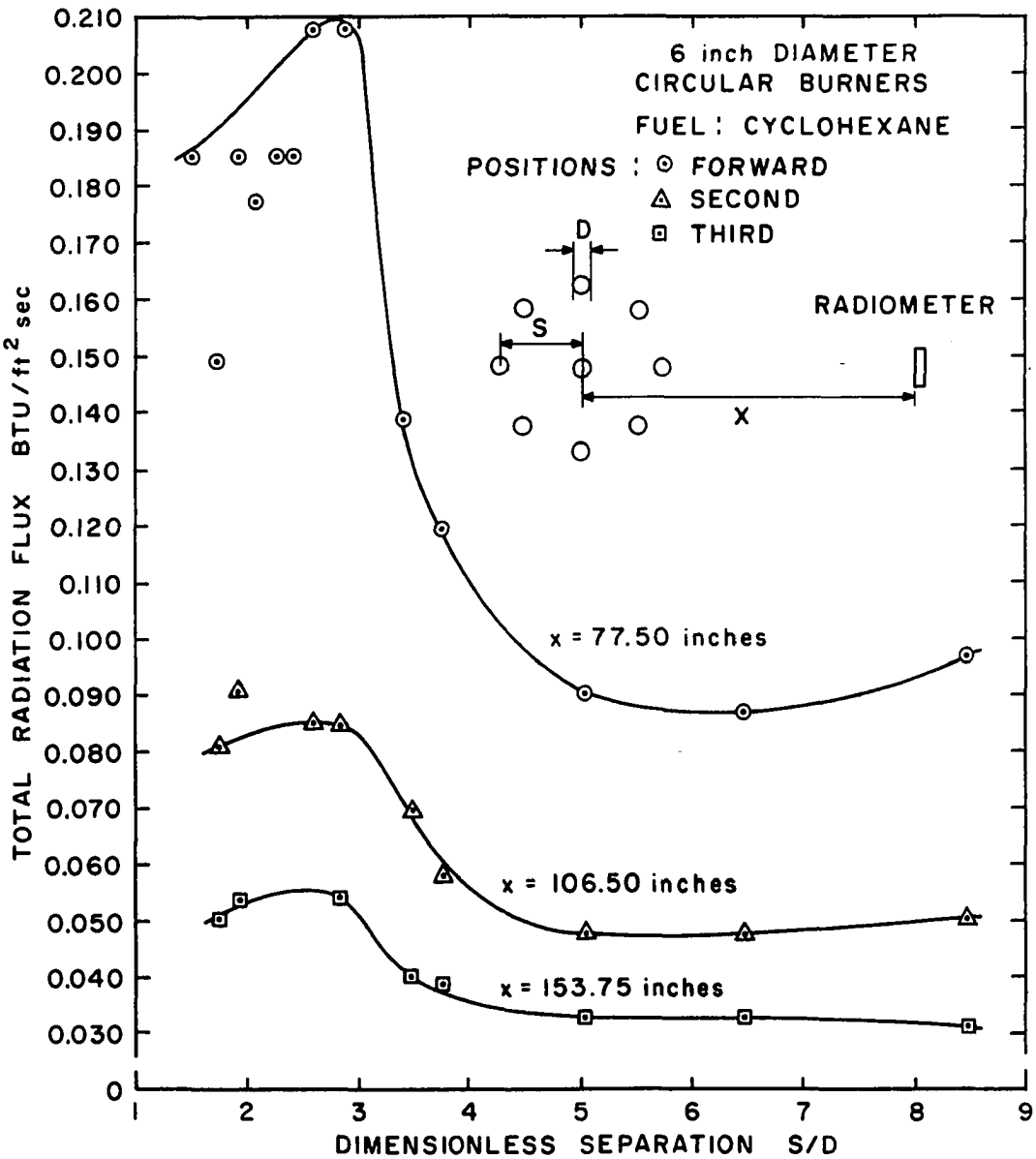

Figure 76. Radiation Flux of Interacting 6-Inch Cyclohexane Fires.

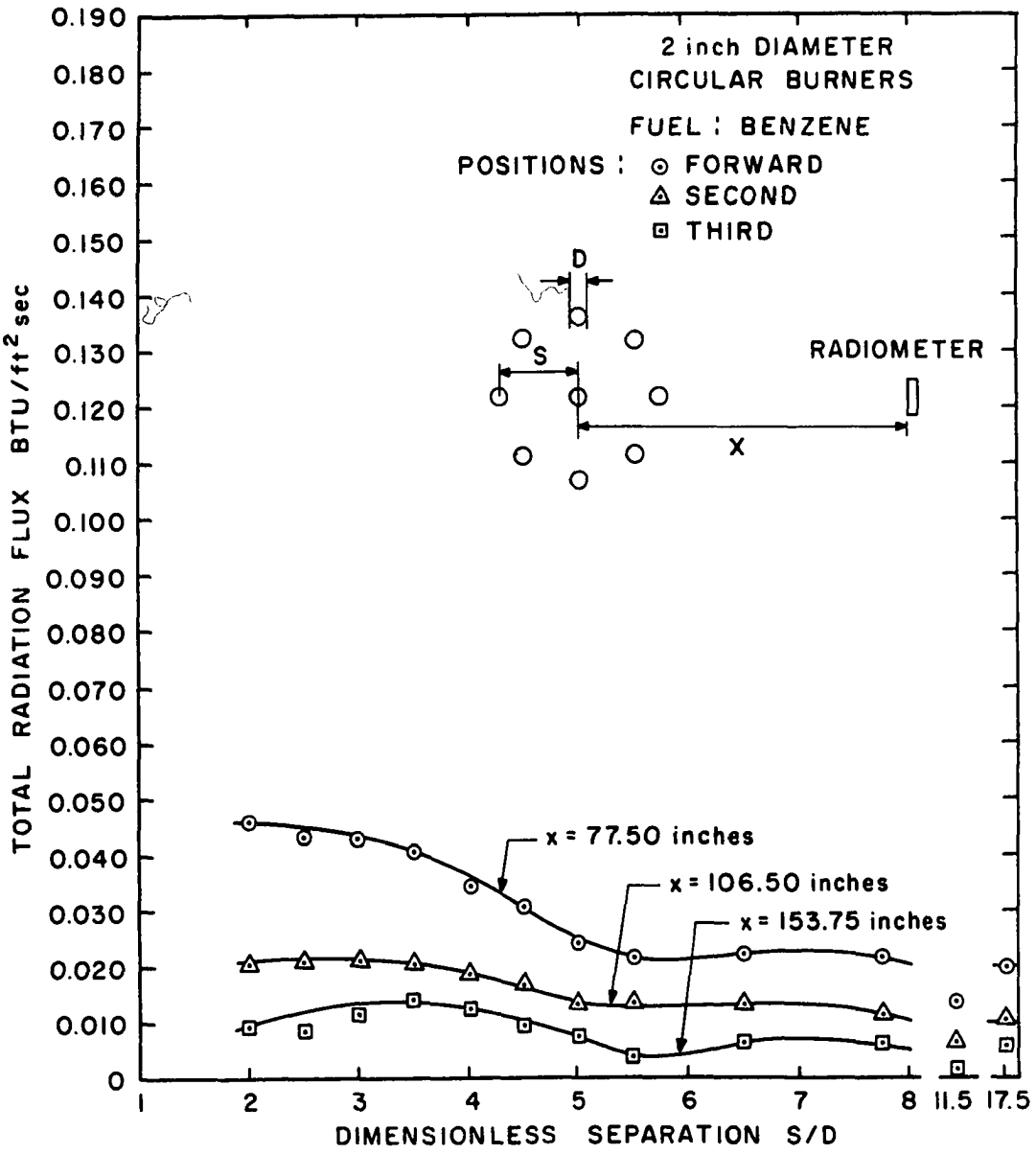

Figure 77. Radiation Flux of Interacting 2-Inch Benzene Fires.

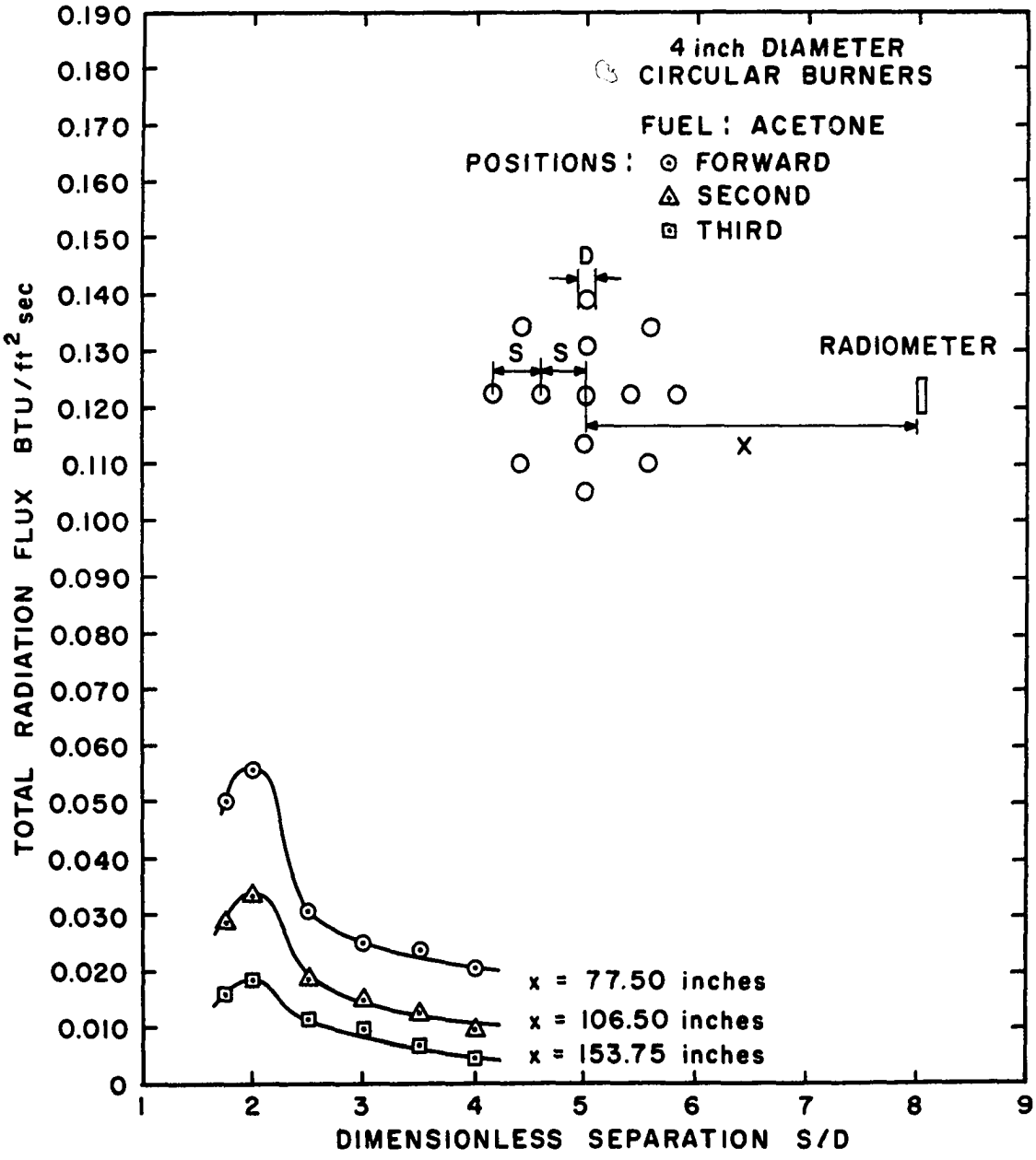

Figure 78. Radiation Flux of Interacting 4-Inch Acetone Fires (Thirteen-Burner Pattern).

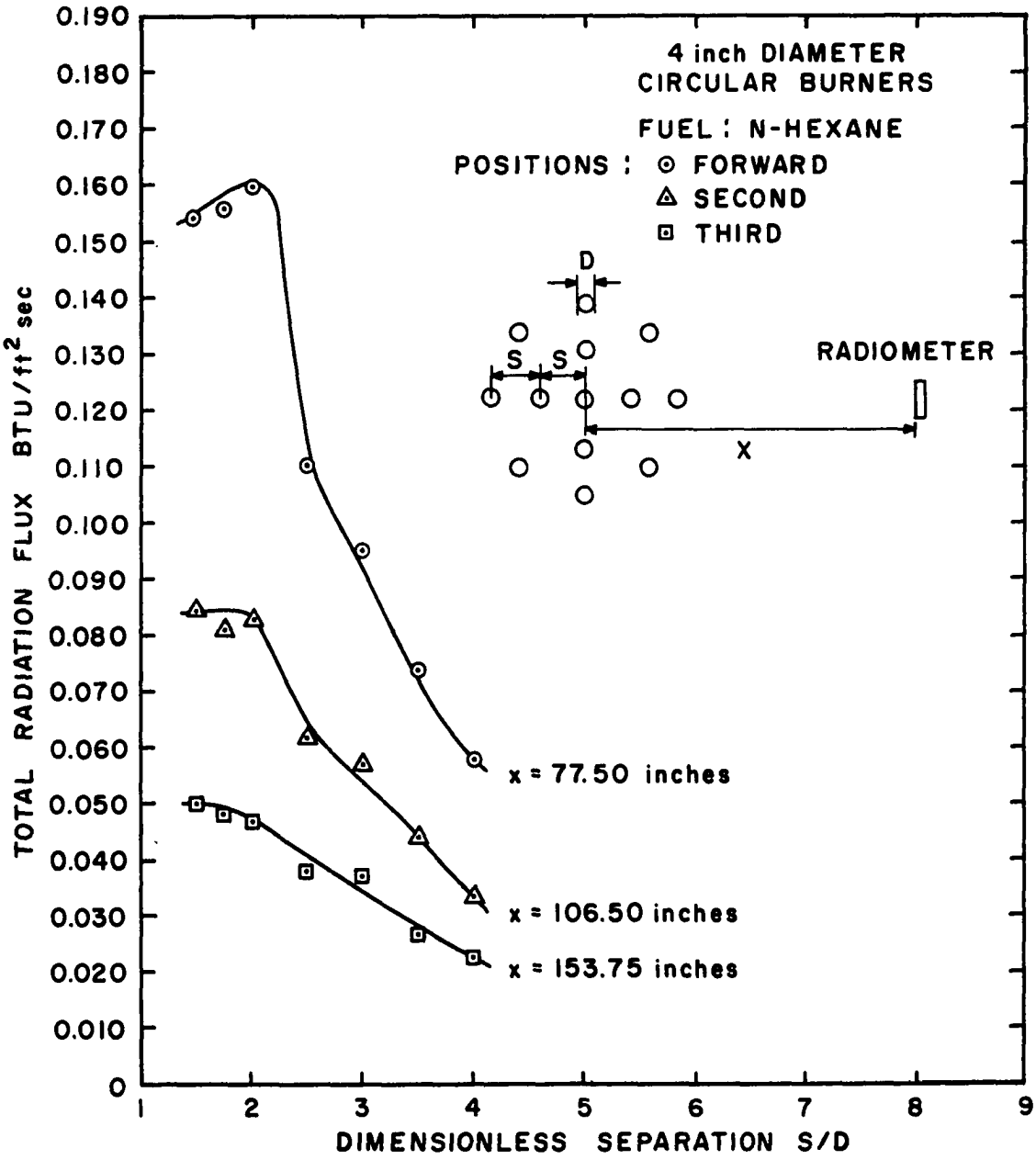

Figure 79. Radiation Flux of Interacting 4-Inch n-Hexane Fires (Thirteen-Burner Pattern).

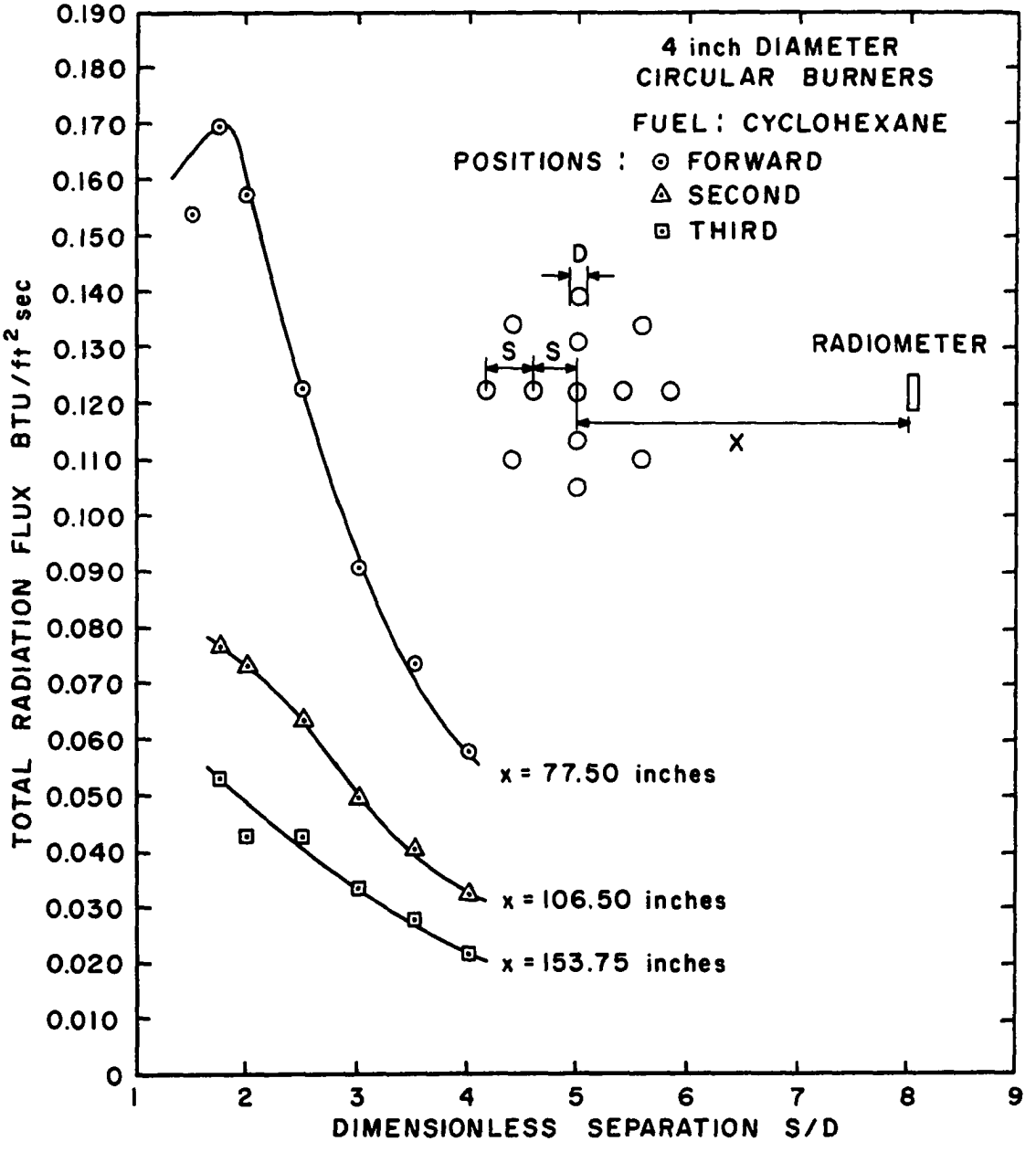

Figure 80. Radiation Flux of Interacting 4-Inch Cyclohexane Fires (Thirteen-Burner Pattern).

the fuel sources; therefore, more radiation was given off to the surroundings.

For the 4-inch acetone fires in Figure 69 and the 6-inch acetone fires in Figure 70, the radiation flux is seen to decrease as the burners are brought closer together, then rise sharply as the flame merging begins to take place. The initial decrease in the radiometer reading takes place because some of the flames are rather close to the radiometer when the burner separation distance is large. In making these measurements the burners were moved closer to the center of the burning table while the radiometer position was fixed. The radiation flux from the flame array was approximately the same for all burner positions until the interaction and merging effects began to be noticed at the smaller separation distances, although the radiometer reading decreased as the peripheral burner positions were changed due to the increased distance between the flames and the radiometer.

A comparison of Figures 37 and 70 for the burning rates and radiation flux, respectively, from the 6-inch acetone fires shows that the slight increase in burning rate at the beginning of interaction between the fires occurs at the same separation distance as the increase in radiation flux. It should also be noted that the maximum values of burning rate and radiation flux also occur at approximately the same burner separation distance for acetone,

as well as for the other fuels and burner sizes used.

The ratio of radiation flux to the average burning rate was plotted versus dimensionless burner separation distance in Figure 81 for several typical series of tests. For this curve the data from the radiometer at the two farthest positions from the table center were used. In addition, the data were restricted to those small burner separation distances at which the fires were interacting or merging. By limiting the data to these radiometer and burner positions, the effects of variation in the distance between the flame column and the radiometer can be considered to be at a minimum. From the curves, the ratio of the radiation flux to the average burning rate was seen to be approximately constant for merging fires. The ratio for several of the larger, smokier fires was seen to decrease at the smallest separation distances, indicating that the radiation flux dropped to a greater extent than did the burning rate. The decrease in the ratio of the radiation flux to the average burning rate at these close burner separations was due primarily to the buildup of smoke and combustion gases in the test room, which lowered the radiometer readings.

The ventilation system in the static test room proved to be inadequate to handle the large volume of smoke obtained from the large merging fires from several of the fuels such as hexane and cyclohexane, as well as the 2-inch benzene fires. Since data from the two farthest radiometer positions were taken

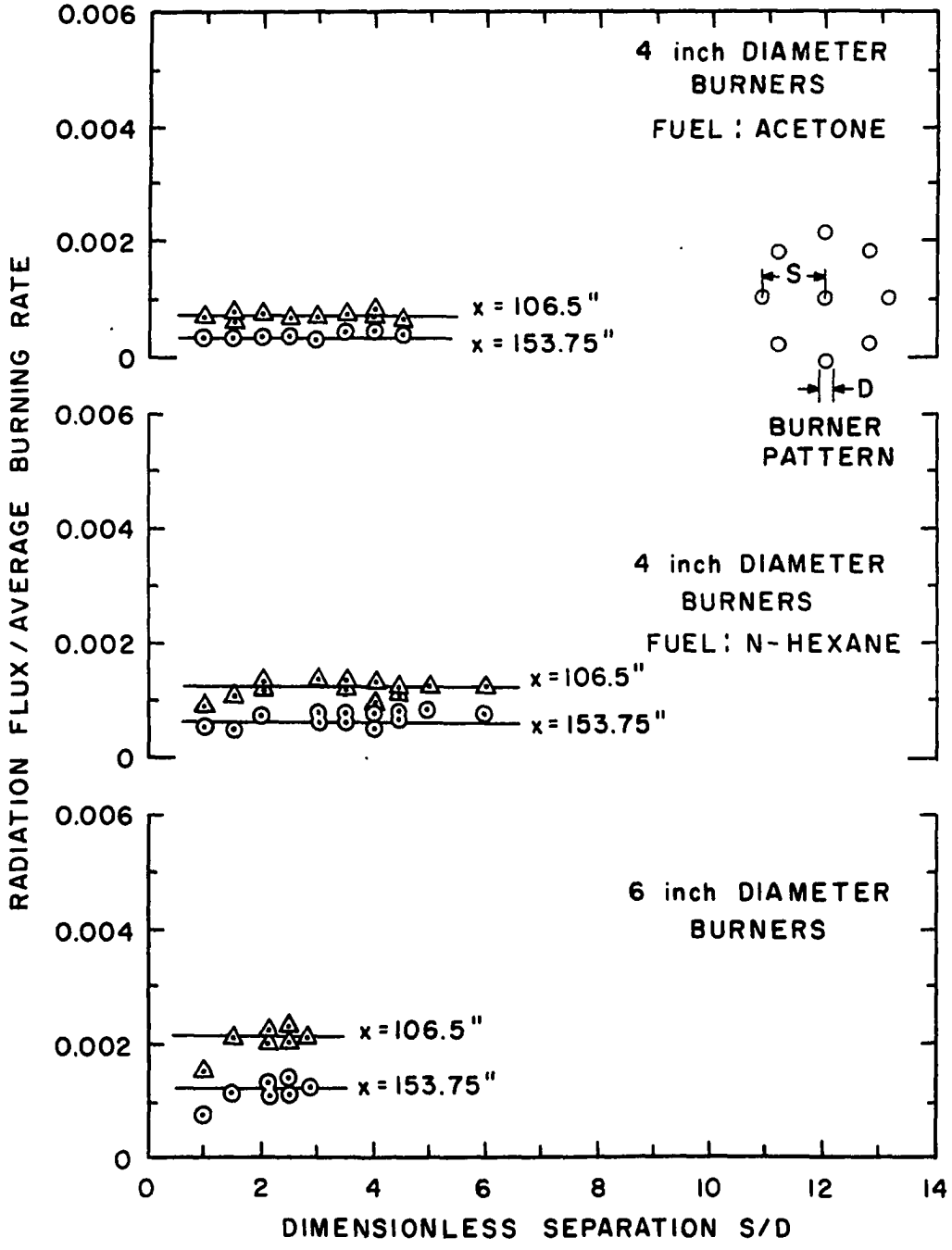

Figure 81. Ratio of Radiation Flux to Surroundings to Average Burning Rate as a Function of Burner Separation.

toward the end of a test, enough smoke and combustion gases from these fires accumulated in the test room for the flame radiation to be partially obscured from the radiometer sensing element. After a steady radiometer reading had been observed for a short time, the value of the reading would gradually decline as the amount of smoke in the room increased. The problem with the radiometer reading decreasing with time was not observed for the acetone fires, or for the smaller hexane or cyclohexane fires.

In order to assess the effect of flame radiation on the burning rate of a liquid fuel, the radiation at the fuel surface supporting the flame was measured. The radiation flux reaching the fuel surface is different from the intensity of radiation outside the flame. As mentioned previously, a blanket of fuel vapor was observed to cover the center of the burner array for several of the fuels when the fires were merging. This fuel vapor absorbs some of the flame radiation before it can reach the liquid fuel surface. The burners used in the tests were too small to place a radiometer directly in a fuel burner without influencing the burning rate, and consequently, the flame column over the burner and the amount of radiation back to the burner. Readings were therefore obtained with the radiometer positioned in the burning table surface next to the center burner. When the flames were merging, the fire column was spread over the entire center section of the

burner array and readings from this radiometer can be expected to give a good approximation of the actual radiation flux back to the center-burner fuel surface. When the flames were not merged, the center radiometer could see only part of the center fire; therefore, the readings at the larger burner separation distances are of little value. The radiation flux measured from the center radiometer is shown in Tables 3 and 4. The maximum values of this radiation flux back to the center radiometer are seen to occur at the same burner separation distances as the maximum values of the corresponding center-burner burning rate curves.

The fluctuations in the flame column over the radiometer caused the output readings of the center radiometer as a function of time to assume a sawtoothed shape although the difference between the maxima and minima of this curve was usually 15 per cent of the average value. The data recorded in Tables 3 and 4 are the average radiometer output values obtained from these curves. The radiation flux values obtained for benzene and the larger cyclohexane fires were probably too low. Even though the center radiometer window was gas purged, soot was observed to settle on this window when merging fires were obtained from these two fuels. As the soot would build-up on the window during a test, the radiometer reading would gradually decrease even though the steady burning rate had been reached for the test.

The radiometer data closely followed the trends in the burning rate data, even for the previously mentioned merging acetone test repeats. The main difficulty with these radiometer readings was caused by the accumulation of soot and combustion gases, as noted previously.

In summary, the curves of radiation flux to the surroundings as a function of burner separation were seen to correspond closely to the nine-burner average burning rate curves for the corresponding tests. In addition, the maximum values of flame radiation measurements made at the center of the burner array occurred at the same burner separation distances as the maximum values of the corresponding center-burner burning rate curves.

Heights of Flames from Interacting and Merging Fires

It was noted that the larger merging fire columns tended to form continually in a mushroom shape which would travel very quickly up the column and would break off from the main fire column just before disappearing. This pulsing effect, as well as other flame turbulence, necessitated a rather long film exposure in order to obtain a representative flame height. With the exposure used, photographs of the main body of the fire columns were slight overexposed, with the few instantaneous flickers at the top of the columns being recorded rather dimly on the film. The average flame height was interpreted as being the length of the overexposed portion of the fire column; the maximum

flame height was considered to be the entire length of the flame column recorded in the photograph. The cross-sectional area of the merging fire columns was measured from the photographs by means of a planimeter. The overexposed portion of the fire column was also considered to represent the average cross-sectional area of the column. The average flame heights for the interacting and merging fires, as well as the average cross-sectional area of the merging fire columns, are recorded in Tables 3 and 4. Photographs of a flame array at several burner separation distances are shown in Figure 11.

As merging of the individual flames occurred, the overall shape of the merging fire changed from conical to cylindrical, corresponding to a great increase in the height of the fire column. The data in Tables 3 and 4 show that as the flames became fully merged and the burning rate dropped, the size of the fire column also decreased.

The data on flame height and average fire column area obtained for the larger hexane and cyclohexane merging fires show a rather large amount of scatter. Distinct pictures of the largest fires could not be taken due to the accumulation of smoke in the test room. The outline of the average fire column area was therefore rather difficult to define for these smoky fires.

Thomas (25) in his studies of the flame heights of single wood cribs, developed a relation between the height

of a turbulent, buoyancy-controlled diffusion flame and the burning rate. This relation was of the form

$$L/D_{eq} = f(m/\rho_a\sqrt{g\ D_{eq}^5}) \quad , \qquad (20)$$

where L is the flame height, D_{eq} is the fuel source dimension, m is the mass flow rate of fuel, and ρ_a is the density of the surrounding air. The air density was used because the density of the wood volatiles was not properly known. This relation was developed by assuming the burning rate was independent of the heat feedback to the fuel.

Waterman, et al. (27) applied this flame height relation to their studies of multiple wood crib fires. The values of D_{eq} for these multiple fires was taken to be the dimension of the multiple crib array rather than that of a single crib. The above-mentioned flame height relation was applied to the multiple, liquid-fueled fires of the present study, and is shown in Figure 82 as a log-log plot of L/D_{eq} versus $(m/\rho_a\sqrt{g\ D_{eq}^5})$. Data for the burning rate at the onset of merging and the single-burner burning rate were plotted for the various fuels and sizes of rimless burners used in the present tests. The diameter of the burner array (2S) was used as D_{eq} for the multiple-fire burning rates. The data for wood cribs shown in Figure 82 was that given by Waterman, et al. (27) for single and multiple cribs and by Thomas (25) for single wood cribs. The sizes of

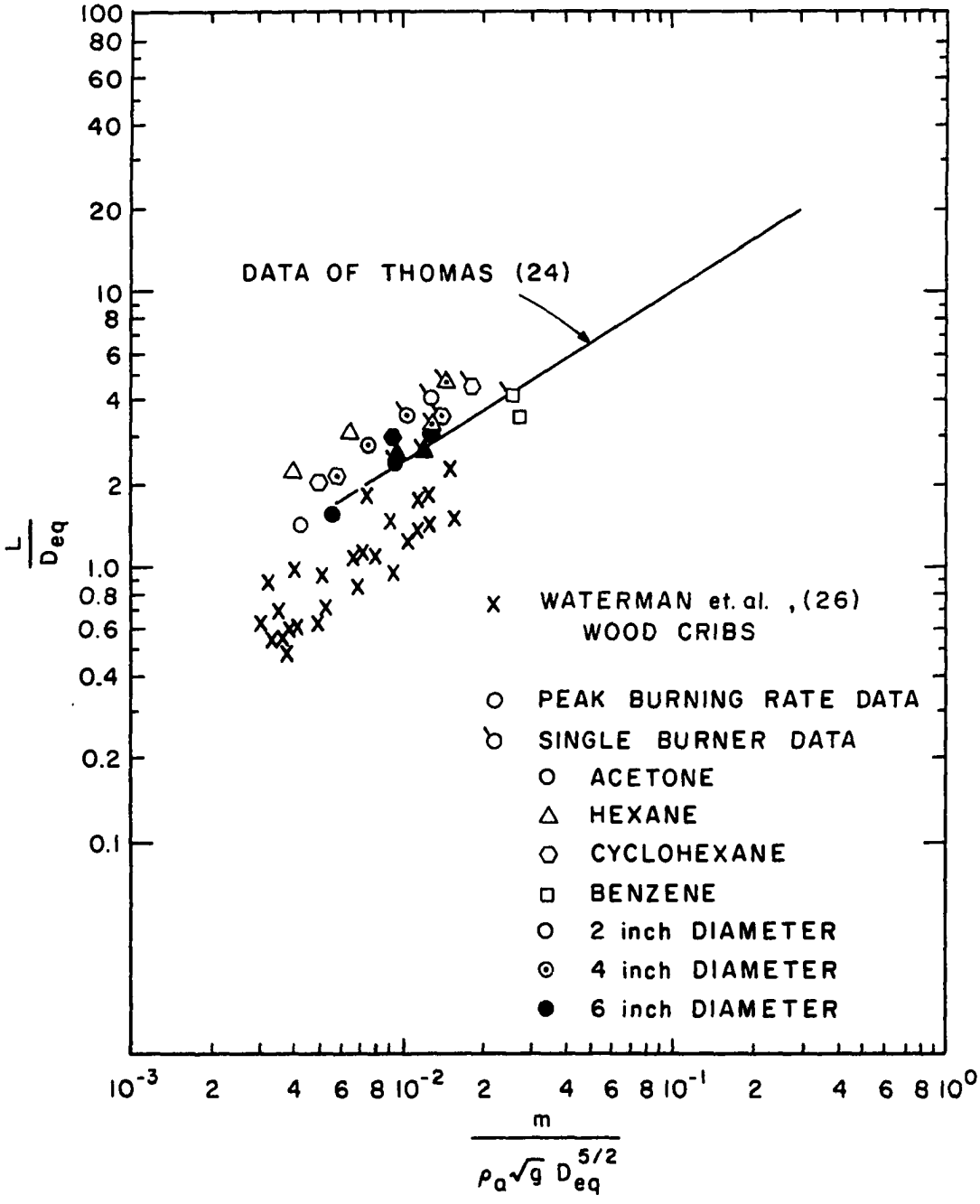

Figure 82. Effect of Burning Rate on Flame Height of Single and Multiple Fires.

Thomas' single wood cribs ranged from less than 2 feet to about 6 feet in width. Waterman's multiple cribs ranged from four, 3' x 3' cribs to sixteen, 3' x 3' cribs. The present liquid fuel data are seen to fall on or slightly above the line representing Thomas' data, whereas Waterman's multiple crib data had values of L/D_{eq} below Thomas' data. For Waterman's data, the spacing between the cribs was very small compared with the width of the cribs, making D_{eq} approximately equal to the actual dimension of the fuel surface. For the multiple liquid-fueled fires, the spacing between the liquid fuel burners was somewhat greater than the diameter of the burners, causing the values of D_{eq} to be much greater than the actual dimension of the fuel surface. The scatter in the data presented in the flame height correlation of Figure 82 shows the need for including additional parameters.

Flame Trailing

The flame trailing effect which was observed for the peripheral interacting fires was similar to that observed in the wind tunnel testing of liquid fuel fires. The fires were burning on the top of a flat surface with the air flow into the flame array causing the flame to trail along the table top toward the center of the array. The trailing is shown in Figure 83 for a 6-inch acetone fire. The flame trailing effect tends to cause the flames to merge at a greater burner

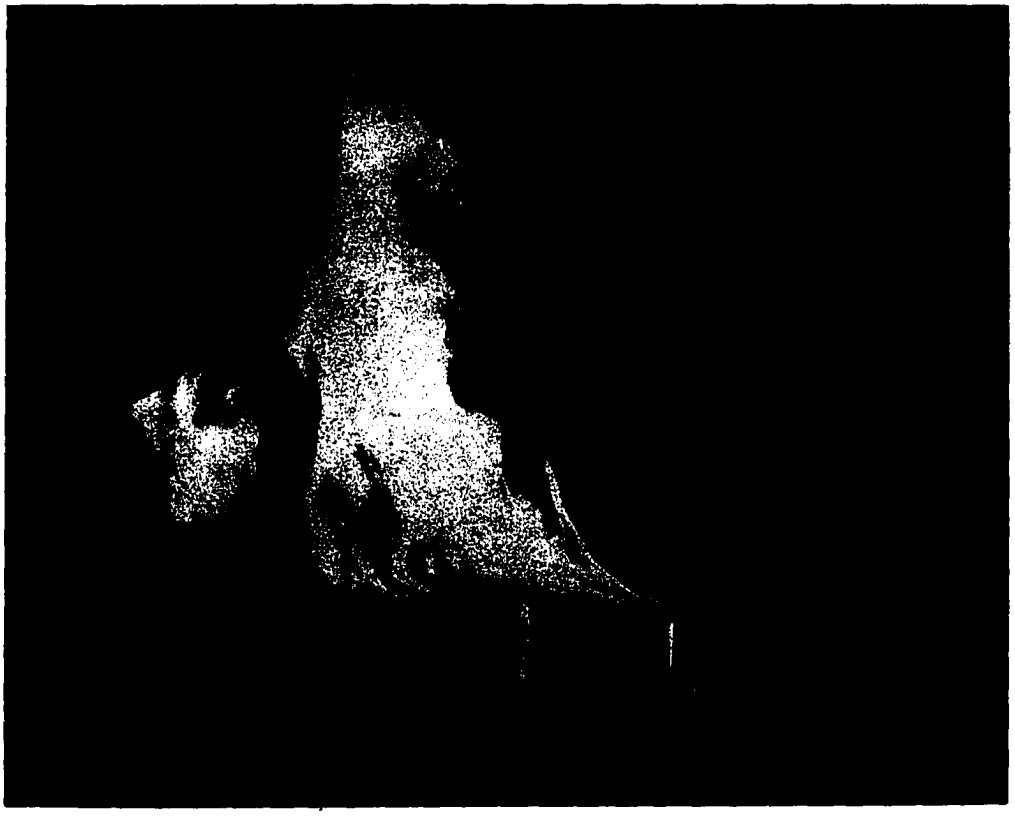

Figure 83. Bending and Trailing of Interacting Flames. (The white marks in the photograph denote the burner edges.)

separation distance than if the trailing did not occur. The trailing was greater for n-hexane and cyclohexane than for acetone, and it was even more pronounced for benzene. Larger burner sizes also increased the trailing effect.

Measurements of the flame trailing length were made for some of the tests by means of photographs. Photographic measurements could only be made for burner separation distances which were so large that the individual flames had not yet begun to merge. The air flow which caused the flames to trail toward the array center was due to entrainment of air by the flames. Greater air flows caused a greater trailing length. The anemometer was used to measure this air flow to one of the peripheral burners, and it was assumed that this flow was symmetrical with respect to the flame array. The trailing length and anemometer data are shown in Table 7.

The pulsing of the flames, as mentioned previously in connection with the flame height data, apparently caused variations in the anemometer readings since the entrainment of air by the flames was essentially the sole source of wind in the room. For very small fires spaced widely apart, no detectable anemometer readings were obtained. For larger interacting fires the results shown in Table 7 were obtained. For this particular data only a small amount of fluctuation was obtained in the readings. The data used were the average values read from the anemometer. When the fires merged

and very large flame columns were formed, the air entrainment as measured by the anemometer was greatly increased. The increased turbulence of the fire column caused very wide oscillations in the anemometer readings obtained.

Welker (28) in his wind tunnel studies developed a correlation for the flame trailing length as a function of the air velocity. He found by dimensional analysis that the ratio of flame trailing length to burner diameter (D'/D) could be correlated as a function of the Froude number and the ratio of fuel vapor density at the fuel boiling point to the density of the surrounding air. His data for five different sizes of single burners and five fuels were plotted as

$$\frac{D'}{D}\left(\frac{\rho_g}{\rho_a}\right)^{-0.48} \text{ versus } \frac{u^2}{gD} \quad .$$

The resulting equation was

$$\frac{D'}{D}\left(\frac{\rho_g}{\rho_a}\right)^{-0.48} = 2.1 \left(\frac{u^2}{gD}\right)^{0.21} \qquad (21)$$

The data for flame trailing lengths and the anemometer readings for the interacting fires were plotted on Welker's correlation. The resulting plot is shown in Figure 84. The interacting fire data are seen to fit the curve about as well as did the previous wind tunnel data.

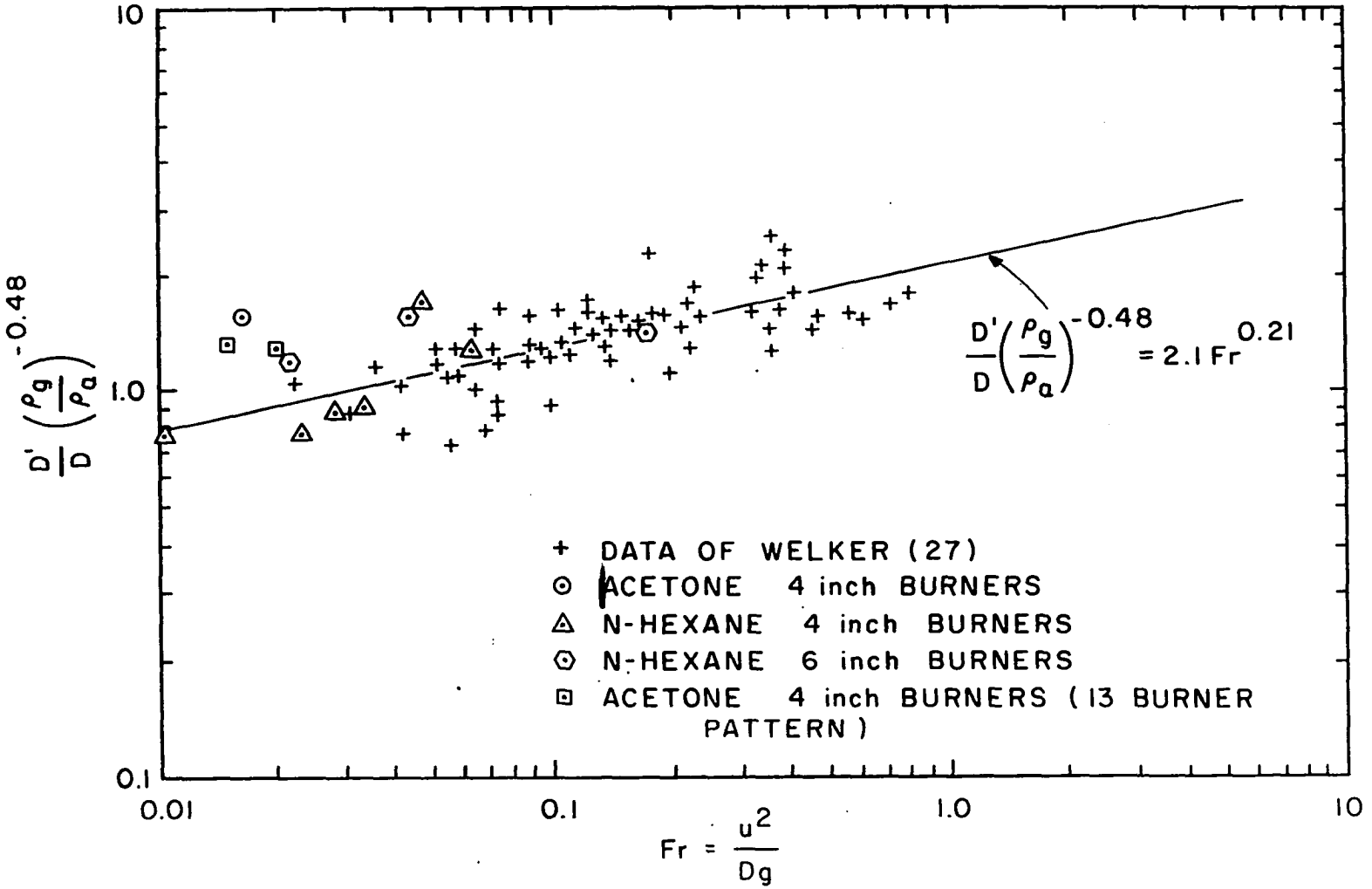

Figure 84. Flame Trailing Correlation for Interacting Fires.

Thermocouple Measurements and Brightness Temperatures

Data from thermocouples placed above the burning table were taken in an attempt to measure the temperature of the convective columns over the fires. Since the test room was rather small for the sizes of some of the fires burned during the tests, the air turbulence created in the room and the buildup of hot gases during a test caused the thermocouple data obtained to be of little value. For the largest merging fires obtained, the height of the fire column was sometimes above the height of the thermocouple grid, so that the thermocouples over the center of the table were completely enveloped in flame. Temperatures of up to 220°F were obtained from the thermocouples positioned over the outermost portion of the burning table for the merging hexane and cyclohexane fires in 6-inch burners. For the largest merging fires, temperatures above 1500°F were obtained from the thermocouples over the center of the table, since they were immersed in the fire column. The actual values measured by these thermocouples could not be read since the recorder would only record temperatures up to 1500°F. The previously described nickel-coated thermocouple radiation shields were used to minimize radiation effects on the temperature readings. These shields became blackened by the soot from the smoky fires; therefore, the shields would absorb radiation rather than reflect it. The hot shields increased the readings obtained from the thermocouples.

The optical pyrometer measured flame brightness temperatures of about 1800°F to about 2100°F for the various fuels. As mentioned previously, the flickering of the flames made the brightness temperatures very difficult to read. Variations in the temperature reading of about 200°F could be obtained during a particular test due to this flickering.

CHAPTER VI

CONCLUSIONS AND RECOMMENDATIONS

This study has been the first systematic investigation of the effects of merging of buoyant diffusion flames from burning pools of liquids. The effect of flame merging on the burning rate and radiation flux given off by the flames was studied for a number of different situations. Six liquid fuels: methanol, acetone, n-hexane, cyclohexane, napalm test solvent, and benzene were studied. Circular burners ranging in size from 1¼ to 6 inches in diameter were used in either nine-burner or thirteen-burner circular patterns, and 3-inch square burners were used in a nine-burner square pattern. The effect of exposing the burner walls to radiation from adjacent fires was also investigated by burning fires in both exposed-rim and rimless burners. For the rimless burners, the center-burner burning rate and the burning rate of the peripheral burners of the array were measured separately.

The trends in the burning rates as burner separation distance was varied depended both on the fuel and burners which were used. For large burner separation distances where there was no interaction between the individual fires, slight

variations in burner separation had no effect on the burning rate. With the exception of the methanol flames, the fires started to interact at the smaller burner separations and the burning rate began to increase. When the burner spacing was such that the flames began to merge into one fire column, the burning rate was greatly increased. Depending on the fuel and burners used, the nine-burner average burning rates for the merging fires ranged from two to approximately four times the corresponding burning rates for the non-interacting fires. The center-burner burning rate for the merging fires for some fuels increased to nearly six times the corresponding burning rate for the non-interacting fires.

As the fires became fully merged, the burning rates for the exposed-rim burners peaked and then dropped with further decreases in separation distance, as shown in Figure 15. The burning rates for most of the rimless-burner fires also dropped, although the burning rates for the benzene fires and the largest n-hexane and cyclohexane fires continued to increase as the fires became fully merged, as shown for cyclohexane in Figure 43.

A comparison of Figure 15 and Figures 36, 39, and 42 shows that the burning rates of the interacting or merging flames were always higher for the exposed-rim burners than for rimless burners of the same size; in fact, the peak hexane burning rate for the exposed-rim burners was more than twice as great as the peak burning rate for the rimless burners.

The greater burning rates of the exposed-rim burners were caused by the conduction of heat through the exposed burner wall to the fuel.

The curves of radiation flux to the surroundings as a function of burner separation were seen to correspond closely to the nine-burner average burning rate curves for the corresponding tests when either exposed-rim or rimless burners were used. In addition, the maximum values of flame radiation measurements made at the center of the rimless-burner array occurred at the same burner separation distances as the maximum values of the corresponding center-burner burning rate curves.

The burning rate of liquid-fueled fires is heavily dependent on the heat feedback from flame to fuel. The rimless burners were designed so that conduction of heat through the burner walls to the fuel could be considered negligible. The trends in the burning rate versus burner separation curves for these rimless-burner tests can therefore be explained by considering the variations in radiative and convective heat feedback to the fuel. The main cause of the large increase in burning rate as the fires begin to merge is the increase in radiation to the fuel surface from the adjacent flames, although increased convective heat feedback due to the proximity of other fires contributes to the burning rate increase. For the smaller as well as the more transparent fully-merged fires, the blockage of air to the fire array

center by the outer portion of the fire array causes a decrease in heat feedback to the fuel with a resulting drop in burning rate. For the larger as well as the more opaque merged fires, the increased radiative heat feedback to the peripheral-burner fuel due to the change in fire column shape is enough to offset any decrease in convective heat feedback; therefore, the peripheral-burner burning rates did not drop as these fires became fully merged.

Burning rate correlations were developed which allow the burning rate of interacting or merging, multiple, liquid-fueled fires to be predicted. These correlations were developed for two situations: where heating of the fuel-source rim is an important mode of heat feedback to the fuel (exposed-rim burners), and where this heating is unimportant (rimless burners). Correlations of the nine-burner average burning rates for the exposed-rim burners were developed which have the general form

$$\dot{m}\left(\frac{m_p}{m_s}\right)\left(\frac{\Delta H_c}{\Delta H_v}\right)^b \text{ versus } \left(\frac{S}{D}\right)\left(\dot{m}_s\right)^a$$

For the rimless burners, the burning rate correlations have the general form

$$\frac{\dot{m}}{\dot{m}_s}\left(\frac{\Delta H_c}{\Delta H_v}\right)\left(\frac{\rho_g}{\rho_a}\right)^b \text{ versus } \frac{S}{D}\left[\frac{m_p}{m_s}\left(\frac{\rho_g}{\rho_a}\right)\right]^a$$

for the center-burner burning rate and

$$\frac{m}{m_s}\left(\frac{\Delta H_c}{\Delta H_v}\right)\left(\frac{\rho_g}{\rho_a}\right)^b \text{ versus } \frac{S}{D}\left(\frac{m_p}{m_s}\right)^a$$

for the nine-burner average burning rate. "a" and "b" are empirical constants having different values for the center and average rimless-burner rates as well as the burning rates of the exposed-rim burners. Only the burning rate of a single source of the fuel, along with several properties of the fuel such as heat of combustion (ΔH_c), the heat of vaporization plus the sensible heat of raising the fuel from ambient temperature up to the boiling point (ΔH_v), and the ratio of fuel vapor density to ambient air density (ρ_g/ρ_a), needs to be known. The burning rate at the onset of merging, as well as the separation distance between the multiple fuel sources at which this merging occurs, can be predicted from Figures 19 or 20 for the exposed-rim burners, and from Figures 65 and 66 for the rimless burners.

As shown in Figures 38 through 40, the peak values of n-hexane burning rate per unit area at the onset of merging (m_p) showed little or no increase as the burner size was increased. For opaque flames from fuels such as n-hexane, much of the radiation from the merged fire column is absorbed by the fire itself before it can reach the fuel; therefore, the larger flame columns over the large burners contribute little extra radiation back to the fuel surface. In addition, for the fuels with opaque flames, the ratios of burning rate at

the onset of merging to the burning rate under interaction-free conditions (m_p/m_s) were observed to become smaller with increasing burner size. For the more transparent acetone fires these ratios (m_p/m_s) continued to increase with burner diameter but at a progressively reduced rate.

The above mentioned trends in burning rates as the fire size became larger indicates that the burning rate enhancement due to merging will become less as the fire size is increased. The burning rates per unit area for the merging fires (m_p), as well as the ratio (m_p/m_s), may well become constant for somewhat larger fire sizes than those tested in the present studies. If these burning rates do indeed become constant the merging-fire burning rate trends would be in accord with the burning rate trends observed by Blinov and Khudiakov for single-burner fires over a large range of burner sizes.

As will be discussed further in Appendix B, interesting similarities can be seen between the heat feedback to the fuel source of a very large single fire and to the center fuel source of an array of small multiple fires. These similarities in heat feedback lead to the possibility of predicting large-fire burning rates by burning small multiple fires.

In order to investigate larger multiple fires than those of the present study, as well as large single fires, a larger indoor testing facility would be needed. Due to the sensitivity of the liquid-fueled fires to stray winds,

adequate control over these fires cannot be exercised unless such tests are conducted indoors. A more adequate ventilation system would be necessary, enabling larger fires from fuels such as benzene to be studied. An improved ventilation system would also allow more reliable measurements to be made of the radiation flux to the surroundings for the large fires since smoke and combustion gases would not collect in the test room during a test.

APPENDIX A

TABLE 1

SUMMARY OF EXPOSED-RIM BURNER FLAME INTERACTION AND MERGING DATA[a]

Run No.[b]	Fuel[c]	Burner Diameter (inches)	Dimensionless Separation S/D	Average Burning Rate ($lb/hr-ft^2$)
1	A	1.25	8.5	27.0
2	A	1.25	6.9	24.0
3	A	1.25	6.1	28.7
4	A	1.25	5.3	32.0
5	A	1.25	4.5	34.6
6	A	1.25	3.7	28.6
7	A	1.25	2.8	37.1
8	A	1.25	2.1	45.8
9	M	1.25	8.5	14.7
10	M	1.25	6.9	14.4
11	M	1.25	6.1	11.8
12	M	1.25	5.3	14.2
13	M	1.25	4.5	14.9
14	M	1.25	3.7	13.2
15	M	1.25	2.8	13.2
16	M	1.25	2.1	13.2
17	A	2.063	4.4	19.8
18	A	2.063	6.3	17.1
19	A	2.063	5.4	17.5
20	A	2.063	3.4	22.0
21	M	2.063	6.3	8.2
22	M	2.063	5.4	9.0
23	M	2.063	4.4	8.6
24	M	2.063	3.4	8.2
25	M	2.063	2.9	9.5
26	M	2.063	2.4	9.7
27	M	2.063	2.0	11.3
28	M	2.063	1.5	12.8
29	M	2.063	2.4	11.1
30	A	2.063	2.9	32.7

[a] 9-burner circular pattern
[b] Run number denotes sequence in which tests were made.
[c] Fuels are denoted as follows: A - acetone; M - methanol.

TABLE 1 (Continued)

Run No.[b]	Fuel[c]	Burner Diameter (inches)	Dimensionless Separation S/D	Average Burning Rate ($lb/hr-ft^2$)
31	A	2.063	2.4	43.8
32	A	2.063	2.0	51.0
33	A	2.063	1.5	44.7
34	A	2.563	3.2	26.8
35	A	2.563	2.5	42.0
36	A	2.563	4.0	17.7
37	M	2.563	4.0	8.4
38	M	2.563	3.2	11.6
39	M	2.563	2.5	11.8
40	M	2.563	2.1	12.1
41	M	2.563	1.7	12.6
42	A	2.563	2.1	40.0
43	M	2.563	5.2	8.9
44	A	2.563	5.2	15.5
45	M	2.563	4.0	9.4
46	A	2.563	6.7	15.6
47	M	2.563	6.7	8.5
48	A	2.563	8.3	15.2
49	A	2.563	4.0	19.5
50	A	2.563	3.6	21.3
51	A	2.563	7.5	15.6
52	A	1.25	1.3	32.0

[b] Run number denotes sequence in which tests were made.
[c] Fuels are denoted as follows: A - acetone; M - methanol.

TABLE 2

SUMMARY OF EXPOSED-RIM BURNER FLAME INTERACTION AND MERGING DATA

Run No.[b]	Fuel[c]	Burner Dimensions (inches)	Dimensionless Separation (S/D)	Average Burning Rate ($lbs/hr\text{-}ft^2$)	Radiometer Readings[a] ($Btu/ft^2\text{-}sec$)
57	A	4-3/16 (Circular)	6.96	13.0	--
58	A		6.24	15.3	--
59	A		5.76	14.4	--
60	A		5.28	15.1	--
61	A		4.80	15.2	--
62	A		4.33	14.5	--
63	A		3.84	15.1	--
64	A		3.36	15.3	--
65	A		2.87	18.6	--
66	A		2.65	20.0	--
67	A		2.41	28.0	--
68	A		2.17	36.8	--
69	A		1.93	38.5	--
70	A		1.69	40.3	--
71	A		1.45	35.0	--
75	H		6.95	33.8	--
76	H		6.25	37.0	--
77	H		5.75	39.7	--
78	H		5.27	48.0	--
79	H		4.80	53.0	--
80	H		4.32	69.5	--
81	H		3.84	74.5	--
82	H		3.36	82.6	--

[a] Radiometer position at level of top of burners and 32 inches from edge of circular burning table top (64 inches from center of table).

[b] Run number denotes sequence in which tests were made.

[c] Fuels denoted as follows: A-acetone; B-benzene; C-cyclohexane; H-hexane; M-methanol; NTS-Napalm Test Solvent

TABLE 2 (Continued)

Run No.[b]	Fuel[c]	Burner Dimensions (inches)	Dimensionless Separation (S/D)	Average Burning Rate (lbs/hr-ft^2)	Radiometer Readings[a] (Btu/ft^2-sec)
83	H	4-3/16 Circular)	2.88	87.5	--
84	H		1.94	103.0	--
86	H		1.33	74.5	--
87	M		6.95	9.6	--
88	M		6.25	12.2	--
89	M		5.27	11.3	--
90	M		4.32	10.5	--
91	M		3.36	10.5	--
92	M		2.88	11.3	--
93	M		1.93	12.4	--
94	M		1.33	16.5	--
95	A	3 x 3 (Square)	5.84	21.1	--
96	A		5.16	24.2	--
97	A		3.83	30.6	--
98	A		3.16	36.8	--
99	A		2.50	51.4	--
100	A		2.16	63.0	--
101	A		1.83	61.0	--
102	A		1.50	47.0	--
103	A		1.00	27.3	--
104	H		6.17	66.6	--
105	H		5.16	68.6	--
106	H		4.50	103.2	--
107	H		3.83	105.6	--
108	H		3.16	138.5	--
109	H		2.50	118.5	--
110	H		2.16	103.5	--
111	H		1.83	103.0	--
112	H		1.50	90.9	--

[a] Radiometer position at level of top of burners and 32 inches from edge of circular burning table top (64 inches from center of table).

[b] Run number denotes sequence in which tests were made.

[c] Fuels denoted as follows: A-acetone; B-benzene; C-cyclohexane; H-hexane; M-methanol; NTS-Napalm Test Solvent.

TABLE 2 (Continued)

Run No.[b]	Fuel[c]	Burner Dimensions (inches)	Dimensionless Separation (S/D)	Average Burning Rate (lbs/hr-ft^2)	Radiometer Reading[a] (Btu/ft^2-sec)
113	C	3 x 3 (Square)	6.17	72.2	0.141
114	C		5.16	83.7	0.163
115	C		4.50	103.0	0.179
116	C		3.83	134.5	0.235
117	C		3.16	142.5	0.238
118	C		1.83	112.5	0.191
119	C		2.50	130.0	0.218
120	C		1.50	100.0	0.175
121	C		1.00	67.6	0.120
122	H		1.00	67.5	0.128
123	B		6.17	126.5	0.184
124	C	4-3/16 (Circular)	6.24	57.2	0.113
125	C		5.28	59.6	0.128
126	C		4.33	70.0	0.163
127	C		3.84	76.5	0.195
128	C		3.36	91.0	0.222
129	C		2.87	98.6	0.234
130	C		2.17	81.2	0.179
131	C		1.93	84.4	0.184
132	C		1.31	78.6	0.175
133	NTS	3 x 3 (Square)	6.17	100.0	0.140
134	NTS		5.16	114.0	0.143
135	NTS		4.5	134.0	0.185
136	NTS		4.0	179.0	0.244
137	NTS		3.16	161.0	0.238
138	NTS		2.5	154.0	0.218
139	NTS		1.83	133.5	0.175
140	NTS		1.0	94.5	0.113

[a]Radiometer position at level of top of burners and 32 inches from edge of circular burning table top (64 inches from center of table).

[b]Run number denotes sequence in which tests were made.

[c]Fuels denoted as follows: A-acetone; B-benzene; C-cyclohexane; H-hexane; M-methanol; NTS-Napalm Test Solvent.

TABLE 2 (Continued)

Run No.[b]	Fuel[c]	Burner Dimensions (inches)	Dimensionless Separation (S/D)	Average Burning Rate (lbs/hr-ft^2)	Radiometer Reading[a] (Btu/ft^2-sec)
141	NTS	4-3/16 (Circular)	6.24	50.7	0.135
142	NTS		5.28	74.6	0.147
143	NTS		4.33	88.2	0.187
144	NTS		3.84	97.0	0.214
145	NTS		3.36	105.0	0.244
146	NTS		2.87	--	0.248
147	NTS		2.41	97.0	0.195
148	NTS		1.93	80.0	0.156
149	NTS		1.31	--	0.206
150	M	3 x 3 (Square)	6.17	14.5	0.007
151	M		4.5	12.7	0.007
152	M		3.16	12.7	0.005
153	M		2.5	13.5	0.005
154	M		1.83	15.2	0.007
155	M		1.0	14.2	0.008
156	B	3 x 3 (Square)	5.16	133.4	0.206
157	B		4.5	172.0	0.230
158	B		3.83	205.1	0.270
159	B		3.16	172.0	0.274
160	B		2.5	169.0	0.253
161	B		1.83	137.0	0.222
162	B		1.0	94.6	0.215

[a]Radiometer position at level of top of burners and 32 inches from edge of circular burning table top (64 inches from center of table).

[b]Run number denotes sequence in which tests were made.

[c]Fuels denoted as follows: A-acetone; B-benzene; C-cyclohexane; H-hexane; M-methanol; NTS-Napalm Test Solvent.

TABLE 3

SUMMARY OF RIMLESS-BURNER FLAME INTERACTION AND MERGING DATA[a]

Run[c] No.	Fuel[b]	Nominal Burner Diameter (inches)	Dimensionless Burner Separation S/D	Burning Rate Per Unit Area (lb/hr-ft^2)			Radiation Flux to Surroundings (Btu/ft^2-sec)			Radiation Flux to Center Radiometer (Btu/ft^2-sec)	Average Flame Height (inches)	Average Flame Column Cross-Sectional Area (ft^2)
				Center Burner	Peripheral Burners	9-Burner Average	x=77.5 (inches)	x=106.5 (inches)	x=153.75 (inches)			
1201	M	4	4.9	10.9	9.5	9.6	--	--	--	--	8	--
1202	M	4	4.0	11.3	11.5	11.4	--	--	--	--	8	--
1202-A	M	4	4.0	9.4	10.6	10.4	--	--	--	--	7	--
1203	M	4	3.5	8.5	8.8	8.8	--	--	--	--	--	--
1203-A	M	4	3.5	9.4	9.3	9.3	--	--	--	--	--	--
1204	M	4	3.25	10.0	9.7	9.7	--	--	--	--	7	--
1205	M	4	3.0	9.8	9.7	9.7	--	--	--	--	7	--
1206	M	4	2.75	9.6	9.7	9.7	--	--	--	0.77	6	--
1207	M	4	2.5	9.6	12.4	12.0	--	--	--	1.03	7	--
1208	M	4	2.25	9.6	12.4	12.0	--	--	--	1.60	7	--
1209	M	4	2.0	10.7	11.5	11.4	--	--	--	1.76	7	--
1212	M	4	1.75	10.4	10.4	10.4	0.0062	--	--	--	8	--
1213	M	4	1.5	14.3	11.3	11.6	0.0096	--	--	--	16	--
1301	M	6	7.1	7.9	9.0	8.9	0.0123	0.0069	--	0.28	7	--
1302	M	6	5.1	7.9	9.9	9.7	0.0131	0.0069	--	0.28	7	--
1303	M	6	3.75	8.4	9.3	9.2	0.0131	0.0077	--	0.38	10	--
1304	M	6	3.2	8.4	10.5	10.3	0.0127	0.0073	--	0.50	9	--
1305	M	6	2.8	8.9	10.4	10.2	0.0127	0.0077	--	0.55	8	--
1306	M	6	2.5	8.9	10.0	10.0	0.0138	--	--	0.70	9	--
1307	M	6	2.3	9.0	10.3	10.0	0.0108	--	--	0.70	10	--
1308	M	6	2.2	10.0	11.1	11.0	0.0138	--	--	0.93	9	--
1309	M	6	2.0	10.2	10.9	10.8	0.0131	--	--	1.08	11	--
1309-A	M	6	2.0	10.7	10.9	10.9	0.0131	--	--	0.95	11	--
1310	M	6	1.8	11.3	11.2	11.2	0.0146	--	--	1.30	10	--
1310-A	M	6	1.8	10.2	10.8	10.7	0.0123	--	--	1.23	11	--
1311	M	6	1.5	13.9	11.2	11.5	0.0150	--	--	2.02	--	--

[a] 9-Burner Circular Pattern.

[b] Fuels are denoted as follows: A - acetone; B - benzene; C - cyclohexane; H - n-hexane; M - methanol.

[c] See footnote at end of Table 3.

TABLE 3 (Continued)

Run[c] No.	Fuel[b]	Nominal Burner Diameter (inches)	Dimensionless Burner Separation S/D	Burning Per Unit Area (lb/hr-ft^2)			Radiation Flux to Surroundings (Btu/ft^2-sec)			Radiation Flux to Center Radiometer (Btu/ft^2-sec)	Average Flame Height (inches)	Average Flame Column Cross-Sectional Area (ft^2)
				Center Burner	Peripheral Burners	9-Burner Average	x=77.5 (inches)	x=106.5 (inches)	x=153.75 (inches)			
2101	A	2	15.5	12.2	14.1	13.9	0.0021	--	--	0.28	7	--
2102	A	2	9.5	10.9	12.8	12.6	0.0022	--	--	0.28	7	--
2103	A	2	6.5	12.6	14.1	13.9	0.0025	--	--	0.38	8	--
2104	A	2	5.5	13.9	14.1	14.1	0.0033	--	--	0.45	8	--
2105	A	2	4.5	13.1	15.0	14.8	0.0033	--	--	0.60	9	--
2106	A	2	4.0	14.3	15.0	14.9	0.0036	--	--	0.77	9	--
2107	A	2	3.5	18.2	15.9	16.1	0.0036	--	--	1.03	9	--
2108	A	2	3.0	26.5	16.3	18.5	0.0045	--	--	1.60	13	0.6
2109	A	2	2.5	34.1	21.6	23.0	0.0058	--	--	1.76	14	0.9
2110	A	2	2.0	34.1	21.2	22.6	0.0075	--	--	1.63	27	1.1
2201	A	4	6.0	11.5	14.6	14.2	0.0154	--	--	0.50	12	--
2202	A	4	7.9	11.5	13.9	13.6	0.0161	--	--	0.30	12	--
2203	A	4	10.0	12.1	13.2	13.1	0.0177	0.0100	--	0.38	13	--
2204	A	4	4.4	14.5	15.2	15.1	0.0169	--	--	0.95	13	--
2205	A	4	4.0	16.6	16.3	16.3	0.0177	--	--	1.03	15	--
2206	A	4	3.5	18.3	18.1	18.1	0.0177	0.0100	0.0046	1.35	15	--
2207	A	4	3.25	17.5	17.2	17.2	0.0192	0.0123	0.0062	1.40	15	2.0
2207-A	A	4	3.25	25.9	19.3	20.0	0.0231	0.0131	0.0073	1.05	17	2.1
2208	A	4	3.0	22.1	19.2	19.5	0.0200	0.0123	0.0062	1.50	18	2.0
2208-A	A	4	3.0	30.9	21.5	22.5	0.0261	0.0154	0.0092	1.20	19	2.4
2209	A	4	2.75	25.3	18.3	19.0	0.0208	0.0131	0.0054	2.08	19	1.9
2209-A	A	4	2.75	30.7	19.3	20.5	0.0238	0.0150	0.0088	1.80	--	--
2210	A	4	2.5	28.1	22.5	23.1	0.0238	0.0138	0.0069	2.68	23	2.1
2211	A	4	2.25	37.1	23.4	24.8	0.0315	0.0161	0.0085	3.45	31	2.5
2212	A	4	2.0	40.9	23.8	25.7	0.0354	0.0192	0.0092	3.90	43	2.9
2212-A	A	4	2.0	50.3	30.0	32.1	0.0415	0.0246	0.0138	2.35	41	3.4
2213	A	4	1.75	36.6	29.6	30.3	0.0346	0.0177	0.0092	3.45	47	3.9
2213-A	A	4	1.75	41.0	28.1	29.4	0.0400	0.0231	0.0138	1.70	43	3.8
2214	A	4	1.5	27.7	23.4	23.8	0.0300	0.0169	0.0085	2.85	49	3.5
2215	A	4	Single Burner	13.6	--	13.6	0.0019	--	--	2.84	14	0.3

[b]Fuels are denoted as follows: A - acetone; B - benzene; C - cyclohexane; H - n-hexane; M - methanol.

[c]See footnote at end of Table 3.

TABLE 3 (Continued)

Run[c] No.	Fuel[b]	Nominal Burner Diameter (inches)	Dimensionless Burner Separation S/D	Burning Rate Per Unit Area (lb/hr-ft^2)			Radiation Flux to Surroundings (Btu/ft^2-sec)			Radiation Flux to Center Radiometer (Btu/ft^2-sec)	Average Flame Height (inches)	Average Flame Column Cross-Sectional Area (ft^2)
				Center Burner	Peripheral Burners	9-Burner Average	x=77.5 (inches)	x=106.5 (inches)	x=153.75 (inches)			
2301	A	6	8.4	15.4	15.7	15.7	0.0630	0.0399	0.0284	0.50	15	--
2302	A	6	6.4	19.0	16.9	17.1	0.0569	0.0384	0.0284	0.50	14	--
2303	A	6	5.1	19.2	19.4	19.4	0.0646	0.0423	0.0323	0.75	17	--
2303-A	A	6	5.1	16.5	16.0	16.1	0.0408	0.0238	0.0154	--	16	--
2304	A	6	3.75	18.1	17.9	17.9	0.0484	0.0285	0.0169	1.08	21	--
2304-A	A	6	3.75	20.0	17.5	17.7	0.0461	0.0261	0.0161	--	20	--
2305	A	6	3.2	24.0	20.2	20.6	0.0576	0.0338	0.0177	1.98	20	--
2306	A	6	2.8	29.0	21.2	22.1	0.0654	0.0377	0.0207	2.78	24	3.8
2307	A	6	2.6	34.1	22.9	24.1	0.0707	0.0399	0.0215	3.30	27	3.8
2308	A	6	2.4	36.5	22.1	23.7	0.0769	0.0477	0.0284	3.90	27	4.1
2309	A	6	2.25	48.4	25.2	27.8	0.0946	0.0576	0.0346	4.43	40	4.5
2310	A	6	2.1	52.8	26.6	29.5	0.1015	0.0600	0.0369	4.15	42	5.7
2310-A	A	6	2.1	65.3	30.7	34.6	0.1015	0.0600	0.0361	--	50	5.8
2311	A	6	1.9	50.5	26.5	29.1	0.0984	0.0576	0.0384	4.63	58	6.2
2311-A	A	6	1.9	55.8	30.1	32.9	0.0961	0.0561	0.0354	--	53	6.2
2312	A	6	1.75	46.7	24.0	26.5	0.0946	0.0576	0.0354	4.25	56	6.1
2313	A	6	1.5	35.4	24.4	25.6	0.0769	0.0454	0.0246	4.13	52	6.1
2314	A	6	Single Burner	13.4	--	13.4	0.0042	--	--	3.75	18	0.6
3101	H	2	17.5	12.1	12.5	12.4	0.0082	--	--	0.375	9	--
3102	H	2	11.5	14.5	15.9	15.7	0.0092	0.0052	0.0035	0.45	8	--
3103	H	2	7.75	20.8	16.7	17.1	0.0098	0.0055	0.0033	0.50	10	--
3104	H	2	6.5	24.8	17.8	18.5	0.0106	0.0058	0.0034	1.35	12	--
3105	H	2	5.5	33.2	20.3	21.7	0.0118	0.0062	0.0035	1.80	12	--
3106	H	2	5.0	27.2	18.8	19.7	0.0104	0.0058	0.0032	1.60	15	--
3107	H	2	4.5	42.5	23.2	25.3	0.0141	0.0073	0.0038	2.30	14	1.3
3108	H	2	4.0	46.8	24.7	27.1	0.0159	0.0085	0.0042	2.93	19	1.4
3109	H	2	3.5	71.6	39.1	42.6	0.0261	0.0140	0.0075	4.20	28	1.7
3110	H	2	3.0	70.2	36.8	40.4	0.0259	0.0131	0.0067	3.83	33	2.0
3111	H	2	2.5	59.5	30.9	34.0	0.0193	0.0106	0.0056	3.38	33	2.1
3112	H	2	2.0	38.6	30.9	31.7	0.0171	0.0088	0.0044	2.70	31	2.2
3113	H	2	Single Burner	10.6	--	10.6	0.0015	--	--	0.30	12	0.3

[b]Fuels are denoted as follows: A - acetone; B - benzene; C - cyclohexane; H - n-hexane; M - methanol.

[c]See footnote at end of Table 3.

TABLE 3 (Continued)

Run[c] No.	Fuel[b]	Nominal Burner Diameter (inches)	Dimensionless Burner Separation S/D	Burning Rate Per Unit Area (lb/hr-ft^2)			Radiation Flux to Surroundings (Btu/ft^2-sec)			Radiation Flux to Center Radiometer (Btu/ft^2-sec)	Average Flame Height	Average Flame Column Cross-Sectional Area (ft^2)
				Center Burner	Peripheral Burners	9-Burner Average	x=77.5 (inches)	x=106.5 (inches)	x=153.75 (inches)			
3201	H	4	8.75	20.1	17.1	17.4	0.0469	0.0261	0.0185	0.75	13	--
3202-A	H	4	7.9	20.4	18.3	18.5	0.0438	0.0246	0.0169	0.53	15	--
3203	H	4	5.9	25.7	20.0	20.6	0.0500	0.0269	0.0177	0.93	15	--
3204	H	4	4.4	38.0	22.5	24.1	0.0569	0.0277	0.0161	1.80	16	--
3205	H	4	4.0	54.5	27.1	30.0	0.0677	0.0369	0.0231	2.70	22	--
3206	H	4	3.5	75.5	34.3	38.8	0.0884	0.0484	0.0323	4.13	24	--
3207	H	4	3.25	78.3	39.5	43.7	0.0984	0.0561	0.0331	4.13	--	--
3207-A	H	4	3.25	81.4	42.0	46.3	0.0961	0.0523	0.0300	--	38	4.2
3208	H	4	3.0	81.1	39.5	44.0	0.1038	0.0584	0.0346	4.43	--	4.3
3208-A	H	4	3.0	78.7	40.6	44.7	0.0892	0.0438	0.0223	--	41	4.3
3209	H	4	2.75	81.1	41.6	45.9	0.1100	0.0615	0.0361	4.65	43	4.9
3209-A	H	4	2.75	76.8	45.1	48.5	0.0946	0.0554	0.0308	--	51	4.8
3210	H	4	2.5	77.6	42.7	46.4	0.1100	0.0615	0.0361	4.58	52	5.5
3210-A	H	4	2.5	73.4	41.8	45.2	0.1015	0.0600	0.0308	--	62	5.4
3211-A	H	4	2.25	62.5	43.2	45.3	0.1000	0.0577	0.0346	--	57	6.1
3212	H	4	2.0	52.4	44.8	45.5	0.1000	0.0600	0.0346	3.45	63	5.9
3212-A	H	4	2.0	57.3	45.3	46.5	0.1077	0.0596	0.0346	--	67	6.9
3213-A	H	4	1.75	46.2	39.0	39.7	0.0825	0.0438	0.0208	--	67	6.3
3213-B	H	4	1.75	55.8	41.5	43.0	0.0846	0.0492	0.0285	--	57	6.0
3214-A	H	4	1.5	49.4	37.5	38.7	0.0715	0.0385	0.0208	--	56	4.9
3214-B	H	4	1.5	48.7	44.0	44.4	--	--	--	--	54	4.6
3215	H	4	Single Burner	25.4	--	25.4	--	--	--	0.63	19	0.8

[b]Fuels are denoted as follows: A - acetone; B - benzene; C - cyclohexane; H - n-hexane; M - methanol.

[c]See footnote at end of Table 3.

TABLE 3 (Continued)

Run[c] No.	Fuel[b]	Nominal Burner Diameter (inches)	Dimensionless Burner Separation S/D	Burning Rate Per Unit Area (lb/hr-ft^2)			Radiation Flux to Surroundings (Btu/ft^2-sec)			Radiation Flux to Center Radiometer (Btu/ft^2-sec)	Average Flame Height (inches)	Average Flame Column Cross-Sectional Area (ft^2)
				Center Burner	Peripheral Burners	9-Burner Average	x=77.5 (inches)	x=106.5 (inches)	X=153.75 (inches)			
3301	H	6	8.4	19.9	22.6	22.3	0.1153	0.0615	0.0361	0.20	15	--
3301-A	H	6	8.4	18.6	22.2	21.8	0.1153	0.0615	0.0368	0.23	17	--
3302	H	6	6.4	19.9	22.6	22.3	0.1015	0.0554	0.0361	0.43	--	--
3303	H	6	5.1	28.4	23.2	23.8	0.1023	0.0538	0.0338	0.65	--	--
3304	H	6	3.75	57.7	27.4	30.7	0.1291	0.0731	0.0361	2.93	18	--
3305	H	6	2.8	80.5	37.4	42.2	0.1884	0.0884	0.0492	4.43	--	--
3306-A	H	6	2.6	81.9	43.0	47.3	0.2076	0.1115	0.0631	3.45	80	12.1
3307	H	6	2.4	74.5	41.6	45.2	0.1923	0.0984	0.0538	3.45	81	9.6
3307-A	H	6	2.4	75.5	40.3	44.2	0.1692	0.0923	0.0569	4.73	74	8.9
3308	H	6	2.25	66.1	38.8	41.8	0.1615	0.0877	0.0500	3.00	79	11.4
3308-A	H	6	2.25	69.5	40.4	43.6	0.1730	0.1023	0.0638	4.43	65	10.4
3309	H	6	2.1	72.6	43.3	46.6	0.1692	0.0938	0.0538	3.08	77	10.3
3309-A	H	6	2.1	72.6	41.6	45.0	0.1747	0.1015	0.0615	4.13	65	8.9
3310	H	6	1.9	71.2	49.2	51.6	0.1730	--	--	2.63	82	--
3311	H	6	1.75	61.0	45.4	47.1	0.1676	0.1015	0.0554	2.70	85	11.7
3312	H	6	1.5	61.5	47.8	49.3	0.1530	0.0777	0.0400	2.55	75	11.0
3312-A	H	6	1.5	55.4	46.8	47.7	--	--	--	--	--	--
3313	H	6	Single Burner	22.5	--	22.5	0.0146	0.0087	0.0056	0.40	30	1.5
4101	C	2	17.5	17.8	16.0	16.2	0.0088	0.0046	0.0021	0.25	9	--
4102	C	2	11.5	12.2	18.8	18.1	0.0092	0.0050	0.0023	0.63	9	--
4103	C	2	7.75	18.7	18.8	18.8	0.0094	0.0052	0.0028	0.88	10	--
4104	C	2	6.5	20.0	22.0	21.8	0.0098	0.0056	0.0032	0.94	8	--
4105	C	2	5.5	40.4	29.3	30.6	0.0181	0.0119	0.0080	--	13	--
4106	C	2	5.0	45.0	28.6	30.5	0.0200	0.0127	0.0087	--	12	--
4107	C	2	4.5	55.6	37.5	39.5	0.0240	0.0146	0.0088	--	15	1.1
4108	C	2	4.0	62.3	34.7	37.9	0.0246	0.0154	0.0100	--	16	1.3
4109	C	2	3.5	88.0	51.6	55.8	0.0346	0.0208	0.0123	--	28	2.1
4110	C	2	3.0	81.4	48.8	52.5	0.0311	0.0185	0.0100	--	29	2.1
4111	C	2	2.5	82.8	55.4	58.7	0.0315	0.0161	0.0069	--	33	2.5
4112	C	2	2.0	54.7	51.4	51.8	0.0246	0.0154	0.0069	--	32	2.5

[b]Fuels are denoted as follows: A - acetone; B - benzene; C - cyclohexane; H - n-hexane; M - methanol.

[c]*See footnote at end of Table 3.*

TABLE 3 (Continued)

Run[c] No.	Fuel[b]	Nominal Burner Diameter (inches)	Dimensionless Burner Separation S/D	Burning Rate Per Unit Area (lb/hr-ft^2)			Radiation Flux to Surroundings (Btu/ft^2-sec)			Radiation Flux to Center Radiometer (Btu/ft^2-sec)	Average Flame Height (inches)	Average Flame Column Cross-Sectional Area (ft^2)
				Center Burner	Peripheral Burners	9-Burner Average	x=77.5 (inches)	x=106.5 (inches)	x=153.75 (inches)			
4201	C	4	10.9	16.8	16.9	16.8	0.0392	0.0177	0.0073	--	12	--
4202	C	4	7.9	28.1	18.4	19.5	0.0400	0.0192	0.0092	--	12	--
4203	C	4	5.9	17.7	18.7	18.6	0.0361	0.0200	0.0100	--	13	--
4204	C	4	5.0	27.3	23.1	23.5	0.0488	0.0261	0.0135	0.78	14	--
4205	C	4	4.0	60.3	34.2	37.0	0.0707	0.0392	0.0238	2.00	20	--
4206	C	4	3.5	73.5	42.4	45.8	0.0984	0.0531	0.0323	2.70	33	3.9
4207	C	4	3.25	85.9	46.1	50.4	0.1000	0.0500	0.0269	3.15	38	5.0
4208	C	4	3.0	86.7	48.4	52.5	0.1077	0.0531	0.0323	3.68	40	4.3
4209	C	4	2.75	85.9	53.5	56.9	0.1100	0.0523	0.0308	3.60	41	4.4
4210	C	4	2.5	81.8	49.2	52.7	0.1115	0.0600	0.0338	4.13	47	4.0
4210-A	C	4	2.5	77.7	52.0	54.8	0.0961	0.0538	0.0346	4.13	43	4.2
4211	C	4	2.25	78.5	51.8	54.7	0.1061	0.0592	0.0354	3.08	50	4.7
4212	C	4	2.0	74.3	52.7	55.0	0.0984	0.0538	0.0292	2.78	45	6.3
4213	C	4	1.75	65.2	50.8	52.3	0.0946	0.0554	0.0323	2.23	48	5.9
4214	C	4	1.5	47.1	43.7	43.9	0.0769	0.0446	0.0246	1.88	58	3.7
4301	C	6	8.4	22.0	19.7	19.9	0.0961	0.0500	0.0308	0.18	13	--
4302	C	6	6.4	26.6	22.5	23.0	0.0869	0.0477	0.0323	0.30	13	--
4303	C	6	5.1	28.6	23.7	24.3	0.0900	0.0477	0.0323	0.50	15	--
4304	C	6	3.75	48.4	28.7	30.9	0.1192	0.0577	0.0385	1.18	15	--
4305	C	6	3.4	64.9	32.7	36.3	0.1382	0.0692	0.0400	1.60	21	--
4306	C	6	2.8	83.6	41.8	46.4	0.2076	0.0846	0.0538	3.60	52	8.6
4307	C	6	2.6	83.6	41.8	46.4	0.2076	0.0846	--	3.88	74	10.1
4308	C	6	2.4	79.2	42.6	46.6	0.1846	--	--	3.88	54	7.4
4309	C	6	2.25	78.1	45.0	48.7	0.1846	--	--	3.30	55	7.6
4310	C	6	2.1	72.6	44.2	47.4	0.1769	--	--	3.23	70	9.2
4311	C	6	1.9	68.2	47.7	49.1	0.1846	0.0907	0.0538	3.23	70	10.0
4312	C	6	1.75	62.7	46.3	48.1	0.1492	0.0807	0.0500	3.15	72	8.8
4313	C	6	1.5	60.5	46.7	48.2	0.1846	--	--	2.78	70	10.8
4314	C	6	Single Burner	25.4	--	25.4	0.1730	0.1023	0.0669	0.63	28	1.8

[b]Fuels are denoted as follows: A - acetone; B - benzene; C - cyclohexane; H - n-hexane; M - methanol.

[c]See footnote at end of Table 3.

TABLE 3 (Continued)

Run[c] No.	Fuel[b]	Nominal Burner Diameter (inches)	Dimensionless Burner Separation S/D	Burning Rate Per Unit Area (lb/hr-ft^2)			Radiation Flux to Surroundings (Btu/ft^2-sec)			Radiation Flux to Center Radiometer (Btu/ft^2-sec)	Average Flame Height (inches)	Average Flame Column Cross-Sectional Area (ft^2)
				Center Burner	Peripheral Burners	9-Burner Average	x=77.5 (inches)	x=106.5 (inches)	x=153.75 (inches)			
5101	B	2	17.5	33.2	32.3	32.4	0.0200	0.0108	0.0054	0.60	7	--
5102	B	2	11.5	23.0	31.2	30.3	0.0138	0.0062	0.0015	0.40	8	--
5103	B	2	7.75	23.0	34.7	33.3	0.0215	0.0115	0.0062	--	11	--
5104	B	2	6.5	29.4	38.1	37.1	0.0223	0.0131	0.0062	--	12	--
5105	B	2	5.5	56.6	37.2	39.5	0.0215	0.0138	0.0038	--	--	--
5106	B	2	5.0	60.9	41.3	43.6	0.0246	0.0131	0.0077	--	--	--
5107	B	2	4.5	73.3	52.4	54.8	0.0308	0.0169	0.0046	--	9	--
5108	B	2	4.0	87.0	48.3	52.9	0.0346	0.0185	0.0123	--	--	--
5109	B	2	3.5	97.1	60.4	64.6	0.0408	0.0204	0.0142	--	--	--
5110	B	2	3.0	124.2	71.8	77.9	0.0423	0.0208	0.0112	--	23	1.4
5111	B	2	2.5	108.0	79.4	82.7	0.0431	0.0208	0.0081	--	34	2.7
5112	B	2	2.0	78.5	84.5	83.8	0.0454	0.0200	0.0092	--	28	2.0

[b]Fuels are denoted as follows: A - acetone; B - benzene; C - cyclohexane; H - n-hexane; M - methanol.

[c]All run numbers for the rimless burner tests consist of four digits. The first digit denotes the fuel: 1 - methanol; 2 - acetone; 3 - n-hexane; 4 - cyclohexane; 5 - benzene. The second digit denotes the burner diameter and number of burners: 1 - 2-inch diameter (9-burners); 2 - 4-inch diameter (9-burners); 3 - 6-inch diameter (9-burners); 4 - 4-inch diameter (13-burners). The third and fourth digits denote the sequence in which a series of tests (a particular fuel, burner size and number of burners) was made. The letters A and B after some of the run numbers denote that the test of a particular run number has been repeated under the same conditions: A - first repeat of a run; B - second repeat of a run. Example: Run No. 2307-A denotes a repeat of the seventh test of the series for which acetone was burned in nine, 6-inch diameter rimless burners.

TABLE 4

SUMMARY OF RIMLESS-BURNER FLAME INTERACTION AND MERGING DATA[a]

Run[c] No.	Fuel[b]	Dimensionless Burner Separation S/D	Burning Rate Per Unit Area (lb/hr-ft^2)				Radiation Flux to Surroundings (Btu/ft^2-sec)			Radiation Flux to Center Radiometer (Btu/ft^2-sec)	Average Flame Height (inches)	Average Flame Column Cross-Sectional Area (ft^2)
			Center Burner	Intermediate Burners	Peripheral Burners	13-Burner Average	x=77.5 (inches)	x=106.5 (inches)	x=153.75 (inches)			
2401	A	4.0	14.1	13.8	13.9	13.9	0.0202	0.0096	0.0044	0.60	13	--
2402	A	3.5	16.1	14.8	15.4	15.2	0.0235	0.0123	0.0065	0.78	14	--
2403	A	3.0	18.8	16.5	15.0	15.2	0.0250	0.0146	0.0092	0.78	14	--
2404	A	2.5	25.1	19.8	16.6	18.2	0.0308	0.0185	0.0112	1.25	15	--
2405	A	2.0	57.1	44.1	23.6	32.5	0.0554	0.0331	0.0185	2.55	25	3.7
2406	A	1.75	44.8	36.0	19.8	26.7	0.0500	0.0285	0.0157	3.68	28	--
3401	H	4.0	29.3	25.5	18.7	21.6	0.0577	0.0331	0.0223	0.88	13	--
3402	H	3.5	35.1	32.0	20.3	25.0	0.0731	0.0438	0.0269	1.18	16	--
3403	H	3.0	48.5	49.4	26.1	35.0	0.0946	0.0570	0.0369	1.70	24	--
3404	H	2.5	78.9	47.3	28.4	38.1	0.1099	0.0615	0.0377	3.68	27	--
3405-A	H	2.0	94.4	85.1	45.9	61.7	0.1592	0.0823	0.0461	3.98	55	9.2
3406	H	1.75	83.9	78.8	47.6	59.9	0.1553	0.0807	0.0477	4.43	64	9.6
3407	H	1.5	71.5	72.5	50.0	58.4	0.1476	0.0846	0.0500	3.68	60	9.1
4401	C	4.0	29.2	26.1	17.9	21.3	0.0577	0.0323	0.0215	0.85	16	--
4402	C	3.5	35.2	35.2	22.3	27.3	0.0731	0.0408	0.0277	1.12	15	--
4403	C	3.0	58.5	47.5	25.3	34.6	0.0907	0.0492	0.0331	2.18	20	--
4404	C	2.5	77.1	71.7	34.5	49.2	0.1230	0.0638	0.0423	4.05	--	--
4405	C	2.0	106.3	87.0	48.5	64.8	0.1575	0.0731	0.0423	4.13	58	7.3
4406	C	1.75	95.4	87.0	55.3	68.1	0.1692	0.0769	0.0523	4.50	--	6.6
4407	C	1.5	81.5	78.2	60.9	67.8	0.1538	--	--	3.93	71	9.9

[a] 13-burner pattern (4-inch diameter burners).

[b] Fuels are denoted as follows: A - acetone; C - cyclohexane; H - n-hexane.

[c] See footnote at end of Table 3.

TABLE 5

DATA FOR EXPOSED-RIM BURNER FLAME MERGING CORRELATION

Fuel	Burner Pattern	$\frac{\Delta H_c}{\Delta H_v}$	m_s[a] (lb/hr-ft^2)	m_p (lb/hr-ft^2)	$\frac{m_p}{m_s}$	$\left(\frac{S}{D}\right)_p$
Acetone	9-burner	48.5	16.5	70	4.24	2.1
n-hexane	square	99.4	42.2	146	3.46	3.3
Cyclohexane	pattern	91.0	47.9	150	3.13	3.7
NTS[b]	(3 x 3	87.2	62.1	179	2.88	4.0
Benzene	inch square burner	79.3	101.5	213	2.10	4.4
Acetone	9-burner	48.5	16.5	40	2.44	1.7
n-hexane	square	99.4	42.2	103	2.44	2.0
Cyclohexane	pattern	91.0	47.9	105	2.2	2.6
NTS[b]	(4 3/16-inch circular burners)	87.2	62.1	121	1.95	2.8

[a]Data of 3 x 3-inch single square burner used.

[b]Napalm test solvent.

TABLE 6

DATA FOR RIMLESS BURNER FLAME MERGING CORRELATIONS

Fuel[a]	Burner Pattern	Nominal Burner Diameter (inches)	$\frac{\Delta H_c}{\Delta H_v}$	Single Burner Burning Rate ($lb/hr\text{-}ft^2$)	$\frac{m_p}{m_s}$ (Average Burning Rate)	$\frac{m_p}{m_s}$ (Center Burner)	$\left(\frac{S}{D}\right)_p$ (Center Burner)	$\left(\frac{S}{D}\right)_p$ (Outer Burners)
A	9-burner	2	48.5	11.5	2.0	3.0	2.5	2.5
H	pattern	2	99.4	13.0	3.3	5.5	3.5	3.5
C		2	91.0	15.0	3.9	5.8	3.5	2.75
B		2	79.3	22.5	3.7	5.5	3.0	--
A		4	48.5	13.5	2.4	3.7	2.0	2.0
H		4	99.4	17.0	2.9	4.8	3.0	2.25
C		4	91.0	17.5	3.3	5.0	3.0	2.75
A		6	48.5	14.0	2.5	4.6	2.1	2.1
H		6	99.4	18.5	2.8	4.4	2.6	2.75
C		6	91.0	20.0	2.5	4.2	2.75	--
A	13-burner	4	48.5	13.5	2.4	4.22	2.0	2.0
H	pattern	4	99.4	17.0	3.6	5.53	2.0	2.0
C		4	91.0	17.5	3.9	6.06	2.0	1.75

[a] A = Acetone, H = n-Hexane, C = Cyclohexane, B = Benzene.

TABLE 7

DATA FOR RIMLESS BURNER FLAME TRAILING CORRELATION

Run No.[b]	Fuel[c]	Dimensionless Burner Separation	Velocity of Entrained Air (Ft/Min)			Flame Trailing Length (inches)
			Low Reading	Average Reading[a]	High Reading	
2307A	A	3.25	15	25	30	7.5
2403	A	3.0	20	27	35	6.0
2405	A	2.0	15	23	35	6.3
3201	H	8.75	13	19	22	5.0
3202	H	7.9	24	30	35	4.7
8202A	H	7.9	27	33	37	5.3
8203	H	5.9	30	40	45	5.7
3204	H	4.4	45	50	55	7.6
3205	H	4.0	30	42	45	10.0
3301	H	8.4	25	35	45	10.5
3302	H	6.4	35	50	65	13.8
3303	H	5.1	60	90	100	12.0

[a]Average anemometer readings are used in correlation.

[b]See footnote at end of Table 3.

[c]Fuels are denoted as follows: A - acetone; H - n-hexane.

APPENDIX B

THE PREDICTION OF LARGE-FIRE BURNING RATES FROM SMALL MULTIPLE FIRES

The behavior of the modes of heat transfer to the fuel surface of a large single fire can be compared with the behavior of the heat transfer back to the surface of small multiple fires from liquid fuels. The similarities between the heat feedback to a large single fire and to the center fuel source of an array of small multiple fires lead to the possibility of predicting large-fire burning rates by burning small multiple fires.

As noted by Hottel (12) and expressed in Equation 1, radiative heat feedback will be constant and will predominate at large burner diameters. Conduction is an edge effect and will be negligible for large burners. The studies of Akita and Yumoto (1) showed that the contribution of convective heat transfer to the liquid decreases with distance from the outer edge of the flame column base. However, convective heat transfer is still present near the center of the large fire since hot combustion gases are often swept over the liquid fuel surface due to the turbulent motion of the large fire column. A layer of unburned fuel vapor is present over the entire portion of the large-

fire fuel surface since the heat feedback causes the fuel to vaporize faster than it can be consumed. This vapor layer blocks some of the flame radiation to the fuel surface since, as mentioned previously, data taken by Burgess, et al. (6) showed that a fuel vapor tends to absorb its own flame radiation.

In the present multiple fire studies, the burners were recessed up to their rims in an insulated table surface so that, as noted above for large single fires, the conduction of heat through the burner walls could be considered negligible. As noted previously, the burning rate, particularly for the fuel in the center burner of the burner pattern, was greatly increased by the presence of the surrounding fires as these fires began to interact and merge.

As the multiple fires began to merge into one fire column, the radiation heat transfer to the center-burner fuel surface was greatly increased due to the presence of the fire from the surrounding burners. For some of the more opaque fires from fuels such as cyclohexane, the merged fire column was large enough that radiation from the outer portion of the fire column was absorbed by the fire itself before it could reach the center-burner fuel surface. The radiative heat feedback to the center-burner fuel surface was therefore as a maximum since any increase in the fire column size would not increase the radiative heat feedback to this fuel surface. As noted in Reference 5, the radiative

heat feedback per unit fuel surface area to a very large liquid-fueled fire is also at a maximum. The radiative heat feedback to the center burner of the opaque merged fires is therefore similar to the radiative feedback for a very large fire. In addition, a vapor layer, similar to that mentioned in connection with the large single fires, was formed over the center portion of the burner pattern for the fully merged fires.

When the multiple fires were interacting but were not close enough together to be completely merged, the air entrained to the center-burner fires was heated since it had to pass over the hot table surface between the peripheral fires of the pattern. This hot entrained air, along with the turbulence in the center-burner flame column created by the surrounding fires, caused the convective heat transfer to the center-burner fuel surface to be greater than that for interaction-free burning. When the burner separation distance was further decreased, the fires merged into a single fire column, and the fire from the peripheral burners completely surrounded the center burner. This fully merged fire column blocked the air flow to the center burner and decreased the convective heat feedback to the center-burner fuel. Therefore, the greatest convective heat feedback to the center-burner fuel surface occurred before the fires had become sufficiently merged to block air flow to the center burner. As noted previously, the convective heat feedback

to a large single fire decreases with distance from the outer edge of the flame column base. For the fully merged fires, the convective heat transfer to the center burner was therefore similar to the convective transfer to a large single fire. In addition, the merged fire column is turbulent enough that the previously-mentioned convective heat transfer due to fire turbulence is present.

At the onset of merging, the heat transfer back to the center-burner liquid, and therefore the burning rate of the center-burner liquid, is at a maximum. As noted previously, the heat feedback to the center-burner fuel of a fully merged, opaque fire is similar to the heat feedback to a large single fire. In addition, the heat feedback to the center-burner fuel at the onset of merging is greater than that for the fully merged fire, mainly due to the greater convective heat feedback to the center-burner fuel at the onset of merging. Therefore, for the fires which are opaque enough that the radiative heat feedback is at a maximum, the peak burning rate per unit area (at the onset of merging) of the center burner is at least as great as the large-fire burning rate per unit area.

If a successful empirical correlation between the peak multiple-fire burning rate and the large-fire burning rate can be found, an actual prediction of the large single-fire burning rate can be made by burning only small multiple

sources of the liquid fuel. If not, at least an upper bound on the value of burning rate per unit area of a single large fire can be obtained.

APPENDIX C

REFERENCES

1. Akita, K., and T. Yumoto, "Heat Transfer in Small Pools and Rates of Burning of Methanol," Tenth Symposium (International) on Combustion, 943-948, The Combustion Institute, Pittsburgh, Pennsylvania (1965).

2. Baldwin, R., P. H. Thomas, and H. G. H. Wraight, "The Merging of Flames from Separate Fuel Beds," Fire Research Note No. 551, Joint Fire Research Organization, England, May 1964.

3. Baldwin, R., "Some Tentative Calculations of Flame Merging in Mass Fires," Fire Research Note No. 629, Joint Fire Research Organization, England.

4. Blinov, V. I., and G. N. Khudiakov, "Certain Laws Governing Diffusive Burning of Liquids," Acad. Nauk. USSR Doklady, 113, 1094 (1957).

5. Burgess, D. C., J. Grumer, and H. G. Wolfhard, "Burning Rates of Liquid Fuels in Large and Small Open Trays," The Use of Models in Fire Research, NAS-NRC Pub. 786, 68 (1961).

6. Burgess, D. S., A. Strasser, and J. Grumer, "Diffusive Burning of Liquid Ruels in Open Trays," Fire Research Abstracts and Reviews, 3, 177 (1961).

7. Burgess, D., and J. Grumer, "Comments on 'The Burning Rate of Liquid Fuels from Open Trays by Natural Convection' by D. B. Spalding," Fire Research Abstracts and Reviews, 4, 236 (1962).

8. Burgess, D. S., and M. G. Zabetakis, "Fire and Explosion Hazards Associated with Liquefied Natural Gas," Bureau of Mines R. I. 6099, 1962.

9. Countryman, C. M., "Mass Fires and Fire Bheavior," First Interim Report for Office of Civil Defense, Office of the Secretary of the Army, Pacific Southwest Forest and Range Experiment Station (1964).

10. Emmons, H. W., "Some Observations on Pool Burning," The Use of Models in Fire Research, NAS-NRC Pub. 786, 50 (1961).

11. Fons, W. L., "Rate of Combustion from Free Surfaces of Liquid Hydrocarbons," Combustion and Flame, 5, 283 (1961).

12. Hottel, H. C., Review of Reference 4, Fire Research Abstracts and Reviews, 1, 41 (1959).

13. Hottel, H. C., "Fire Modeling," The Use of Models in Fire Research, NAS-NRC Pub. 786, 32 (1961).

14. Magnus, G., "Tests on Combustion Velocity of Liquid Fuels and Temperature Distribution in Flames and Beneath Surface of the Burning Liquid," The Use of Models in Fire Research, NAS-NRC Pub. 786, 76 (1961).

15. Putnam, A. A., and C. F. Speich, "A Model Study of the Interaction Effects of Mass Fires," Summary Report No. 2, Battelle Memorial Institute, Columbus, Ohio, Research Report, March 27, 1963.

16. Putnam, A. A., and C. F. Speich, "A Model Study of the Interaction of Multiple Turbulent Diffusion Flames." Ninth International Symposium on Combustion, Academic Press, New York (1963).

17. Rasbash, D. J., Z. E. Rogowski, and G. W. V. Stark, "Properties of Fires of Liquids," Fuel, 35, 94 (1956).

18. Rios, J., "Interaction Effects of Wind-Blown Proximate Flames From Burning Wood Cribs," Ph.D. Dissertation, The University of Oklahoma (1966).

19. Spalding, D. B., Some Fundamentals of Combustion, Butterworths, London (1955).

20. Spalding, D. B., "The Burning Rate of Liquid Fuels from Open Trays by Natural Convection," Fire Research Abstracts and Reviews, 4, 234 (1962).

21. Spalding, D. B., "The Art of Partial Modeling," Ninth International Symposium on Combustion, Academic Press, New York (1963).

22. Stempel, F. C., and D. L. Rall, "Applications and Advancements in the Field of Direct Heat Transfer Measurements," Preprint of paper presented at Instrument Society of America 18th Annual Conference, Sept. 9-12, 1963, Chicago.

23. Strasser, A., and J. Grumer, "Air Flows into Uncontrolled Fires," Final Report No. 3909, Bureau of Mines (Jan. 8, 1964).

24. Thomas, P. H., C. T. Webster, and M. M. Raftery, "Some Experiments on Buoyant Diffusion Flames," Combustion and Flames, 5, 359-367 (1961).

25. Thomas, P. H., "The Size of Flames from Natural Fires," Ninth International Symposium on Combustion, Academic Press, New York (1963).

26. Thomas, P. H., R. Baldwin, and A. J. M. Heselden, "Buoyant Diffusion Flames: Some Measurements of Air Entrainment, Heat Transfer and Flame Merging," Tenth Symposium (International) on Combustion, 983-996, The Combustion Institute, Pittsburgh, Pennsylvania (1965).

27. Waterman, T. E., W. G. Labes, F. Salzberg, J. E. Temney, and F. J. Vodvarka, "Prediction of Fire Damage to Installations and Built-up Areas from Nuclear Weapons," Final Report - Phase III, Experimental Studies - Appendices A-G, IIT Research Institute Report for National Military Command System Support Center, Contract No. DCA-8, November, 1964.

28. Welker, J. R., "The Effect of Wind on Uncontrolled Buoyant Diffusion Flames from Burning Liquids," Ph.D. Dissertation, The University of Oklahoma (1965).

29. Western, A. M., "A Preliminary Analysis of Some Flambeau Data," SA/PR-113 Home Office Scientific Advisors Report 1966.

30. Zabetakis, M. G., and D. S. Burgess, "Research on the Hazards Associated with the Production and Handling of Liquid Hydrogen," Bureau of Mines R.I. 5707, 1961.

APPENDIX D

NOMENCLATURE

a = empirical coefficient

b = empirical coefficient

D = burner diameter

D' = flame trailing length, measured as length that flame trailed over table surface plus value of burner diameter

Fr = Froude number

g = acceleration due to gravity

ΔH_c = lower heat of combustion of fuel

ΔH_v = heat of vaporization at the fuel boiling point plus the integrated heat capacity of the fuel

L = flame height

m = burning rate per unit of fuel surface area

S = distance between center of center burner of array and either the center of a peripheral burner (for 9-burner pattern) or center of an intermediate burner (for 13-burner pattern)

u = entrained air velocity

x = distance from track radiometer to center of burner array

ρ = density

Subscripts

a = air

eq = equivalent

g = fuel vapor

p = peak, or at the onset of merging

s = single burner, or interaction-free burning